THE PROTEIN NETWORK OF HIV-1 BUDDING

by

Melissa Diane Stuchell Brereton

A dissertation submitted to the faculty of
The University of Utah
in partial fulfillment of the requirements for the degree of

Doctor of Philosophy

Department of Biochemistry

The University of Utah

December 2010

The University of Utah Graduate School

STATEMENT OF DISSERTATION APPROVAL

The dissertation of **Melissa Diane Stuchell Brereton**

has been approved by the following supervisory committee members:

Wesley I. Sundquist	, Chair	**11/24/10** Date Approved
Michael Kay	, Member	**11/24/10** Date Approved
Dennis Winge	, Member	**11/24/10** Date Approved
David Myszka	, Member	**11/24/10** Date Approved
Darrel Davis	, Member	**11/24/10** Date Approved

and by **Wesley I. Sundquist and Chris Hill**, Chair of the Department of **Biochemistry**

and by Charles A. Wight, Dean of The Graduate School.

ABSTRACT

HIV-1 is an enveloped RNA virus that recruits cellular machinery to facilitate virus budding. HIV-1 Gag, the structural protein that drives the assembly and budding processes, binds directly to two cellular factors, TSG101 and ALIX. Both TSG101 and ALIX are proteins in the endosomal sorting complexes required for transport (ESCRT) pathway and are required for inward vesicle formation at late endosomes or multivesicular bodies (MVBs). Most ESCRT proteins are subunits one of five hetero-oligomeric complexes named ESCRT-0, ESCRT-I, ESCRT-II, ESCRT-III, and the VPS4 AAA ATPases (vacuolar protein sorting), which are sequentially recruited to sites of vesicle formation and virus budding. TSG101 is a member of the ESCRT-I complex and is involved in recognition of cargos and recruitment of ESCRT-II. ESCRT-II recruits ESCRT-III, which is composed of charged multivesicular body proteins (CHMPs) that coassemble to form a lattice on the surface of endosomal membranes. ALIX interacts with proteins in both ESCRT-I and ESCRT-III, but is not a constitutive member of either complex. ESCRT-III proteins bind directly to the VPS4 AAA ATPases, which are the only known enzymes in the pathway. ATP hydrolysis by the VPS4 ATPases releases all assembled ESCRT machinery, allowing multiple rounds of vesicle formation or viral egress. This thesis focuses on the identification and characterization of components of the human ESCRT protein network involved in HIV-1 budding.

Chapter 2 describes my contribution to the identification of the protein network involved in HIV-1 budding. Discovery of new protein-protein interactions in the ESCRT pathway defined bridges between complexes that act early in the pathway and those that act late. Chapter 3 describes the role of ESCRT-I in HIV-1 budding. Specifically, I identified four previously unknown subunits of human ESCRT-I (VPS37A-D) and characterized the biochemistry of VPS37B. Finally, Chapter 4, Appendix and Appendix B describe the interaction between the CHMPs of ESCRT-III and the VPS4 MIT domains. My contribution to these sections was the identification of the regions of required for the complex interactions. Specifically, I identified a C-terminal motif found in CHMP 1-3 that binds the VPS4 MIT domains. Structural studies of the VPS4B/CHMPB complex revealed that the CHMP2B peptide binds to the antiparallel three helix bundle of the VPS4B MIT domain between helices two and three, and suggested two plausible models for the complex. Overall, the data presented here support the model that HIV-1 usurps the human ESCRT pathway to enable virus budding, and help to define the interactions that allow this pathway to facilitate MVB vesicle formation and HIV-1 budding.

TABLE OF CONTENTS

CHAPTER 1

INTRODUCTION

HIV and AIDS Prevalence

Acquired immune deficiency syndrome (AIDS) is one of the most devastating diseases to affect the world today. In 1981, five patients in Los Angeles area hospitals presented with symptoms of pneumonia, only to discover later that this was only a secondary infection. These patients were infected with a virus. Their diagnosis and the subsequent identification of the human immunodeficiency virus (HIV) were key early events that presented the AIDS epidemic to the world (Barre-Sinoussi et al., 1983; Gallo et al., 1984). Since that time, AIDS and AIDS-related illnesses have killed more than 25 million people. According to the World Health Organization (WHO) and the Joint United Nations Programme on HIV/AIDS (UNAIDS), Africa remains the epicenter of the AIDS pandemic, and more than a third of the recorded deaths in 2005 occurred in Sub-Saharan Africa. This large number of deaths in Africa has literally affected the fabric of society, as economic growth decreases and the number of orphaned children increases. Today it is estimated that 40 million people worldwide are living with HIV (UNAIDS, 2006). A detailed understanding of HIV molecular biology therefore remains a key objective as part of the effort to defeat this disease and epidemic.

HIV is an enveloped ribonucleic acid (RNA) virus of the *retroviridae* family of viruses. HIV-1 and HIV-2 are the two known HIV types and account for all current and

new infections of today. There are at least nine distinct HIV-1 subtypes (Geretti, 2006; Julg & Goebel, 2005). Most subtypes can be effectively treated by the Antiretroviral treatments (ARTs) available today. However, these drugs are not a cure and only prolong the lives of AIDS patients by inhibiting or slowing certain steps in the HIV life cycle. Moreover, ART-resistant strains are now prevalent, which necessitates the identification of new targets for antiviral therapies (Geretti, 2006; Wainberg, 2004).

In recent years, there has been significant progress understanding the late stage of retroviral replication called budding. The process of HIV-1 budding occurs when the virus becomes entrapped by the plasma membrane, and a membrane fission event releases the virion from the cell. We now understand that HIV-1, the focus of this dissertation, does not encode the machinery required for viral egress, suggesting that these activities must be provided by host factors. In 2001, the cellular host factor TSG101 was shown to be required for efficient virus budding (Demirov et al., 2002; Garrus et al., 2001; Martin-Serrano et al., 2001; VerPlank et al., 2001). The work, described herein, contributed to the identification and characterization of the cellular protein network that functions together with TSG101 to aid in the HIV-1 budding process.

The HIV-1 Life Cycle

The HIV-1 life cycle begins when the virus binds a host cell via a direct interaction between the viral Env glycoproteins on the virion exterior and CD4 receptors on the surface of target cells (Figure 1.1) (Gomez & Hope, 2005; Wang et al., 2000). This interaction facilitates a subsequent interaction with one of two co-receptors that are also located on the surface of the host cell (CXCR4 or CCR5). These interactions trigger

Figure 1.1. The life cycle of HIV-1.

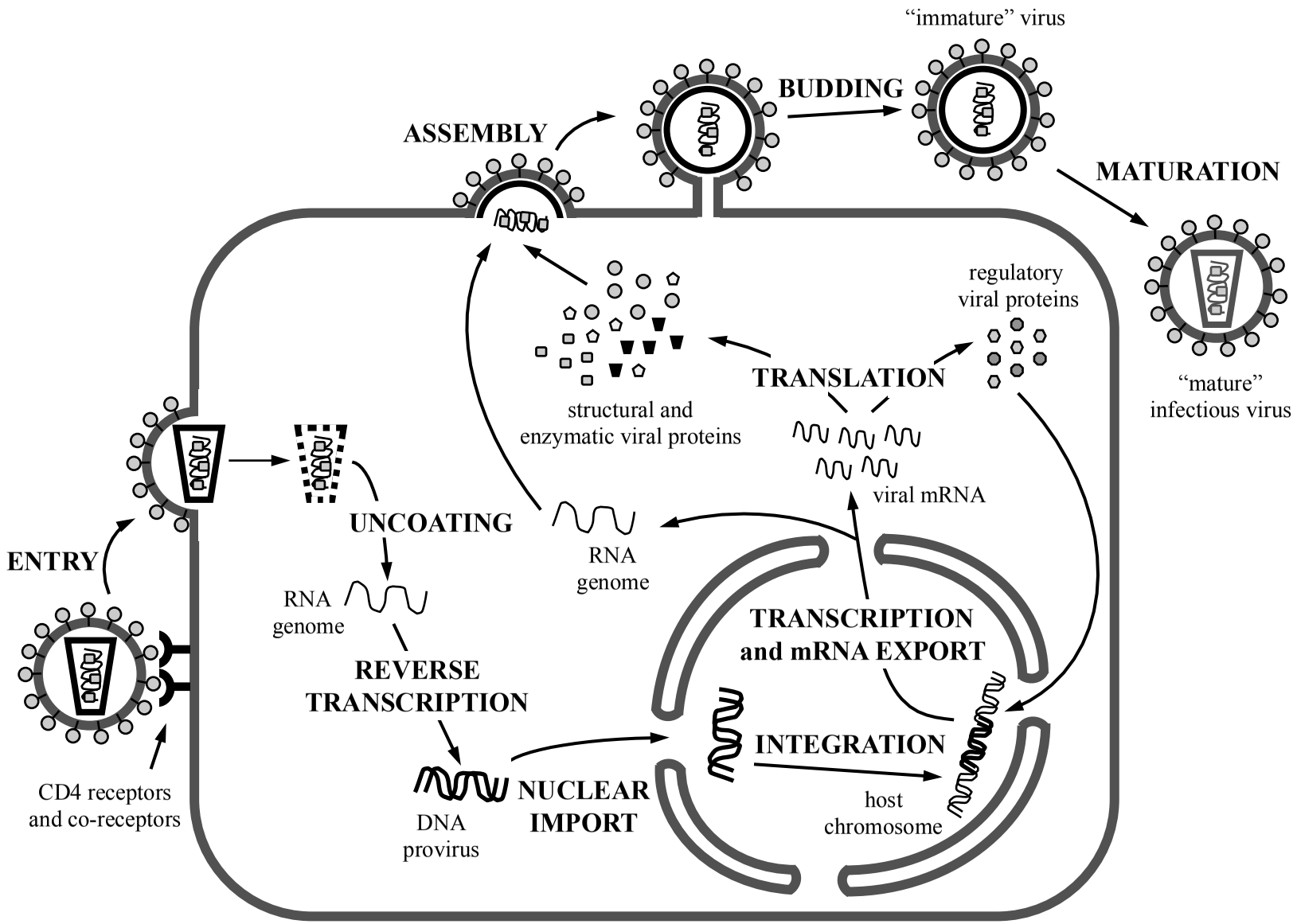
"immature" virus
BUDDING
ASSEMBLY
MATURATION
regulatory
viral proteins
"mature"
infectious virus
TRANSLATION
structural and
enzymatic viral proteins
viral mRNA
UNCOATING
ENTRY
RNA
genome
RNA
genome
TRANSCRIPTION
and mRNA EXPORT
REVERSE
TRANSCRIPTION
INTEGRATION
NUCLEAR
IMPORT
DNA
provirus
host
chromosome
CD4 receptors
and co-receptors

conformational changes in the viral glycoproteins that juxtapose the cellular and viral membranes and facilitate membrane fusion. Fusion of the viral and cellular membranes releases the viral "core" into the cytoplasm where it loses its outer capsid shell (a process termed "uncoating") which releases the viral RNA genome (Gomez & Hope, 2005). Reverse transcriptase (RT), a viral enzyme that is packaged within the viral core, reverse transcribes the HIV genome to produce a DNA copy of the viral genome (Freed, 2001). This DNA genome and associated viral and cellular proteins are called the preintegration complex (PIC). The PIC is imported into the nucleus, where the viral DNA genome is integrated at random sites in the host chromosomal DNA. This integrated viral DNA copy (termed the "provirus") is transcribed by RNA polymerase II under the control of the viral Tat transactivator to produce both full length viral RNA genomes as well as unspliced and singly spliced viral mRNAs (Gomez & Hope, 2005). Incompletely spliced viral RNAs are exported from the nucleus by the viral Rev proteins. In the cytoplasm these RNAs serve as templates for translation of the various viral proteins, including the viral Gag (structural proteins), Pol (viral enzymes), and Env (receptor binding/fusion) polyproteins. Approximately 3000 copies of Gag assemble to form each virion. Gag proteins recognize the plasma membrane through the N-terminal matrix (MA) domain, and package full length RNA genomes through direct interactions with the downstream nucleocapsid (NC) domains (Freed, 2001). Once virion components have been recruited, a spherical particle begins to extrude from the surface of the cell (Figure 1.2). The virion is then released through a fission mechanism that reseals the viral and plasma membranes (budding). The newly released immature virus is not infectious until it advances through a maturation process, which involves cleavage of the assembled Gag and Gag-Pol

Figure 1.2. Spherical HIV particles arrested at a late stage of budding.
EM images of thin-sectioned 293T cells transfected with an HIV expression vector and expression constructs for dominant negative (A) DsRed-CHMP4B and (B) DsRed-CHMP2A proteins (Adapted from von Schwedler et al., 2003, Figure 6 in Chapter 2).

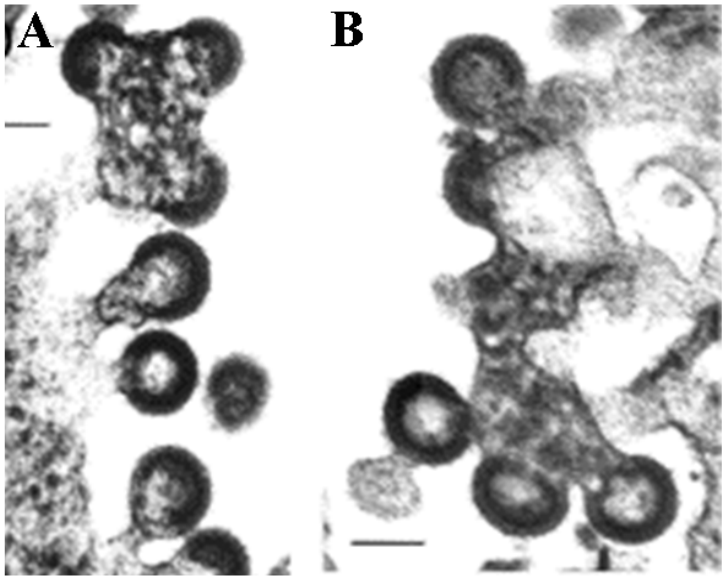
A
B

polyproteins by the viral protease followed by reorganization of the cleaved products (Freed, 2001). Viral maturation initiates during budding and is completed soon thereafter. Rearrangements during maturation create a central core particle that contains the viral RNA genome and associated enzymes, and is surrounded by a conical shell called the capsid (Freed, 2001). Maturation creates an infectious particle, and completes the viral lifecycle. This dissertation focuses on the mechanism by which immature virions are released from the infected cell—the process of viral budding.

The HIV-1 Genome and Virion Organization

HIV-1 is a positive sense single stranded RNA (ssRNA) lentivirus. Lentiviruses are defined by their virion structure and organization, genetic composition and manner of replication (Coffin et al., 1997). Lentiviral cores are predominantly conical in shape and contain the material required for replication. The viral RNA genome is approximately 9 kilobases in size and encodes nine open reading frames (ORFs). Translation of the ORFs ultimately leads to the production of 15 viral proteins because the major proteins are initially produced as polyproteins that are processed into a series of smaller mature proteins. The three major polyproteins are Gag, Gag-Pol and Env (Figure 1.3A). About 5% of the time, ribosomal frameshifting during Gag translation produces the longer Gag-Pol polyprotein (Freed, 2001; Jacks, 1990). Gag-Pol co-assembles with Gag and Gag-Pol cleavage produces the essential viral enzymes (Freed, 2001). The six remaining ORFs encode for accessory proteins that aid HIV at multiple stages of viral replication.

Gag Polyprotein

The Gag polyprotein is comprised of four distinct regions that are required for

Figure 1.3. HIV-1 genome and *gag* open reading frame.
(A) Schematic of the HIV-1 genome with nine viral ORFs and two long terminal repeats or LTRs. (B) *gag* open reading frame enlarged to show organization of MA, CA, NC, p6 and two spacer proteins.

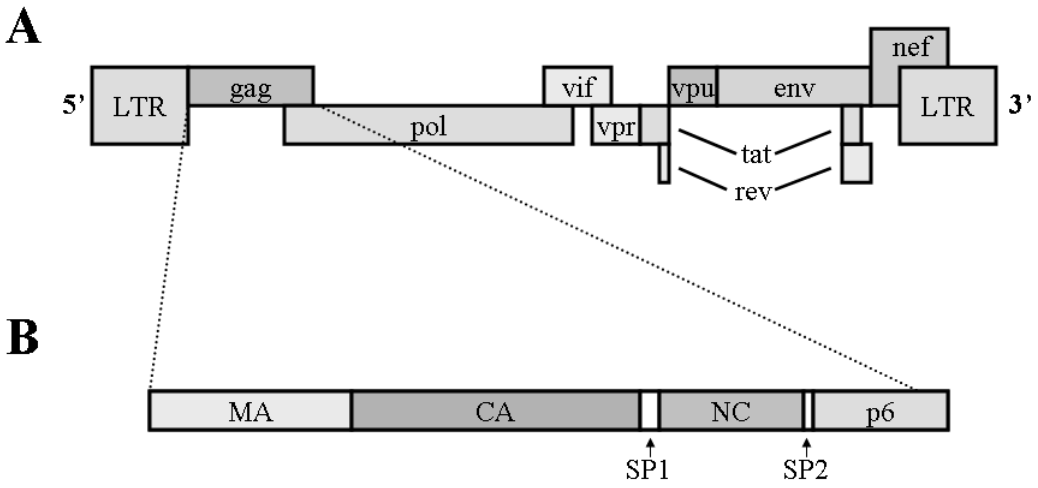
A
5'
LTR
gag
pol
vif
vpr
vpu
env
nef
LTR
3'
tat
rev
B
MA
CA
NC
p6
SP1
SP2

assembly of the virion and viral egress. These four domains are cleaved from each other by a viral protease during maturation into four structural proteins; MA (matrix), CA (capsid), NC (nucleocapsid), and p6 (Figure 1.3B) (Freed, 2001). The MA protein is located at the N-terminus of Gag and is required for directing both Gag and Gag-Pol precursor polyproteins to the site of virus assembly (Freed, 2001). MA associates with the plasma membrane via an N-terminal myristyl group and a binding site for the phosphatidyl inositol(4,5)diphosphate ($PI(4,5)P_2$ (Freed, 2006; Saad et al., 2006). The CA protein is internally positioned between MA and NC in the Gag polyprotein. Once cleaved it forms the viral capsid, which encapsulates the viral genome along with NC and other viral enzymes. The NC protein is also internally situated in Gag and binds and packages the viral RNA genome. The C-terminal p6 region of the Gag polyprotein is responsible for incorporating Vpr (Checroune et al., 1995; Huang et al., 1995; Kondo et al., 1995; Lu et al., 1995), an accessory protein described later, and for recruiting the cellular factors required for efficient viral egress.

In addition to the four proteins described above, Gag also encodes two spacer proteins, SP1 and SP2. SP2 is located between NC and p6, while SP1 is farther upstream between CA and NC. These additional spacer proteins are essential for viral infectivity and aid in the viral maturation process (Gottlinger et al., 1989; Krausslich et al., 1995; von Poblotzki et al., 1993). One model holds that SP1 assists in the assembly process of the capsid core by providing an α-helix in the C-terminal domain that is transiently required for proper rearrangement during maturation (Accola et al., 1998).

Pol Polyprotein

The Pol polyprotein contains three enzymes essential for viral replication: PR

(protease), RT (reverse transcriptase), and IN (integrase). The viral PR enzyme is responsible for processing the Gag and Gag-Pol polyproteins. This cleavage releases the final MA, CA, NC, p6, PR, RT, and IN proteins from their respective polyproteins, allowing necessary rearrangements during viral maturation (Freed, 2001). The RT enzyme is required for reverse transcription of the RNA genome. RT is a heterodimer containing two subunits, p66 and p51 (Hill et al., 2005). The longer p66 subunit contains an additional ribonuclease H (RNase H) domain, which is responsible for cleaving the RNA strands of the RNA-DNA hybrids generated during reverse transcription (Frankel & Young, 1998; Hill et al., 2005). IN is required for integration of the viral genome into the host genome (Hill et al., 2005). The integration process takes place after reverse transcription and can occur at many target sites along the host chromosomal DNA.

Env Polyprotein

The Env polyprotein is composed of two glycoproteins required for viral entry: SU (surface/or gp120) and TM (transmembrane/or gp41) (Freed, 2001). The SU glycoprotein recognizes and binds to CD4 and chemokine co-receptors on the surface of human cells while the TM glycoprotein spans the viral membrane. The SU/TM heterodimer trimerizes to create spikes on the exterior of the assembled virus (Figure 1.4) (Freed, 2001). HIV entry begins via binding of SU to specific receptors found on the surface of T cells, primary macrophages and some dendritic cells. CD4 is the initial receptor for HIV-1; and this interaction induces a conformational change that allows SU to interact with chemokine co-receptors (Gomez & Hope, 2005). The two most common co-receptors used by HIV-1 are CXCR4 and CCR5 (Gomez & Hope, 2005). These co-

Figure 1.4. Organization of the mature HIV-1 virion.

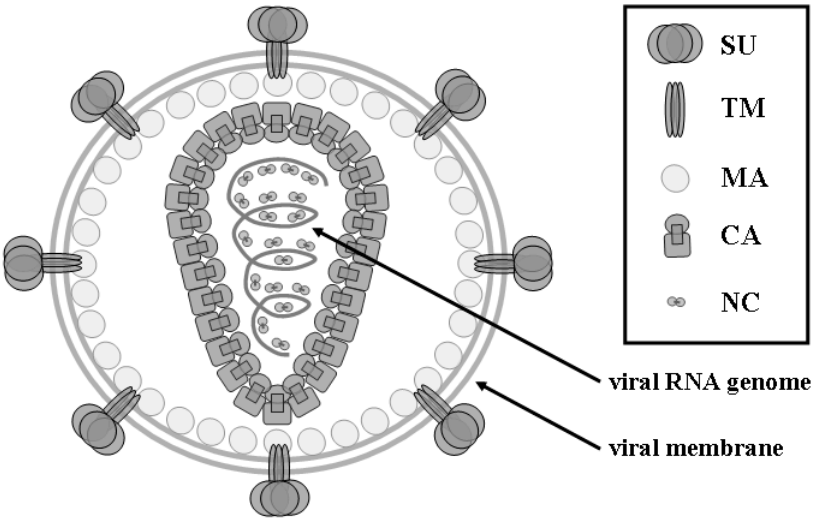
SU
TM
MA
CA
NC
viral RNA genome
viral membrane

receptors are normally involved in cellular activities such as leukocyte chemotaxis (Dunfee et al., 2006; Lusso, 2006).

HIV-1 strains exhibit one of two distinct patterns of infectivity, (M)-tropism or (T)-tropism. Macrophage (M)-tropic viruses replicate in macrophages and commonly use the CCR5 co-receptor to infect CD4+ cells. (T)-tropic or T cell tropic isolates enter cells using the CXCR4 co-receptor and replicate in T cells. These isolates are more likely to induce cell fusion in culture, whereas (M)-tropic isolates are non-syncytium inducing (Coffin et al., 1997; Dunfee et al., 2006; Frankel & Young, 1998). Once SU engages the co-receptors, TM undergoes a conformation change that facilitates fusion of the viral membrane with the cell membrane (Dunfee et al., 2006; Frankel & Young, 1998).

Accessory Viral Proteins

Six additional open reading frames encode for accessory proteins that aid in the viral life cycle. Tat enhances the processivity of the transcribing polymerases, resulting in production of full length transcripts. Rev is responsible for transporting unspliced and singly spliced mRNAs to the cytoplasm after transcription of the integrated viral genome (Hope & Pomerantz, 1995). Vpu is involved in the degradation of CD4 receptors (to reduce the number of receptors that bind to Env in the endoplasmic reticulum), down regulation of MHC class I protein (which normally attracts T lymphocytes to destroy the cell), and virus release (through antagonism of the cellular innate immune restriction factor, tetherin) (Neil et al., 2008; Nomaguchi et al., 2008; Waheed et al., 2008). Vif is an accessory protein that allows HIV to persist in cells that would normally be resistant to infection. Vif functions by inducing the degradation of the innate immune restriction

factor, APOBEC3 (Stopak & Greene, 2005). Nef acts similarly to Vpu and assists in CD4 receptor downregulation by rerouting them to the lysosome (Arien & Verhasselt, 2008; Malim & Emerman, 2008). Finally, Vpr assists early stages of viral replication in some cell types, probably by antagonizing another host immune restriction system (Malim & Emerman, 2008; Pandey et al., 2009).

The HIV-1 virion is spherical and is approximately 110-150nm in diameter (Gentile et al., 1994). The organization of the viral proteins is shown in Figure 1.4. The outermost surface of the virion is a lipid bilayer that anchors and displays the glycoproteins making them available to recognize CD4+ host cells. The MA protein lines the inside of the lipid layer and is believed to aid in anchoring the transmembrane Env proteins (Buchschacher et al., 1995; Cosson, 1996; Freed & Martin, 1996; Murakami & Freed, 2000). The conical viral core is composed of a layer of CA protein (the "capsid"), which surrounds two copies of the RNA genome complexed with the viral NC protein (Freed, 2001). The capsid core also encloses a number of other viral proteins such as the essential IN and RT enzymes as well as Vif, Nef and Vpr (Freed, 2001; Gomez & Hope, 2005). The following sections provide detailed descriptions of the HIV-1 assembly and budding processes.

HIV-1 Assembly and Budding

As described previously, Gag is the structural polyprotein that coordinates viral assembly and budding (Freed, 1998; Freed, 2001; Gomez & Hope, 2005). The four regions of the full length Gag polyprotein (MA, CA, NC, and p6) provide the functions necessary to carry out these important steps of the life cycle (Freed, 2001; Gomez & Hope, 2005). The MA region directs the Gag and Gag-Pol polyproteins to the plama

membrane sites of viral assembly (Freed, 2001). The CA region aids in Gag assembly through a carboxy-terminal dimerization site (Accola et al., 2000; Liang et al., 2003; Worthylake et al., 1999). The NC region packages the viral RNA genome virion by binding a packaging signal (ψ) located just 5' of the Gag gene (Tang et al., 1999). NC is also thought to assist in Gag interactions during assembly via an RNA tether (Gomez & Hope, 2005). The Gag protein is the only viral protein required for assembly (Gottlinger, 2001) yet cannot sever the membrane, suggesting that cellular factors are recruited to facilitate this process. The p6 domain of Gag recruits such cellular budding proteins through short sequence motifs known as late domains (Freed, 2002).

Late Domains

Cellular factors required for budding are recruited to the HIV-1 assembly site via a tetrapeptide motif, Pro-(Thr/Ser)-Ala-Pro (P(S/T)AP), or late domain located within p6 (Figure 1.5). Deletion of p6 or point mutations in the P(T/S)AP motif arrests virus budding at a late stage (Figure 1.2), in which the virus has fully assembled but remains connected to the cell via a membranous stalk (Gottlinger et al., 1991; Huang et al., 1995). Consequently, this motif is referred to as a "late domain" (Parent et al., 1995; Wills & Craven, 1991). P(T/S)AP late domains are also required for efficient release of other enveloped viruses, including Ebola virus (Martin-Serrano et al., 2001) and the matrix protein of human T cell leukemia virus type 1 (HTLV-1) (Bouamr et al., 2003). Since the initial discovery of the P(T/S)AP late domain in HIV-1, three other types of late domains have been discovered in the structural proteins of other enveloped RNA viruses. The YPDL late domain was discovered in the p9 domain of equine infectious anemia virus (EIAV) and is required for budding of this virus (Puffer et al., 1997). HIV-1 p6

Figure 1.5. Late domain motifs in structural proteins of enveloped RNA viruses. Abbreviations: EIAV, equine infectious anemia virus; HIV-1, human immunodeficiency virus type 1; HTLV-1, human T cell leukemia virus type 1; MMuLV, Moloney murine leukemia virus; MPMV, Mason-Pfizer monkey virus; RSV, Rous sarcoma virus; VSV, vesicular stomatitis virus; LCMV, lymphocytic choriomeningitis virus; SV5, Simian virus 5 (Adapted from Morita and Sundquist, 2004).

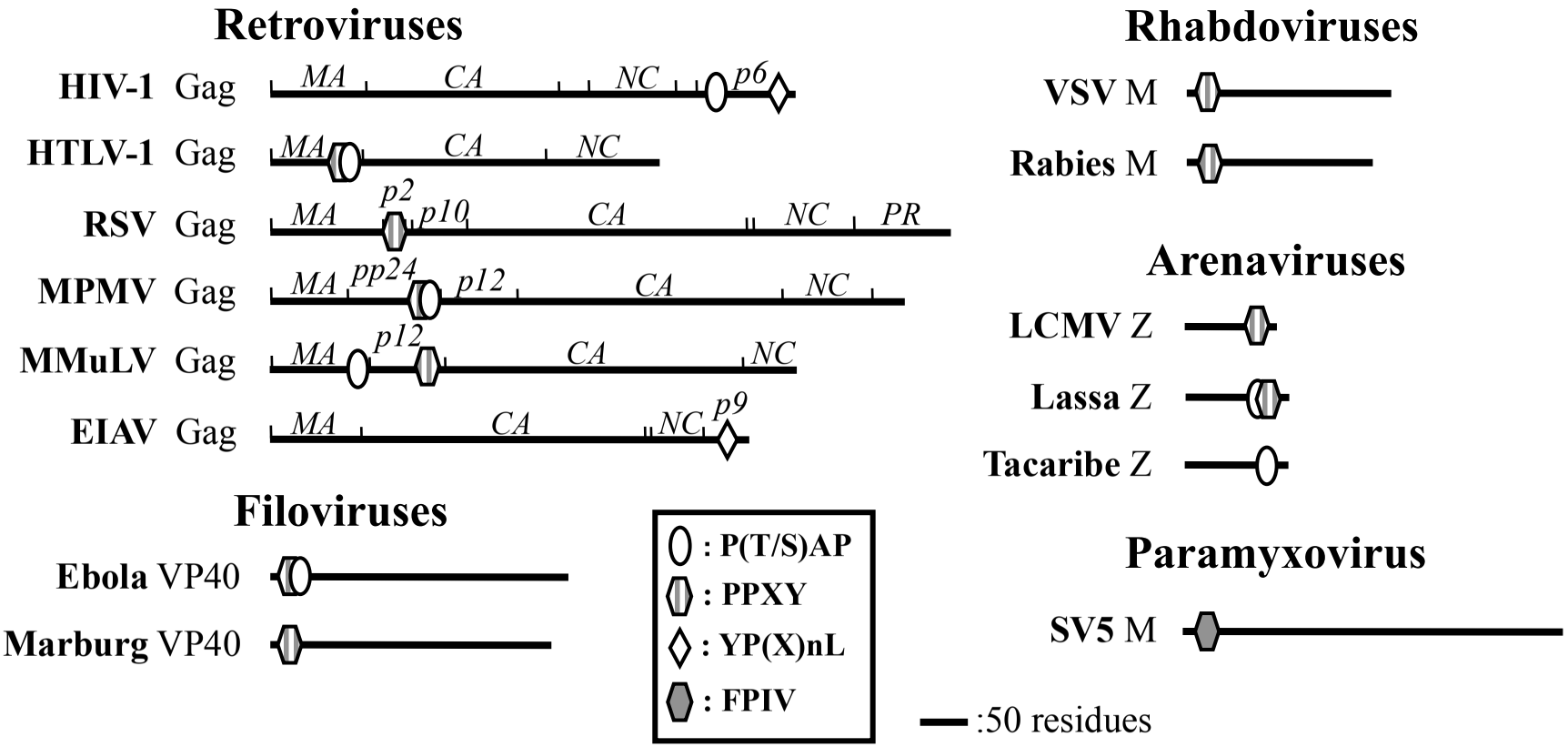
Retroviruses
HIV-1 Gag
MA
CA
NC
p6
HTLV-1 Gag
MA
CA
NC
RSV Gag
MA
p2
p10
CA
NC
PR
MPMV Gag
MA
pp24
p12
CA
NC
MMuLV Gag
MA
p12
CA
NC
EIAV Gag
MA
CA
NC
p9
Filoviruses
Ebola VP40
Marburg VP40
: P(T/S)AP
: PPXY
: YP(X)nL
: FPIV
Rhabdoviruses
VSV M
Rabies M
Arenaviruses
LCMV Z
Lassa Z
Tacaribe Z
Paramyxovirus
SV5 M
:50 residues

contains a functional YPXL late domain, although in most cell types its activity is less important than the p6 P(T/S)AP late domain (Chen et al., 2005; Morita & Sundquist, 2004; Puffer et al., 1997; Strack et al., 2003). The PPXY late domain (where X is typically Pro) was originally identified in the Gag protein of the Rous sarcoma virus (RSV) (Parent et al., 1995; Wills et al., 1994). Since its discovery, PPXY late domains have been identified in many other viruses, including rhabdo-, filo-, arena- and retroviruses (Bouamr et al., 2003; Craven et al., 1999; Harty et al., 2000; Perez et al., 2003; Strecker et al., 2003; Yasuda & Hunter, 1998; Yuan et al., 1999). Subsequently, FPIV late domains have been discovered in paramyxoviruses (Schmitt et al., 2005). This motif has not been fully characterized, but can functionally exchange with P(T/S)AP and YPDL late domains (Schmitt et al., 2005). Figure 1.5 depicts the different late domain motifs and the structural viral proteins in which they are located. The identification of late domain motifs in many enveloped viruses together with the fact that these motifs can often function interchangeably, suggests that most (but not all) enveloped viruses bud from their host cells using similar pathways (Morita & Sundquist, 2004).

Late Domain Binding Partners

Binding partners have now been identified for all of the known late domains except the FPIV late domain. The late domain activity of the PTAP motif in HIV-1 and Ebola virus were initially shown too bind and recruit the cellular protein TSG101 (tumor susceptibility gene 101) (Demirov et al., 2002; Garrus et al., 2001; Gottlinger et al., 1991; Huang et al., 1995; Martin-Serrano et al., 2001; VerPlank et al., 2001). TSG101 is orthologous to the yeast protein Vps23p, which normally functions in the sorting of proteins in the ESCRT (endosomal sorting complexes required for transport) pathway

(Babst et al., 2000; Bishop & Woodman, 2001; Katzmann et al., 2001). This pathway controls vacuolar (lysosomal in mammals) degradation of membrane proteins. The ESCRT pathway functions to sort cargoes, destined for lysosomal degradation into vesicles that bud into the lumen of the late endosome or multivesicular body (MVB). The topology of vesicles budding into the MVB is similar to that of virus formation. In both cases the vesicle or virus particle buds away from the cytoplasm into the lumen of the endosome or into the extracellular space, respectively (Figure 1.6). This appears to be the reason that the cellular ESCRT pathway is usurped by HIV-1 and other viruses to facilitate viral egress.

The YPDL late domain motif of EIAV and other retroviruses facilitates budding by binding to the cellular factor, ALIX (also known as AIP-1) (Martin-Serrano et al., 2003a; Strack et al., 2003; Vincent et al., 2003; von Schwedler et al., 2003), which also functions in the ESCRT pathway. The PPXY motif has been shown to bind WW domains found in members of the NEDD4 family of ubiquitin E3 ligases (Macias et al., 2002), and will be discussed in more detail later. NEDD4 proteins also appear to function in the ESCRT pathway, although their precise function is less well understood than TSG101 and ALIX.

The ESCRT Pathway and MVB Formation

Genetic screens performed in yeast have identified 18 ESCRT proteins that function in MVB vesicle formation (Babst, 2005; Katzmann et al., 2002). These proteins were originally identified as *vps* (vacuolar protein sorting) mutants that induced aberrant endosomes (also known as "Class E" compartments) (Raymond et al., 1992). These

Figure 1.6. HIV-1 virus budding and vacuolar protein sorting. Schematic illustrations of HIV assembly and budding, vacuolar protein sorting (VPS) and exosome formation. HIV Gag proteins are shown in dark blue, and protein cargos that are sorted through the VPS pathway are shown in magenta, green and light blue. For clarity, not all of the possible protein trafficking pathways are shown (Pornillos et al., 2002b).

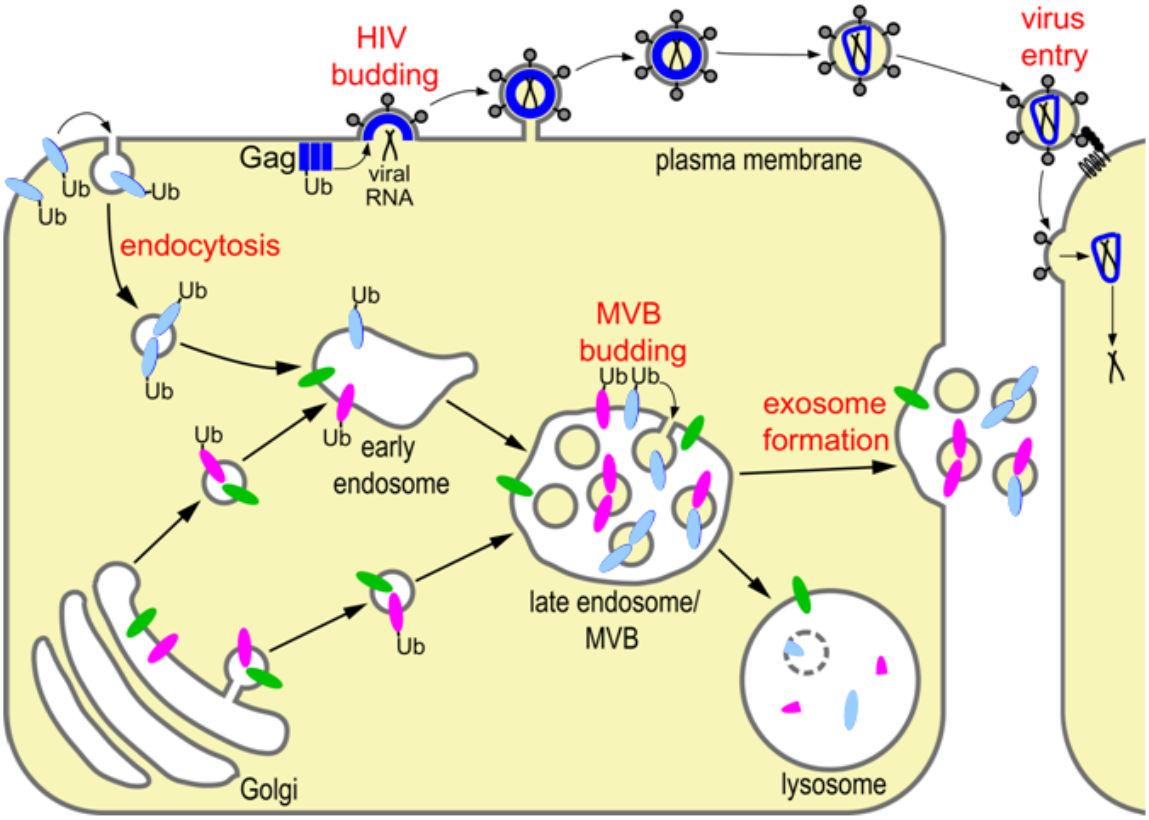
HIV
budding
virus
entry
Gag
viral
RNA
plasma membrane
Ub
endocytosis
MVB
budding
exosome
formation
early
endosome
late endosome/
MVB
Golgi
lysosome

enlarged compartments are essentially endosomes that fail to mature into multivesicular bodies, which forces the limiting membrane of the organelle to accumulate.

The ESCRT proteins form five distinct oligomeric complexes that are sequentially recruited to endosomal sites of vesicle formation (Babst et al., 2002a; Babst et al., 2002b; Bache et al., 2003; Bilodeau et al., 2003; Katzmann et al., 2001; Katzmann et al., 2003). The yeast and human ESCRT pathways are similar in outline and there is at least one human ortholog for each of the yeast Class E VPS proteins (Table 1.1) (Bache et al., 2004; Eastman et al., 2005; Martin-Serrano et al., 2003a; Stuchell et al., 2004; von Schwedler et al., 2003; Ward et al., 2005). The mammalian ESCRT pathway is considerably more complex than the yeast system and yeast MVB formation will therefore be described first, followed by a description of the mammalian ESCRT system and its involvement in HIV-1 budding.

The Yeast ESCRT Pathway

MVB formation is the key step in the committed lysosomal degradation pathway (Figure 1.6). This pathway is responsible for the degradation of essentially all membrane proteins, for example it mediates ligand-induced down regulation of receptors from the cell surface. Such receptors are typically marked for degradation by ubiquitylation, endocytosed, and delivered to endosomal compartments (Babst, 2005). Once there, ubiquitylated receptors on the limiting membrane are bound by the first oligomeric complex in the ESCRT pathway, the Vps27p-Hse complex (ESCRT-0 or HRS-STAM complex in mammals) (Bilodeau et al., 2002). This complex recognizes ubiquitylated cargoes and concentrates them into specific domains on the endosomal membrane (Babst, 2005).

Table 1.1 Human and yeast Class E VPS proteins

Complex	Human Protein[b]	Protein Length	Other Names	Yeast Ortholog	Percent Homology	Number of Residues Compared	NCBI Locus Link Gene ID# (Human Protein)
STAM/HRS	HRS	777	HGS	Vps27p	25	366	9146
	STAM1	540		Hse1p	22	472	8027
	STAM2	525	HBP/EAST	Hse1p	26	263	10254
ESCRT-I	TSG101	390		Vps23p	23	287	7251
	VPS28	221		Vps28p	30	225	51160
	VPS37A	397	HCRP1/FLJ32642	Vps37p	22	213	137492
	VPS37B	285	FLJ12750	Vps37p	14	213	79720
	VPS37C	523	FLJ20847	Vps37p	15	213	55048
	VPS37D	397	WBSCR24	Vps37p	16	213	137492
	MVB12	319	FAM125B	Mvb12p	20	101	89853
ESCRT-II	EAP20	176	hVPS25/MGC10540	Vps25p	29	185	84313
	EAP30	258		Vps22p	36	233	11267
	EAP45	386	CGI-145	Vps36p	21	157	51028
ESCRT-III	CHMP1A	196	PCOLN3/CHMP1	Did2p	47	197	5119
	CHMP1B	199	CHMP1.5	Did2p	41	196	57132
	CHMP2A	222	BC-2	Vps2p/Did4p	35	181	27243
	CHMP2B	213	CHMP2.5/CGI-84	Vps2p/Did4p	26	139	25978
	CHMP3	222	CGI-149/NEDF	Vps24p	32	142	51652
	CHMP4A[a]	224	CAC14088/C20orf178	Vps32p/Snf7p	37	152	128866

Table 1.1 continued

Complex	Human Protein[b]	Protein Length	Other Names	Yeast Ortholog	Percent Homology	Number of Residues Compared	NCBI Locus Link Gene ID# (Human Protein)
ESCRT-III	CHMP4B[a]	265	CDA04/HSPC134	Vps32p/Snf7p	38	134	29082
	CHMP4C	233	MGC22825	Vps32p/Snf7p	34	143	92421
	CHMP5	219	HSPC177/CGI-34	Vps60p/Mos10p	29	155	51510
	CHMP6	201	FLJ11749	Vps20p	30	146	79643
	CHMP7	453	MGC29816	Vps32p/Snf7p	23	133	91782
	IST1	364	PM28	Ist1p	26	298	9798
VPS4	VPS4A	437	VPS4	Vps4p	60	446	27183
	VPS4B	444	SKD1	Vps4p	60	449	9525
	LIP5	307	C6orf55/DRG1/My012	Vta1p	24	737	51534
Others	ALIX	868	HP95/AIP1	Vps31p/Bro1p	23	102	10015
	SLC9A6[c]	669	NHE6/KIAA0267	Vps44p/Nhx1p	36	491	10479

[a] Note that the names for CHMP4A and CHMP4B are reversed in some publications (e.g., see Katoh et al., 2003).

[b] The human ESCRT proteins were identified in BLASTp searches (www.ncbi.nlm.nih.gov/blast) using the yeast Class E proteins as a starting point. The minimal acceptable blast score was 50 (next best score 43.5), BLAST scores ranged from 52-1325.

[c] Yeast NHX1/Vps44p is a sodium/proton exchanger that functions to help acidify the endosomal compartment (Bowers et al., 2000).

Abbreviations used in the first three columns: HRS, hepatocyte growth factor (HGF)-regulated tyrosine kinase substrate; STAM, signal-transducing adaptor molecule; ESCRT, endosome associated complexes required for transport; VPS, vacuolar protein sorting; TSG101, Tumor susceptibility gene 101; EAP, RNA polymerase II elongation factor ELL-associated protein; CHMP, charged multivesicular body protein; ALIX, ALG-2-interacting protein X; LIP5, lysosomal trafficking regulator (LYST) interacting protein 5; IST1, increased sodium tolerance 1; MVB12, multivesicular body protein 12

(Figure updated from Morita and Sundquist, 2004 and von Schwedler et al., 2003).

The Vps27-Hse complex then recruits the endosomal sorting complex required for transport I (ESCRT-I) (Katzmann et al., 2003). The ~350 kDa ESCRT-I complex is comprised of four proteins, Vps23p, Vps28p, Vps37p, and Mvb12p. Like the Vps27-Hse complex, ESCRT-I can also bind directly to ubiquitylated cargoes (Katzmann et al., 2001). ESCRT-I, in turn, recruits a heterotetrameric complex (~155kDa) called ESCRT-II, which contains single copies of Vps36p and Vps22p, and two copies of Vps25p. ESCRT-II has ubiquitin binding activity and again binds directly to ubiquitylated protein cargoes (Babst, 2005; Babst et al., 2002b; Bowers et al., 2004). ESCRT-II recruits ESCRT-III, which forms large endosome-associated lattices, that contain multiple copies of the highly charged ESCRT-III proteins: Vps2p, Vps24p, Vps20p, and Snf7p (Babst et al., 2002a). These lattices are thought to mediate membrane fission albeit through an unknown mechanism.

Unlike ESCRT-I and ESCRT-II components, ESCRT-III subunits are monomeric in the cytoplasm and only oligomerize when recruited to the membrane (Babst et al., 2002a). One ESCRT-III subcomplex, comprised of Vps20p-Snf7p, is required for ESCRT-III association with the membrane via a myristyl group found at the N-terminus of Vps20p (Babst et al., 2002a). The second ESCRT-III subcomplex, composed of Vps2p and Vps24p recruits the final ESCRT complex, Vps4p (Babst et al., 2002a; Babst et al., 1998). Vps4p, is a AAA-type ATPase that utilizes ATP hydrolysis to release ESCRT machinery from the membrane, which allows for multiple rounds of vesicle formation (Babst et al., 2002a; Babst et al., 2002b; Katzmann et al., 2001).

In addition to the ESCRT complexes described above, there are several additional ESCRT proteins that aid in the formation of vesicles at the yeast MVB. Bro1p (the yeast

ALIX homolog) associates with endosomal membranes through a recruitment that is specifically dependent on an interaction with the ESCRT-III protein, Snf7p (Odorizzi et al., 2003). Did2p and Vps60p are ESCRT-III like proteins that display a weak Class E phenotype when deleted (Babst et al., 2002a; Raymond et al., 1992; Shiflett et al., 2004). These proteins facilitate recruitment of the Vps4p complex (Azmi et al., 2006; Bajorek et al., 2009; Kieffer et al., 2008; Lottridge et al., 2006; McCullough et al., 2008; Nickerson et al., 2006). Vta1p is another Vps4p cofactor that interacts directly with both Vps4p and Vps60p (Azmi et al., 2006; Shiflett et al., 2004). Doa4p, is a deubiquitinating enzyme that removes ubiquitin from cargoes as they are sorted into MVB vesicles (Dupre & Haguenauer-Tsapis, 2001; Reggiori & Pelham, 2001). Localization of Doa4p to endosomal membranes is dependent on an interaction with the ESCRT-III protein, Vps24p (Amerik et al., 2000), and Bro1p (Luhtala & Odorizzi, 2004). Because the yeast ESCRT proteins were identified from a genetic screen that examined only essential genes, the identification of additional essential ESCRT proteins seems likely (Raymond et al., 1992). Indeed, the ubiquitin ligase Rsp5p (the yeast homolog of the mammalian NEDD4 proteins) is an essential yeast protein that is required for ESCRT-mediated sorting (Nikko & Andre, 2007). Collectively, these aforementioned factors comprise the essential yeast ESCRT machinery.

The Human ESCRT Proteins

Human ESCRT proteins are believed to function is a manner similar to that described for the yeast system. To date 30 human ESCRT proteins have been identified (Agromayor et al., 2009; Bache et al., 2004; Bajorek et al., 2009; Eastman et al., 2005; Martin-Serrano et al., 2003a; Morita et al., 2007; Stuchell et al., 2004; von Schwedler et

al., 2003; Ward et al., 2005). Once the human ESCRT proteins were tentatively identified, it was important to test whether they exhibited similar interactions to those of their yeast counterparts. The work described in Chapter 2 of this dissertation, together with similar work performed in the Bieniasz lab, characterized the protein-protein interactions that take place in this network of proteins (Figure 1.7) (Martin-Serrano et al., 2003a; von Schwedler et al., 2003). These studies were the first to show that the human ESCRT proteins also form five oligomeric complexes that are analogous to those of the yeast ESCRT pathway system: HRS-STAM, ESCRT(I-III), and VPS4 (Martin-Serrano et al., 2003a; von Schwedler et al., 2003).

Like its yeast counterpart, the mammalian HRS-STAM complex recognizes ubiquitylated membrane proteins on endosomal membranes and targets then for incorporation into MVB vesicles (Asao et al., 1997; Bean et al., 2000; Raiborg et al., 2002; Raiborg et al., 2001b; Shih et al., 2002). This HRS recognition step appears to be bypassed when HIV usurps the ESCRT pathway to facilitate virus budding (Pornillos et al., 2003), as will be discussed later in this chapter. This HRS-STAM complex then recruits the ESCRT-I complex through an interaction between HRS and TSG101 that involves a PSAP sequence motif on HRS (the equivalent of the P(T/S)AP late domain in HIV-1 Gag).

Mammalian tumor susceptibility gene 101 (TSG101), the human ortholog of yeast Vps23p (Babst et al., 2000), functions as a member of the cytoplasmic human ESCRT-I complex along with the human VPS28 protein (the ortholog of yeast Vps28p) (Babst et al., 2000; Bishop & Woodman, 2001; Katzmann et al., 2001). When I began my work, it was known that the yeast ESCRT-I complex consisted of at least three proteins, but

Figure 1.7. Human ESCRT Protein Network.
Schematic showing 28 human proteins, their subcomplexes, and their known protein-protein interactions. Interactions between proteins are denoted by arrows and are color coded based on the studies that identified the interaction (Bache et al., 2004: blue green, Eastman et al., 2004: green, Garrus et al., 2001: black, Martin-Serrano et al., 2003: gray, Howard et al., 2001: pink, Scott et al., 2005b: dark purple, Strack et al., 2003: dark blue, Stuchell et al., 2004: slate, von Schwedler et al., 2003: orange, Horii et al., 2006: brown) (Figure modified from von Schwedler et al., 2003).

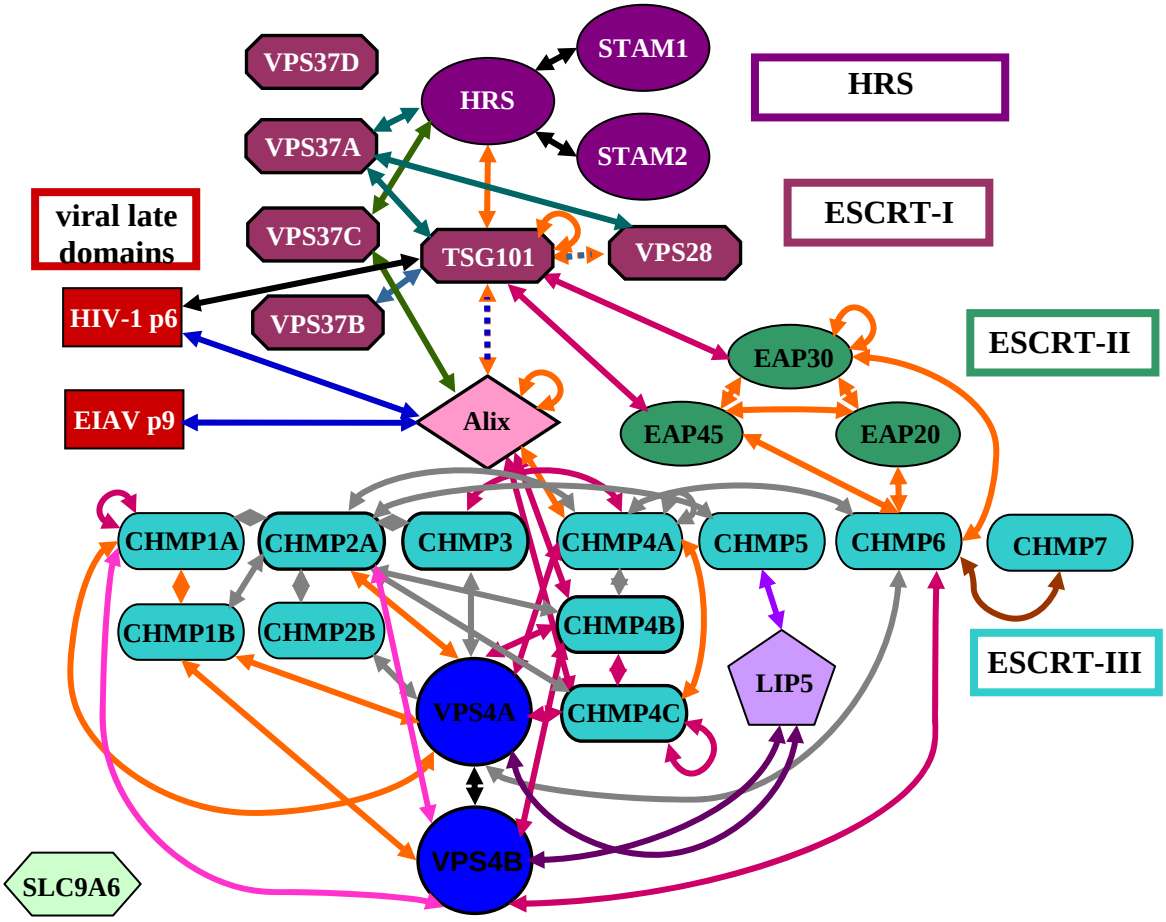
VPS37D
STAM1
HRS
HRS
VPS37A
STAM2
viral late domains
ESCRT-I
VPS37C
TSG101
VPS28
HIV-1 p6
VPS37B
ESCRT-II
EAP30
EIAV p9
Alix
EAP45
EAP20
CHMP1A
CHMP2A
CHMP3
CHMP4A
CHMP5
CHMP6
CHMP7
CHMP1B
CHMP2B
CHMP4B
ESCRT-III
LIP5
VPS4A
CHMP4C
VPS4B
SLC9A6

human VPS37 orthologs were not known owing to their significant divergence in the primary sequence. Several labs, including ours, therefore used both biochemical and bioinformatic approaches to identify four human VPS37 proteins (Bache et al., 2004; Eastman et al., 2005; Stuchell et al., 2004). The identification and characterization of the human VPS37 proteins is described in Chapter 3. The human ESCRT-I complex is also involved in the recognition of ubiquitylated cargoes, specifically through direct TSG101-Ub interactions, and this topic will be discussed in detail later.

By analogy to yeast, the human ESCRT-II and ESCRT-III complexes are presumed to be sequentially recruited to sites of MVB vesicle formation. The human ESCRT-II complex is composed of three proteins, EAP20, EAP30 and EAP45, which are orthologous to yeast Vps25p, Vps22p, and Vps36p, respectively (Kamura et al., 2001; Martin-Serrano et al., 2003a; von Schwedler et al., 2003). This complex was originally discovered as a putative RNA polymerase II elongation factor, and the subunits were therefore named ELL-associating proteins or EAPs (Kamura et al., 2001). The TSG101 subunit of ESCRT-I interacts with both EAP30 and EAP45 to recruit the ESCRT-II complex to the endosomal membrane (Langelier et al., 2006; Slagsvold et al., 2005). EAP45 has ubiquitin binding ability, and the importance of ubiquitin recognition by EAP45 will be discussed later. ESCRT-II can in turn recruit the ESCRT-III complex through an interaction between EAP20 and the charge multivesicular body protein 6 (CHMP6) (Langelier et al., 2006).

Human ESCRT-III proteins are composed of a family of highly charged proteins, most of which are called CHMP proteins (for charged multivesicular body proteins) (Table 1.1 and Figure 1.7). There are more human than yeast ESCRT-III

proteins. To date, 12 human ESCRT-III proteins have been identified. They generally share a similar domain structure, and most are ~200 amino acids in length. The human CHMP proteins can be organized into eight subclasses (CHMP1-7, and IST1) according to their homology to one another (Agromayor et al., 2009; Bajorek et al., 2009; Horii et al., 2006; von Schwedler et al., 2003). The CHMP1-6 and IST1 families correspond to the seven yeast ESCRT-III-like proteins (Agromayor et al., 2009; Bajorek et al., 2009; von Schwedler et al., 2003). An additional CHMP-like protein, CHMP7, is most similar to the CHMP6 subclass but is a much larger protein consisting of 453 amino acids (Horii et al., 2006). CHMP7 interacts with CHMP4B and also functions in the mammalian endosomal pathway (Horii et al., 2006). The human ESCRT-III complex appears to form lattices that are presumably similar to yeast ESCRT-III lattices. The structure of the CHMP3 protein core was recently determined and shown to be a four helix bundle that forms a flat overall structure (Muziol et al., 2006). Similarities in sequence, charge and domain structure suggest that all CHMP proteins will adopt similar structures (Muziol et al., 2006).

The CHMP4 subset of human ESCRT-III proteins (CHMP4A, CHMP4B, and CHMP4C) interact directly with ALIX (ALG-2-interacting protein X) (Martin-Serrano et al., 2003a; von Schwedler et al., 2003). ALIX also binds ESCRT-I, but is not a constitutive member of either ESCRT complex (Katoh et al., 2003; Katoh et al., 2005; Martin-Serrano et al., 2003a; Strack et al., 2003; von Schwedler et al., 2003). ALIX can, in priciple, bridge ESCRT-I and ESCRT-III, thus providing an additional way to recruit ESCRT-III to site of vesicle formation.

ESCRT-III proteins also bind and recruit the VPS4 AAA ATPases, which then remove them from the membrane and thereby allow them to recycle and repeat the sorting process on other substrates (Martin-Serrano et al., 2003a; Scott et al., 2005b; Tsang et al., 2006; von Schwedler et al., 2003). VPS4 proteins are ATPases associated with diverse cellular activities (AAA). Humans have two VPS4 proteins, VPS4A and VPS4B, that share ~80% sequence similarity. VPS4 proteins are composed of three different regions: an N-terminal microtubule interacting and trafficking (MIT) domain, a C-terminal AAA ATPase cassette, and a three-stranded, anti-parallel β-domain that is inserted into the small domain of the ATPase cassette (Scott et al., 2005a; Scott et al., 2005b; Takasu et al., 2005). The VPS4 proteins can form two stacked hexameric rings, which is similar to structures formed by the p97 AAA ATPase (Scott et al., 2005a). The β-domain of VPS4 has been shown to associate with LIP5 (Vta1p in yeast) (Scott et al., 2005a). Vta1p and LIP5 stimulate VPS4 assembly and ATPase activites. LIP5 also binds specifically to the ESCRT-III protein CHMP5 (Scott et al., 2005a).

The interactions of VPS4 AAA ATPases with several different ESCRT-III proteins are described in Chapter 2, Chapter 4, Appendix A and Appendix B (Fujita et al., 2004; Lin et al., 2005; Martin-Serrano et al., 2003a; Scott et al., 2005a; von Schwedler et al., 2003). Specifically, I characterized how the N-terminal MIT domain of VPS4 binds a short peptide sequence tag located at the C-terminus of many CHMP proteins; CHMP1A-1B, CHMP2A-2B, and CHMP3 (Chapter 4 of this dissertation). These C-terminal tags also bind other MIT-domain containing proteins, including AMSH and UBPY (Agromayor & Martin-Serrano, 2006).

AMSH (associated molecule with the SH3 domain of STAM) and UBPY are deubiquitylating enzymes that are associated with the ESCRT pathway.(McCullough et al., 2004; Mizuno et al., 2006; Row et al., 2007; Row et al., 2006; Urbe et al., 2006). Both can also interact with the STAM (signal transducing adaptor molecule) subunit of the HRS complex (Kim et al., 2006; McCullough et al., 2004; McCullough et al., 2006; Urbe et al., 2006). AMSH and UBPY can deubiquitylate MVB vesicle cargoes, although the exact sequence of deubiquitylation remains somewhat controversial (Agromayor & Martin-Serrano, 2006; McCullough et al., 2006; Mizuno et al., 2006; Row et al., 2006).

ESCRT - Lipid Interactions

Several ESCRT proteins bind lipids, and these interactions help recruit them to endosomal sites of membrane fission. Endosomes are enriched in phosphotidyl inositol 3-phophate (PI(3)P). HRS contains a FYVE domain, which specifically binds to PI(3)P (Katzmann et al., 2003; Komada & Soriano, 1999; Raiborg et al., 2001a). Similarly, EAP45, a component of the ESCRT-II complex, also binds PI(3)P and other phosphatidyl (3) phosphates (Gill et al., 2007; Slagsvold et al., 2005). Late endosomes are also enriched in PI(3,5)P2 and one member of the ESCRT-III complex, CHMP3, has been reported bind PI(3,5)P_2 (Gillooly et al., 2000; Gillooly et al., 2003; Whitley et al., 2003). Another ESCRT-III protein, CHMP6, binds membranes via an N-terminal myristoyl group, albeit without any known lipid specificity (Yorikawa et al., 2005). Both Bro1p and ALIX are thought to interact with membranes through their boomerang-shaped Bro1 domain (Kim et al., 2005) and ALIX has been reported to bind lysobisphosphatidic acid (LBPA), which is a cone shaped lipid that plays a role MVB vesicle formation (Matsuo et

al., 2004). The apparent importance of lipids, in MVB vesicle formation is emphasized by the fact that three out of the five oligomeric ESCRT complexes bind endosomal lipids.

Ubiquitin in the ESCRT Pathway

The ubiquitin post translational modification plays an important role in targeting cargoes for lysosomal degradation, and several ESCRT proteins have ubiquitin binding activities (Hicke & Dunn, 2003; Katzmann et al., 2001). HRS contains two UIM motifs (ubiquitin interacting motifs) that are required for sorting ubiquitylated cargoes (Bilodeau et al., 2002; Polo et al., 2002; Raiborg et al., 2002; Shih et al., 2002; Swanson et al., 2003). TSG101 contains a UEV (ubiquitin E2 variant) domain, that is structurally similar to ubiquitin E2 ligases but lacks the active site cysteine residue that is required for ubiquitin transfer. TSG101 can therefore bind, but not transfer ubiquitin (Pornillos et al., 2002a; Sundquist et al., 2004; Teo et al., 2004). The human ESCRT-II subunit, EAP45, contains a GLUE (Gram-like Ub binding to EAP45) domain, which allows this complex to recognize ubiquitin (Alam et al., 2006; Hirano et al., 2006; Langelier et al., 2006; Slagsvold et al., 2005). In yeast, this activity is provided instead by the ubiquitin binding zinc finger motif. Thus, the HRS, ESCRT-I, and ESCRT-II complexes all have ubiquitin binding activities that are required for cargo sorting. Apparently, these different complexes cooperate to concentrate ubiquitylated proteins on endosomal membranes. As those cargoes are sorted and sequestered inside vesicles, the covalently attached ubiquitins are removed and recycled by the UBPY and/or AMSH deubiquitylating enzymes (Agromayor & Martin-Serrano, 2006; McCullough et al., 2004; McCullough et al., 2006; Mizuno et al., 2006; Row et al., 2006; Tsang et al., 2006).

Ubiquitin in HIV-1 Budding

Ubiquitylation also plays a role in the budding of viruses that contain the late domain motifs, P(T/S)AP and PPXY (Patnaik et al., 2000; Vogt, 2000). Interestingly, the $YP(X)_nL$ late domain appears to function independently of a ubiquitin requirement (Patnaik et al., 2002). As noted earlier, the P(T/S)AP motif recruits TSG101/ESCRT-I, while the PPXY motif interacts with NEDD4 family of ubiquitin ligases, and both of these host factors are involved in ubiquitin transfer or recognition. Thus, it seems possible that Gag proteins may, in part, have evolved to mimic the ubiquitylated cargoes that are sorted into budding viruses. Other observations that tie ubiquitin to virus budding include: (1) ubiquitin is enriched inside the virions of many retroviruses (Ott et al., 1998; Putterman et al., 1990), (2) Gag proteins of HIV-1 and MuLV are monoubiquitylated at multiple sites (Ott et al., 2000), (3) the concentration of ubiquitin found on Gag proteins can be altered depending on the presence or absence of late domains (Martin-Serrano et al., 2004; Strack et al., 2000), and (4) depleting cellular ubiquitin levels can arrest virus budding at a late stage (Patnaik et al., 2000; Schubert et al., 2000; Strack et al., 2000).

ESCRT Proteins and HIV-1 Budding

As noted above, retroviruses interact with several human ESCRTs, which apparently serve as entry points into the ESCRT pathway. As illustrated in Figure 1.8, late domains within viral structural proteins can interact with TSG101, ALIX, and/or the NEDD4 proteins to “hijack” them to sites of virus assembly. In principle, gaining an understanding of how the proteins in this pathway are involved in retroviral budding could lead to the discovery of potential new drug targets.

Figure 1.8. The human ESCRT pathway and the entry sites of different enveloped viruses.

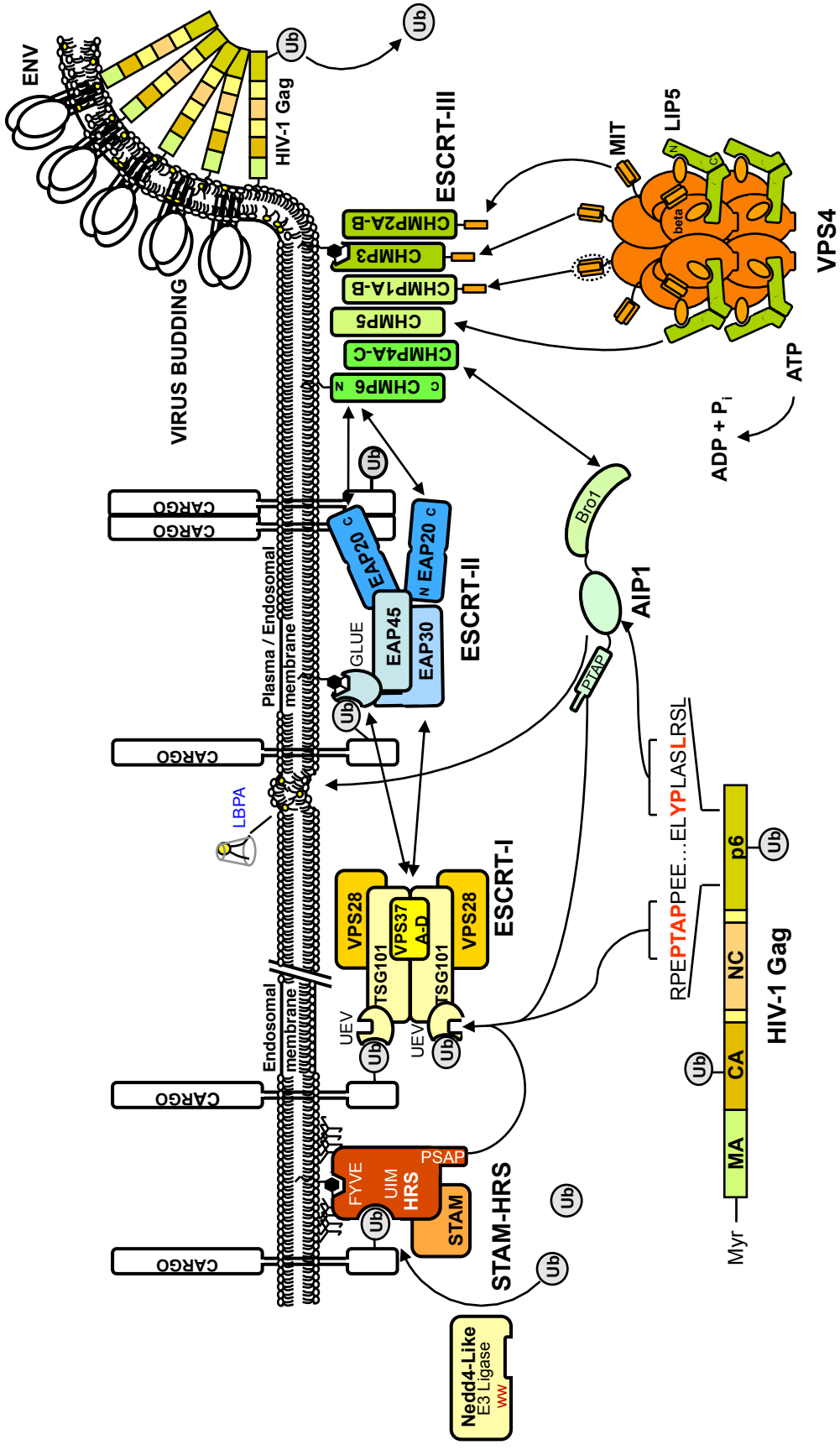
ENV
HIV-1 Gag
Ub
VIRUS BUDDING
ESCRT-III
CHMP2A-B
CHMP3
CHMP1A-B
CHMP5
CHMP4A-C
CHMP6
MIT
LIP5
VPS4
ATP
ADP + Pi
CARGO
Plasma / Endosomal membrane
EAP20
EAP45
EAP30
GLUE
ESCRT-II
Bro1
AIP1
PTAP
LBPA
Endosomal membrane
VPS28
TSG101
VPS37 A-D
UEV
ESCRT-I
FYVE
UIM
HRS
PSAP
STAM
STAM-HRS
Nedd4-Like
E3 Ligase
WW
RPEPTAPPEE...ELYPLASLRSL
Myr
MA
CA
NC
p6
HIV-1 Gag

To date, a number of downstream ESCRT proteins have been shown to be required for viral egress. Specifically, subunits of the ESCRT-I complex, have been shown to be important for budding of HIV-1 (Demirov et al., 2002; Garrus et al., 2001; Goff et al., 2003; Goila-Gaur et al., 2003; Martin-Serrano et al., 2001; Martin-Serrano et al., 2003b; VerPlank et al., 2001), Ebola (Licata et al., 2003; Martin-Serrano et al., 2001; Shehu-Xhilaga et al., 2004; Timmins et al., 2003), HTLV-1 (Bouamr et al., 2003), MPMV (Gottwein et al., 2003), and possibly RSV (Johnson et al., 2005; Medina et al., 2005). Thus, TSG101/ESCRT-I appears to be important for all viruses that bud using P(T/S)AP late domains. Similarly, the VPS28 binding site on TSG101 is required for HIV budding, suggesting that VPS28 also plays a role in PTAP-dependent budding (Martin-Serrano et al., 2003b; Stuchell et al., 2004). Similarly, VPS37B, VPS37C, and MVB12 have also been shown to inhibit late domain dependent virus release (Eastman et al., 2005; Morita et al., 2007). Thus, the entire ESCRT-I complex is required for efficient HIV-1 budding.

Several ESCRT-II and ESCRT-III components have also been tested for their requirement in viral egress. Surprisingly, ESCRT-II does not appear to be required because the essential EAP20 subunit can be depleted without affecting virus release (Langelier et al., 2006). Several ESCRT-III proteins, including CHMP2A, CHMP3, CHMP4B and CHMP4C, can potently inhibit the HIV-1 budding pathway when they are over expressed as dominant negative constructs, indicating that they are involved in (or can dominantly inhibit) HIV budding (von Schwedler et al., 2003). However, siRNA knockdown of CHMP6 does not affect the ability of HIV-1 to release from cells. Therefore, it is not yet clear how the ESCRT-III proteins contribute to the budding

process.

VPS4 is the only known enzyme in the MVB pathway, and it uses the energy of ATP hydrolysis to release the ESCRT machinery for use in multiple rounds of vesicle formation. The VSP4 proteins play an important role in the budding of many enveloped viruses, including HIV-1 (Garrus et al., 2001; Scott et al., 2005b) , MPMV (Gottwein et al., 2003) , Ebola virus (Licata et al., 2003) and MLV (Garrus et al., 2001) budding.

ALIX is another ESCRT protein that binds directly to YPXL late domains. Not surprisingly, ALIX is required for the release EIAV (Strack et al., 2003). In contrast, ALIX is not essential for HIV-1 budding in most cell types, though it can contribute to the efficiency of HIV, Ebola and MLV budding (Martin-Serrano et al., 2004; Strack et al., 2003). Moreover, ALIX is present in HIV-1 particles and HIV budding can be supported by ALIX when the Gag P(T/S)AP late domain is mutated (Strack et al., 2003; von Schwedler et al., 2003). It is therefore likely that HIV-1 has evolved to "hedge its bets" by entering the ESCRT pathway at different sites.

The NEDD4 family of ubiquitin E3 ligases can also facilitate retroviral release and are recruited through an interaction between their WW domains and PPXY late domain motif. The requirement for NEDD4 family members has been tested for a number of different viruses including RSV (Kikonyogo et al., 2001; Martin-Serrano et al., 2004; Strack et al., 2000), HTLV-1 (Blot et al., 2004; Bouamr et al., 2003), Ebola (Timmins et al., 2003; Yasuda et al., 2003) MPMV (Yasuda et al., 2002) and HIV-1 (Chung et al., 2008; Usami et al., 2008). However, there is some disagreement as to which ligase can function for the different viruses, and the mechanistic roles of these ligases in budding is not yet clear.

In summary, it is now clear that the human ESCRT protein network is usurped by many enveloped viruses to escape from cells. However, not all of the relevant factors are known, and the exact mechanism of fission has yet to be elucidated. Research in these areas therefore remains active with the ultimate goal of moving the field closer to understanding the detailed process of viral budding.

Thesis Overview

The goal of my thesis research was to characterize the pathway required for HIV-1 budding—the human ESCRT pathway. Chapter 2 describes the identification and characterization of most of the components of the human ESCRT protein network. My specific contribution to Chapter 2 was to identify candidate human ESCRT proteins based upon bioinformatic homolog searches and to test their protein-protein interactions using directed yeast two hybrid experiments and other biochemical methods. Chapter 3 describes the bioinformatic and biochemical approaches I used to identify the third class of proteins that form subunits of human ESCRT-I (VPS37A-D), and to characterize the requirement of ESCRT-I proteins involved in HIV-1 budding. My contribution to Chapter 3 was to identify VPS37B and characterize its interactions within the human ESCRT-I complex. Chapter 4 describes the identification and characterization of VPS4 binding sites on human ESCRT-III proteins and the determination of three dimensional structures of VPS4 MIT-ESCRT-III complexes. Chapter 5 summarizes my research and discusses important new directions in the ESCRT field.

References

Accola MA, Hoglund S, Gottlinger HG (1998) A putative alpha-helical structure which overlaps the capsid-p2 boundary in the human immunodeficiency virus type 1 Gag precursor is crucial for viral particle assembly. *Journal of virology* **72:** 2072-2078

Accola MA, Strack B, Gottlinger HG (2000) Efficient particle production by minimal Gag constructs which retain the carboxy-terminal domain of human immunodeficiency virus type 1 capsid-p2 and a late assembly domain. *Journal of virology* **74:** 5395-5402

Agromayor M, Carlton JG, Phelan JP, Matthews DR, Carlin LM, Ameer-Beg S, Bowers K, Martin-Serrano J (2009) Essential role of hIST1 in cytokinesis. *Molecular biology of the cell* **20:** 1374-1387

Agromayor M, Martin-Serrano J (2006) Interaction of AMSH with ESCRT-III and deubiquitination of endosomal cargo. *The Journal of biological chemistry* **281:** 23083-23091

Alam SL, Langelier C, Whitby FG, Koirala S, Robinson H, Hill CP, Sundquist WI (2006) Structural basis for ubiquitin recognition by the human ESCRT-II EAP45 GLUE domain. *Nature structural & molecular biology* **13:** 1029-1030

Amerik AY, Nowak J, Swaminathan S, Hochstrasser M (2000) The Doa4 deubiquitinating enzyme is functionally linked to the vacuolar protein-sorting and endocytic pathways. *Molecular biology of the cell* **11:** 3365-3380

Arien KK, Verhasselt B (2008) HIV Nef: role in pathogenesis and viral fitness. *Current HIV research* **6:** 200-208

Asao H, Sasaki Y, Arita T, Tanaka N, Endo K, Kasai H, Takeshita T, Endo Y, Fujita T, Sugamura K (1997) Hrs is associated with STAM, a signal-transducing adaptor molecule. Its suppressive effect on cytokine-induced cell growth. *The Journal of biological chemistry* **272:** 32785-32791

Azmi I, Davies B, Dimaano C, Payne J, Eckert D, Babst M, Katzmann DJ (2006) Recycling of ESCRTs by the AAA-ATPase Vps4 is regulated by a conserved VSL region in Vta1. *The Journal of cell biology* **172:** 705-717

Babst M (2005) A protein's final ESCRT. *Traffic (Copenhagen, Denmark)* **6:** 2-9

Babst M, Katzmann D, Estepa-Sabal E, Meerloo T, Emr S (2002a) Escrt-III. An endosome-associated heterooligomeric protein complex required for mvb sorting. *Developmental cell* **3:** 271-282

Babst M, Katzmann D, Snyder W, Wendland B, Emr S (2002b) Endosome-Associated Complex, ESCRT-II, Recruits Transport Machinery for Protein Sorting at the Multivesicular Body. *Developmental cell* **3:** 283-289

Babst M, Odorizzi G, Estepa EJ, Emr SD (2000) Mammalian tumor susceptibility gene 101 (TSG101) and the yeast homologue, Vps23p, both function in late endosomal trafficking. *Traffic (Copenhagen, Denmark)* **1:** 248-258

Babst M, Wendland B, Estepa EJ, Emr SD (1998) The Vps4p AAA ATPase regulates membrane association of a Vps protein complex required for normal endosome function. *The EMBO journal* **17:** 2982-2993

Bache KG, Brech A, Mehlum A, Stenmark H (2003) Hrs regulates multivesicular body formation via ESCRT recruitment to endosomes. *The Journal of cell biology* **162:** 435-442

Bache KG, Slagsvold T, Cabezas A, Rosendal KR, Raiborg C, Stenmark H (2004) The Growth-Regulatory Protein HCRP1/hVps37A is a Subunit of Mammalian ESCRT-I and Mediates Receptor Downregulation. *Molecular biology of the cell* **15:** 4337-4346

Bajorek M, Morita E, Skalicky JJ, Morham SG, Babst M, Sundquist WI (2009) Biochemical analyses of human IST1 and its function in cytokinesis. *Molecular biology of the cell* **20:** 1360-1373

Barre-Sinoussi F, Chermann JC, Rey F, Nugeyre MT, Chamaret S, Gruest J, Dauguet C, Axler-Blin C, Vezinet-Brun F, Rouzioux C, Rozenbaum W, Montagnier L (1983) Isolation of a T-lymphotropic retrovirus from a patient at risk for acquired immune deficiency syndrome (AIDS). *Science* **220:** 868-871

Bean AJ, Davanger S, Chou MF, Gerhardt B, Tsujimoto S, Chang Y (2000) Hrs-2 regulates receptor-mediated endocytosis via interactions with Eps15. *The Journal of biological chemistry* **275:** 15271-15278

Bilodeau PS, Urbanowski JL, Winistorfer SC, Piper RC (2002) The Vps27p Hse1p complex binds ubiquitin and mediates endosomal protein sorting. *Nat Cell Biol* **4:** 534-539

Bilodeau PS, Winistorfer SC, Kearney WR, Robertson AD, Piper RC (2003) Vps27-Hse1 and ESCRT-I complexes cooperate to increase efficiency of sorting ubiquitinated proteins at the endosome. *The Journal of cell biology* **163:** 237-243

Bishop N, Woodman P (2001) TSG101/mammalian VPS23 and mammalian VPS28 interact directly and are recruited to VPS4-induced endosomes. *The Journal of biological chemistry* **276:** 11735-11742

Blot V, Perugi F, Gay B, Prevost MC, Briant L, Tangy F, Abriel H, Staub O, Dokhelar MC, Pique C (2004) Nedd4.1-mediated ubiquitination and subsequent recruitment of Tsg101 ensure HTLV-1 Gag trafficking towards the multivesicular body pathway prior to virus budding. *Journal of cell science* **117:** 2357-2367

Bouamr F, Melillo JA, Wang MQ, Nagashima K, de Los Santos M, Rein A, Goff SP (2003) PPPYVEPTAP motif is the late domain of human T-cell leukemia virus type 1 Gag and mediates its functional interaction with cellular proteins Nedd4 and Tsg101 [corrected]. *Journal of virology* **77:** 11882-11895

Bowers K, Lottridge J, Helliwell SB, Goldthwaite LM, Luzio JP, Stevens TH (2004) Protein-protein interactions of ESCRT complexes in the yeast Saccharomyces cerevisiae. *Traffic (Copenhagen, Denmark)* **5:** 194-210

Buchschacher GL, Jr., Freed EO, Panganiban AT (1995) Effects of second-site mutations on dominant interference by a human immunodeficiency virus type 1 envelope glycoprotein mutant. *Journal of virology* **69:** 1344-1348

Checroune F, Yao XJ, Gottlinger HG, Bergeron D, Cohen EA (1995) Incorporation of Vpr into human immunodeficiency virus type 1: role of conserved regions within the P6 domain of Pr55gag. *J Acquir Immune Defic Syndr Hum Retrovirol* **10:** 1-7

Chen C, Vincent O, Jin J, Weisz OA, Montelaro RC (2005) Functions of early (AP-2) and late (AIP1/ALIX) endocytic proteins in equine infectious anemia virus budding. *The Journal of biological chemistry* **280:** 40474-40480

Chung HY, Morita E, von Schwedler U, Muller B, Krausslich HG, Sundquist WI (2008) NEDD4L overexpression rescues the release and infectivity of human immunodeficiency virus type 1 constructs lacking PTAP and YPXL late domains. *Journal of virology* **82:** 4884-4897

Coffin JM, Hughes SH, Varmus HE (1997) *Retroviruses*, Plainview, New York: Cold Spring Harbor Press.

Cosson P (1996) Direct interaction between the envelope and matrix proteins of HIV-1. *The EMBO journal* **15:** 5783-5788

Craven RC, Harty RN, Paragas J, Palese P, Wills JW (1999) Late domain function identified in the vesicular stomatitis virus M protein by use of rhabdovirus-retrovirus chimeras. *Journal of virology* **73:** 3359-3365

Demirov DG, Ono A, Orenstein JM, Freed EO (2002) Overexpression of the N-terminal domain of TSG101 inhibits HIV-1 budding by blocking late domain function. *Proceedings of the National Academy of Sciences of the United States of America* **99:** 955-960

Dunfee R, Thomas ER, Gorry PR, Wang J, Ancuta P, Gabuzda D (2006) Mechanisms of HIV-1 neurotropism. *Current HIV research* **4:** 267-278

Dupre S, Haguenauer-Tsapis R (2001) Deubiquitination step in the endocytic pathway of yeast plasma membrane proteins: crucial role of doa4p ubiquitin isopeptidase. *Mol Cell Biol* **21:** 4482-4494

Eastman SW, Martin-Serrano J, Chung W, Zang T, Bieniasz PD (2005) Identification of human VPS37C, a component of endosomal sorting complex required for transport-I important for viral budding. *The Journal of biological chemistry* **280:** 628-636

Frankel AD, Young JA (1998) HIV-1: fifteen proteins and an RNA. *Annu Rev Biochem* **67:** 1-25

Freed EO (1998) HIV-1 gag proteins: diverse functions in the virus life cycle. *Virology* **251:** 1-15

Freed EO (2001) HIV-1 replication. *Somatic cell and molecular genetics* **26:** 13-33

Freed EO (2002) Viral late domains. *Journal of virology* **76:** 4679-4687

Freed EO (2006) HIV-1 Gag: flipped out for PI(4,5)P(2). *Proceedings of the National Academy of Sciences of the United States of America* **103:** 11101-11102

Freed EO, Martin MA (1996) Domains of the human immunodeficiency virus type 1 matrix and gp41 cytoplasmic tail required for envelope incorporation into virions. *Journal of virology* **70:** 341-351

Fujita H, Umezuki Y, Imamura K, Ishikawa D, Uchimura S, Nara A, Yoshimori T, Hayashizaki Y, Kawai J, Ishidoh K, Tanaka Y, Himeno M (2004) Mammalian class E Vps proteins, SBP1 and mVps2/CHMP2A, interact with and regulate the function of an AAA-ATPase SKD1/Vps4B. *Journal of cell science* **117:** 2997-3009

Gallo RC, Salahuddin SZ, Popovic M, Shearer GM, Kaplan M, Haynes BF, Palker TJ, Redfield R, Oleske J, Safai B, et al. (1984) Frequent detection and isolation of cytopathic retroviruses (HTLV-III) from patients with AIDS and at risk for AIDS. *Science* **224:** 500-503

Garrus JE, von Schwedler UK, Pornillos OW, Morham SG, Zavitz KH, Wang HE, Wettstein DA, Stray KM, Cote M, Rich RL, Myszka DG, Sundquist WI (2001) Tsg101 and the vacuolar protein sorting pathway are essential for HIV-1 budding. *Cell* **107:** 55-65

Gentile M, Adrian T, Scheidler A, Ewald M, Dianzani F, Pauli G, Gelderblom HR (1994) Determination of the size of HIV using adenovirus type 2 as an internal length marker. *Journal of virological methods* **48:** 43-52

Geretti AM (2006) HIV-1 subtypes: epidemiology and significance for HIV management. *Current opinion in infectious diseases* **19:** 1-7

Gill DJ, Teo H, Sun J, Perisic O, Veprintsev DB, Vallis Y, Emr SD, Williams RL (2007) Structural studies of phosphoinositide 3-kinase-dependent traffic to multivesicular bodies. *Biochemical Society symposium***:** 47-57

Gillooly DJ, Morrow IC, Lindsay M, Gould R, Bryant NJ, Gaullier JM, Parton RG, Stenmark H (2000) Localization of phosphatidylinositol 3-phosphate in yeast and mammalian cells. *The EMBO journal* **19:** 4577-4588

Gillooly DJ, Raiborg C, Stenmark H (2003) Phosphatidylinositol 3-phosphate is found in microdomains of early endosomes. *Histochemistry and cell biology* **120:** 445-453

Goff A, Ehrlich LS, Cohen SN, Carter CA (2003) Tsg101 control of human immunodeficiency virus type 1 Gag trafficking and release. *Journal of virology* **77:** 9173-9182

Goila-Gaur R, Demirov DG, Orenstein JM, Ono A, Freed EO (2003) Defects in human immunodeficiency virus budding and endosomal sorting induced by TSG101 overexpression. *Journal of virology* **77:** 6507-6519

Gomez C, Hope TJ (2005) The ins and outs of HIV replication. *Cellular microbiology* **7:** 621-626

Gottlinger HG (2001) The HIV-1 assembly machine. *AIDS (London, England)* **15:** S13-20

Gottlinger HG, Dorfman T, Sodroski JG, Haseltine WA (1991) Effect of mutations affecting the p6 gag protein on human immunodeficiency virus particle release. *Proceedings of the National Academy of Sciences of the United States of America* **88:** 3195-3199

Gottlinger HG, Sodroski JG, Haseltine WA (1989) Role of capsid precursor processing and myristoylation in morphogenesis and infectivity of human immunodeficiency virus type 1. *Proceedings of the National Academy of Sciences of the United States of America* **86:** 5781-5785

Gottwein E, Bodem J, Muller B, Schmechel A, Zentgraf H, Krausslich HG (2003) The Mason-Pfizer monkey virus PPPY and PSAP motifs both contribute to virus release. *Journal of virology* **77:** 9474-9485

Harty RN, Brown ME, Wang G, Huibregtse J, Hayes FP (2000) A PPxY motif within the VP40 protein of ebola virus interacts physically and functionally with a ubiquitin ligase: implications for filovirus budding. *Proceedings of the National Academy of Sciences of the United States of America* **97:** 13871-13876

Hicke L, Dunn R (2003) Regulation of membrane protein transport by ubiquitin and ubiquitin-binding proteins. *Annual review of cell and developmental biology* **19:** 141-172

Hill M, Tachedjian G, Mak J (2005) The packaging and maturation of the HIV-1 Pol proteins. *Current HIV research* **3:** 73-85

Hirano S, Suzuki N, Slagsvold T, Kawasaki M, Trambaiolo D, Kato R, Stenmark H, Wakatsuki S (2006) Structural basis of ubiquitin recognition by mammalian Eap45 GLUE domain. *Nature structural & molecular biology* **13:** 1031-1032

Hope T, Pomerantz RJ (1995) The human immunodeficiency virus type 1 Rev protein: a pivotal protein in the viral life cycle. *Current topics in microbiology and immunology* **193:** 91-105

Horii M, Shibata H, Kobayashi R, Katoh K, Yorikawa C, Yasuda J, Maki M (2006) CHMP7, a novel ESCRT-III-related protein, associates with CHMP4b and functions in the endosomal sorting pathway. *The Biochemical journal* **400:** 23-32

Huang M, Orenstein JM, Martin MA, Freed EO (1995) p6Gag is required for particle production from full-length human immunodeficiency virus type 1 molecular clones expressing protease. *Journal of virology* **69:** 6810-6818

Jacks T (1990) Translational suppression in gene expression in retroviruses and retrotransposons. *Current topics in microbiology and immunology* **157:** 93-124

Johnson MC, Spidel JL, Ako-Adjei D, Wills JW, Vogt VM (2005) The C-terminal half of TSG101 blocks Rous sarcoma virus budding and sequesters Gag into unique nonendosomal structures. *Journal of virology* **79:** 3775-3786

Julg B, Goebel FD (2005) HIV genetic diversity: any implications for drug resistance? *Infection* **33:** 299-301

Kamura T, Burian D, Khalili H, Schmidt SL, Sato S, Liu WJ, Conrad MN, Conaway RC, Conaway JW, Shilatifard A (2001) Cloning and characterization of ELL-associated proteins EAP45 and EAP20. a role for yeast EAP-like proteins in regulation of gene expression by glucose. *The Journal of biological chemistry* **276:** 16528-16533

Katoh K, Shibata H, Suzuki H, Nara A, Ishidoh K, Kominami E, Yoshimori T, Maki M (2003) The ALG-2-interacting protein Alix associates with CHMP4b, a human homologue of yeast Snf7 that is involved in multivesicular body sorting. *The Journal of biological chemistry* **278:** 39104-39113

Katoh K, Suzuki H, Terasawa Y, Mizuno T, Yasuda J, Shibata H, Maki M (2005) The penta-EF-hand protein ALG-2 directly interacts with the ESCRT-I component TSG101 and Ca 2+-dependently colocalizes to aberrant endosomes with dominant-negative AAA ATPase SKD1/Vps4B. *The Biochemical journal* **391:** 677-685

Katzmann DJ, Babst M, Emr SD (2001) Ubiquitin-dependent sorting into the multivesicular body pathway requires the function of a conserved endosomal protein sorting complex, ESCRT-I. *Cell* **106:** 145-155

Katzmann DJ, Odorizzi G, Emr SD (2002) Receptor downregulation and multivesicular-body sorting. *Nat Rev Mol Cell Biol* **3:** 893-905

Katzmann DJ, Stefan CJ, Babst M, Emr SD (2003) Vps27 recruits ESCRT machinery to endosomes during MVB sorting. *The Journal of cell biology* **162:** 413-423

Kieffer C, Skalicky JJ, Morita E, De Domenico I, Ward DM, Kaplan J, Sundquist WI (2008) Two distinct modes of ESCRT-III recognition are required for VPS4 functions in lysosomal protein targeting and HIV-1 budding. *Developmental cell* **15:** 62-73

Kikonyogo A, Bouamr F, Vana ML, Xiang Y, Aiyar A, Carter C, Leis J (2001) Proteins related to the Nedd4 family of ubiquitin protein ligases interact with the L domain of Rous sarcoma virus and are required for gag budding from cells. *Proceedings of the National Academy of Sciences of the United States of America* **98:** 11199-11204

Kim J, Sitaraman S, Hierro A, Beach BM, Odorizzi G, Hurley JH (2005) Structural basis for endosomal targeting by the Bro1 domain. *Developmental cell* **8:** 937-947

Kim MS, Kim JA, Song HK, Jeon H (2006) STAM-AMSH interaction facilitates the deubiquitination activity in the C-terminal AMSH. *Biochemical and biophysical research communications* **351:** 612-618

Komada M, Soriano P (1999) Hrs, a FYVE finger protein localized to early endosomes, is implicated in vesicular traffic and required for ventral folding morphogenesis. *Genes Dev* **13:** 1475-1485

Kondo E, Mammano F, Cohen EA, Gottlinger HG (1995) The p6gag domain of human immunodeficiency virus type 1 is sufficient for the incorporation of Vpr into heterologous viral particles. *Journal of virology* **69:** 2759-2764

Krausslich HG, Facke M, Heuser AM, Konvalinka J, Zentgraf H (1995) The spacer peptide between human immunodeficiency virus capsid and nucleocapsid proteins is essential for ordered assembly and viral infectivity. *Journal of virology* **69:** 3407-3419

Langelier C, von Schwedler U, Fisher RD, De Dominco I, White PL, Hill CP, Kaplan J, Ward D, Sundquist WI (2006) Human ESCRT-II complex and its role in human immunodeficiency virus type 1 release. *Journal of virology* **80:** 9465-9480

Liang C, Hu J, Whitney JB, Kleiman L, Wainberg MA (2003) A structurally disordered region at the C terminus of capsid plays essential roles in multimerization and membrane binding of the gag protein of human immunodeficiency virus type 1. *Journal of virology* **77:** 1772-1783

Licata JM, Simpson-Holley M, Wright NT, Han Z, Paragas J, Harty RN (2003) Overlapping motifs (PTAP and PPEY) within the Ebola virus VP40 protein function independently as late budding domains: involvement of host proteins TSG101 and VPS-4. *Journal of virology* **77:** 1812-1819

Lin Y, Kimpler LA, Naismith TV, Lauer JM, Hanson PI (2005) Interaction of the mammalian endosomal sorting complex required for transport (ESCRT) III protein hSnf7-1 with itself, membranes, and the AAA+ ATPase SKD1. *The Journal of biological chemistry* **280:** 12799-12809

Lottridge JM, Flannery AR, Vincelli JL, Stevens TH (2006) Vta1p and Vps46p regulate the membrane association and ATPase activity of Vps4p at the yeast multivesicular body. *Proceedings of the National Academy of Sciences of the United States of America* **103:** 6202-6207

Lu YL, Bennett RP, Wills JW, Gorelick R, Ratner L (1995) A leucine triplet repeat sequence (LXX)4 in p6gag is important for Vpr incorporation into human immunodeficiency virus type 1 particles. *Journal of virology* **69:** 6873-6879

Luhtala N, Odorizzi G (2004) Bro1 coordinates deubiquitination in the multivesicular body pathway by recruiting Doa4 to endosomes. *The Journal of cell biology* **166:** 717-729

Lusso P (2006) HIV and the chemokine system: 10 years later. *The EMBO journal* **25:** 447-456

Macias MJ, Wiesner S, Sudol M (2002) WW and SH3 domains, two different scaffolds to recognize proline-rich ligands. *FEBS Lett* **513:** 30-37

Malim MH, Emerman M (2008) HIV-1 accessory proteins--ensuring viral survival in a hostile environment. *Cell host & microbe* **3:** 388-398

Martin-Serrano J, Perez-Caballero D, Bieniasz PD (2004) Context-dependent effects of L domains and ubiquitination on viral budding. *Journal of virology* **78:** 5554-5563

Martin-Serrano J, Yaravoy A, Perez-Caballero D, Bieniasz PD (2003a) Divergent retroviral late-budding domains recruit vacuolar protein sorting factors by using alternative adaptor proteins. *Proceedings of the National Academy of Sciences of the United States of America* **100:** 12414-12419

Martin-Serrano J, Zang T, Bieniasz PD (2001) HIV-1 and Ebola virus encode small peptide motifs that recruit Tsg101 to sites of particle assembly to facilitate egress. *Nature medicine* **7:** 1313-1319

Martin-Serrano J, Zang T, Bieniasz PD (2003b) Role of ESCRT-I in Retroviral Budding. *Journal of virology* **77:** 4794-4804

Matsuo H, Chevallier J, Mayran N, Le Blanc I, Ferguson C, Faure J, Blanc NS, Matile S, Dubochet J, Sadoul R, Parton RG, Vilbois F, Gruenberg J (2004) Role of LBPA and Alix in multivesicular liposome formation and endosome organization. *Science* **303:** 531-534

McCullough J, Clague MJ, Urbe S (2004) AMSH is an endosome-associated ubiquitin isopeptidase. *The Journal of cell biology* **166:** 487-492

McCullough J, Fisher RD, Whitby FG, Sundquist WI, Hill CP (2008) ALIX-CHMP4 interactions in the human ESCRT pathway. *Proceedings of the National Academy of Sciences of the United States of America* **105:** 7687-7691

McCullough J, Row PE, Lorenzo O, Doherty M, Beynon R, Clague MJ, Urbe S (2006) Activation of the endosome-associated ubiquitin isopeptidase AMSH by STAM, a component of the multivesicular body-sorting machinery. *Curr Biol* **16:** 160-165

Medina G, Zhang Y, Tang Y, Gottwein E, Vana ML, Bouamr F, Leis J, Carter CA (2005) The functionally exchangeable L domains in RSV and HIV-1 Gag direct particle release through pathways linked by Tsg101. *Traffic (Copenhagen, Denmark)* **6:** 880-894

Mizuno E, Kobayashi K, Yamamoto A, Kitamura N, Komada M (2006) A deubiquitinating enzyme UBPY regulates the level of protein ubiquitination on endosomes. *Traffic (Copenhagen, Denmark)* **7:** 1017-1031

Morita E, Sandrin V, Alam SL, Eckert DM, Gygi SP, Sundquist WI (2007) Identification of human MVB12 proteins as ESCRT-I subunits that function in HIV budding. *Cell host & microbe* **2:** 41-53

Morita E, Sundquist WI (2004) Retrovirus budding. *Annual review of cell and developmental biology* **20:** 395-425

Murakami T, Freed EO (2000) Genetic evidence for an interaction between human immunodeficiency virus type 1 matrix and alpha-helix 2 of the gp41 cytoplasmic tail. *Journal of virology* **74:** 3548-3554

Muziol T, Pineda-Molina E, Ravelli RB, Zamborlini A, Usami Y, Gottlinger H, Weissenhorn W (2006) Structural basis for budding by the ESCRT-III factor CHMP3. *Developmental cell* **10:** 821-830

Neil SJ, Zang T, Bieniasz PD (2008) Tetherin inhibits retrovirus release and is antagonized by HIV-1 Vpu. *Nature* **451:** 425-430

Nickerson DP, West M, Odorizzi G (2006) Did2 coordinates Vps4-mediated dissociation of ESCRT-III from endosomes. *The Journal of cell biology* **175:** 715-720

Nikko E, Andre B (2007) Split-ubiquitin two-hybrid assay to analyze protein-protein interactions at the endosome: application to Saccharomyces cerevisiae Bro1 interacting

with ESCRT complexes, the Doa4 ubiquitin hydrolase, and the Rsp5 ubiquitin ligase. *Eukaryotic cell* **6:** 1266-1277

Nomaguchi M, Fujita M, Adachi A (2008) Role of HIV-1 Vpu protein for virus spread and pathogenesis. *Microbes and infection / Institut Pasteur* **10:** 960-967

Odorizzi G, Katzmann DJ, Babst M, Audhya A, Emr SD (2003) Bro1 is an endosome-associated protein that functions in the MVB pathway in Saccharomyces cerevisiae. *Journal of cell science* **116:** 1893-1903

Ott DE, Coren LV, Chertova EN, Gagliardi TD, Schubert U (2000) Ubiquitination of HIV-1 and MuLV Gag. *Virology* **278:** 111-121

Ott DE, Coren LV, Copeland TD, Kane BP, Johnson DG, Sowder RC, 2nd, Yoshinaka Y, Oroszlan S, Arthur LO, Henderson LE (1998) Ubiquitin is covalently attached to the p6Gag proteins of human immunodeficiency virus type 1 and simian immunodeficiency virus and to the p12Gag protein of Moloney murine leukemia virus. *Journal of virology* **72:** 2962-2968

Pandey RC, Datta D, Mukerjee R, Srinivasan A, Mahalingam S, Sawaya BE (2009) HIV-1 Vpr: a closer look at the multifunctional protein from the structural perspective. *Current HIV research* **7:** 114-128

Parent LJ, Bennett RP, Craven RC, Nelle TD, Krishna NK, Bowzard JB, Wilson CB, Puffer BA, Montelaro RC, Wills JW (1995) Positionally independent and exchangeable late budding functions of the Rous sarcoma virus and human immunodeficiency virus Gag proteins. *Journal of virology* **69:** 5455-5460

Patnaik A, Chau V, Li F, Montelaro RC, Wills JW (2002) Budding of equine infectious anemia virus is insensitive to proteasome inhibitors. *Journal of virology* **76:** 2641-2647

Patnaik A, Chau V, Wills JW (2000) Ubiquitin is part of the retrovirus budding machinery. *Proceedings of the National Academy of Sciences of the United States of America* **97:** 13069-13074

Perez M, Craven RC, De La Torre JC (2003) The small RING finger protein Z drives arenavirus budding: Implications for antiviral strategies. *Proceedings of the National Academy of Sciences of the United States of America* **100:** 12978-12983

Polo S, Sigismund S, Faretta M, Guidi M, Capua MR, Bossi G, Chen H, De Camilli P, Di Fiore PP (2002) A single motif responsible for ubiquitin recognition and monoubiquitination in endocytic proteins. *Nature* **416:** 451-455

Pornillos O, Alam SL, Rich RL, Myszka DG, Davis DR, Sundquist WI (2002a) Structure and functional interactions of the Tsg101 UEV domain. *The EMBO journal* **21:** 2397-2406

Pornillos O, Garrus JE, Sundquist WI (2002b) Mechanisms of enveloped RNA virus budding. *Trends Cell Biol* **12**: 569-579

Pornillos O, Higginson DS, Stray KM, Fisher RD, Garrus JE, Payne M, He GP, Wang HE, Morham SG, Sundquist WI (2003) HIV Gag mimics the Tsg101-recruiting activity of the human Hrs protein. *The Journal of cell biology* **162:** 425-434

Puffer BA, Parent LJ, Wills JW, Montelaro RC (1997) Equine infectious anemia virus utilizes a YXXL motif within the late assembly domain of the Gag p9 protein. *Journal of virology* **71:** 6541-6546

Putterman D, Pepinsky RB, Vogt VM (1990) Ubiquitin in avian leukosis virus particles. *Virology* **176:** 633-637

Raiborg C, Bache KG, Gillooly DJ, Madshus IH, Stang E, Stenmark H (2002) Hrs sorts ubiquitinated proteins into clathrin-coated microdomains of early endosomes. *Nat Cell Biol* **4:** 394-398

Raiborg C, Bache KG, Mehlum A, Stenmark H (2001a) Function of Hrs in endocytic trafficking and signalling. *Biochemical Society transactions* **29:** 472-475

Raiborg C, Bremnes B, Mehlum A, Gillooly DJ, D'Arrigo A, Stang E, Stenmark H (2001b) FYVE and coiled-coil domains determine the specific localisation of Hrs to early endosomes. *Journal of cell science* **114:** 2255-2263

Raymond CK, Howald-Stevenson I, Vater CA, Stevens TH (1992) Morphological classification of the yeast vacuolar protein sorting mutants: evidence for a prevacuolar compartment in class E vps mutants. *Molecular biology of the cell* **3:** 1389-1402

Reggiori F, Pelham HR (2001) Sorting of proteins into multivesicular bodies: ubiquitin-dependent and -independent targeting. *The EMBO journal* **20:** 5176-5186

Row PE, Liu H, Hayes S, Welchman R, Charalabous P, Hofmann K, Clague MJ, Sanderson CM, Urbe S (2007) The MIT domain of UBPY constitutes a CHMP binding and endosomal localization signal required for efficient epidermal growth factor receptor degradation. *The Journal of biological chemistry* **282:** 30929-30937

Row PE, Prior IA, McCullough J, Clague MJ, Urbe S (2006) The ubiquitin isopeptidase UBPY regulates endosomal ubiquitin dynamics and is essential for receptor down-regulation. *The Journal of biological chemistry* **281:** 12618-12624

Saad JS, Miller J, Tai J, Kim A, Ghanam RH, Summers MF (2006) Structural basis for targeting HIV-1 Gag proteins to the plasma membrane for virus assembly. *Proceedings of the National Academy of Sciences of the United States of America* **103:** 11364-11369

Schmitt AP, Leser GP, Morita E, Sundquist WI, Lamb RA (2005) Evidence for a new viral late-domain core sequence, FPIV, necessary for budding of a paramyxovirus. *Journal of virology* **79:** 2988-2997

Schubert U, Ott DE, Chertova EN, Welker R, Tessmer U, Princiotta MF, Bennink JR, Krausslich HG, Yewdell JW (2000) Proteasome inhibition interferes with gag polyprotein processing, release, and maturation of HIV-1 and HIV-2. *Proceedings of the National Academy of Sciences of the United States of America* **97:** 13057-13062

Scott A, Chung HY, Gonciarz-Swiatek M, Hill GC, Whitby FG, Gaspar J, Holton JM, Viswanathan R, Ghaffarian S, Hill CP, Sundquist WI (2005a) Structural and mechanistic studies of VPS4 proteins. *The EMBO journal* **24:** 3658-3669

Scott A, Gaspar J, Stuchell-Brereton MD, Alam SL, Skalicky JJ, Sundquist WI (2005b) Structure and ESCRT-III protein interactions of the MIT domain of human VPS4A. *Proceedings of the National Academy of Sciences of the United States of America* **102:** 13813-13818

Shehu-Xhilaga M, Ablan S, Demirov DG, Chen C, Montelaro RC, Freed EO (2004) Late domain-dependent inhibition of equine infectious anemia virus budding. *Journal of virology* **78:** 724-732

Shiflett SL, Ward DM, Huynh D, Vaughn MB, Simmons JC, Kaplan J (2004) Characterization of Vta1p, a class E Vps protein in Saccharomyces cerevisiae. *The Journal of biological chemistry* **279:** 10982-10990

Shih SC, Katzmann DJ, Schnell JD, Sutanto M, Emr SD, Hicke L (2002) Epsins and Vps27p/Hrs contain ubiquitin-binding domains that function in receptor endocytosis. *Nat Cell Biol* **4:** 389-393

Slagsvold T, Aasland R, Hirano S, Bache KG, Raiborg C, Trambaiolo D, Wakatsuki S, Stenmark H (2005) Eap45 in mammalian ESCRT-II binds ubiquitin via a phosphoinositide-interacting GLUE domain. *The Journal of biological chemistry* **280:** 19600-19606

Stopak K, Greene WC (2005) Protecting APOBEC3G: a potential new target for HIV drug discovery. *Curr Opin Investig Drugs* **6:** 141-147

Strack B, Calistri A, Accola MA, Palu G, Gottlinger HG (2000) A role for ubiquitin ligase recruitment in retrovirus release. *Proceedings of the National Academy of Sciences of the United States of America* **97:** 13063-13068

Strack B, Calistri A, Craig S, Popova E, Gottlinger HG (2003) AIP1/ALIX Is a Binding Partner for HIV-1 p6 and EIAV p9 Functioning in Virus Budding. *Cell* **114:** 689-699

Strecker T, Eichler R, Meulen J, Weissenhorn W, Klenk HD, Garten W, Lenz O (2003) Lassa virus Z protein is a matrix protein sufficient for the release of virus-like particles. *Journal of virology* **77:** 10700-10705

Stuchell MD, Garrus JE, Muller B, Stray KM, Ghaffarian S, McKinnon R, Krausslich HG, Morham SG, Sundquist WI (2004) The Human Endosomal Sorting Complex Required for Transport (ESCRT-I) and Its Role in HIV-1 Budding. *The Journal of biological chemistry* **279:** 36059-36071

Sundquist WI, Schubert HL, Kelly BN, Hill GC, Holton JM, Hill CP (2004) Ubiquitin recognition by the human TSG101 protein. *Molecular cell* **13:** 783-789

Swanson KA, Kang RS, Stamenova SD, Hicke L, Radhakrishnan I (2003) Solution structure of Vps27 UIM-ubiquitin complex important for endosomal sorting and receptor downregulation. *The EMBO journal* **22:** 4597-4606

Takasu H, Jee JG, Ohno A, Goda N, Fujiwara K, Tochio H, Shirakawa M, Hiroaki H (2005) Structural characterization of the MIT domain from human Vps4b. *Biochemical and biophysical research communications* **334:** 460-465

Tang H, Kuhen KL, Wong-Staal F (1999) Lentivirus replication and regulation. *Annual review of genetics* **33:** 133-170

Teo H, Veprintsev DB, Williams RL (2004) Structural insights into ESCRT-I recognition of ubiquitinated proteins. *The Journal of biological chemistry* **279:** 28689-28696

Timmins J, Schoehn G, Ricard-Blum S, Scianimanico S, Vernet T, Ruigrok RW, Weissenhorn W (2003) Ebola Virus Matrix Protein VP40 Interaction with Human Cellular Factors Tsg101 and Nedd4. *Journal of molecular biology* **326:** 493-502

Tsang HT, Connell JW, Brown SE, Thompson A, Reid E, Sanderson CM (2006) A systematic analysis of human CHMP protein interactions: Additional MIT domain-containing proteins bind to multiple components of the human ESCRT III complex. *Genomics* **88:** 333-346

UNAIDS JUNPoHA. (2006) 2006 Report on the global AIDS epidemic: Executive Summary. *UNAIDS*. UNAIDS, 20 AVENUE APPIA, CH-1211 GENEVA 27, SWITZERLAND, pp. 1-26

Urbe S, McCullough J, Row P, Prior IA, Welchman R, Clague MJ (2006) Control of growth factor receptor dynamics by reversible ubiquitination. *Biochemical Society transactions* **34:** 754-756

Usami Y, Popov S, Popova E, Gottlinger HG (2008) Efficient and specific rescue of human immunodeficiency virus type 1 budding defects by a Nedd4-like ubiquitin ligase. *Journal of virology* **82:** 4898-4907

VerPlank L, Bouamr F, LaGrassa TJ, Agresta B, Kikonyogo A, Leis J, Carter CA (2001) Tsg101, a homologue of ubiquitin-conjugating (E2) enzymes, binds the L domain in HIV type 1 Pr55Gag. *Proceedings of the National Academy of Sciences of the United States of America* **98:** 7724-7729

Vincent O, Rainbow L, Tilburn J, Arst Jr HN, Jr., Penalva MA (2003) YPXL/I Is a Protein Interaction Motif Recognized by Aspergillus PalA and Its Human Homologue, AIP1/Alix. *Mol Cell Biol* **23:** 1647-1655

Vogt VM (2000) Ubiquitin in retrovirus assembly: actor or bystander? *Proceedings of the National Academy of Sciences of the United States of America* **97:** 12945-12947

von Poblotzki A, Wagner R, Niedrig M, Wanner G, Wolf H, Modrow S (1993) Identification of a region in the Pr55gag-polyprotein essential for HIV-1 particle formation. *Virology* **193:** 981-985

von Schwedler UK, Stuchell M, Muller B, Ward DM, Chung HY, Morita E, Wang HE, Davis T, He GP, Cimbora DM, Scott A, Krausslich HG, Kaplan J, Morham SG, Sundquist WI (2003) The protein network of HIV budding. *Cell* **114:** 701-713

Waheed AA, Ablan SD, Soheilian F, Nagashima K, Ono A, Schaffner CP, Freed EO (2008) Inhibition of human immunodeficiency virus type 1 assembly and release by the cholesterol-binding compound amphotericin B methyl ester: evidence for Vpu dependence. *Journal of virology* **82:** 9776-9781

Wainberg MA (2004) HIV-1 subtype distribution and the problem of drug resistance. *AIDS (London, England)* **18 Suppl 3:** S63-68

Wang WK, Chen MY, Chuang CY, Jeang KT, Huang LM (2000) Molecular biology of human immunodeficiency virus type 1. *Journal of microbiology, immunology, and infection = Wei mian yu gan ran za zhi* **33:** 131-140

Ward DM, Vaughn MB, Shiflett SL, White PL, Pollock AL, Hill J, Schnegelberger R, Sundquist WI, Kaplan J (2005) The role of LIP5 and CHMP5 in multivesicular body formation and HIV-1 budding in mammalian cells. *The Journal of biological chemistry* **280:** 10548-10555

Whitley P, Reaves BJ, Hashimoto M, Riley AM, Potter BV, Holman GD (2003) Identification of mammalian Vps24p as an effector of phosphatidylinositol 3,5-bisphosphate-dependent endosome compartmentalization. *The Journal of biological chemistry* **278:** 38786-38795

Wills JW, Cameron CE, Wilson CB, Xiang Y, Bennett RP, Leis J (1994) An assembly domain of the Rous sarcoma virus Gag protein required late in budding. *Journal of virology* **68:** 6605-6618

Wills JW, Craven RC (1991) Form, function, and use of retroviral gag proteins. *AIDS (London, England)* **5:** 639-654

Worthylake DK, Wang H, Yoo S, Sundquist WI, Hill CP (1999) Structures of the HIV-1 capsid protein dimerization domain at 2.6 A resolution. *Acta crystallographica* **55:** 85-92

Yasuda J, Hunter E (1998) A proline-rich motif (PPPY) in the Gag polyprotein of Mason-Pfizer monkey virus plays a maturation-independent role in virion release. *Journal of virology* **72:** 4095-4103

Yasuda J, Hunter E, Nakao M, Shida H (2002) Functional involvement of a novel Nedd4-like ubiquitin ligase on retrovirus budding. *EMBO Rep* **3:** 636-640

Yasuda J, Nakao M, Kawaoka Y, Shida H (2003) Nedd4 regulates egress of Ebola virus-like particles from host cells. *Journal of virology* **77:** 9987-9992

Yorikawa C, Shibata H, Waguri S, Hatta K, Horii M, Katoh K, Kobayashi T, Uchiyama Y, Maki M (2005) Human CHMP6, a myristoylated ESCRT-III protein, interacts directly with an ESCRT-II component EAP20 and regulates endosomal cargo sorting. *The Biochemical journal* **387:** 17-26

Yuan B, Li X, Goff SP (1999) Mutations altering the moloney murine leukemia virus p12 Gag protein affect virion production and early events of the virus life cycle. *The EMBO journal* **18:** 4700-4710

CHAPTER 2

THE PROTEIN NETWORK OF HIV BUDDING

Uta K. von Schwedler, Melissa Stuchell, Barbara Muller, Diane M. Ward, Hyo-Young Chung, Eiji Morita, Hubert E. Wang, Thaylon Davis, Gong-Ping He, Daniel M. Cimbora, Anna Scott, Hans-Georg Krausslich, Jerry Kaplan, Scott G. Morham, and Wesley Sundquist

Reprinted from Cell, Vol. 114, pages 701-713, Copyright 2003.

Note: Cloning of human Class E genes into activation and DNA binding constructs and the directed yeast two-hybrid experiments were performed by Melissa D. Stuchell-Brereton and contributed to Figures 1A, 1C, and 2B. Cloning of constructs, production of protein, and GST-pulldown experiments were performed by Melissa D. Stuchell-Brereton and contributed to Figure 3C. Identification of the human Class E genes through literature and BLAST searches was performed by Anna Scott and confirmed by Melissa D. Stuchell-Brereton. Work described in Figure 1B of this chapter was performed by Myriad Genetics, Inc. Work described in Figures 2B, 3A, 3B of this chapter was performed by Hyo-young Chung. Work described in Figure 4A was performed by Barbara Muller. Work described in Figures 4B, 5A, 5B, and 6 was performed by Uta K. von Schwedler.

Cell, Vol. 114, 701–713, September 19, 2003, Copyright ©2003 by Cell Press

The Protein Network of HIV Budding

Uta K. von Schwedler,[1] Melissa Stuchell,[1] Barbara Müller,[3] Diane M. Ward,[2] Hyo-Young Chung,[1] Eiji Morita,[1] Hubert E. Wang,[4] Thaylon Davis,[4] Gong-Ping He,[4] Daniel M. Cimbora,[4] Anna Scott,[1] Hans-Georg Kräusslich,[3] Jerry Kaplan,[2] Scott G. Morham,[4] and Wesley I. Sundquist[1,*]

[1]Department of Biochemistry
[2]Department of Pathology
University of Utah
Salt Lake City, Utah 84132
[3]Abteilung Virologie
Universitätsklinikum Heidelberg
D-69120 Heidelberg
Germany
[4]Myriad Pharmaceuticals, Inc.
Salt Lake City, Utah 84108

Summary

HIV release requires TSG101, a cellular factor that sorts proteins into vesicles that bud into multivesicular bodies (MVB). To test whether other proteins involved in MVB biogenesis (the class E proteins) also participate in HIV release, we identified 22 candidate human class E proteins. These proteins were connected into a coherent network by 43 different protein-protein interactions, with AIP1 playing a key role in linking complexes that act early (TSG101/ESCRT-I) and late (CHMP4/ESCRT-III) in the pathway. AIP1 also binds the HIV-1 $p6^{Gag}$ and EIAV $p9^{Gag}$ proteins, indicating that it can function directly in virus budding. Human class E proteins were found in HIV-1 particles, and dominant-negative mutants of late-acting human class E proteins arrested HIV-1 budding through plasmal and endosomal membranes. These studies define a protein network required for human MVB biogenesis and indicate that the entire network participates in the release of HIV and probably many other viruses.

Introduction

HIV spreads via extracellular particles that can enter and exit cells. The characterization of viral and cellular proteins involved in HIV entry has provided a greater understanding of early stages in the viral life cycle, and led to new therapeutics (Biscone et al., 2002). In contrast, the equally important process of HIV release is less well understood, and many of the cellular factors involved in this fundamental stage of the viral life cycle remain to be identified and characterized (for recent reviews see Freed, 2002; Pornillos et al., 2002c).

Efficient HIV release requires the *cis*-acting, tetrapeptide P(S/T)AP "late domain" found in the p6 domain of all HIV Gag proteins, and also in the structural proteins of other pathogenic human viruses including Ebola and HTLV-I (Freed, 2002; Pornillos et al., 2002c). PTAP late domains recruit the cellular protein TSG101 to facilitate virus budding (Demirov et al., 2002a; Garrus et al., 2001; Martin-Serrano et al., 2001; VerPlank et al., 2001). In uninfected cells, TSG101 functions in the biogenesis of the *m*ultive*s*icular *b*ody (MVB) (Katzmann et al., 2002), which suggests that HIV may bind TSG101 in order to gain access to the downstream machinery that catalyzes MVB vesicle budding. Consistent with this model, a dominant-negative Vps4A protein that inhibits MVB biogenesis also blocks release of HIV-1 and other enveloped viruses (Garrus et al., 2001; Licata et al., 2003; Martin-Serrano et al., 2003). The mammalian MVB pathway is not yet fully defined, however. Hence, it is unclear whether other proteins in the MVB pathway participate in HIV-1 budding.

Genetic screens in yeast have defined 17 different proteins that appear to play direct roles in MVB biogenesis (reviewed in Katzmann et al., 2002). All are required for *v*acuolar *p*rotein *s*orting (VPS), and are termed "class E" proteins because their deletion or inactivation induces formation of abnormally enlarged, highly tubulated endosomal membrane compartments that fail to mature normally into MVBs (termed "class E compartments"). Recent studies by Emr and coworkers have revealed that most class E proteins exist predominantly as soluble proteins or subcomplexes that are sequentially recruited from the cytoplasm to function at sites of MVB vesicle formation (termed ESCRTs, for *E*ndosomal *S*orting *C*omplexes *R*equired for *T*ransport) (Babst et al., 2002a, 2002b; Katzmann et al., 2003; Odorizzi et al., 2003). After proteins are sorted into MVB vesicles, the assembled class E proteins are then released upon ATP binding/hydrolysis by the AAA ATPase, Vps4p. Thus, the different factors and stages of yeast MVB biogenesis are now understood in outline. The present studies were undertaken with the goals of defining the network of proteins required for human MVB biogenesis and testing whether HIV-1 budding requires the function of proteins that act later in this pathway.

Results

Modeling the Human Protein Interaction Network Required for MVB Biogenesis

A systematic search for human homologs of yeast class E proteins yielded at least one acceptable match for all 17 yeast proteins, with the exception of Vps37p (Figure 1 and Supplemental Table S1 available at http://www.cell.com/cgi/content/full/114/6/701/DC1). The resulting 22 human proteins can be grouped in analogy to the yeast ESCRT subcomplexes, and the groupings shown in Figure 1A are consistent with studies in mammalian systems indicating that: (1) HRS, STAM1/2, TSG101, and VPS28 all act early in MVB formation (Asao et al., 1997; Babst et al., 2000; Bache et al., 2003a, 2003b; Bishop et al., 2002; Bishop and Woodman, 2001; Lu et al., 2003; Pornillos et al., 2003), and (2) the ESCRT-II proteins

*Correspondence: wes@biochem.utah.edu

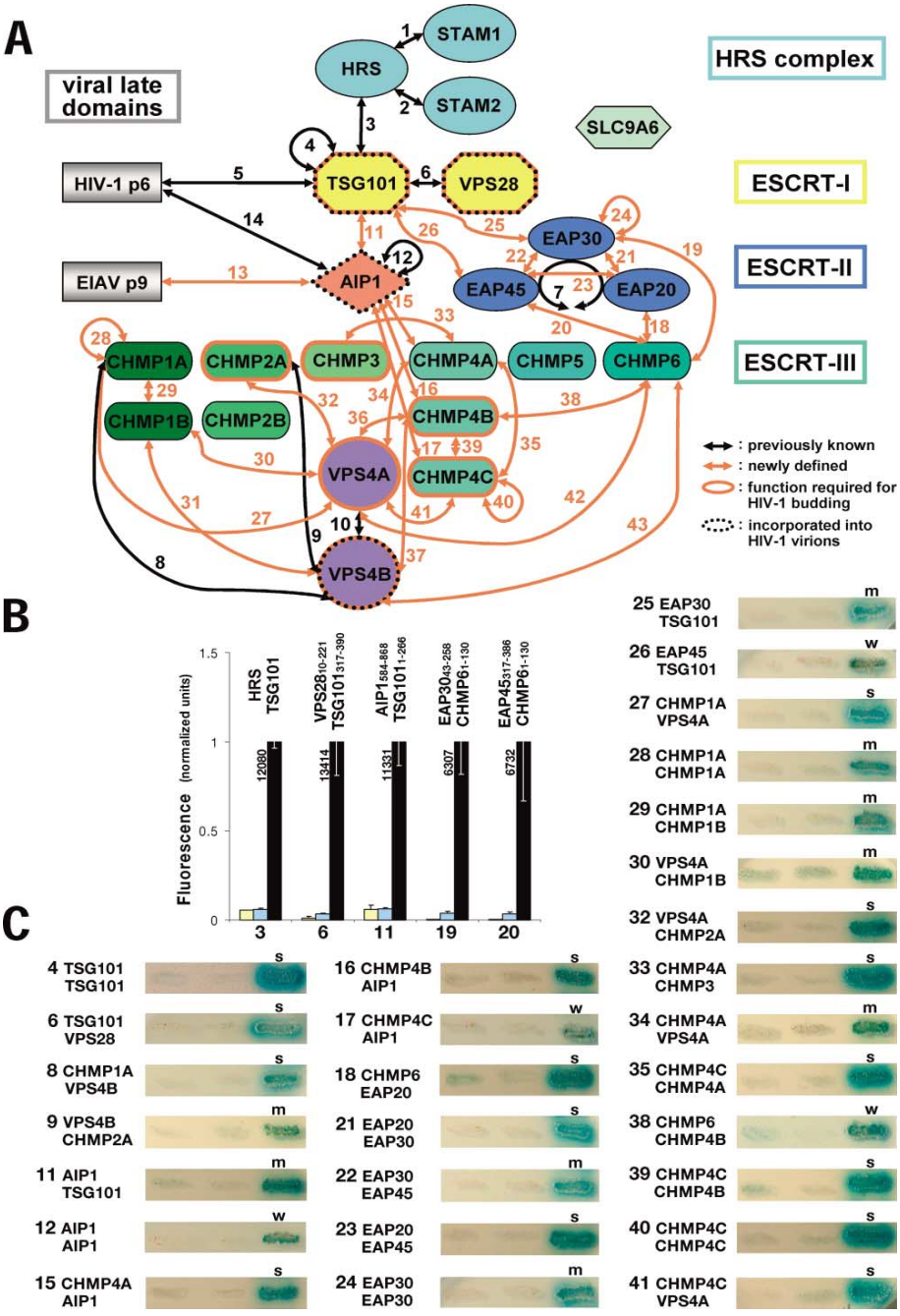

Figure 1. Model for the Human Class E Protein Interaction Network

(A) Schematic illustration showing 22 putative human class E proteins, their subcomplexes, and interactions. Interactions between proteins are denoted by arrows and are color-coded as previously known (black) or novel (red). ESCRT-I, II, III complexes are modeled after analogous yeast complexes (Katzmann et al., 2002). Detection methods, interactions (in brackets) and relevant protein fragments (in parentheses) were: a) Yeast two-hybrid screens of cDNA libraries: [6] ($TSG101_{317–390}$/$VPS28_{10–221}$), [11] ($TSG101_{1–266}$/$AIP1_{584–868}$), [19] ($EAP30_{43–259}$/$CHMP6_{1–130}$), [20] ($EAP45_{317–386}$/$CHMP6_{1–130}$); b) Directed yeast two-hybrid screens [4, 6, 8–9, 11–12, 15–18, 21–30, 32–35, and 38–41] (all full-length proteins); c) Interactions between purified proteins detected using GST pull-down assays: [13] ($AIP1_{1–716}$/EIAV p9), [14] ($AIP_{1–716}$/HIV-1 p6), [16] ($AIP1_{1–716}$/CHMP4B), and [9, 30–32, 36–37, 42–43] (all full-length proteins); d) Interactions between purified proteins detected using Biacore biosensor: [11] ($Tsg101_{1–145}$/$AIP1_{714–723}$). References for previously reported interactions are: [1] and [2] (Asao et al., 1997), [3] (Bache et al., 2003a; Lu et al., 2003; Pornillos et al., 2003), [4] (Martin-Serrano et al., 2003), [5] (Demirov et al., 2002a; Garrus et al., 2001; Martin-Serrano et al., 2001;

form a stable complex in mammalian cells (Kamura et al., 2001).

In several cases, a single yeast protein apparently has two or more human orthologs, implying greater complexity in the mammalian MVB pathway. This is most evident late in the pathway; e.g., the single yeast Vps4p protein has two apparent human orthologs: VPS4A and VPS4B, and the six related proteins of the yeast ESCRT-III class have 10 apparent human orthologs, the *ch*arged *M*VB *p*roteins or CHMP proteins. The six yeast proteins perform distinct functions: two (Vps32p/Snf7p and Vps20p) form a proximal lattice that binds directly to the MVB membrane, two (Vps2p/Did4p and Vps24p) form a distal layer on the first, and the remaining two (Did2p and Vps60p/Mos10p) apparently have partially redundant and/or regulatory roles (Babst et al., 2002a). A phylogenetic analysis showed that the 10 related human CHMP proteins can also be subdivided into six analogous groups (Figure 1A and Supplemental Figure S1 available on *Cell* website).

Protein Interactions within the Human Vps Class E Protein Network

Extensive yeast two-hybrid analyses were performed to test our model for the human MVB pathway and to identify new protein-protein interactions that could link the entire protein network together, which has not been possible in any system including yeast. Potential interactions between human class E proteins were tested using both random library screening and directed yeast two-hybrid assays, which provided overlapping and complementary information (Figure 1, Supplemental Figure S1 and Table S1 available on *Cell* website). In the random screen, early (TSG101) and late (CHMP6) acting class E proteins were used as baits in automated screens of human cDNA libraries, with multiple constructs employed to identify interacting domains. These screens confirmed one previously known TSG101 interaction, TSG101/VPS28 (Bishop and Woodman, 2001), and revealed three novel interactions: TSG101/AIP1, CHMP6/EAP30, and CHMP6/EAP45. All four interactions were confirmed in semiquantitative liquid β-galactosidase two-hybrid assays (Figure 1B).

The directed screen tested for all possible intra- and intermolecular interactions between the 18 human class E proteins predicted to act downstream of TSG101 (including TSG101 itself). A total of 28 interactions were identified and 16 of the 18 proteins tested interacted with at least one other class E protein (Figures 1A and 1C). CHMP5 constructs were toxic or self-activating, and CHMP2B did not show any positive interactions. Our experiments reconfirmed several yeast two-hybrid interactions described previously in mammalian systems: TGS101/TSG101 (Martin-Serrano et al., 2003), TSG101/VPS28 (Bishop and Woodman, 2001), AIP1/AIP1 (Chatellard-Causse et al., 2002), CHMP1A/VPS4B, and CHMP2A/VPS4B (Howard et al., 2001). We also found a series of interactions that were previously undocumented in mammalian systems, but were analogous to interactions previously described in yeast (e.g., CHMP4B/CHMP6, AIP1/CHMP4A-C) (Babst et al., 2002a; Odorizzi et al., 2003), or were consistent with biochemical or genetic experiments in yeast (e.g., ESCRT-I recruits ESCRT-II to the endosomal membrane (Babst et al., 2002b), Snf7p (CHMP4A-C) recruits Bro1p (AIP1) (Odorizzi et al., 2003), and ESCRT-II recruits Vps20p (CHMP6) (Babst et al., 2002b). It is therefore apparent that the MVB pathway is conserved in outline from yeast to man.

Importantly, our two screens revealed 25 new class E protein-protein interactions that had not previously been described in any system. These included the first links between ESCRT-I and ESCRT-II (TSG101/EAP45, TSG101/EAP30), and between ESCRT-I and AIP1 (TSG101/AIP1). Collectively, our data imply a hierarchy of protein interactions required for MVB formation, with HRS complex recruiting ESCRT-I; ESCRT-I recruiting AIP1 and ESCRT-II; AIP1 and ESCRT-II recruiting ESCRT-III; and ESCRT-III recruiting VPS4A/B (see Figure 1A).

TSG101/AIP1 Interactions

The novel interaction between TSG101 and AIP1 detected in the yeast two-hybrid experiments was characterized in greater detail because it provided, to our knowledge, the first direct link between the human ESCRT-I and ESCRT-III complexes. Deletion analyses revealed that the N-terminal UEV domain of TSG101 (residues 1–145) bound the proline-rich C-terminal region of AIP1 (residues 586–868) (Figures 1B and 2A). The TSG101 UEV domain binds specifically to P(S/T)AP sequences, but a mutation in the UEV domain (M95A) abolishes P(S/T)AP binding (Pornillos et al., 2002a, 2002b). The M95A mutation also eliminated AIP1 binding to both the full-length and $TSG101_{1–145}$ proteins (Figure 2A, far right, red bar), indicating that the TSG101 UEV domain bound a P(S/T)AP-like sequence in the proline-rich region of AIP1.

There is a conserved PSAP motif within the proline-rich region of AIP1 (residues 717–720), and we therefore tested whether the TSG101 UEV domain could bind this

VerPlank et al., 2001), [6] (Bishop and Woodman, 2001), [7] (Kamura et al., 2001), [8] and [9] (Howard et al., 2001), [10] (Scheuring et al., 2001), [12] (Chatellard-Causse et al., 2002) and [14] (Strack et al., 2003).

(B) Protein-protein interactions detected in yeast two-hybrid library screens and confirmed using semiquantitative β-galactosidase assays. Positive signals from yeast expressing prey-AD/bait-BD pairs (black bars) are shown together with signals from control cells expressing AD/bait-BD (yellow) and prey-AD/BD pairs (blue). Interaction numbers (below) correspond to those in Figure 1A, and the HRS/TSG101 interaction served as a positive control (Pornillos et al., 2003). Signals were normalized relative to the appropriate positive signal (given in fluorescence units adjacent to black bars).

(C) Directed yeast two-hybrid interactions between human class E proteins detected in X-α-gal assays. From left to right, each image shows X-α-gal signals from yeast patches containing AD/bait-BD (negative control), prey-AD/BD (negative control), and prey-AD/bait-BD (positive interaction). All interactions shown were positive in multiple repetitions of these experiments and are denoted as strong (s, signal in 1–2 days), medium (m, signal in 3 days), and weak (w, signal in 4 or more days). Very weak interactions not scored as positive were: CHMP3/CHMP4B, CHMP1B/VPS4B, CHMP4B/EAP45, and CHMP6/VPS4A. Note that some two-hybrid interactions could be mediated via bridging yeast proteins.

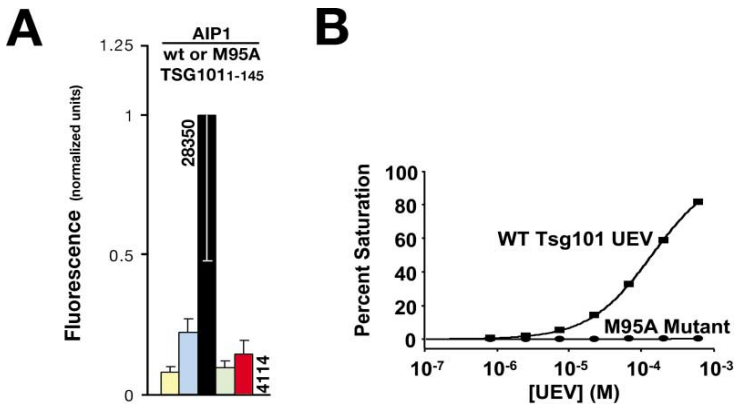

Figure 2. TSG101/AIP1 Interactions

(A) β-galactosidase assays showing two-hybrid interactions between AD/TSG101$_{1–145}$-BD (yellow, negative control), AIP1-AD/BD (blue, negative control), AIP1-AD/TSG101$_{1–145}$-BD (black), AD/M95A-TSG101$_{1–145}$-BD (green, negative control), and AIP1-AD/M95A-TSG101$_{1–145}$-BD (red).

(B) Biosensor binding isotherms for GST-AIP1$_{714–723}$ binding to wt (squares, $K_D = 142 \pm 0.5$ μM) or M95A mutant (ovals) TSG101 UEV. Raw binding data for this figure are given in Supplemental Figure S2A (available on *Cell* website).

motif directly using Biacore biosensor experiments. Pure recombinant TSG101 UEV domain bound specifically to a peptide spanning AIP1 residues 714–723 (denoted AIP1$_{714–723}$; $K_D = 142 \pm 0.5$ μM), and binding was again eliminated by the TSG101 M95A mutation (Figure 2B and Supplemental Figure S2A available on *Cell* website). Hence, the TSG101 UEV domain binds directly to the $_{717}$PSAP$_{720}$ element of AIP1.

AIP1/CHMP4 Interactions

The yeast two-hybrid data also indicated that AIP1 interacts with all three members of the CHMP4 family of ESCRT-III proteins, but not with other CHMP proteins. GST pull-down assays were performed to test for direct, specific protein-protein interactions between AIP1$_{1–716}$ and representatives from 5 of the 6 different CHMP subclasses (1B, 2A, 3, 4B, and 6; GST-CHMP4A, -CHMP4C, and -CHMP5 were poorly soluble and therefore not tested). As shown in Figure 3A, AIP1$_{1–716}$ bound CHMP4B, but not the other CHMP proteins. A single point mutation (L217A) near the C terminus of CHMP4B blocked AIP1 binding (Figure 3A, compare lanes 7 and 8). Although the functional interactions between AIP1 and CHMP4 proteins presumably occur primarily within membrane bound complexes, it was possible to coimmunoprecipitate AIP1-Myc and CHMP4B-FLAG proteins that were overexpressed in 293T cells (Figure 3B). Overall, we conclude that AIP1 binds directly and specifically to the CHMP4 proteins, but not to CHMP proteins from other families.

Interactions of AIP1 and Viral Proteins

Recent evidence suggests that AIP1 may play a direct role in the release of several enveloped viruses, includ-

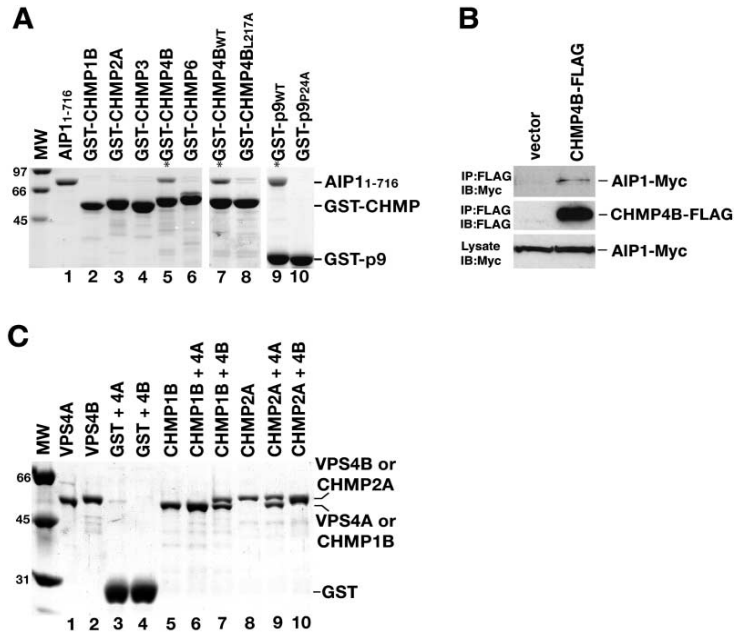

Figure 3. CHMP Protein Interactions

(A) CHMP/AIP1 interactions analyzed in GST pull-down assays. Excess pure AIP1$_{1–716}$ (lane 1, 10% of input) was incubated with glutathione beads prebound with different GST fusion proteins (lanes 2–10, lower bands). Bound AIP$_{1–716}$ was separated by SDS-PAGE and visualized by Coomassie blue staining (upper bands in lanes with asterisks).

(B) Coimmunoprecipitation of CHMP4B and AIP1. 293T cells were cotransfected with AIP1-Myc expression vector and with either pcDNA3.1 control vector (lane 1) or CHMP4B-FLAG expression vector (lane 2). Proteins were immunoprecipitated (IP) from the lysates using anti-FLAG antibodies and detected by Western blotting with anti-Myc (top image) or anti-FLAG (middle image). A Western blot (anti-Myc) of the soluble lysate is shown in the bottom image (1% input).

(C) CHMP/VPS4 interactions analyzed by GST pull-down assays. Pure VPS4A or VPS4B (lanes 1 and 2; 0.7 μg, 5% of input, ~10-fold molar excess) were incubated with glutathione beads prebound with GST alone (lanes 3 and 4), GST-CHMP1B (lanes 6 and 7), or GST-CHMP2A (lanes 9 and 10). GST-CHMP1B and GST-CHMP2A alone are shown in lanes 5 and 8, respectively. Note that GST-CHMP1B/VPS4A and GST-CHMP2A/VPS4B comigrate in lanes 6 and 10, respectively.

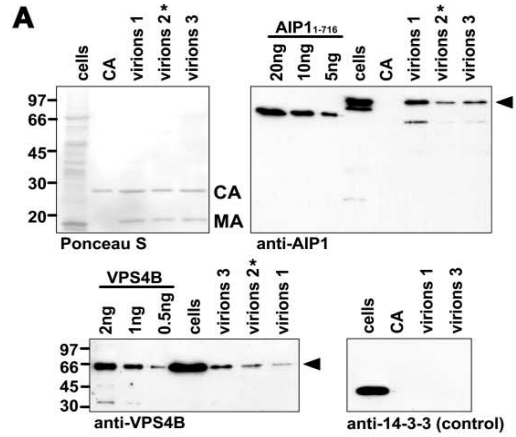

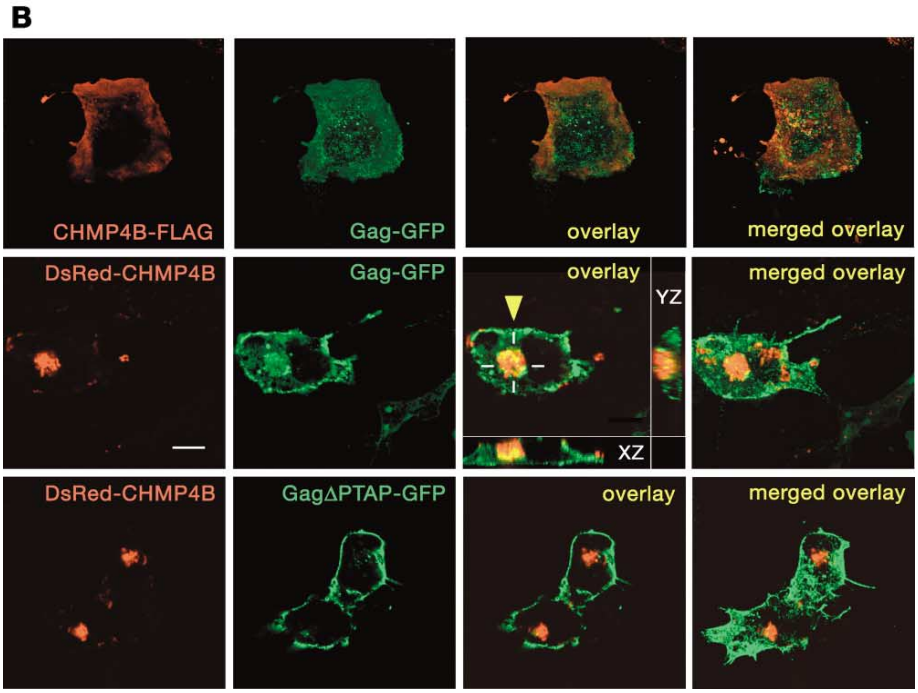

Figure 4. Virion Incorporation and HIV-1 Gag Redistribution to Class E Compartments

(A) Cellular and HIV-1-associated proteins detected by Ponceau S staining (upper left blot) and Western blotting with the indicated antibodies. Lanes labeled "cells" correspond to extracts from 10^5 uninfected MT4 cells (positive control), lanes labeled "CA" correspond to 1 μg pure CA (negative and loading control). Lanes labeled virions 1–3 correspond to independent preparations of purified HIV-1 particles (1 μg CA equivalent), sample 2* was treated with subtilisin. Recombinant $AIP_{1–716}$ and VPS4B protein standards are also shown. Full-length AIP1 protein (arrowhead) is 868 amino acids long, and the presence of multiple bands in the cell and virion lanes presumably reflects multiple protein isoforms, posttranslational modification, degradation products, and/or crossreacting proteins.

(B) Confocal fluorescence microscopic images showing the distribution of CHMP4B (first column, red) and Gag-GFP or GagΔPTAP-GFP (second column, green) in cells expressing CHMP4B-FLAG (top row, negative control) or dominant-negative DsRed-CHMP4B (middle and lower rows). Overlaid red and green images at right show colocalization at the class E compartment of DsRed-CHMP4B with Gag-GFP (yellow arrow). White cross bars mark the directions of the reslicing done in the XZ (bottom inset) and YZ planes (right inset). Single Z-sections are shown in the first three columns, and merged Z-stacks ("merged overlay") are shown in the fourth. Scale bar is 10 μm.

ing HIV-1. As shown above, AIP1 binds directly to TSG101, which in turn binds the $_7$PTAP$_{10}$ late domain of HIV-1 p6^{Gag} and facilitates virus budding. Moreover, Göttlinger and coworkers now report that AIP1 can bind directly to a downstream $_{41}$LRSL$_{44}$ motif within p6 (Strack et al., 2003). We have confirmed their observation and shown that both conserved leucines are required for full affinity AIP1 binding (Supplemental Figure S2B available on *Cell* website). It is therefore likely that Gag forms a ternary complex with both TSG101 and AIP1 during viral

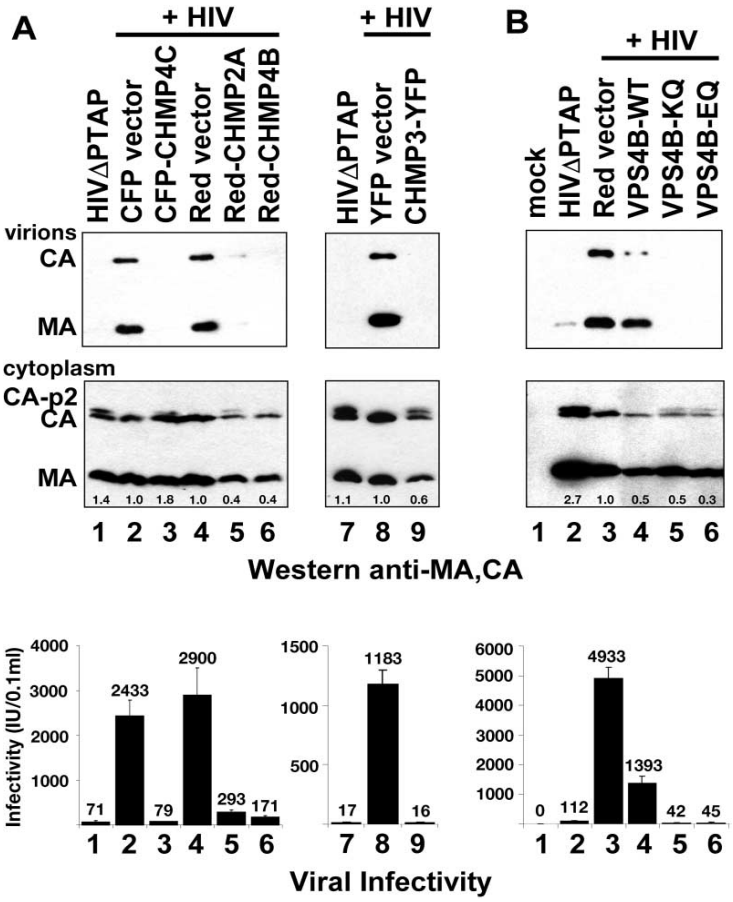

Figure 5. HIV-1 Release and Infectivity Are Inhibited by Dominant-Negative CHMP and VPS4B Proteins

Analyses of HIV-1 Gag protein expression (Western blot, middle image), virion release (top image), and viral infectivity (lower image) in the presence of the dominant-negative CHMP and VPS4B proteins: (A) CFP-CHMP4C, DsRed-CHMP4B, DsRed-CHMP2A or CHMP-YFP and (B) mutant VPS4B proteins. Levels of cytoplasmic Gag proteins relative to the relevant controls were determined by integrating the CA and MA band intensities in lighter exposures (numbers given at bottom of the blot). Note the characteristic late defect in intracellular processing of the CA-p2 protein seen in all cases where virus release is inhibited. Viral titers were determined in single-cycle MAGI infectivity assays of supernatants from transfected cells (blue cells/0.1 ml supernatant).

budding. However, mutations that disrupt the TSG101/Gag interaction typically inhibit HIV-1 release to a much greater extent than do mutations that disrupt the AIP1/Gag interaction, indicating that the class E proteins are probably recruited primarily through the TSG101/Gag interaction (Demirov et al., 2002b; Göttlinger et al., 1991).

It has also been suggested that AIP1 may bind to the YPDL late domain found in the p9 domain of the equine infectious anemia virus (EIAV) Gag (Vincent et al., 2003). Although AP-2 was initially described as a cellular binding partner for the YPDL late domain (Puffer et al., 1998), this has been puzzling because AP-2 functions primarily in endocytosis rather than MVB formation. More recently, however, AIP1 has been proposed as an alternative binding partner for the EIAV late domain because AIP1 orthologs from several organisms can bind YPXL sequences (Vincent et al., 2003). We therefore tested whether AIP1 and EIAV-p9 could form a complex in vitro. As shown in Figure 3A (lane 9), $AIP1_{1–716}$ bound GST-p9 and this interaction was specific for the $p9_{23}YPDL_{26}$ late domain motif, because binding was abolished (lane 10) by a mutation of the central proline residue (P24A) that also inhibits EIAV release (Puffer et al., 1997). Thus, AIP1 can bind both HIV-1 p6 and EIAV p9, indicating that both viruses enter the mammalian class E protein network, at least in part, through direct interactions with AIP1.

CHMP Proteins Bind VPS4 Proteins

Yeast two-hybrid interactions linked many of the ESCRT-III/CHMP proteins to the two human VPS4 proteins, and we therefore tested whether recombinant VPS4 and CHMP proteins could interact directly. As shown in Figure 3C, pure recombinant mammalian VPS4A and VPS4B proteins bound to GST-CHMP1B (lanes 6 and 7) and GST-CHMP2A (lanes 9 and 10) but not to GST alone (lanes 3 and 4). Analogous VPS4 binding interactions were also seen for the two other CHMP proteins tested (CHMP4B and CHMP6, data not shown). These observations imply that, as in yeast (Babst et al., 2002a), the mammalian VPS4 enzymes likely act directly on the subunits of the CHMP protein lattice.

HIV-1 Packaging and Gag Colocalization of Human Class E Proteins

Cellular factors that participate in viral budding may be packaged into virions, and we have previously shown that the ESCRT-I proteins TSG101 and VPS28 are specifically packaged into HIV-1 virions (J.E. Garrus, K.M. Stray, B.M., H.-G.K., and W.I.S., unpublished data). Proteins that act later in the MVB pathway have not yet been tested for virion incorporation, however. We therefore analyzed purified HIV-1 particles from acutely infected human MT4 cells for the presence of AIP1, CHMP1A,

CHMP2A, VPS4A, and VPS4B. The purity of the virion preparations was evaluated on silver stained SDS-gels (not shown) and by Western blotting, which revealed no detectable contamination with a series of cellular proteins such as the abundant 14-3-3 protein (Figure 4A, bottom right and data not shown; see also Muller et al., 2002).

All of the proteins tested were readily detected in cell extracts (Figure 4A and data not shown). However, only AIP1 and VPS4B were present in multiple independent preparations of HIV-1 particles, with a significantly stronger signal for AIP1 (Figure 4A, lanes labeled virions 1, 2*, and 3). Subtilisin treatment, which degrades proteins on the virion exterior (Ott et al., 2000), did not significantly reduce the AIP1 or VPS4B signals (lanes labeled virions 2*), indicating that these proteins were located inside the viral particles. Absolute levels of virion-associated proteins were estimated by comparing virus-associated CA, AIP1, and VPS4B proteins against known quantities of recombinant proteins. 5–10 ng of AIP1 and 0.1–0.5 ng of VPS4B per μg of CA were detected. Assuming that there are ~5000 Gag molecules per virion (V. Vogt, personal communication), this implies that, on average, 3–12.5 molecules of AIP1 and 0.5–2.5 molecules VPS4B were incorporated into each viral particle.

The PTAP Late Domain Helps Target HIV-1 Gag to Mammalian Class E Compartments

In most cell lines, HIV-1 Gag is released primarily from the plasma membrane, whereas in macrophages the virus buds directly into MVB/late endosomal compartments (Pelchen-Matthews et al., 2003; Raposo et al., 2002). These two observations can be unified by a model in which: (1) Gag is targeted to the late endosome through interactions with the class E proteins; (2) Gag then traffics to the plasma membrane via an endosomal pathway; and (3) viral budding can occur at different stages along this pathway depending on the cell type. This model suggests that HIV-1 Gag may accumulate on endosomal membranes upon arrest of MVB formation, as is the case for the class E proteins themselves (see Supplemental Figure S3 available on *Cell* website).

To test this idea, we examined whether dominant-negative CHMP4B and VPS4B proteins altered HIV-1 Gag-GFP localization. A dominant-negative (DN) VPS4B protein was created by mutating residues required for ATP binding (K180Q) or hydrolysis (E235Q) (see also Fujita et al., 2003), and a dominant-negative CHMP4B protein was created by fusing DsRed to the protein's N terminus (Howard et al., 2001). The expected class E phenotypes induced by expression of VPS4B-K180Q, VPS4B-E235Q, and DsRed-CHMP4B were confirmed in a series of control experiments showing that: (1) the DN VPS4B proteins inhibited ligand-induced lysosomal degradation of surface MHC-I and EGFR proteins (Supplemental Figure S3A–S3F available on *Cell* website); (2) the DN VPS4B and CHMP4B proteins induced formation of aberrantly enlarged, vacuolated "mammalian class E" compartments that stained positive for both lysosomal and endosomal markers (Supplemental Figure S4 available on *Cell* website); and (3) the soluble, nondominant-negative CHMP4B-FLAG protein relocalized to the class E compartments induced by expression of the DN VPS4-E235Q protein (Supplemental Figure S4 available on *Cell* website).

Gag-GFP redistributed significantly from the plasma membrane/cell periphery into class E compartments upon expression of either DsRed-CHMP4B (Figure 4B) or VPS4B-E235Q (data not shown). Similar results were obtained for dominant-negative versions of the CHMP2A and VPS4A proteins (data not shown). Moreover, the degree to which Gag-GFP redistributed apparently depended upon TSG101 binding to Gag, as colocalization of wt Gag-GFP/DsRed-CHMP4B was observed in 68% of the cells examined ($n = 19$), whereas colocalization of mutant GagΔPTAP-GFP/DsRed-CHMP4B was uncommon (18%, $n = 48$; Figure 4B, bottom image). Our data therefore support a model in which nonfunctional CHMP and VPS4 proteins cause Gag proteins to accumulate together with TSG101 and other trapped class E proteins on the surface of aberrant late endosomal compartments.

Dominant-Negative CHMP and VPS4B Proteins Block HIV-1 Release and Infectivity

The functional involvement of the CHMP and VPS4B proteins in HIV-1 release was also tested using dominant-negative proteins. A DN CHMP1A protein can be created by fusing large polypeptides to the protein's C terminus (Howard et al., 2001). We found, however, that many such CHMP fusion constructs were cytotoxic and reduced Gag protein expression. We therefore surveyed a series of 25 N- and C-terminal CHMP fusion proteins for the ability to inhibit virus release without strongly reducing Gag expression (see Supplemental Table S2 available on *Cell* website).

As shown in Figure 5A, HIV-1 release was dramatically inhibited by coexpression with CFP-CHMP4C, DsRed-CHMP2A, DsRed-CHMP4B, and CHMP3-YFP. Virus release was analyzed by: (1) Western blot detection of virion-associated MA and CA proteins released by cells expressing HIV-1 (upper images), and (2) reductions of viral titers in single cycle MAGI assays (lower images). Intracellular Gag protein expression was analyzed by Western blot detection of cytoplasmic MA and CA proteins (middle images). Controls for these experiments included the appropriate empty vectors (negative controls) and HIVΔPTAP mutants (positive controls for arrested HIV-1 budding).

The most dramatic effects were observed for the CFP-CHMP4C construct, which did not alter cellular Gag expression levels, but reduced virus release to nearly undetectable levels in the Western blot assay and reduced the release of infectious virus more than 30-fold. DsRed-CHMP2A, DsRed-CHMP4B, and CHMP3-YFP also reduced viral infectivity significantly (10-, 17-, and 73-fold, respectively), albeit with modest reductions in Gag protein expression (2- to 3-fold).

Coexpression of the dominant-negative VPS4B proteins inhibited virus release >100-fold for both mutants (Figure 5B), although Gag expression levels were again reduced modestly (2- to 3-fold in the Western blot assay, middle image). In contrast, the wt VPS4B (negative control) produced a comparable 2-fold reduction in cellular Gag expression levels, but with no additional reduction

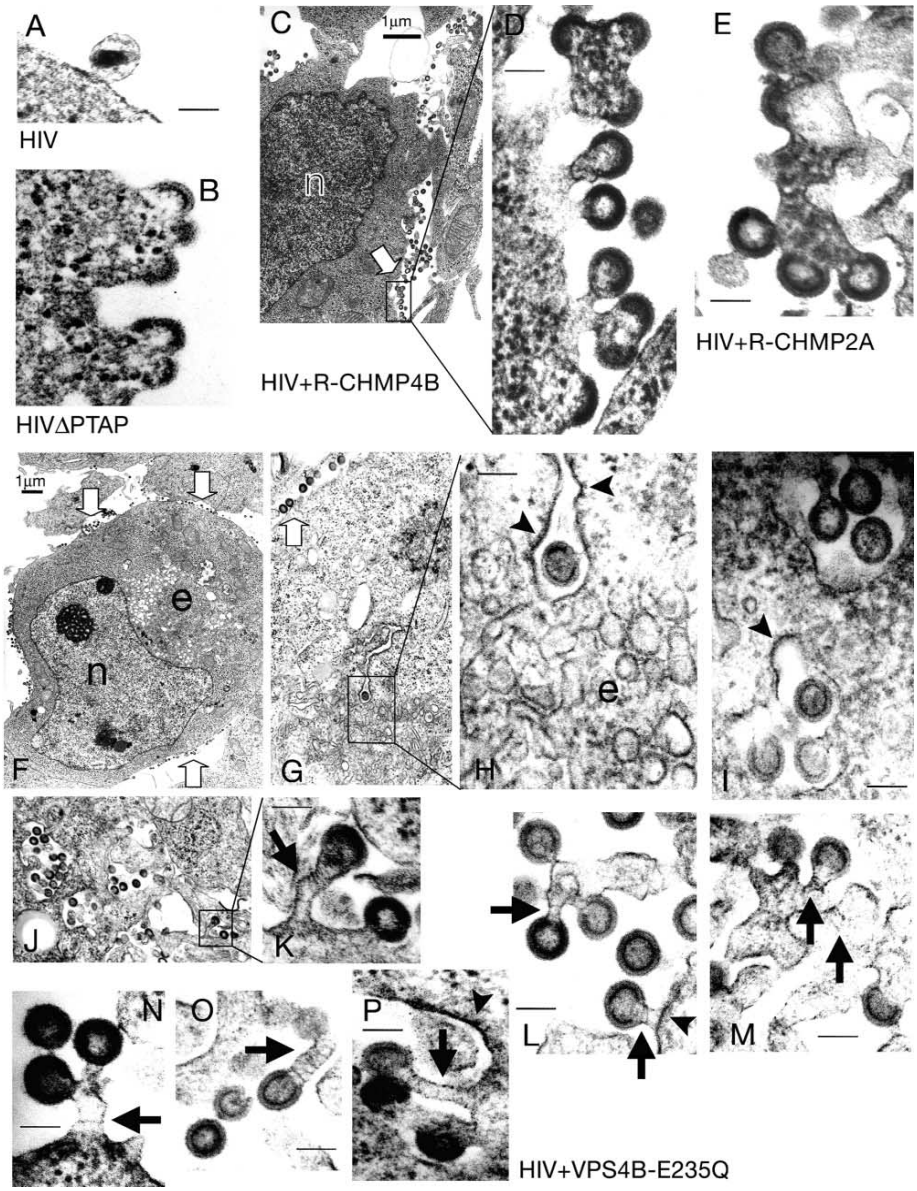

Figure 6. HIV-1 Budding Arrest Induced by Dominant-Negative CHMP and VPS4B Proteins

EM images of thin-sectioned 293T cells transfected with HIV alone (A), HIVΔPTAP (B), or HIV and dominant-negative DsRed-CHMP4B (C and D), DsRed-CHMP2A (E), or DsRed-VPS4B-E235Q (F–P). Thick scale bars are 1 μm; thin scale bars are 100 nm. Open arrows indicate virions arrested in budding at the plasma membrane; arrowheads indicate thickened protein coats on plasma or endosomal membranes; and black arrows indicate striations in the stalks of arrested virions. n: nucleus; e: highly vacuolated class E compartment.

in viral titer (3.5-fold). These data demonstrate that the dominant-negative CHMP and VPS4 proteins diminish particle release and infectivity very significantly, indicating that they likely play a functional role in HIV-1 release.

Dominant-Negative VPS4B and CHMP Proteins Arrest HIV-1 Budding at a Late Stage

Electron microscopy was used to determine the stage at which virus release was arrested by the dominant-negative CHMP2A, CHMP4B, and VPS4B proteins. Thin-sectioned 293T cells transfected with wt HIV-1 DNA alone displayed very few cell-associated virions, and these typically exhibited the conical viral cores that are the hallmark of the mature infectious virus (Figure 6A). In contrast, coexpression of HIV-1 with dominant-negative DsRed-CHMP2A, DsRed-CHMP4B, or VPS4B proteins caused viruses to arrest at a very late stage in assembly, in which extensive clusters of immature particles accu-

mulated at the plasma membrane but remained connected via membrane stalks (Figure 6, open arrows). This arrest resembled a late domain phenotype, except that Gag∆PTAP mutants frequently arrested at a somewhat earlier stage (often following membrane distortion, but prior to stalk formation; Figure 6B and see Garrus et al., 2001), suggesting that virus release may proceed through multiple stages and that the dominant-negative VPS4B, CHMP4B, and CHMP2A proteins inhibited a very late step(s) in release.

Cells coexpressing HIV-1 and VPS4B-E235Q proteins exhibited aberrant clusters of tubules and vacuoles that were not observed in control cells. These presumably corresponded to the class E compartments seen by fluorescence microscopy (Figures 6F–6H, labeled "e" and see Supplemental Figure S4 available on *Cell* website). Strikingly, we frequently observed HIV particles arrested in the process of budding into the vacuoles associated with these compartments (Figures 6G and 6H) as well as into other, smaller clusters of intracellular vacuoles (Figures 6I, 6J, and 6P). Viruses arrested while budding through intracellular and plasma membranes were morphologically indistinguishable, and we therefore conclude that VPS4B-E235Q imposes similar blocks at internal and external membranes.

The size and appearance of the internal compartments varied considerably, as did the morphologies of the arrested virions (e.g., in content and in stalk length and width). Nevertheless, there were two indications that cellular protein complexes might be functioning at the sites of viral budding. Firstly, we and others often observed a thickening of the cytoplasmic faces of membranes near sites of virus budding, which may correspond to the ESCRT-III protein coat (see Figures 6H, 6I, 6L and 6P, arrowheads) (Pelchen-Matthews et al., 2003). Secondly, ring-like striations were sometimes observed within the membrane stalks of viruses arrested by the dominant-negative VPS4B-E235Q protein (Figures 6K–6P, highlighted by black arrows). These striations were not observed for ∆PTAP viruses (which are presumably defective in recruiting TSG101 and other class E proteins and rarely showed narrow membrane stalks). We therefore speculate that the membrane coats and/or striations may represent trapped cellular machinery that might normally help to catalyze protein sorting, membrane fission, and/or virus release from wild-type cells.

Discussion

Our experiments define the human class E protein network and strongly support the idea that HIV-1 utilizes this entire network during viral egress (see Figure 7). Most importantly, HIV-1 release can be arrested at a late stage by deletion or mutation of at least 8 different human class E proteins, which function both early (TSG101, VPS28) (Garrus et al., 2001; Martin-Serrano et al., 2001, 2003), and late (CHMP2A, CHMP3, CHMP4B, CHMP4C, VPS4A, VPS4B) in the MVB pathway. In addition, HIV-1 particles package multiple copies of proteins that act both early (TSG101, VPS28), and later (AIP1) in the MVB pathway. They are also enriched in at least one protein that functions very late in the pathway (VPS4B),

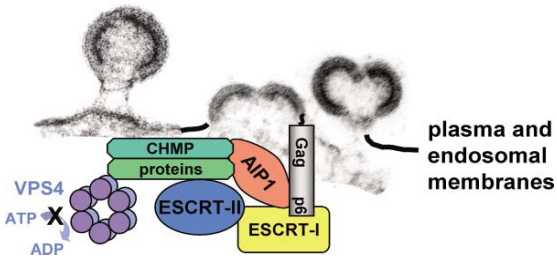

Figure 7. Schematic Model for the HIV-1 Budding Arrest Induced by Expression of Dominant-Negative VPS4 Proteins

The illustration emphasizes how nascent viral particles arrest together with class E protein complexes at both endosomal and plasma membranes when VPS4 proteins are unable to hydrolyze ATP (denoted by the black X). Proteins and complexes are color-coded as in Figure 1A. The figure is simplified in that oligomeric proteins are represented only once (e.g., Gag, TSG101, AIP1, and CHMP proteins), only the plasma membrane arrest is shown, and many temporal and spatial details of the illustrated interactions remain to be elucidated.

indicating that VPS4B acts near sites of viral assembly and release. Although additional studies will be required to understand HIV-1 release in molecular detail, the apparent requirement for more than 20 cellular proteins in this essential viral process provides many potential new targets for therapeutic intervention.

Our studies also begin to define the different roles of human class E proteins in MVB biogenesis. As in yeast, human CHMP6 appears to be recruited by the ESCRT-II complex, whereas the CHMP4 proteins are recruited by AIP1 (see Figures 1 and 7) (Babst et al., 2002b; Odorizzi et al., 2003). Importantly, we also found that TSG101 and AIP1 make a series of key interactions along the MVB pathway: HRS/TSG101→TSG101/EAP30,45; TSG101/AIP1→AIP1/CHMP4A-C that collectively link the human HRS, ESCRT I, II, and III complexes (Bache et al., 2003a; Pornillos et al., 2003, and this work).

It is striking that the UEV domain of TSG101 can bind to PTAP motifs found in three different proteins in the pathway (HRS, TSG101 itself, and AIP1) (Bache et al., 2003a; Katzmann et al., 2003; Lu et al., 2003; Pornillos et al., 2003) as well as in the HIV-1 $p6^{Gag}$ protein (Demirov et al., 2002a; Garrus et al., 2001; Martin-Serrano et al., 2001; VerPlank et al., 2001). TSG101 could, in principle, bind multiple partners simultaneously as it self-oligomerizes in two-hybrid assays (Figures 1A and 1C). Alternatively, TSG101 may bind sequentially to the different PTAP elements, producing conformational changes that could give directionality to the pathway. In either case, we speculate that viral protein binding to the recognition domains of TSG101 and AIP1 may serve not only to recruit the machinery of vesicle formation, but also to alter normal protein-protein interactions required during protein sorting and MVB vesicle formation. This could activate the vesicle fission machinery and/or allow viral proteins to substitute for cellular protein cargos.

Although it is not yet clear where HIV-1 Gag first meets (or recruits) the human class E proteins, the retroviral Moloney Murine Leukemia Gag protein traffics along endosomal membranes before appearing at the plasma

membrane (Basyuk et al., 2003). Moreover, several groups have demonstrated that in macrophages, HIV-1 buds primarily into intracellular compartments that correspond to multivesicular bodies (Pelchen-Matthews et al., 2003; Raposo et al., 2002). Our studies also support a role for endosomal compartments in both Gag trafficking and virus budding. Specifically, we find that even in nonmacrophage lineages (293T cells), where viruses seem to bud predominantly from the plasma membrane, induction of a class E phenotype causes HIV-1 Gag to concentrate and arrest while budding into class E compartments.

Intracellular budding is particularly noticeable under class E conditions because arrested viral particles accumulate on membranes, and possibly also because the trapped class E proteins may recruit Gag more efficiently than in wild-type cells (where the class E proteins are predominantly cytosolic). Nevertheless, we and others (Sherer et al., 2003; M. Thali, personal communication) have observed intracellular HIV-1 budding even in wild-type 293T cells, particularly with the HIVΔPTAP mutant (which again facilitates visualization because the viruses arrest while budding). Conversely, we (and many others) have observed wt virus in the process of budding directly from the plasma membranes of 293T and HeLa cells (e.g., see Supplemental Figure S5 available on *Cell* website). It therefore appears that HIV-1 can bud into both internal endosomal and plasma membranes, and the degree to which the alternate sites are utilized in different cell types may simply reflect differences in the relative rates of virus budding versus Gag trafficking to the plasma membrane. Importantly, virions that bud into intracellular compartments can still emerge from the cell via the exosome pathway, i.e., when the limiting MVB membranes fuse with the plasma membrane and release their vesicles (or viruses) as exosomes (Denzer et al., 2000; Pornillos et al., 2002c; Raposo et al., 2002). The parallels between exosomes and viruses are further emphasized by the fact that AIP1 and TSG101, as well as MLV Gag proteins, are found in preparations of murine exosomes (Thery et al., 2001). A full discussion of the potential relationships between exosomes and viruses is given in Gould et al. (2003).

It will be of interest to understand what factors influence where the virus buds, how Gag traffics via the endosomal network to the plasma membrane, and whether viruses can control these events. These issues could impact viral pathogenesis because endosomal pathways could be used to promote directional release (e.g., see Igakura et al., 2003; McDonald et al., 2003) and because the primary sites of virus release likely change during AIDS disease progression as the tropism of the virus evolves from macrophages (internal budding) to T cells (plasma membrane budding).

A final important finding implied by this and related work is that multiple different classes of enveloped viruses exit cells via the same MVB pathway. In support of this idea, two human class E proteins (AIP1 and TSG101) bind directly to structural proteins from two different viruses (HIV-1 p6/TSG101/AIP1 and EIAV p9/AIP1) and link them directly into the MVB pathway. Moreover, a dominant-negative VPS4A protein that induces a class E phenotype blocks the release of viruses that bud via all known late domains (PTAP, PPXY, YPDL, and/or LXXL) (Garrus et al., 2001; Martin-Serrano et al., 2003).

In conclusion, multiple classes of enveloped viruses utilize the unique budding topology of MVB vesicles as a nonlytic mechanism for escaping cells. Here, we have identified an extensive network of human proteins involved in both cellular protein trafficking and virus release, setting the stage for understanding how these proteins help catalyze protein sorting, membrane deformation, and fission from the cytoplasmic face of a budding vesicle or virus.

Experimental Procedures

Yeast Two-Hybrid Experiments

Directed two-hybrid assays with full-length human class E genes (Supplemental Table S1 available at *Cell* website) were performed using the Matchmaker GAL4 Yeast Two-Hybrid 3 system (Clontech). Library screening was performed as described (Garrus et al., 2001), with eleven different TSG101 and four different CHMP6 baits screened against 3-11 $\times$ 10^6 activation domain (AD) fusions derived from human spleen, brain, and macrophage cDNA libraries.

Two-hybrid interactions were tested in -Leu, -Trp, -Ade, -His, X-α-gal (50 μg/mL) plate assays (Figure 1C) or in semiquantitative liquid culture β-galactosidase activity assays (Figure 1B). In liquid assays, yeast transformants were picked and grown in 100 μl (-Leu, -Trp) SD media in 96 well flat-bottomed plates to an average A_{610} of $\sim$0.4. Resorufin β-D-galactopyranoside (RDG) assay solutions were 1:1 mixtures of: (1) 25 mM PIPES, [pH 7.2]; 10 mM RDG, and (2) 250 mM PIPES, [pH 7.2]; 10% NP-40; 0.24 Units/ml lyticase. 20 μl of the RDG mix was added to each well, and fluorescence was measured after 0 and 1–2 hr of incubation at 37°C (SpectraMAX GeminiXS, Molecular Devices, Inc. Sunnyvale, CA; excitation at 566 nm, emission at 628 nm, with a 610 nm cutoff filter).

Protein Expression and Purification

Expression Constructs

The EIAV p9 gene was PCR-amplified as an NdeI–BamHI-fragment from a proviral $EIAV_{UK}$ plasmid (a gift from Frank Cook, University of Kentucky) (Cook et al., 1998). Other genes were amplified by PCR (with the first 5 codons optimized for *E. coli* expression) from templates listed in Supplemental Table S1 (available on *Cell* website). Genes were subcloned into the NdeI/BamHI sites of a modified pGEX2T vector (WISP01-69, for GST fusion proteins) or pET11a (Novagene, for $AIP1_{1–716}$) and verified by sequencing. $AIP1_{1–716}$ lacked the proline-rich region, which hindered expression of full-length AIP1. Mutations were introduced by PCR megaprimer mutagenesis.

Protein Expression

BL21(DE3) *E. coli* cells were grown to mid log, induced with 0.5 mM IPTG, and recombinant proteins were allowed to accumulate for 2–4 hr (23°C). Cells were harvested, lysed using lysozyme (10 μg/l culture) and sonication, and insoluble material was removed by centrifugation (30 min at 25,000 $\times$ g).

GST fusion proteins were purified by glutathione affinity chromatography, cleaved to remove glutathione, and repurified by conventional chromatography (Pornillos et al., 2002a). Untagged $AIP1_{1–716}$ was precipitated with 55% saturated ammonium sulfate after a 27% precut, redissolved in 25 mM MOPS [pH 7.0], 5 mM β-ME, and purified by Q-Sepharose chromatography (Amersham Pharmacia; elution at $\sim$250 mM NaCl from a linear gradient of 0–1 M over 400 mL). Fractions containing $AIP1_{1–716}$ were pooled, adjusted to 1 M ammonium sulfate, and purified by phenyl-Sepharose chromatography (Amersham Pharmacia; pure $AIP1_{1–716}$ eluted at $\sim$80 mM ammonium sulfate from a linear gradient of 1–0 M over 200 ml). Mass spectrometry confirmed the identity of $AIP_{1–716}$ (minus the N-terminal methionine). Yields were typically 20 mg $AIP_{1–716}$ per liter culture. The expression and purification of human VPS4 proteins will be described elsewhere (A.S., F.G. Whitby, W.I.S., and C.P. Hill, unpublished data).

Protein Interactions

Biosensor Measurements

Binding affinities of pure Tsg101 UEV domains to immobilized GST-AIP1$_{714–723}$ (AREPSAPSIP) were quantified using a Biacore biosensor (20°C in 20 mM sodium phosphate, 150 mM NaCl, 0.01% P20, 50 μg/mL BSA, [pH 7.2]) (Garrus et al., 2001).

GST Affinity Cochromatography

GST-CHMP fusion proteins used in affinity cochromatography (pull-down) assays (Figure 3) were expressed from pGEX vectors in BL21(DE3) *E. coli*, prebound to glutathione agarose (Amersham-Pharmacia), and tested for binding to AIP1$_{1–716,}$ VPS4A, or VPS4B following manufacturer's instructions.

Immunoprecipitations

293T cells (10 cm plate) were cotransfected (Lipofectamine 2000, Invitrogen) with 6 μg pcAIP1-Myc expression vector (see below) and 6 μg CHMP4B-FLAG or control vector (modified from pcDNA3.1). Cells were harvested (24 hr), lysed for 30 min on ice in 20 mM Tris·HCl [pH 7.4], 150 mM NaCl, 0.5% NP-40, with 2 μM pepstatin, 1 mM PMSF, 10 μg/mL leupeptin, 5 μg/mL aprotinin, and clarified by centrifugation (16,000 × g for 30 min). Lysate (1 mg total protein) was incubated (3 hr, 4°C) with 1 μg of anti-FLAG antibody (M2, Sigma) and antimouse IgG rabbit antibody (Zymed) conjugated to Protein A Sepharose (Amersham Bioscience). Unbound proteins were removed by washing with lysis buffer, and bound proteins analyzed by Western blotting with anti-FLAG (1:5000; Sigma M2) or anti-Myc antibodies (clone 9E10, 1:1000, Covance Inc.).

Antibody Production

Antibodies to recombinant AIP1$_{1–716}$ (sera UT324 + UT325), CHMP2A (UT318), VPS4A (UT289), and VPS4B (UT292) were raised in New Zealand White Rabbits (Covance Inc.). Affinity columns were prepared with 1 mg of purified GST fusion proteins coupled to NHS-activated crosslinked agarose (1 ml HiTrapTM NHS-activated HP column, Amersham Biosciences) following manufacturer's instructions. Antiserum (1 mL) was applied to PBS-equilibrated columns, incubated (1 hr, 23°C), and washed with 10 ml PBS. Bound antibody was eluted in 50 mM glycine, 150 mM NaCl, [pH 2.5], neutralized immediately by addition of 0.2 M Tris·HCl, [pH 8.0], concentrated using Vivaspin 0.5 ml concentrators (Vivascience) and dialyzed against PBS. Anti-CHMP1A was a gift from Dan Stauffer.

Detection of Proteins Incorporated into HIV-1 Particles

Human MT4 cells were infected with HIV-1$_{NL4-3}$ by coculture as described previously (Welker et al., 2000). Culture medium was harvested and virus purified by pelleting through a 20% (w/w) sucrose cushion followed by velocity centrifugation through an iodixanol gradient (Dettenhofer and Yu, 1999) and concentration by ultracentrifugation. Subtilisin treatment was performed on virus preparation 2 following the initial 20% sucrose cushion (Ott et al., 2000). For Western blots, virus particles corresponding to 1 μg CA (adjusted by comparison with purified recombinant CA protein) (Gross et al., 1997) were separated by 15% SDS-PAGE (acrylamide:bisacrylamide 200:1) and compared to 1 μg recombinant CA (negative and loading control) and to extracts from 10^5 uninfected MT4 cells. Proteins were transferred to nitrocellulose and detected by ECL using Super Signal West Pico (Pierce) according to manufacturer's instructions. Primary antibodies used were affinity purified anti-VPS4B (1:500) and anti-AIP1 (1:250) sera, or polyclonal anti-14-3-3γ (C-16, Santa Cruz Biotechnology; 1:1000), respectively.

Mammalian Expression Constructs

For DsRed-VPS4B expression, DNA encoding VPS4B was amplified from pGEX-VPS4B by PCR and cloned into the EcoRI/BamHI sites of pDsRed2-C1 (Clontech). VPS4B mutations were introduced by PCR megaprimer mutagenesis, with mutant primers introducing a KpnI site (K180Q) or ClaI site (E235Q), respectively. CHMP genes were cloned into the same sites of pDsRed-C1, pDsRed-N1, pEGFP-C1, pCFP-C1, and/or pYFP-N1 (Clontech), and in pcDNA3.1(−)/Myc-HisA (Invitrogen) either with C-terminal FLAG tags or as fusions with the vector Myc tags (see Supplemental Table S2 available on *Cell* website). AIP1 was cloned into pcDNA3.1(−)/Myc-His. Full cloning details are available upon request. Expression vectors for HIV-1$_{NL4-3}$ (R9 and R9ΔPTAP), Gag-GFP (a gift from Marilyn Resh), and GagΔ-PTAP-GFP have been described (Garrus et al., 2001; Hermida-Matsumoto and Resh, 2000)

Immunofluorescence

COS-7 cells growing on glass cover slips in 60 mm dishes (in DMEM/10% FBS) were transfected with 2 μg plasmid DNA and 12 μl GeneJammer (Stratagene) as per manufacturer's instructions. Twenty-four hr posttransfection, cells were fixed in 3.7% formaldehyde/PBS and permeabilized in 0.1% Triton X-100/PBS/1%BSA. Cells were incubated with either rabbit anti-M6PR (1:200, from Peter Lobel) or mouse anti-Lamp-2 (1:200, Developmental Hybridoma) at 23°C for 60 min. Samples were washed and incubated with goat antirabbit or antimouse Alexa 488-conjugated antibodies (1:750, Molecular Probes). FLAG-tagged CHMP4 proteins were detected using Alexa 488-or Alexa 594-congugated anti-FLAG (1:750, Sigma M2). Images were collected as single wavelengths on an Olympus FVX confocal fluorescent microscope with a 60× Pianapo objective (1.4 NA oil), using Fluoview 2.0.39 software. 0.5 μm thick Z sections or merged Z stacks are shown. Reslicing and three-dimensional representation of Z sections were created with Volocity imaging software (Improvision).

HIV Protein Expression in 293T Cells

For Western blots of Gag expression, infectivity assays and EM, 293T cells in 6-well plates were transfected with 9 μl Lipofectamine 2000 (Invitrogen) per 2 μg HIV-R9 + 1 μg other expression vectors per well as described (Garrus et al., 2001).

Gag Western Blots and Viral Replication Assays

Cytoplasmic proteins and sucrose-pelleted virions (Figure 5) were harvested 36 hr after transfection, resolved by 12% SDS-PAGE, blotted, and detected by ECL as described (von Schwedler et al., 1998). Primary antibodies were rabbit anti-CA #40 at 1:2000 and rabbit anti-MA at 1:20,000. HIV infectious titers were assayed by MAGI assays in P4 cells (von Schwedler et al., 1998).

Electron Microscopy

For EM studies, transfected 293T cells were fixed, stained, and embedded in Spurr's plastic 48 hr after transfection (Garrus et al., 2001), and EM images were obtained at magnifications of 5000–150,000×.

Acknowledgments

We thank Cynthia Lodding, Mimi Payne, Collin Kieffer, and Sanaz Ghaffarian for cloning and technical assistance; David Myszka and the University of Utah Protein Interactions facility for Biacore biosensor measurements; Chris Rodesh for confocal microscope training; and Mark Marsh and Heinrich Göttlinger for sharing their unpublished manuscripts. This work was supported by NIH grants to W.I.S. and J.K.

Received: May 13, 2003
Revised: August 22, 2003
Accepted: August 25, 2003
Published: September 18, 2003

References

Asao, H., Sasaki, Y., Arita, T., Tanaka, N., Endo, K., Kasai, H., Takeshita, T., Endo, Y., Fujita, T., and Sugamura, K. (1997). Hrs is associated with STAM, a signal-transducing adaptor molecule. Its suppressive effect on cytokine-induced cell growth. J. Biol. Chem. *272*, 32785–32791.

Babst, M., Odorizzi, G., Estepa, E.J., and Emr, S.D. (2000). Mammalian tumor susceptibility gene 101 (TSG101) and the yeast homologue, Vps23p, both function in late endosomal trafficking. Traffic *1*, 248–258.

Babst, M., Katzmann, D., Estepa-Sabal, E., Meerloo, T., and Emr, S. (2002a). Escrt-III: an endosome-associated heterooligomeric protein complex required for mvb sorting. Dev. Cell *3*, 271–282.

Babst, M., Katzmann, D., Snyder, W., Wendland, B., and Emr, S. (2002b). Endosome-associated complex, ESCRT-II, recruits trans-

port machinery for protein sorting at the multivesicular body. Dev. Cell *3*, 283–289.

Bache, K.G., Brech, A., Mehlum, A., and Stenmark, H. (2003a). Hrs regulates multivesicular body formation via ESCRT recruitment to endosomes. J. Cell Biol. *162*, 435–442.

Bache, K.G., Raiborg, C., Mehlum, A., and Stenmark, H. (2003b). STAM and Hrs are subunits of a multivalent ubiquitin-binding complex on early endosomes. J. Biol. Chem. *278*, 12513–12521.

Basyuk, E., Galli, T., Mougel, M., Blanchard, J.M., Sitbon, M., and Bertrand, E. (2003). Retroviral genomic RNAs are transported to the plasma membrane by endosomal vesicles. Dev. Cell *5*, 161–174.

Biscone, M.J., Pierson, T.C., and Doms, R.W. (2002). Opportunities and challenges in targeting HIV entry. Curr. Opin. Pharmacol. *2*, 529–533.

Bishop, N., and Woodman, P. (2001). TSG101/mammalian VPS23 and mammalian VPS28 interact directly and are recruited to VPS4-induced endosomes. J. Biol. Chem. *276*, 11735–11742.

Bishop, N., Horman, A., and Woodman, P. (2002). Mammalian class E vps proteins recognize ubiquitin and act in the removal of endosomal protein-ubiquitin conjugates. J. Cell Biol. *157*, 91–101.

Chatellard-Causse, C., Blot, B., Cristina, N., Torch, S., Missotten, M., and Sadoul, R. (2002). Alix (ALG-2-interacting protein X), a protein involved in apoptosis, binds to endophilins and induces cytoplasmic vacuolization. J. Biol. Chem. *277*, 29108–29115.

Cook, R.F., Leroux, C., Cook, S.J., Berger, S.L., Lichtenstein, D.L., Ghabrial, N.N., Montelaro, R.C., and Issel, C.J. (1998). Development and characterization of an in vivo pathogenic molecular clone of equine infectious anemia virus. J. Virol. *72*, 1383–1393.

Demirov, D.G., Ono, A., Orenstein, J.M., and Freed, E.O. (2002a). Overexpression of the N-terminal domain of TSG101 inhibits HIV-1 budding by blocking late domain function. Proc. Natl. Acad. Sci. USA *99*, 955–960.

Demirov, D.G., Orenstein, J.M., and Freed, E.O. (2002b). The late domain of human immunodeficiency virus type 1 p6 promotes virus release in a cell type-dependent manner. J. Virol. *76*, 105–117.

Denzer, K., Kleijmeer, M.J., Heijnen, H.F., Stoorvogel, W., and Geuze, H.J. (2000). Exosome: from internal vesicle of the multivesicular body to intercellular signaling device. J. Cell Sci. *113*, 3365–3374.

Dettenhofer, M., and Yu, X.F. (1999). Highly purified human immunodeficiency virus type 1 reveals a virtual absence of Vif in virions. J. Virol. *73*, 1460–1467.

Freed, E.O. (2002). Viral late domains. J. Virol. *76*, 4679–4687.

Fujita, H., Yamanaka, M., Imamura, K., Tanaka, Y., Nara, A., Yoshimori, T., Yokota, S., and Himeno, M. (2003). A dominant negative form of the AAA ATPase SKD1/VPS4 impairs membrane trafficking out of endosomal/lysosomal compartments: class E vps phenotype in mammalian cells. J. Cell Sci. *116*, 401–414.

Garrus, J.E., von Schwedler, U.K., Pornillos, O.W., Morham, S.G., Zavitz, K.H., Wang, H.E., Wettstein, D.A., Stray, K.M., Cote, M., Rich, R.L., et al. (2001). Tsg101 and the vacuolar protein sorting pathway are essential for HIV-1 budding. Cell *107*, 55–65.

Göttlinger, H.G., Dorfman, T., Sodroski, J.G., and Haseltine, W.A. (1991). Effect of mutations affecting the p6 gag protein on human immunodeficiency virus particle release. Proc. Natl. Acad. Sci. USA *88*, 3195–3199.

Gould, S.J., Booth, A.M., and Hildreth, J.E.K. (2003). The Trojan exosome hypothesis. Proc. Natl. Acad. Sci. USA *100*, 10592–10597.

Gross, I., Hohenberg, H., and Krausslich, H.G. (1997). In vitro assembly properties of purified bacterially expressed capsid proteins of human immunodeficiency virus. Eur. J. Biochem. *249*, 592–600.

Hermida-Matsumoto, L., and Resh, M.D. (2000). Localization of human immunodeficiency virus type 1 Gag and Env at the plasma membrane by confocal imaging. J. Virol. *74*, 8670–8679.

Howard, T.L., Stauffer, D.R., Degnin, C.R., and Hollenberg, S.M. (2001). CHMP1 functions as a member of a newly defined family of vesicle trafficking proteins. J. Cell Sci. *114*, 2395–2404.

Igakura, T., Stinchcombe, J.C., Goon, P.K., Taylor, G.P., Weber, J.N., Griffiths, G.M., Tanaka, Y., Osame, M., and Bangham, C.R. (2003). Spread of HTLV-I between lymphocytes by virus-induced polarization of the cytoskeleton. Science *299*, 1713–1716.

Kamura, T., Burian, D., Khalili, H., Schmidt, S.L., Sato, S., Liu, W.J., Conrad, M.N., Conaway, R.C., Conaway, J.W., and Shilatifard, A. (2001). Cloning and characterization of ELL-associated proteins EAP45 and EAP20. A role for yeast EAP-like proteins in regulation of gene expression by glucose. J. Biol. Chem. *276*, 16528–16533.

Katzmann, D.J., Odorizzi, G., and Emr, S.D. (2002). Receptor down-regulation and multivesicular-body sorting. Nat. Rev. Mol. Cell Biol. *3*, 893–905.

Katzmann, D.J., Stefan, C.J., Babst, M., and Emr, S.D. (2003). Vps27 recruits ESCRT machinery to endosomes during MVB sorting. J. Cell Biol. *162*, 413–423.

Licata, J.M., Simpson-Holley, M., Wright, N.T., Han, Z., Paragas, J., and Harty, R.N. (2003). Overlapping motifs (PTAP and PPEY) within the Ebola virus VP40 protein function independently as late budding domains: involvement of host proteins TSG101 and VPS-4. J. Virol. *77*, 1812–1819.

Lu, Q., Hope, L.W., Brasch, M., Reinhard, C., and Cohen, S.N. (2003). TSG101 interaction with HRS mediates endosomal trafficking and receptor down-regulation. Proc. Natl. Acad. Sci. USA *100*, 7626–7631.

Martin-Serrano, J., Zang, T., and Bieniasz, P.D. (2001). HIV-1 and Ebola virus encode small peptide motifs that recruit Tsg101 to sites of particle assembly to facilitate egress. Nat. Med. *7*, 1313–1319.

Martin-Serrano, J., Zang, T., and Bieniasz, P.D. (2003). Role of ESCRT-I in retroviral budding. J. Virol. *77*, 4794–4804.

McDonald, D., Wu, L., Bohks, S.M., KewalRamani, V.N., Unutmaz, D., and Hope, T.J. (2003). Recruitment of HIV and its receptors to dendritic cell-T cell junctions. Science *300*, 1295–1297.

Muller, B., Patschinsky, T., and Krausslich, H.G. (2002). The late-domain-containing protein p6 is the predominant phosphoprotein of human immunodeficiency virus type 1 particles. J. Virol. *76*, 1015–1024.

Odorizzi, G., Katzmann, D.J., Babst, M., Audhya, A., and Emr, S.D. (2003). Bro1 is an endosome-associated protein that functions in the MVB pathway in Saccharomyces cerevisiae. J. Cell Sci. *116*, 1893–1903.

Ott, D.E., Coren, L.V., Johnson, D.G., Kane, B.P., Sowder, R.C., 2nd, Kim, Y.D., Fisher, R.J., Zhou, X.Z., Lu, K.P., and Henderson, L.E. (2000). Actin-binding cellular proteins inside human immunodeficiency virus type 1. Virology *266*, 42–51.

Pelchen-Matthews, A., Kramer, B., and Marsh, M. (2003). Infectious HIV-1 assembles in late endosomes in primary macrophages. J. Cell Biol. *162*, 443–455.

Pornillos, O., Alam, S., Rich, R.L., Myszka, D.G., Davis, D.R., and Sundquist, W.I. (2002a). Structure and functional interactions of the Tsg101 UEV domain. EMBO J. *21*, 2397–2406.

Pornillos, O., Alam, S.L., Davis, D.R., and Sundquist, W.I. (2002b). Structure of the Tsg101 UEV domain in complex with the PTAP motif of the HIV-1 p6 protein. Nat. Struct. Biol. *9*, 812–817.

Pornillos, O.P., Garrus, J.E., and Sundquist, W.I. (2002c). Mechanisms of enveloped RNA virus budding. Trends Cell Biol. *12*, 569–579.

Pornillos, O., Higginson, D.S., Stray, K.M., Fisher, R.D., Garrus, J.E., Payne, M., He, G.P., Wang, H.E., Morham, S.G., and Sundquist, W.I. (2003). HIV Gag mimics the Tsg101-recruiting activity of the human Hrs protein. J. Cell Biol. *162*, 425–434.

Puffer, B.A., Parent, L.J., Wills, J.W., and Montelaro, R.C. (1997). Equine infectious anemia virus utilizes a YXXL motif within the late assembly domain of the Gag p9 protein. J. Virol. *71*, 6541–6546.

Puffer, B.A., Watkins, S.C., and Montelaro, R.C. (1998). Equine infectious anemia virus Gag polyprotein late domain specifically recruits cellular AP-2 adapter protein complexes during virion assembly. J. Virol. *72*, 10218–10221.

Raposo, G., Moore, M., Innes, D., Leijendekker, R., Leigh-Brown, A., Benaroch, P., and Geuze, H. (2002). Human macrophages accumulate HIV-1 particles in MHC II compartments. Traffic *3*, 718–729.

Scheuring, S., Rohricht, R.A., Schoning-Burkhardt, B., Beyer, A.,

Muller, S., Abts, H.F., and Kohrer, K. (2001). Mammalian cells express two VPS4 proteins both of which are involved in intracellular protein trafficking. J. Mol. Biol. *312*, 469–480.

Sherer, N.M., Lehmann, M.J., Jimenez-Soto, L.F., Ingmundson, A., Haner, S.M., Cicchetti, G., Allen, P.G., Pypaert, M., Cunningham, J.A., and Mothes, W. (2003). Visualization of retroviral replication in living cells reveals budding into multivascular bodies. Traffic, in press.

Strack, B., Calistri, A., Craig, S., Popova, E., and Göttlinger, H.G. (2003). AIP1/ALIX is a binding partner for HIV-1 p6 and EIAV p9 functioning in virus budding. Cell, *114*, 689–699.

Thery, C., Boussac, M., Veron, P., Ricciardi-Castagnoli, P., Raposo, G., Garin, J., and Amigorena, S. (2001). Proteomic analysis of dendritic cell-derived exosomes: a secreted subcellular compartment distinct from apoptotic vesicles. J. Immunol. *166*, 7309–7318.

VerPlank, L., Bouamr, F., LaGrassa, T.J., Agresta, B., Kikonyogo, A., Leis, J., and Carter, C.A. (2001). Tsg101, a homologue of ubiquitin-conjugating (E2) enzymes, binds the L domain in HIV type 1 Pr55Gag. Proc. Natl. Acad. Sci. USA *98*, 7724–7729.

Vincent, O., Rainbow, L., Tilburn, J., Arst Jr, H.N., Jr., and Penalva, M.A. (2003). YPXL/I Is a protein interaction motif recognized by aspergillus PalA and its human homologue, AIP1/Alix. Mol. Cell. Biol. *23*, 1647–1655.

von Schwedler, U.K., Stemmler, T.L., Klishko, V.Y., Li, S., Albertine, K.H., Davis, D.R., and Sundquist, W.I. (1998). Proteolytic refolding of the HIV-1 capsid protein amino-terminus facilitates viral core assembly. EMBO J. *17*, 1555–1568.

Welker, R., Hohenberg, H., Tessmer, U., Huckhagel, C., and Krausslich, H.G. (2000). Biochemical and structural analysis of isolated mature cores of human immunodeficiency virus type 1. J. Virol. *74*, 1168–1177.

CHAPTER 3

THE HUMAN ENDOSOMAL SORTING COMPLEX REQUIRED FOR TRANSPORT (ESCRT-I) AND ITS ROLE IN HIV-1 BUDDING

Melissa D. Stuchell, Jennifer E. Garrus, Barbara Muller, Kirsten M. Stray, Sanaz Ghaffarian, Rena McKinnon, Hans-Georg Krausslich, Scott G. Morham, and Wesley Sundquist

Reprinted from The Journal of Biological Chemistry, Vol. 279, pages 36059-36071,

Note: Melissa D. Stuchell-Brereton analyzed the data shown in Figures 2-5 of this chapter, provided the graphic art in Figure 1B and performed the work shown in Figures 3, 4, 5A, and 5B. Graphic art in Figure 1A was provided by Sanaz Ghaffarian. Work described in Figure 2A and 2B was performed by Sanaz Ghaffarian. Work described in Figure 2C was performed by Rena McKinnon. Library yeast two-hybrid experiments shown in Table 1 were performed by Myriad Genetics, Inc. Work described in Figure 7A was performed by Kirsten M. Stray. Work described in Figure 8 was performed by Barbara Muller. Work described in Figures 6 and 7B was performed by Jennifer E. Garrus.

THE JOURNAL OF BIOLOGICAL CHEMISTRY
Vol. 279, No. 34, Issue of August 20, pp. 36059–36071, 2004
Printed in U.S.A.

The Human Endosomal Sorting Complex Required for Transport (ESCRT-I) and Its Role in HIV-1 Budding*[S]♦

Received for publication, May 11, 2004, and in revised form, June 15, 2004
Published, JBC Papers in Press, June 23, 2004, DOI 10.1074/jbc.M405226200

Melissa D. Stuchell‡§, Jennifer E. Garrus‡§¶, Barbara Müller‖, Kirsten M. Stray‡, Sanaz Ghaffarian‡, Rena McKinnon‡¶, Hans-Georg Kräusslich‖, Scott G. Morham, and Wesley I. Sundquist‡ ‡‡**

*From the ‡Department of Biochemistry, University of Utah, Salt Lake City, Utah 84132-3201, the ‖Abteilung Virologie, Universitätsklinikum Heidelberg, D-69120 Heidelberg, Germany, and **Myriad Genetics, Incorporated, Salt Lake City, Utah 84108*

Efficient human immunodeficiency virus type 1 (HIV-1) budding requires an interaction between the PTAP late domain in the viral $p6^{Gag}$ protein and the cellular protein TSG101. In yeast, Vps23p/TSG101 binds both Vps28p and Vps37p to form the soluble ESCRT-I complex, which functions in sorting ubiquitylated protein cargoes into multivesicular bodies. Human cells also contain ESCRT-I, but the VPS37 component(s) have not been identified. Bioinformatics and yeast two-hybrid screening methods were therefore used to identify four novel human proteins (VPS37A–D) that share weak but significant sequence similarity with yeast Vps37p and to demonstrate that VPS37A and VPS37B bind TSG101. Detailed studies produced four lines of evidence that human VPS37B is a Vps37p ortholog. 1) TSG101 bound to several different sites on VPS37B, including a putative coiled-coil region and a PTAP motif. 2) TSG101 and VPS28 co-immunoprecipitated with VPS37B-FLAG, and the three proteins comigrated together in soluble complexes of the correct size for human ESCRT-I (~350 kDa). 3) Like TGS101, VPS37B became trapped on aberrant endosomal compartments in the presence of VPS4A proteins lacking ATPase activity. 4) Finally, VPS37B could recruit TSG101/ESCRT-I activity and thereby rescue the budding of both mutant Gag particles and HIV-1 viruses lacking native late domains. Further studies of ESCRT-I revealed that TSG101 mutations that inhibited PTAP or VPS28 binding blocked HIV-1 budding. Taken together, these experiments define new components of the human ESCRT-I complex and characterize several TSG101 protein/protein interactions required for HIV-1 budding and infectivity.

Like other enveloped viruses, HIV-1[1] must bud from producer cells to spread infection. HIV budding requires both *cis*-acting viral elements and *trans*-acting cellular proteins (reviewed in Ref. 1). Efficient release and replication of HIV-1 in most cell types, including primary cells, require a conserved *cis*-acting P(S/T)AP motif (the "late domain"), located in the C-terminal p6 region of the structural Gag protein (2–5). The P(S/T)AP late domain binds and recruits the cellular protein TSG101 (tumor susceptibility gene 101), which facilitates efficient separation of the viral and cellular membranes during the final stages of virus release (6–9). In addition to HIV-1, several other pathogenic human viruses, including human T-cell leukemia virus type I (Retroviridae), Ebola virus (Filoviridae) and Lassa virus (Arenaviridae), also use P(S/T)AP late domains to recruit TSG101 during virus budding (7, 10–13). In turn, TSG101 helps to recruit a complex set of cellular machinery that is normally used for protein sorting, membrane distortion, and fission at the multivesicular body (MVB) (1).

Much of our understanding of MVB biogenesis comes from studies in yeast (reviewed in Refs. 14 and 15). Vps23p, the yeast ortholog of TSG101, binds two other proteins, Vps28p and Vps37p, to form a stable soluble ~350-kDa complex called ESCRT-I (endosomal sorting complex required for transport) (16). ESCRT-I is recruited to the endosomal membrane through an interaction with the upstream Vps27p-HRS complex (17–21). Once on the membrane, ESCRT-I helps recruit a series of downstream proteins and complexes (the "Class E" proteins), which collectively sort ubiquitylated proteins into vesicles that bud into the maturing endosome to create MVBs. In most cases, these protein sorting and vesiculation events ultimately target proteins for degradation in the interior of the lysosome (vacuole in yeast).

Although the human MVB pathway is more complex and less well characterized than the yeast pathway, there is now good evidence for conservation of ESCRT-I composition and function from yeast to humans. First, TSG101 and VPS28 are required for the ubiquitin-dependent delivery of cathepsin D and endocytosed receptors to the lysosome (*e.g.* Refs. 17 and 22–24). Second, mammalian TSG101 and VPS28 also function together as part of a soluble ~350-kDa ESCRT-I complex (22, 25). However, a significant limitation in our understanding of the human ESCRT-I complex is that orthologs of VPS37 have not yet been identified in animals.

As illustrated in Fig. 1*A*, TSG101 is a multifunctional, multidomain protein composed of an N-terminal ubiquitin E2 variant (UEV) domain (residues 1–145), a proline-rich region (res-

* This work was supported by a National Institutes of Health Grant R01 AI51174 (to W. I. S.) and Deutsche Forschungsgemeinschaft Grant SFB638 (to H.-G. K.). The costs of publication of this article were defrayed in part by the payment of page charges. This article must therefore be hereby marked "*advertisement*" in accordance with 18 U.S.C. Section 1734 solely to indicate this fact.

[S] The on-line version of this article (available at http://www.jbc.org) contains Supplemental "Results" and Supplemental Fig. 1.

♦ This article was selected as a Paper of the Week.

§ Both authors contributed equally to this work.
¶ Present address: Myriad Genetics, Inc., Salt Lake City, UT 84108.
‡‡ To whom correspondence should be addressed: Dept. of Biochemistry, University of Utah School of Medicine, 20 N, 1900 E, Salt Lake City, UT 84132-3201. Tel.: 801-585-5402; Fax: 801-581-7959; E-mail: wes@biochem.utah.edu.

[1] The abbreviations used are: HIV-1, human immunodeficiency virus type 1; MVB, multivesicular body; UEV, ubiquitin E2 variant; WT, wild-type; siRNA, small interfering RNA; GST, glutathione *S*-transferase; GFP, green fluorescent protein; VLP, virus-like particle; DBD, DNA-binding domain; AD, activation domain; X-gal, 5-bromo-4-chloro-3-indolyl-α/β-galactopyranoside.

idues ~146–215), a predicted central coiled-coil region (residues ~240–311), and a conserved helical C-terminal domain (residues ~330–390). TSG101 appears to function primarily as an adaptor protein, and the different regions of TSG101 engage in a series of protein/protein interactions within the ESCRT-I complex, including the following. 1) The TSG101 N-terminal UEV domain binds P(S/T)AP peptide motifs. Potential cellular binding sites include a downstream PTAP motif within TSG101 itself and P(S/T)AP motifs within at least two other Class E proteins, HRS and AIP1 (17–20, 26–28). 2) The C-terminal region of TSG101/Vps23p binds VPS28/Vps28p (14, 25, 29). This interaction is important for MVB formation and may also control the steady-state levels of TSG101 (30). 3) Finally, deletion of a predicted central coiled-coil region within Vps23p blocks incorporation of Vps37p into the ESCRT-I complex, suggesting that this region of Vps23p may form (or contain) the Vps37p-binding site (16).

Given the parallels between MVB vesicle formation and HIV-1 budding, it has become important to characterize the different TSG101 protein/protein interactions that function in ESCRT-I assembly and test their involvement in virus budding. The goals of this study were therefore to identify human VPS37 orthologs and to test the importance of known TSG101/ESCRT-I interactions in HIV-1 budding.

MATERIALS AND METHODS

VPS37 Homology Searches—In one procedure, the yeast Srn2p/Vps37p protein sequence (NCBI accession number NP_013220) was submitted to the NCBI PSI-BLAST search engine and compared with all known proteins. The first iteration identified apparent VPS37 orthologs in fungi and Japanese rice (NCBI accession number AAS01952). A composite profile built from these sequences was then compared with all known proteins to identify VPS37 orthologs in animals. All sequences above the default threshold (18 total) were incorporated into the search profile, and a final iteration identified four human proteins: VPS37A/HCRP1 (hepatocellular carcinoma-related protein 1; NCBI LocusLink 137492), VPS37B (NCBI LocusLink 79720), VPS37C (NCBI LocusLink 55048), and VPS37D/WBSCR24 (Williams-Beuren syndrome chromosome region 24; NCBI LocusLink 155382).

In a second procedure, the five proteins shown to bind TSG101 in a global analysis of protein/protein interactions in *Drosophila* (31) were compared against the human protein data base. One of the *Drosophila* proteins (CG1115-PA; NCBI accession number NP_649518) showed clear sequence similarities to VPS37B and VPS37C ($E \leq 1 \times 10^{-6}$) and weaker similarities to VPS37A ($E = 1.4$) and VPS37D ($E = 0.034$).

Plasmid Construction—Mammalian expression vectors for wild-type (WT) and PTAP mutant HIV-1_{NL4-3}, WT and mutant VPS4A, and small interfering RNA (siRNA)-resistant TSG101 (TSG*-FLAG) have been described (6). Additional point mutations were introduced into pIRES-TSG*-FLAG using Kunkel or QuikChange (Stratagene) mutagenesis. Deletion mutants were created by PCR amplifying the desired region of pIRES-TSG*-FLAG and subcloning the product into pIRES2-EGFP. VPS37B constructs were PCR-amplified from an expressed sequence tag (DDBJ/GenBank™/EBI accession number BE909752; American Type Culture Collection, Manassas, VA) with the sequence encoding the C-terminal FLAG epitope within the 3′-primer. VPS28 (GenBank™ accession number BC019321) constructs were PCR-amplified from a QUICK-Clone human HeLa cDNA pool (Clontech) using gene-specific primers. For expression in *Escherichia coli*, the VPS28 coding region was subcloned into WISP01-69, a modified pGEX2T vector (Amersham Biosciences), to create WISP01-136, which expresses VPS28 as a GST fusion protein.

Yeast Two-hybrid Binding Assays—Global and directed yeast two-hybrid screens were performed as described previously (19, 26). Briefly, directed two-hybrid assays with full-length TSG101 and VPS37B and deletion constructs were performed using the Matchmaker Gal4 yeast two-hybrid 3 system (Clontech). In each experiment, five test clones and five controls were selected at random and tested for α-galactosidase activity in −Leu/−Trp/−Ade/−His X-α-gal (50 μg/ml) plate assays. Directed two-hybrid assays with full-length TSG101 and VPS28 and deletion constructs were performed using the MP30 vector system (32). To identify yeast colonies producing β-galactosidase, cells were lifted onto filter paper disks, lysed by freeze-thawing in liquid nitrogen, and assayed with X-β-gal. For quantitation of β-galactosidase activity, ~20 colonies/plate were randomly selected, pooled, grown on synthetic liquid medium, and assayed with chlorophenol red β-D-galactopyranoside or *o*-nitrophenyl-β-D-galactopyranoside (6).

VPS37B-FLAG Immunoprecipitation Experiments—293T cells (10-cm plate) were transfected using LipofectAMINE 2000 (Invitrogen) with 13 μg of pCIneo-VPS37B-FLAG or the control pCIneo-FLAG vector. Cells were harvested after 24 h; lysed for 30 min on ice in 1 ml of 50 mM Tris-HCl (pH 7.4), 150 mM NaCl, and 0.1% Nonidet P-40 containing 2 μM pepstatin, 1 mM phenylmethylsulfonyl fluoride, 10 μg/ml leupeptin, and 5 μg/ml aprotinin; and then clarified by centrifugation at 16,000 × *g* for 20 min. Lysate (~1 mg of total protein) was incubated overnight at 4 °C with anti-FLAG antibody M2-agarose affinity beads (Sigma, A 2220). Unbound proteins were removed by lysis buffer washes, and bound proteins were stripped by boiling in SDS-PAGE buffer and analyzed by Western blotting.

Western Blotting—Virus from the supernatants of transfected cells was pelleted through a 20% sucrose cushion in a microcentrifuge at 13,000 rpm for 90 min at 4 °C and resuspended in 25 μl of 1× SDS gel loading buffer. Samples (5–7.5 μl) were separated by 12% SDS-PAGE, transferred, blocked (typically with 5% nonfat dry milk, but as low as 0.1% when detecting endogenous TSG101), blotted with antisera, and protein bands were detected by enhanced chemiluminescence (ECL, Pierce). Transfected human embryonic kidney 293T cells (1 well from a 6-well plate) were harvested directly into 40–45 μl of radioimmune precipitation assay buffer (10 mM Tris-Cl (pH 7.0), 150 mM NaCl, 1% Nonidet P-40, and 0.1% SDS) and incubated on ice for 4 min. Samples were clarified by microcentrifugation at 13,000 rpm for 4 min at 4 °C, and lysates were resuspended in an equal volume of 2× SDS gel loading buffer. Aliquots (5–10 μl) were resolved by 12–17.5% SDS-PAGE. Bound antibody was detected by ECL using SuperSignal West Pico (Pierce) according to the manufacturer's instructions. The following primary antibodies were used: rabbit anti-HIV CA protein antibody (1:2000), rabbit anti-HIV MA protein antibody (1:25,000; Didier Trono, Geneva, Switzerland), murine monoclonal anti-TSG101 antibody 4A10 (1:100–1000; GeneTex, Inc.), murine monoclonal anti-FLAG antibody M2 (1:5000; Sigma), and rabbit anti-NEDD4 antibody (1:5000; Pharmingen). Anti-VPS28 antibodies (1:500–1500) were raised against recombinant VPS28 (see below) in New Zealand White rabbits (Covance, Inc.).

Gel Filtration—293T cells transfected with pCIneo-VPS37B-FLAG (as described for the immunoprecipitation experiments) were harvested after 24 h; lysed for 30 min on ice in 1 ml of phosphate-buffered saline (pH 7.4) and 0.1% Tween 20 containing 2 μM pepstatin, 1 mM phenylmethylsulfonyl fluoride, 10 μg/ml leupeptin, and 5 μg/ml aprotinin; and clarified by centrifugation at 16,000 × *g* for 30 min. The lysate was fractionated by gel filtration chromatography on a Sephacryl S300 column (Amersham Biosciences). Proteins in the 1.4-ml fractions were trichloroacetic acid-precipitated, washed with acetone (22), and analyzed by Western blotting. Apparent molecular masses were obtained by comparison with a standard curve derived from chromatography of proteins of known mass.

Immunofluorescence—COS-7 cells grown on glass coverslips on 60-mm dishes were cotransfected with 100 ng of vector expressing VPS37B-FLAG and 900 ng of vector expressing WT or K173Q VPS4A-GFP using 2.5 μl of LipofectAMINE 2000 following the manufacturer's instructions. Cells were fixed and permeabilized 24 h post-transfection in 4% paraformaldehyde and phosphate-buffered saline, incubated with rabbit anti-FLAG antibody (1:500) at 4 °C for 16 h, washed with phosphate-buffered saline, and incubated with Alexa 594-conjugated goat anti-rabbit antibodies (1:500) to detect FLAG-tagged VPS37 proteins. Images were collected as single wavelengths on an Olympus FVX confocal fluorescent microscope using Fluoview Version 2.0.39 software. 0.3–0.7-μm-thick *Z* sections are shown.

Gag-VPS37B Rescue Experiments—All Gag and Gag-VPS37B expression constructs were based on pGag-GFP (a gift from Dr. Marilyn Resh) (33). Expression vectors for GagΔPTAP-GFP and GagΔp6 were created as described (19), and GagΔPTAP-VPS37B and Gag-VPS37B expression constructs were created by replacing the GFP coding region with the VPS37B coding sequence. Plasmid DNA encoding either Gag-GFP or Gag-VPS37B constructs was cotransfected together with GagΔp6 plasmid DNA into 293T cells (2 ml, 6-well plates). Protein expression and release of viruses and virus-like particles (VLPs) were analyzed by Western blotting 24 h post-transfection.

Viral Replication Assays—Infectivity of HIV-1 particles released into the supernatants from cells transfected with R9 constructs was determined in single-cycle MAGIC replication assays as described (34), except that infections were performed at three different dilutions in triplicate in 48- or 96-well plates. Blue cells and syncytia were counted 2 days post-infection.

TSG101 Depletion/Replacement Experiments—Synthetic 21-nucleotide siRNA duplexes with 2-nucleotide 2′-deoxythymidine 3′- or uridine 3′-overhangs were targeted to TSG101 coding nucleotides 413–433 (35). 293T cells in 6-well plates (2-ml culture volume) were transfected twice at 24-h intervals using LipofectAMINE 2000 (6). The first transfection was with 50 nM siRNA duplexes and either 2 μg of pSL1180 carrier plasmid (Amersham Biosciences) or 2 μg of WT or mutant siRNA-resistant pIRES-TSG*-FLAG expression vector. The second transfection was performed with the same siRNA duplex (50 nM) and 500 ng of vector R9. Viral supernatants and cytoplasmic lysates were harvested after an additional 24–28 h and analyzed for protein expression and virus infectivity. All transfections and subsequent analyses were repeated at least three independent times.

Recombinant VPS28 Purification—*E. coli* BL21(DE3) cells transformed with WISP01-136 were induced with 1 mM isopropyl-β-D-thiogalactopyranoside to express recombinant GST-VPS28 and grown for 4 h at room temperature. Following cell lysis, soluble GST-VPS28 was purified by glutathione-Sepharose affinity chromatography (GSTPrep FF, Amersham Biosciences) and eluted with 20 mM glutathione. Following dialysis in 50 mM Tris-HCl (pH 8.0), 100 mM NaCl, and 1 mM dithiothreitol, the fusion protein was cleaved with 1 mg of tobacco etch virus protease/100 mg of protein for 24 h at 23 °C; free GST was removed by two rounds of glutathione-Sepharose affinity chromatography; and VPS28 protein was purified to homogeneity by anion exchange chromatography on immobilized Q-Sepharose (Amersham Biosciences). VPS28 eluted at ~300 mM NaCl from a linear gradient of 50 mM to 1 M NaCl in 25 mM Tris-HCl (pH 8.0) and 5 mM 2-mercaptoethanol.

Detection of Proteins Incorporated into Virus Particles—Human MT-4 T-cells were infected with HIV-1_{NL4-3} by co-culture as described previously (36). 60 h post-infection, a supernatant was harvested, and virus was purified by pelleting through a 20% (w/w) sucrose cushion, followed by velocity centrifugation through an iodixanol gradient as described (37). Particles were concentrated by ultracentrifugation, and the purity of the samples was verified by SDS-PAGE, followed by silver staining. For Western blotting, virus particles corresponding to 1 μg of CA protein (adjusted by comparison with purified recombinant CA protein) (38) and 1 μg of recombinant CA protein (control) and extracts from 10^5 uninfected MT-4 cells were separated by 17.5% SDS-PAGE (200:1 acrylamide/bisacrylamide).

RESULTS

Identification of Candidate Human VPS37 Proteins—As discussed above, the human ESCRT-I complex presumably contains TSG101, VPS28, and VPS37. However, VPS37 orthologs have not yet been identified in humans or any other higher eukaryote, apparently because the primary sequence has diverged considerably from yeast Vps37p (which shares <20% sequence identity with any known human protein). We therefore pursued three different approaches to identify VPS37 candidates, and these approaches *independently* identified the same family of human proteins.

In the first approach, the yeast Vps37p protein sequence was used to search for human VPS37 candidates by creating PSI-BLAST composite profiles of putative VPS37 orthologs from higher eukaryotes (see "Materials and Methods" for details). Four human proteins were identified using this approach: VPS37A/HCRP1 (39), VPS37B, VPS37C, and VPS37D/WB-SCR24. In the second approach, we searched for human homologs of the five proteins previously shown to bind TSG101 in a global map of *Drosophila* protein/protein interactions (31). This approach again yielded the same four proteins as the best human protein matches to one of the five *Drosophila* TSG101-binding partners (Fig. 1*B*). Finally, we performed extensive yeast two-hybrid screens of human spleen cDNA libraries with the goal of identifying human TSG101-binding proteins *de novo*. These screens employed 12 different TSG101 fragments as baits and identified two different "minimal" fragments of VPS37A as binding partners for TSG101-(12–326) (identified nine times in total) (Table I) and one fragment of VPS37B (VPS37B-(1–126), identified once) as a binding partner for TSG101-(12–326).

VPS37A–D are most similar within an ~150-amino acid region that has been designated the mod_r domain (Fig. 1*B*) (40). This is also the region of highest homology to yeast Vps37p and to the putative *Drosophila* VPS37 ortholog. Each mod_r domain contains at least one segment that is strongly predicted to form a coiled coil, as does the yeast Vps37p protein. Interestingly, our yeast two-hybrid screening studies indicated that the TSG101-binding sites on VPS37A and VPS37B span at least part of the mod_r domain. Thus, the screening and alignment analyses suggested that all four human VPS37 proteins might be Vps37p orthologs that bind TSG101 via their conserved mod_r domains. To test this hypothesis, we selected VPS37B for detailed studies because 1) its domain structure most closely resembles that of yeast Vps37p; 2) its mod_r domain has the highest identity to the *Drosophila* VPS37 protein (Fig. 1*B*) (data not shown); and 3) VPS37B mRNA is expressed in a wide variety of tissues (see NCBI UniGene Cluster Hs.77870 *Homo sapiens*), including macrophages and lymphocytes, which are the natural hosts for HIV-1 replication.

Yeast Two-hybrid Binding Studies—"Reverse" library screens were performed using six different VPS37B bait fragments, and these screens identified four different TSG101 fragments as binding partners for one of the baits (VPS37B-(50–170)) (Table I). Thus, unbiased library screens that employed *either* VPS37B or TSG101 baits successfully identified the reciprocal protein as a binding partner. A series of directed yeast two-hybrid experiments were then performed to confirm the interaction and to map the TSG101/VPS37B interaction sites. As shown in Fig. 2*A*, full-length TSG101-DBD and VPS37B-AD proteins interacted strongly, whereas empty vector controls showed no detectable background binding. Deletion mapping experiments revealed that the TSG101 interaction site is located within a central fragment of VPS37B that spans residues 65–112. This minimal binding site is also contained in all of the VPS37B fragments identified in the library screens (Table I). Deletion of an additional 11 residues from the C terminus (to residue 101), which removed even more of the second predicted coiled-coil sequence in VPS37B, blocked TSG101 binding, supporting the idea that the coiled coil is important for the TSG101 interaction.

Deletion analyses were also performed to map the binding site for VPS37B on TSG101 (Fig. 2, *A* and *B*). These analyses were complicated, however, because all three TSG101 fragments initially tested bound VPS37B to some extent. Binding was weakest for TSG101-(1–145), which showed a weak interaction with the full-length VPS37B protein (Fig. 2*A*, *lower panel*) and a moderate interaction with VPS37B-(65–198) (Fig. 2*B*). TSG101-(1–145) corresponds to the PTAP motif-binding UEV domain, and VPS37B contains a PTAP motif (residues 185–188). We therefore tested whether the PTAP site on TSG101 mediates the TSG101-(1–145)/VPS37B-(65–198) interaction using a point mutation (M95A) within the TSG101 UEV domain that blocks PTAP binding (41). This mutation eliminated the TSG101-(1–145)/VPS37B-(65–198) interaction (Fig. 2*B*, *lower panel*), indicating that the TSG101 UEV domain did indeed contact VPS37B-(65–198) through the PTAP motif-binding groove. Similarly, we found that the pure recombinant TSG101 UEV domain (residues 1–145) bound specifically to a nine-amino acid peptide spanning the VPS37B PTAP site as analyzed in biosensor binding experiments (ELAPTAPLPY; K_D = 155 μM) (data not shown). Thus, the N-terminal TSG101 UEV domain binds directly, but weakly, to the VPS37B PTAP motif. Importantly, however, the TSG101 M95A mutation did not appreciably inhibit the interaction between the full-length TSG101 and VPS37B proteins (Fig. 2*A*, *lower panel*). Hence, the VPS37B PTAP motif is not the primary binding site for TSG101. This situation is analogous to the TSG101/HRS inter-

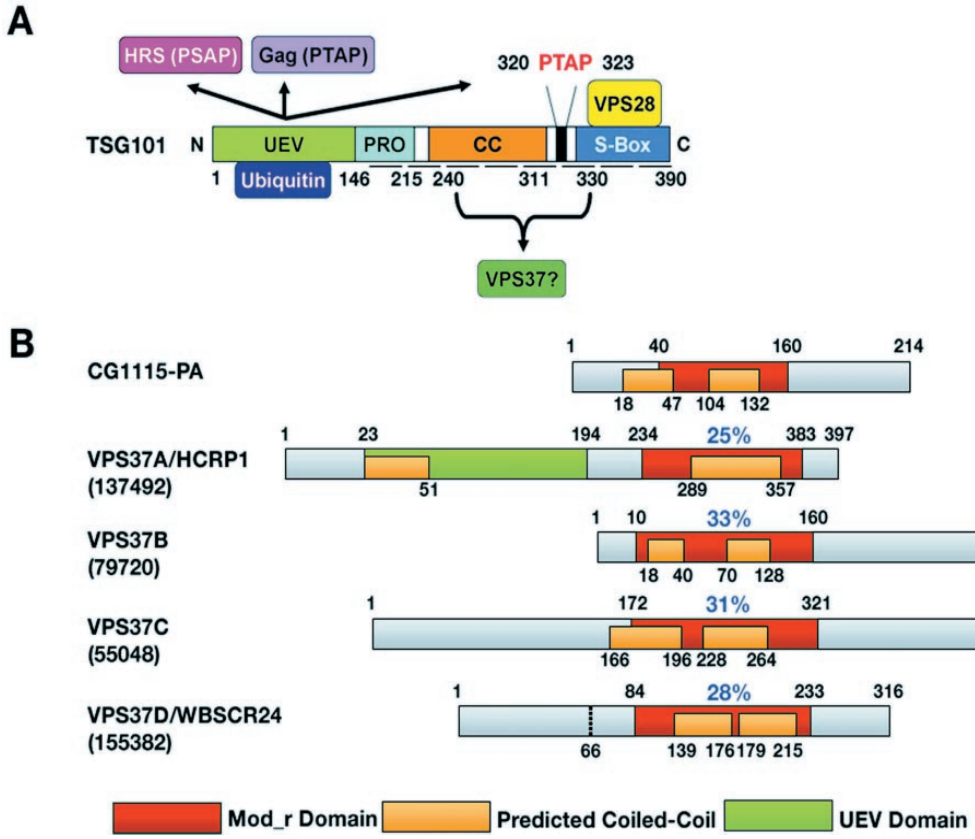

FIG. 1. **Schematic illustrations showing the putative domain structures and binding partners of TSG101 (*A*) and VPS37-like proteins (*B*).** *A*, schematic illustration of TSG101 showing the amino acid numbering scheme and approximate interaction sites of known binding partners. The *dashed line* highlights the observation that the C-terminal two-thirds of TSG101 can bind itself, although the precise sequence requirements for homo-oligomerization have not yet been determined (29). *PRO*, proline-rich region; *CC*, predicted coiled-coil region; *S-Box*, steadiness box region (30). Regions designated as coiled coils had a predicated coiled-coil propensity of >0.1 as analyzed by the program Multicoils (67) or >0.2 as analyzed by the program Coils (68). *B*, VPS37-like proteins from *Drosophila* (CG1115-PA) and humans (as indicated) are shown schematically, together with their NCBI LocusLink identifiers. Percent identities between the mod_r domains of CG1115-PA and the human proteins are shown in *blue*. Note that the N-terminal ends of the VPS37C and VPS37D/WBSCR24 proteins have not been determined experimentally, and the *dashed line* shows an alternative possible N terminus for VPS37D/WBSCR24. Putative domain identities were obtained from the Swiss Protein Knowledgebase (69), except that the E2 domain designation for VPS37A/HCRP1 was changed to "UEV" because the domain lacks an active-site cysteine residue.

TABLE I
TSG101/VPS37 interactions detected in yeast two-hybrid screens of human spleen libraries

Bait	Prey
TSG101-(12–326)	VPS37A-(194–397)
TSG101-(12–326)	VPS37A-(169–315)
TSG101-(12–326)	VPS37B-(1–126)
VPS37B-(50–170)	TSG101-(296–381)
VPS37B-(50–170)	TSG101-(297–390)
VPS37B-(50–170)	TSG101-(132–390)
VPS37B-(50–170)	TSG101-(208–335)

action, where the TSG101 UEV domain can bind an HRS PSAP sequence, but the primary interaction(s) between the two proteins occurs elsewhere (17–20).

TSG101 fragments spanning residues 158–309 and 310–390 also interacted with full-length VPS37B in the yeast two-hybrid experiments (Fig. 2*B*). Indeed, positive VPS37B interactions were detected for a series of non-overlapping fragments spanning the C-terminal end of TSG101 (Fig. 2*B*) (data not shown). It is therefore possible that VPS37B makes multiple contacts both upstream and downstream of TSG101 residue 310. However, we cannot rule out the alternative possibility that the observed TSG101/VPS37B interactions may, in some cases, be bridged via the endogenous yeast ESCRT-I complex, particularly as determinants of TSG101 homo-oligomerization are also found in this region (29). In any event, these complications precluded a more precise mapping of the VPS37B-binding site on TSG101.

Finally, directed yeast two-hybrid experiments were also used to test for VPS37B interactions with other known human Class E proteins, and two human Class E proteins tested positive in these assays: VPS37B itself and HRS (data not shown). The former interaction indicates that VPS37B likely forms homo-oligomeric interactions. The latter interaction suggests that VPS37B may play an important role in helping the upstream HRS complex to recruit ESCRT-I to the endosomal membrane. We note that Bieniasz[2] has similarly found that the VPS37C protein interacts with HRS in two-hybrid assays. Yeast Vps37p exhibits two-hybrid interactions with three additional yeast Class E proteins (Vps20p, Vps28p, and Vps36p) (43), but we did not observe analogous interactions between the human orthologs in our experiments.

Human VPS37B Forms a Complex with TSG101 and VPS28 in Vivo—We next tested whether VPS37B forms stable com-

[2] P. D. Bieniasz, personal communication.

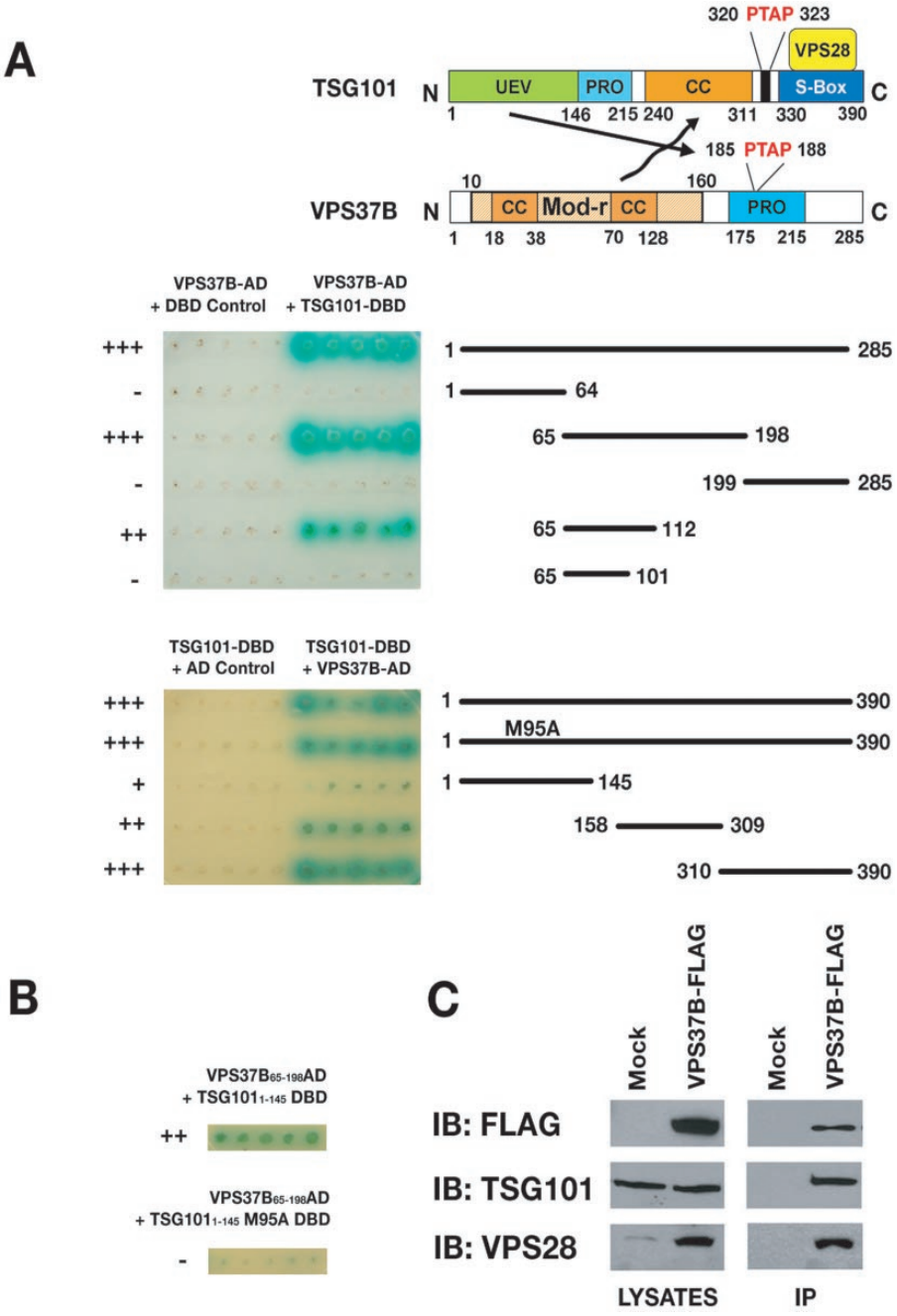

FIG. 2. **TSG101/VPS37B binding studies.** *A*, yeast two-hybrid binding signals arising from coexpression of the indicated pairs of test (*right*) or control (*left*) proteins. In the *upper panel*, a full-length TSG101-DBD fusion protein was coexpressed with the VPS37B-AD fusions shown to the right. In the *lower panel*, full-length VPS37B was coexpressed with the TSG101 fragments shown to the right. Note that VPS37B bound both TSG101-(1–145) and TSG101-(1–157) to a similar extent (not shown). Controls and test interactions were examined for five independent clones expressing the appropriate pairs of proteins. *Blue* indicates positive interactions, and the relative strength of each relevant interaction is summarized to the left. *PRO*, proline-rich region; *CC*, predicted coiled-coil region; *S-Box*, steadiness box region (30). *B*, yeast two-hybrid binding signals arising from coexpression of the designated pairs of proteins or controls. *C*, co-immunoprecipitation of endogenous TSG101 and VPS28 with VPS37B-FLAG. *Left panels*, Western blot signals observed for the input lysate (~50 μg of total protein input); *right panels*, Western blot signals following immunoprecipitation (*IP*) of VPS37B-FLAG (~500 μg of total protein input). *Right lanes*, lysates from cells expressing VPS37B-FLAG; *left lanes*, control cell extracts. *IB*, immunoblot.

plexes with TSG101 and VPS28 in human cells. As shown in Fig. 2*C* (*right panels*, *right lanes*), immunoprecipitation of exogenously expressed VPS37B-FLAG from soluble 293T cell extracts efficiently co-immunoprecipitated both TSG101 and VPS28. This was a specific interaction, as neither TSG101 nor VPS28 was detected in control co-immunoprecipitation reactions with mock-transfected cells (*left lanes*). Interestingly, VPS37B overexpression also increased the steady-state levels

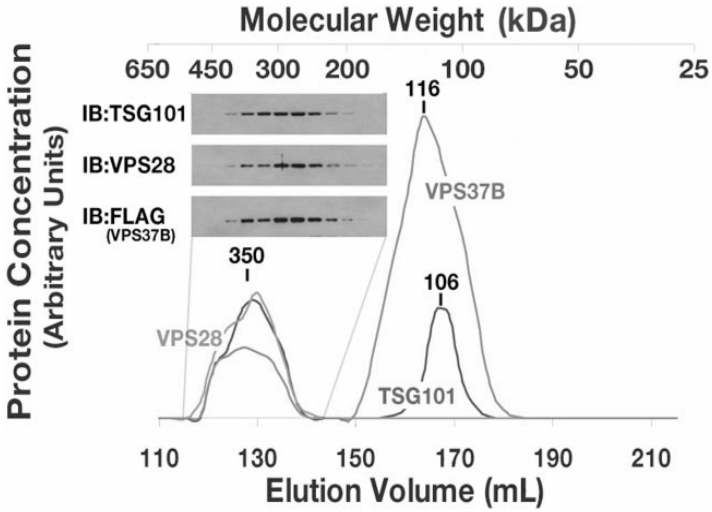

FIG. 3. **Gel filtration analyses of human ESCRT-I components.** Cells overexpressing VPS37B-FLAG protein were lysed, and the soluble lysate was fractionated by gel filtration chromatography. Fractions were analyzed by Western blotting to determine the elution profiles of TSG101, VPS28, and VPS37B. Western blots were digitized, and the intensities were plotted to show relative protein concentration. The elution positions of molecular mass standards are shown above the chromatograph and were used to estimate the apparent molecular masses of the different protein complexes (labeled above the peaks). *Inset*, Western blots from alternating fractions collected through the ESCRT-I elution profile. *IB*, immunoblot.

of VPS28 (*lower left panel*, compare the *two lanes*). This effect was observed in multiple experiments, but the relative increases in VPS28 levels varied between the different experiments. Thus, our data demonstrate that the TSG101, VPS28, and VPS37B-FLAG proteins associate within cells and indicate that elevated VPS37B levels can stabilize VPS28, presumably via ESCRT-I complex formation.

The Human ESCRT-I Complex—Gel filtration chromatography was used to test whether VPS37B, TSG101, and VPS28 form higher order complexes of the size expected for human ESCRT-I. Previous studies have demonstrated that soluble human ESCRT-I complexes elute from gel filtration columns with an apparent molecular mass of ~350 kDa (22, 25). As shown in Fig. 3, exogenously expressed and tagged VPS37B also precisely eluted together with TSG101 and VPS28 in complexes of ~350 kDa. Moreover, all three proteins were present in the same complexes, as immunoprecipitation of VPS37B-FLAG from these fractions again co-immunoprecipitated TSG101 and VPS28 (data not shown). We therefore conclude that VPS37B-FLAG associates stably with the human ESCRT-I complex.

VPS37B-FLAG and endogenous TSG101 were also present in smaller complexes of overlapping but slightly different sizes (~116 and ~106 kDa, respectively). In contrast, VPS28 was found only in the ~350-kDa complex. In the absence of VPS37B overexpression, all of the endogenous TSG101 protein is normally present within the ESCRT-I complex (22), and it is therefore likely that the smaller TSG101 and VPS37B subcomplexes accumulate because VPS28 levels, although increased in the presence of elevated VPS37B, are still limiting when VPS37B is overexpressed.

VPS37B Is Trapped on Endosomal Membranes in the Absence of VPS4A ATPase Activity—Under steady-state conditions, ESCRT-I and other Class E proteins are present primarily in dispersed soluble complexes. To function in MVB cargo sorting and vesicle formation, however, these complexes must transiently associate with endosomal membranes. Following vesicle formation, these complexes then disassemble and are released from the membrane through the action of the VPS4 ATPases associated with a variety of cellular activities (25, 26, 44–50). Thus, in the absence of VPS4 ATPase activity, Class E proteins are recruited to the endosomal membrane, but become trapped on aberrant endosomal compartments (Class E compartments). This behavior can be seen for the VPS4A-GFP protein itself, where the wild-type protein was present in dispersed soluble complexes (Fig. 4*A*, *second panel*), whereas a dominant-negative VPS4A mutant lacking the ability to bind and hydrolyze ATPase activity (K173Q) was trapped on endosomal membranes (Fig. 4*B*, *second panel*).

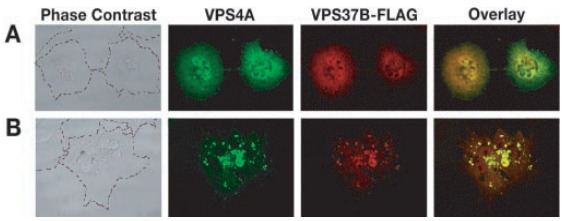

FIG. 4. **Immunofluorescent images showing the localization of VPS37B in the presence of the WT VPS4A-GFP protein (*A*) and the dominant-negative K173Q VPS4A-GFP mutant protein (*B*).** VPS4A-GFP proteins appear *green*, and VPS37B-FLAG proteins appear *red*. The *first panels* in *A* and *B* show the phase-contrast image (with cell boundaries outlined for clarity), and the *fourth panels* show an overlay of the *second* and *third panels*. Note that the dominant-negative K173Q VPS4A mutation caused both VPS4A and VPS37B-FLAG proteins to re-localize to the same sites on the Class E endosomal compartment. The "disperse" localization shown for VPS37B-FLAG in the presence of the WT VPS4A-GFP protein was seen in 90% of the images examined (47/52), whereas the "punctuate/Class E" localization shown for VPS37B-FLAG in the presence of the dominant-negative K173Q VPS4A-GFP protein was seen in 88% of the images examined (29/33).

Analogous experiments were used to test whether VPS37B is recruited to endosomal membranes in a VPS4A-dependent fashion, as has been seen previously for the other mammalian ESCRT-I components (25). As expected, VPS37B-FLAG was distributed throughout the cell as a soluble protein when coexpressed with WT VPSP4A-GFP. This "dispersed" phenotype was observed in nearly all (90%) of the VPS4A-GFP/VPS37B-FLAG cells examined. In contrast, when VPS37B-FLAG was coexpressed together with the dominant-negative K173Q VPS4A-GFP mutant, most of the VPS37B-FLAG protein became concentrated at punctate cytoplasmic sites (88% of the cells examined). These sites corresponded to Class E compartments, as confirmed by the co-localization of VPS37B-FLAG and K173Q VPS4A-GFP (Fig. 4*B*, *fourth panel*). We therefore conclude that VPS37B behaves like the other two ESCRT-I proteins, *i.e.* the protein exists predominantly in dispersed soluble complexes under steady-state conditions, but can also associate transiently with the endosomal membrane and be released by the action of VPS4A.

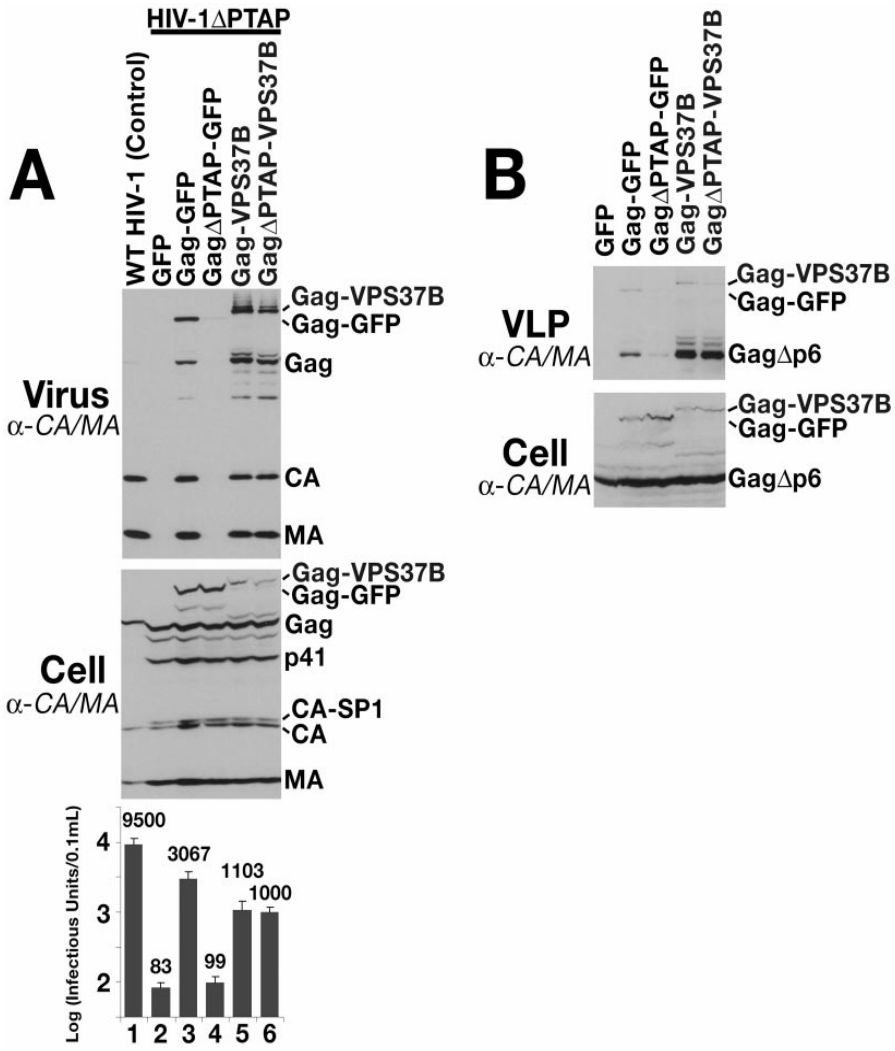

FIG. 5. **VPS37B polypeptides can rescue the release of HIV-1 constructs that lack PTAP late domains (*A*) and GagΔp6 VLPs (*B*).** *A*, VPS37B can rescue the release and infectivity of mutant HIV-1 virions that lack endogenous PTAP late domains. *Upper panel*, Western blot of HIV-1 particle-associated MA and CA proteins released from cells following transfection with 2 μg of WT HIV-1 proviral R9 plasmid (positive control; *lane 1*) or mutant proviral R9 plasmid in which the PTAP late domain of $p6^{Gag}$ was mutated to AAAA (HIV-1ΔPTAP; *lanes 2–6*). Cells were cotransfected with plasmid expressing GFP alone (negative control; *lane 2*), Gag-GFP (1 μg, positive control; *lane 3*), GagΔPTAP-GFP (1 μg, negative control; *lane 4*), Gag-VPS37B (3 μg, control for the infectivity effects of the VPS37B fusion; *lane 5*), or GagΔPTAP-VPS37B (3 μg, test for the ability of VPS37B to rescue virus budding; *lane 6*). Total vector levels were normalized to 5 μg by addition of a vector expressing GFP alone. *Middle panel*, Western blot of the same samples showing cytoplasmic Gag protein expression. Note that the bands labeled p41 and p25 are Gag processing intermediates. *Lower panel*, viral titers in the supernatants of the same samples. Titers were determined in single-cycle MAGIC assays and are plotted on a log scale. *B*, VPS37B can rescue the release of VLPs formed by Gag proteins that lack p6 (GagΔp6). *Upper panel*, Western blot of VLPs released from cells following transfection with 2 μg of plasmid expressing the HIV-1 GagΔp6 protein (*all lanes*). Cells were cotransfected with plasmid expressing GFP alone (negative control; *first lane*), Gag-GFP (positive control; *second lane*), GagΔPTAP-GFP (negative control; *third lane*), Gag-VPS37B (control for any effects of fusing VPS37B to Gag; *fourth lane*), or GagΔPTAP-VPS37B (test for the ability of VPS37B to rescue VLP release; *fifth lane*). Plasmid quantities were the same as described for *A*. *Lower panel*, Western blot of the same samples showing cytoplasmic expression of the various Gag proteins.

Human VPS37B Recruits ESCRT-I Activity—We next tested whether VPS37B can direct functional ESCRT-I activity to HIV-1 budding sites *in vivo*. Previous studies have demonstrated that ESCRT-I can support HIV-1 Gag particle release, even when recruited to sites of viral particle assembly via non-native interactions. For example, mutant retroviral Gag proteins that would otherwise be retained can bud from cells when fused directly to various proteins or domains that can recruit ESCRT-I, including ubiquitin (51), TSG101 (7), VPS28 (52), and HRS (19). In some cases, these Gag fusion proteins can even co-assemble and rescue in *trans* the release of *infectious* HIV-1 virions that lack endogenous late domains, although Gag processing and virus infectivity are typically attenuated when larger proteins are fused to the C-terminal end of Gag. Thus, the heterologous rescue of virus release and infectivity provides a sensitive assay for ESCRT-I activity *in vivo*, and this approach was therefore used to test whether VPS37B can recruit functional ESCRT-I activity to sites of virus budding.

As expected, an HIV-1 construct lacking the $p6^{Gag}$ PTAP late domain (HIV-1ΔPTAP) was not released efficiently from 293T cells and was very poorly infectious (Fig. 5*A*, compare *lanes 1*

and *2*). However, HIV-1ΔPTAP release was rescued by coexpression with a wild-type Gag-GFP protein that could co-assemble with the viral Gag proteins and thereby recruit ESCRT-I activity to the sites of particle assembly (compare *lanes 2* and *3*). Virus infectivity was also substantially (although not fully) rescued by coexpression of the Gag-GFP protein (*lower panel*). The incomplete rescue of virus infectivity presumably reflected the detrimental effects of fusing GFP to the C-terminal end of the Gag protein. As expected, mutation of the PTAP late domain in the Gag-GFP construct abrogated its ability to rescue virus release and infectivity (compare *lanes 3* and *4*), confirming that rescue was late domain-dependent.

Gag-VPS37B fusion constructs could also rescue the release of HIV-1ΔPTAP, and in this case, the rescue *did not* depend upon the presence of the Gag PTAP late domain in the fusion construct (Fig. 5*A*, compare *lanes 5* and *6*). Virus infectivity was substantially rescued as well, albeit to a 3-fold lower level than in the Gag-GFP control (possibly because VPS37B (31 kDa) is even larger than GFP (27 kDa)). Gag-VPS37B fusion proteins also rescued the release of mutant Gag VLPs in *trans* (Fig. 5*B*). Indeed, GagΔPTAP-VPS37B was significantly more effective in mediating VLP release than was the Gag-GFP control construct (compare *second* and *fifth lanes*). We therefore conclude that the VPS37B polypeptide has the ability to recruit functional ESCRT-I activity *in vivo*, as assayed by its ability to rescue the release and infectivity of mutant HIV-1 and the release of mutant Gag VLPs.

Interestingly, additional higher molecular mass species were consistently seen to be associated with the different Gag species in all of the Gag-VPS37B rescue experiments. These additional species likely correspond to mono- and multiubiquitylated Gag proteins based upon the observed mobility shifts (~7 kDa larger). Thus, the VPS37B polypeptide can apparently recruit ubiquitin ligase activity (or, alternatively, reduce ubiquitin hydrolase activity (53)) to sites of virus budding.

TSG101 PTAP Binding Activity Is Essential for HIV-1 Release—We further tested whether other known TSG101/ESCRT-I interactions play important roles in HIV-1 release. To assay the functions of mutant TSG101 proteins, endogenous TSG101 was first depleted from 293T cells using siRNA. This treatment typically inhibited the release of infectious HIV-1 particles up to 50-fold. siRNA-resistant TSG101 expression constructs were then reintroduced into the cells lacking endogenous TSG101, and the ability of the ectopic TSG101 proteins (denoted TSG*) to rescue HIV-1 release and infectivity was tested. Expression of the WT TSG* protein typically rescued virus release to within 2-fold of the undepleted control. Complete rescue was not always achieved, presumably because TSG* expression levels were sometimes lower than endogenous protein levels (see "Supplemental Results" and Supplemental Fig. 1 for full details).

TSG101 depletion/rescue experiments were first used to test whether the PTAP binding activity of TSG101 is required for HIV-1 release. As noted above, the HIV-1 $p6^{Gag}$ ^{7}PTAP^{10} motif binds in a groove in the TSG101 UEV domain, and TSG101 residues that make important contacts include Tyr^{63}, which forms one side of the Pro^{10} binding pocket, and Met^{95}, which makes extensive intermolecular hydrophobic interactions with the p6 Pro^{7} and Ala^{9} residues (54). Alanine substitutions of these two TSG101 residues reduce the affinity of the TSG101 UEV domain/p6 interaction partially (Y63A, 14-fold reduced) or nearly completely (M95A, 52-fold reduced) (54). These mutants were therefore used to test for a correlation between TSG101/p6 binding affinity and the ability of TSG101 to support the release of infectious HIV-1.

Infectious HIV-1 release was reduced 35-fold upon depletion

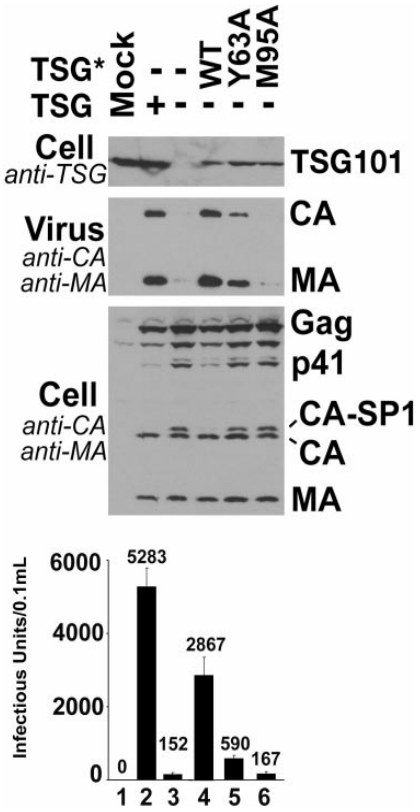

FIG. 6. **TSG101 PTAP binding is essential for HIV-1 release.** Cells were mock-transfected (*lane 1*) or transfected with the proviral R9 plasmid (*lanes 2–6*). Cells were cotransfected with siRNA duplexes to deplete TSG101 (*lanes 3–6*); with an siRNA duplex of inverted sequence (specificity control; *lane 2*); and with vectors expressing siRNA-resistant constructs (TSG*) encoding WT TSG* (*lane 4*), mutant TSG* (*lanes 5* and *6*), or no protein (control; *lane 3*). *First panel*, anti-TSG101 Western blot showing levels of endogenous TSG101 and ectopic TSG*-FLAG; *second panel*, anti-CA and anti-MA Western blot showing particle-associated CA and MA proteins released into the supernatant; *third panel*, anti-CA and anti-MA Western blot showing cytoplasmic lysates from the same samples; *fourth panel*, titers of virus released into the supernatants.

of TSG101 and rescued to within 2-fold of control levels upon reintroduction of WT TSG* (Fig. 6, compare *lanes 2–4*). In contrast, efficient HIV-1 release was not rescued by equivalent levels of either of the two TSG* PTAP motif-binding proteins, as reflected by reduced particle release, accumulation of unprocessed intracellular Gag proteins, and low infectious titers (*lanes 5* and *6*). Nevertheless, the weak binding Y63A mutant did support modest levels of virus release and infectivity (~20% of the WT TSG* control), whereas the non-binding M95A mutant failed to rescue any detectable virus release or infectivity above background levels (6). Thus, TSG101 must bind PTAP sequences with full affinity to support efficient HIV-1 release from 293T cells.

VPS28 Binds the C-terminal Domain of TSG101—Previous work in other laboratories has shown that VPS28 binds TSG101 and that the VPS28-binding site is located in the C-terminal third of TSG101 (16, 25, 29). In good agreement with these observations, VPS28 was identified 28 different times in our yeast two-hybrid library screens that employed TSG101 baits. TSG101-(317–390) was the smallest fragment that bound VPS28 in these screens, which confirmed that VPS28 binds the C-terminal region of TSG101. Similarly, pure recombinant VPS28 bound specifically to GST-TSG101-(330–

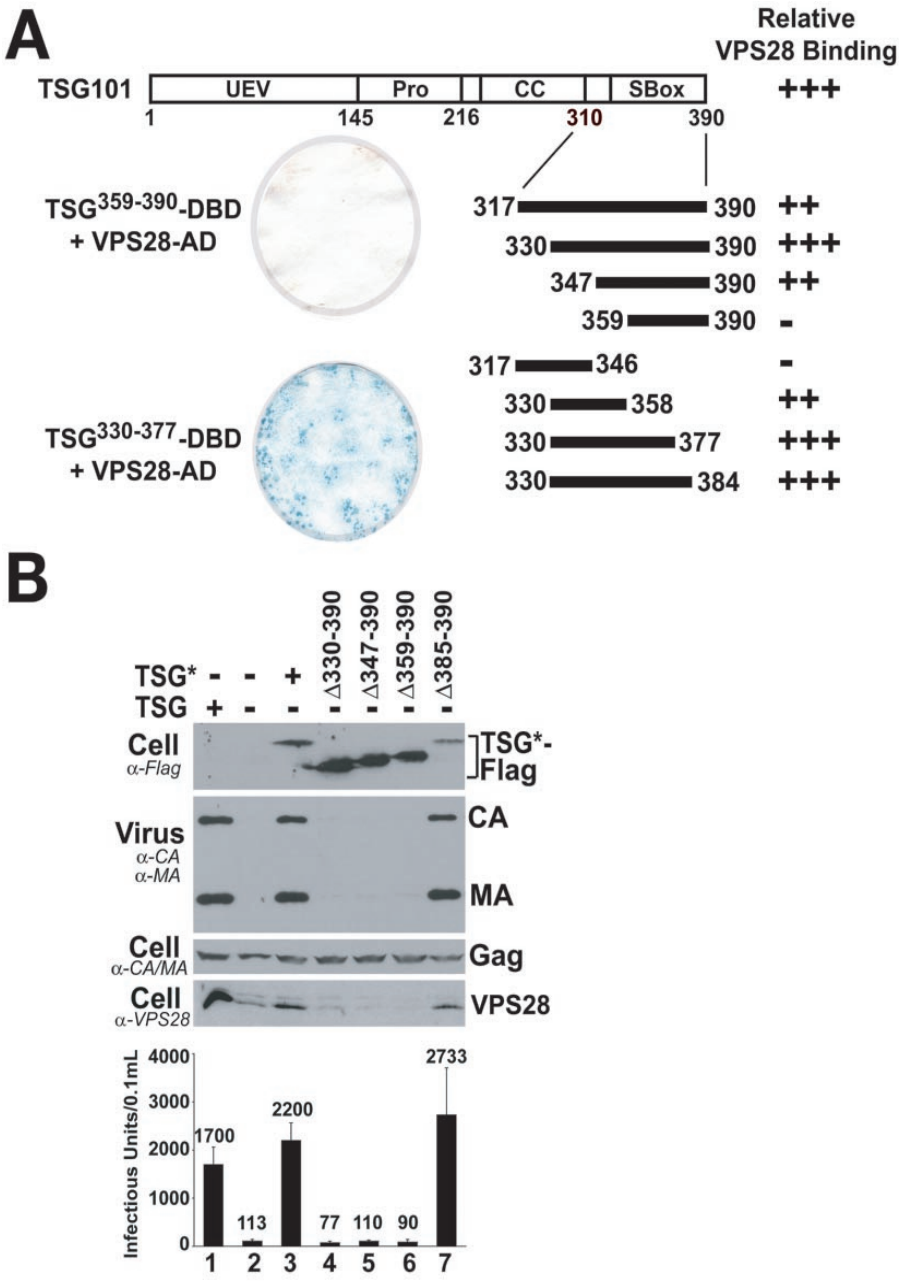

FIG. 7. **TSG101/VPS28 interactions and HIV-1 release.** *A*, the VPS28-binding site is located within the C-terminal domain of TSG101. Schematic illustrations of TSG101 and the TSG101-DBD fusion constructs are shown above. TSG101-DBD binding to VPS28-AD constructs was tested in semiquantitative liquid yeast two-hybrid assays (summarized to the right). Relative β-galactosidase activity was determined and is expressed as +++ (25–40-fold above background levels), ++ (10–25-fold above background levels), or − (undetectable binding). For reference, a filter lift assay showing the relative β-galactosidase activity resulting from the interaction between VPS28 and TSG101-(359–390) (negative) or TSG101-(330–377) (positive) is shown to the left. Note that the TSG-(330–358)-DBD fusion protein activated β-galactosidase expression in the absence of VPS28-AD. Therefore, TSG-(330–358)-AD was tested for binding to a VPS28-DBD fusion protein. *PRO*, proline-rich region; *CC*, predicted coiled-coil region; *S-Box*, steadiness box region (30). *B*, the C-terminal residues of TSG101 are essential for HIV-1 budding. Cells were transfected with the proviral R9 expression construct (*lanes 1–7*), depleted of endogenous TSG101 using a specific siRNA (denoted *TSG−*; *lanes 2–7*) or a control siRNA duplex of inverted sequence (*lane 1*), and cotransfected with plasmids expressing the indicated TSG* protein (*lanes 3–7*). *First panel*, anti-FLAG Western blot showing exogenous TSG*-FLAG levels; *second panel*, anti-CA and anti-MA Western blot of sucrose-pelleted virions showing virus release; *third panel*, anti-CA and anti-MA Western blot of cytoplasmic lysates showing Gag protein expression levels; *fourth panel*, anti-VPS28 Western blot showing endogenous VPS28 levels; *fifth panel*, viral titers in MAGIC infectivity assays of culture supernatants.

390) in "pull-down" experiments, demonstrating that the TSG101/VPS28 interaction is direct (data not shown).

Directed two-hybrid experiments and deletion analyses were used to confirm the initial binding data and to map the VPS28-binding site more precisely. As summarized in Fig. 7, VPS28 bound well to full-length TSG101 and TSG101-(330–377). Deletion of an additional 17 residues from the N-terminal end of this construct (through residue 346) reduced VPS28 binding

significantly, and deletion of 12 more residues (through residue 359) eliminated VPS28 binding entirely. Similarly, C-terminal deletions of TSG101 through residue 359 reduced VPS28 binding, and deletions through residue 347 eliminated detectable VPS28 binding. In all cases, expression of the relevant TSG101-DBD constructs was confirmed by Western blotting with an anti-DBD antibody (data not shown). We therefore conclude that the entire VPS28-binding site spans TSG101 residues ~330–377, although ~20-residue deletions from either end of this region can be tolerated without complete loss of VPS28 binding.

TSG101 Proteins Lacking the VPS28-binding Site Fail to Rescue HIV-1 Release—We next investigated whether the TSG101/VPS28 interaction is required for HIV-1 release by testing whether a series of C-terminally truncated TSG* proteins can support virus release. As shown in Fig. 7*B*, the TSG*Δ330–390, TSG*Δ347–390, and TSG*Δ359–390 proteins all failed to rescue HIV-1 release and infectivity in cells depleted of endogenous TSG101 (compare *lanes 3* and *4–6*). In contrast, a TSG* protein lacking only the final six residues (TSG*Δ385–390) supported efficient HIV-1 release and infectivity (*lane 7*). The failure of the shorter TSG* proteins to rescue release was not due to their impaired expression or stability (*first panel*) or to altered HIV-1 Gag expression (*third panel*). We therefore conclude that TSG101 proteins missing all or part of the VPS28-binding site are unable to support HIV-1 release and hence that this region of TSG101 performs essential function(s) in virus budding.

Analyses of the TSG101 and VPS28 protein levels in our experiments revealed two notable trends. Endogenous VPS28 protein levels were dramatically reduced in the absence of TSG101 proteins with intact VPS28 interaction sites (Fig. 7*B*, *fourth panel*). This was true both in the complete absence of TSG101 (*lane 2*) and in the presence of truncated TSG* proteins lacking the entire VPS28-binding site (*lanes 4–6*). In contrast, VPS28 protein levels were higher in the presence of longer TSG* proteins that were competent to bind VPS28 (*lane 7*), and the absolute levels of VPS28 correlated well with the expression levels of the longer TSG* proteins (*lanes 3* and *7*). These observations suggest that VPS28 may be unstable when it is not bound to TSG101. The presence of cellular VPS28 also correlated well with successful HIV-1 release, as virus release was observed whenever VPS28 levels were high, but not when VPS28 levels were low.

Conversely, deletion of the VPS28-binding region *increased* the steady-state levels of exogenous TSG* (Fig. 7*B*, compare *lanes 3* and *7* with *lanes 4–6*). This observation is consistent with a previous report that the post-translational stability of TSG101 is negatively regulated by an element in the C-terminal region termed the "steadiness box" (residues 346–390) (30). Our data suggest the possibility that the steadiness box corresponds to the VPS28-binding site and, more generally, indicate that formation of a stable TSG101-VPS28 complex (22, 25) helps regulate the steady-state levels of both proteins.

ESCRT-I Incorporation into HIV-1 Particles—Previous studies have shown that overexpressed TSG101 can be recruited to sites of virus budding at the plasma membrane (7), that a fragment of TSG101 spanning the UEV domain can be incorporated into virus particles (8), and that EIAV Gag-VPS28 fusion proteins can recruit TSG101 into VLPs. However, these experiments did not address whether endogenous ESCRT-1 components are normally incorporated into HIV-1 particles, and this information is important for understanding precisely how the complex functions in particle release. We therefore quantitated the levels of VPS28 in highly purified HIV-1 particles.

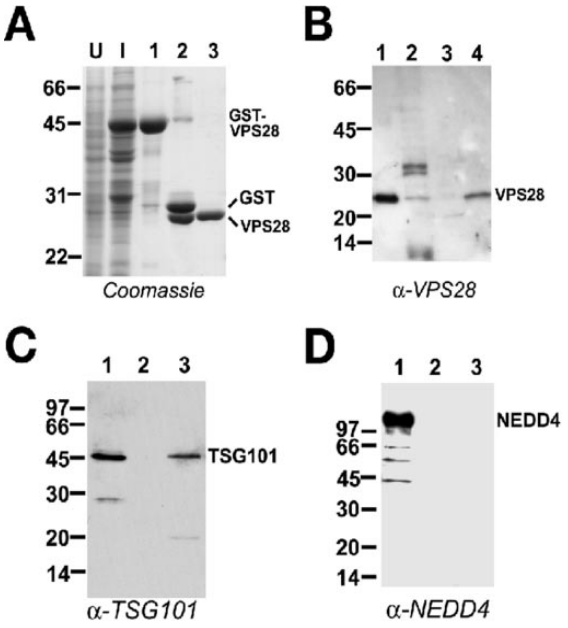

FIG. 8. **Endogenous VPS28 and TSG101 are incorporated into HIV-1 virions, whereas NEDD4 is not.** *A*, Coomassie Blue-stained gel showing the stepwise purification of recombinant VPS28 protein. *Lane U*, uninduced *E. coli* cell extract; *lane I*, induced cell extract; *lane 1*, glutathione-Sepharose-bound proteins; *lane 2*, proteins following tobacco etch virus protease cleavage; *lane 3*, purified VPS28. *B*, anti-VPS28 Western blot of 5 ng of purified recombinant VPS28 (*lane 1*), lysate from 10^5 MT-4 cells (*lane 2*), and purified HIV-1 particles corresponding to 1 μg of CA protein (*lane 4*). 1 μg of CA protein was used as a control (*lane 3*) to rule out antibody cross-reactivity in the virion preparation because VPS28 and CA have similar mobilities. Note that two cross-reacting species of higher molecular mass were observed in the crude lysate (*lane 2*). *C*, anti-TSG101 Western blot of lysate from 10^5 MT-4 cells (*lane 1*), 1 μg of recombinant CA protein (control for antibody cross-reactivity; *lane 2*), and purified HIV-1 particles corresponding to 1 μg of CA protein (*lane 3*). *D*, anti-NEDD4 Western blot of the samples described for *A*. Molecular mass markers (in kilodaltons) are shown to the left of each panel.

As anti-VPS28 antibodies were not commercially available, human VPS28 was expressed in *E. coli*, purified to homogeneity, and used to elicit anti-VPS28 antibodies in rabbits (Fig. 8*A*). High titer HIV-1 preparations (~10^9 infectious units/ml) containing minimal cellular contaminants were obtained from acutely infected MT-4 cells and purified by velocity gradient centrifugation (36). The purity of the sample was evaluated on silver-stained SDS gels, which showed that the Gag proteins were the main constituents and demonstrated minimal contamination with cellular proteins (data not shown) (55).

VPS28 could be detected on Western blots of pure recombinant proteins (Fig. 8*B*, *lane 1*), cell extracts (*lane 2*), and purified HIV-1 virions (*lane 4*). VPS28 incorporation into HIV-1 particles was confirmed in independent virus preparations and by analysis of subtilisin-treated virions, which eliminated contaminating cellular vesicles and degraded proteins on the virion exterior (56), but did not significantly reduce the amount of VPS28 in the preparations (data not shown). The absolute quantities of VPS28 present within the virion were estimated by comparing the levels of virion-associated VPS28 and CA proteins with known quantities of pure recombinant CA and VPS28 (Fig. 8*A*) (data not shown). In different virus preparations, between 1 and 5 ng of VPS28/μg of CA was detected, corresponding to a molar ratio of ~1:200–1000. Assuming ~5000 Gag molecules/virion (57), this implies that 5–25 molecules of VPS28 were incorporated per virion.

We also screened for HIV-1 incorporation of endogenous TSG101 and NEDD4 as well as overexpressed VPS37B-FLAG. These experiments were not quantitative, however, because we lacked the appropriate recombinant protein standards. Nevertheless, endogenous TSG101 was readily detected in both cell extracts and purified virus particles (Fig. 8*C*), indicating that the protein was specifically incorporated by HIV-1. Interestingly, both TSG101 and endogenous murine leukemia viral Gag proteins were also detected in exosomes (MVB vesicles released from cells) (58–60), which further emphasizes the similarities between viral particle release and MVB vesicle biogenesis. In contrast, NEDD4 was not detected in virions (Fig. 8*D*), despite the fact that this protein was readily detected in cell extracts and has been reported to bind TSG101 (61). Several other control proteins that partially localized to the plasma membrane were also undetectable in the purified virus preparations, confirming that these preparations were not contaminated with cellular proteins (data not shown). We therefore conclude that TSG101, like VPS28, is also specifically incorporated into HIV-1 particles, whereas NEDD4 is not. NEDD4 was detected in purified particles of Mason-Pfizer monkey virus, a virus that buds via a different late domain (PPPY) (62), reinforcing the idea that these two different late domains perform distinct functions in virus budding. Finally, we were unable to confirm that VPS37B was specifically incorporated into HIV-1 particles. Although VPS37B-FLAG was detected in purified virions, the levels appeared very low relative to the levels of overexpressed protein in the producer cells (data not shown). These observations raise the possibility that VPS37B may be lost during the process of viral assembly.

DISCUSSION

The $p6^{Gag}$ PTAP late domain is required for efficient HIV-1 replication in most cell types, including primary cells (5). The PTAP late domain recruits TSG101, which in turn functions within a multiprotein complex (ESCRT-I) that links the virus to cellular machinery that normally functions in protein sorting and vesicle formation in the MVB (reviewed in Ref. 1). Previous studies have demonstrated that the N-terminal half of TSG101 (residues 1–249) is not required for virus budding when the C-terminal half of the protein (residues 250–390) is fused directly to the viral Gag protein (7). Thus, the N-terminal half of TSG101 appears to function primarily in recruiting the protein to the sites of virus budding, whereas the C-terminal half of the protein contains binding sites for other proteins that function in virus budding, including the other members of the ESCRT-I complex, VPS28 and VPS37. Our studies were performed with the goals of identifying human orthologs of VPS37 and testing the importance of different TSG101 interactions in HIV-1 release.

TSG101 Recruitment—TSG101 is recruited to sites of virus release, at least in part, through direct interactions with P(S/T)AP late domains found in the structural proteins from a number of different enveloped viruses, including HIV-1 (6–9). Using TSG101 depletion/replacement assays, we found an excellent correlation between the affinities of WT and mutant TSG101 proteins for the HIV-1 PTAP late domain and their ability to support HIV-1 release from 293T cells. The mutations under study presumably also affected TSG101 interactions with cellular binding partners because the TSG101 UEV domain can also bind to P(S/T)AP motifs located within a series of cellular proteins, including HRS (17–20), AIP1 (26–28), TSG101 itself (17), and VPS37B (this work). However, as TSG101 fragments lacking the UEV domain can support virus budding when fused directly to the HIV-1 Gag protein, these TSG101 UEV domain/cellular protein interactions cannot be absolutely essential for HIV budding, although they may help to "activate" the autoinhibited full-length TSG101 protein (17–20). Hence, our experiments further confirm the functional importance of the TSG101 UEV domain/Gag P(S/T)AP interaction for HIV-1 release and indicate that any reductions in PTAP binding affinity (or levels of active TSG101 protein) can be expected to reduce viral titers. This makes the TSG101 UEV domain/PTAP motif-binding pocket an attractive target for inhibitor development.

Identification of Human VPS37 Proteins—As a necessary step in understanding how the human ESCRT-I complex functions in virus release and MVB biogenesis, we identified a series of putative human VPS37 proteins and characterized one of them, VPS37B, in detail. A number of criteria establish human VPS37B as an ortholog of yeast Vps37p, including the following. 1) The two proteins share modest but identifiable sequence similarity. 2) Both proteins bind to central/C-terminal regions of TSG101/Vps23p (16). 3) Both proteins can form stable subunits of ~350-kDa ESCRT-I complexes. 4) Both proteins become trapped on the Class E endosomal compartment in the absence of VPS4 ATPase activity. 5) VPS37B can recruit functional human ESCRT-I activity *in vivo*, as judged by its ability to support the release of infectious HIV-1 virions lacking endogenous PTAP late domains.

VPS37B belongs to a family of four human proteins that share clear sequence similarity (Fig. 1*B*), and our data demonstrate that at least one of the other proteins (VPS37A) binds TSG101. Thus, it appears that *all* of these proteins may be VPS37 orthologs. Although this idea remains to be tested experimentally, there is already precedence for this type of diversity in the mammalian MVB pathway, where other single yeast proteins appear to have diverged into multiple human proteins that perform overlapping or redundant functions (*e.g.* human VPS4A and VPS4B are both orthologs of yeast Vps4p). It will therefore be of interest to determine the relationship between the different human VPS37-like proteins, all of which appear to be widely expressed.

The sequence similarities between the different human VPS37-like proteins (and the putative *Drosophila* VPS37 protein) are strongest within an ~150-residue domain (the mod_r domain). This domain was first identified in the *Drosophila* modifier of rudimentary (Mod_r) protein, which modulates expression of the rudimentary protein (40). Although mod_r domains are found within a number of eukaryotic proteins, their functions are not well understood, and the presence of a mod_r domain therefore cannot yet be used to infer biological activity. Importantly, our mapping experiments indicate that the VPS37B mod_r domain contains the binding site for TSG101, which represents the first well characterized biochemical function for any mod_r domain.

Beyond their conserved mod_r domains, the different human VPS37-like proteins each contain unique elements that suggest interesting and unique biological functions. Specifically, VPS37B uniquely contains a PTAP motif, which is the binding site for the TSG101 UEV domain; VPS37C and VPS37D contain N- and C-terminal extensions of unknown function; and VPS37A/HCRP1 contains a putative UEV domain. This is of potential significance because other UEV domains bind ubiquitin (6, 16, 63, 64) and because ubiquitin performs a number of important roles in the MVB and HIV-1 budding pathways (1, 14, 15). However, the residues known to bind ubiquitin and PTAP sequences are not conserved in alignments of the TSG101 and VPS37A/HCRP1 UEV domains (39), and the function of this domain therefore remains to be determined experimentally.

HCRP1 was previously identified by positional cloning and shown to be down-regulated in hepatocellular carcinoma development (39). Although the protein has not been shown defini-

tively to act as a tumor suppressor *in vivo*, its expression is reduced in human cellular carcinomas, and reduction of VPS37A/HCRP1 levels in the human cellular carcinoma cell line BEL-7404 stimulates cell growth and enhances cell invasiveness *in vitro* (39). Similarly, reductions of TSG101 levels allowed NIH3T3 cells to grow on soft agar and to form metastatic tumors in nude mice (65), although genetic deletions of TSG101 do not induce tumor formation (66). It therefore appears that altered levels (or composition) of ESCRT-I can give rise to improperly regulated cell growth in some contexts.

Human ESCRT-I and HIV-1 Release—In addition to TSG101 and VPS37B, the human ESCRT-I complex also contains VPS28. VPS28 binds a C-terminal site on TSG101 that we have mapped to residues 330–377 and is unstable in the absence of this binding site. As in yeast, it appears that the TSG101, VPS28, and VPS37B proteins must be present in multiple copies to create a complex of ~350 kDa. Consistent with this idea, all three proteins bind to themselves in directed yeast two-hybrid experiments, suggesting that they can form homo-oligomers (Refs. 25, 26, and 29 and this work). At this stage, we cannot rule out the possibility that human ESCRT-I complexes may also contain additional proteins, and the other human VPS37 paralogs are obvious candidates.

Importantly, HIV-1 release was not supported by truncated TSG101 proteins that were missing their VPS28-binding sites (and therefore exhibited reduced VPS28 levels). This observation supports the idea that VPS28 plays a functional role in virus release and is in excellent agreement with previous work of Bieniasz and co-workers (27), who also found that VPS28 is required for HIV-1 release and identified several mutations in TSG101 residues 360–370 that inhibit both VPS28 binding and HIV-1 budding. Further evidence for a direct role for ESCRT-I in virus budding was provided by our observation that endogenous TSG101 and VPS28 were both specifically incorporated into highly purified HIV-1 particles prepared from infected T-cells, although we were unable to demonstrate specific incorporation of VPS37B. We estimate that, on average, 5–25 VPS28 molecules are incorporated into each virus particle. It is likely that virion levels of TSG101 are lower, however, as the stoichiometry of Vps28p to Vps23p in the yeast ESCRT-I complex is estimated to be ~1:6 (16).

In summary, our studies have identified human VPS37B as a new component of the human ESCRT-I complex and revealed that VPS37B can rescue the release of HIV-1 Gag proteins that lack endogenous PTAP late domains. Thus, all three known members of the human ESCRT-I complex are able to support virus release and infectivity (Refs. 7 and 52 and this work), demonstrating remarkable flexibility in the requirements for viral entry into the MVB biogenesis pathway.

Acknowledgments—We thank Drs. Volker Vogt, Harald Stenmark, and Paul Bieniasz for communicating data prior to publication; Dr. Markus Babst for helpful suggestions; Rob Fisher for performing the TSG101 UEV domain/VPS37 PTAP peptide binding experiments; Dan Higginson for constructing the VPS37-FLAG expression construct; and Drs. Heinrich Göttlinger and Harald Stenmark for pointing out the mod_r domain within VPS37D/WBSCR24.

REFERENCES

1. Morita, E., and Sundquist, W. I. (2004) *Annu. Rev. Cell Dev. Biol.*, in press
2. Göttlinger, H. G., Dorfman, T., Sodroski, J. G., and Haseltine, W. A. (1991) *Proc. Natl. Acad. Sci. U. S. A.* **88,** 3195–3199
3. Huang, M., Orenstein, J. M., Martin, M. A., and Freed, E. O. (1995) *J. Virol.* **69,** 6810–6818
4. Wills, J. W., and Craven, R. C. (1991) *AIDS* **5,** 639–654
5. Demirov, D. G., Orenstein, J. M., and Freed, E. O. (2002) *J. Virol.* **76,** 105–117
6. Garrus, J. E., von Schwedler, U. K., Pornillos, O. W., Morham, S. G., Zavitz, K. H., Wang, H. E., Wettstein, D. A., Stray, K. M., Cote, M., Rich, R. L., Myszka, D. G., and Sundquist, W. I. (2001) *Cell* **107,** 55–65
7. Martin-Serrano, J., Zang, T., and Bieniasz, P. D. (2001) *Nat. Med.* **7,** 1313–1319
8. Demirov, D. G., Ono, A., Orenstein, J. M., and Freed, E. O. (2002) *Proc. Natl. Acad. Sci. U. S. A.* **99,** 955–960
9. VerPlank, L., Bouamr, F., LaGrassa, T. J., Agresta, B., Kikonyogo, A., Leis, J., and Carter, C. A. (2001) *Proc. Natl. Acad. Sci. U. S. A.* **98,** 7724–7729
10. Bouamr, F., Melillo, J. A., Wang, M. Q., Nagashima, K., De Los Santos, M., Rein, A., and Goff, S. P. (2003) *J. Virol.* **77,** 11882–11895Q. W.
11. Licata, J. M., Simpson-Holley, M., Wright, N. T., Han, Z., Paragas, J., and Harty, R. N. (2003) *J. Virol.* **77,** 1812–1819
12. Strecker, T., Eichler, R., Meulen, J., Weissenhorn, W., Klenk, H. D., Garten, W., and Lenz, O. (2003) *J. Virol.* **77,** 10700–10705
13. Perez, M., Craven, R. C., and De La Torre, J. C. (2003) *Proc. Natl. Acad. Sci. U. S. A.* **100,** 12978–12983
14. Katzmann, D. J., Odorizzi, G., and Emr, S. D. (2002) *Nat. Rev. Mol. Cell. Biol.* **3,** 893–905
15. Raiborg, C., Rusten, T. E., and Stenmark, H. (2003) *Curr. Opin. Cell Biol.* **15,** 446–455
16. Katzmann, D. J., Babst, M., and Emr, S. D. (2001) *Cell* **106,** 145–155
17. Lu, Q., Hope, L. W., Brasch, M., Reinhard, C., and Cohen, S. N. (2003) *Proc. Natl. Acad. Sci. U. S. A.* **100,** 7626–7631
18. Bache, K. G., Brech, A., Mehlum, A., and Stenmark, H. (2003) *J. Cell Biol.* **162,** 435–442
19. Pornillos, O., Higginson, D. S., Stray, K. M., Fisher, R. D., Garrus, J. E., Payne, M., He, G. P., Wang, H. E., Morham, S. G., and Sundquist, W. I. (2003) *J. Cell Biol.* **162,** 425–434
20. Katzmann, D. J., Stefan, C. J., Babst, M., and Emr, S. D. (2003) *J. Cell Biol.* **162,** 413–423
21. Bilodeau, P. S., Winistorfer, S. C., Kearney, W. R., Robertson, A. D., and Piper, R. C. (2003) *J. Cell Biol.* **163,** 237–243
22. Babst, M., Odorizzi, G., Estepa, E. J., and Emr, S. D. (2000) *Traffic* **1,** 248–258
23. Bishop, N., Horman, A., and Woodman, P. (2002) *J. Cell Biol.* **157,** 91–101
24. Hewitt, E. W., Duncan, L., Mufti, D., Baker, J., Stevenson, P. G., and Lehner, P. J. (2002) *EMBO J.* **21,** 2418–2429
25. Bishop, N., and Woodman, P. (2001) *J. Biol. Chem.* **276,** 11735–11742
26. von Schwedler, U. K., Stuchell, M., Muller, B., Ward, D. M., Chung, H. Y., Morita, E., Wang, H. E., Davis, T., He, G. P., Cimbora, D. M., Scott, A., Krausslich, H. G., Kaplan, J., Morham, S. G., and Sundquist, W. I. (2003) *Cell* **114,** 701–713
27. Martin-Serrano, J., Yaravoy, A., Perez-Caballero, D., and Bieniasz, P. D. (2003) *Proc. Natl. Acad. Sci. U. S. A.* **100,** 12414–12419
28. Strack, B., Calistri, A., Craig, S., Popova, E., and Göttlinger, H. G. (2003) *Cell* **114,** 689–699
29. Martin-Serrano, J., Zang, T., and Bieniasz, P. D. (2003) *J. Virol.* **77,** 4794–4804
30. Feng, G. H., Lih, C. J., and Cohen, S. N. (2000) *Cancer Res.* **60,** 1736–1741
31. Giot, L., Bader, J. S., Brouwer, C., Chaudhuri, A., Kuang, B., Li, Y., Hao, Y. L., Ooi, C. E., Godwin, B., Vitols, E., Vijayadamodar, G., Pochart, P., Machineni, H., Welsh, M., Kong, Y., Zerhusen, B., Malcolm, R., Varrone, Z., Collis, A., Minto, M., Burgess, S., McDaniel, L., Stimpson, E., Spriggs, F., Williams, J., Neurath, K., Ioime, N., Agee, M., Voss, E., Furtak, K., Renzulli, R., Aanensen, N., Carrolla, S., Bickelhaupt, E., Lazovatsky, Y., DaSilva, A., Zhong, J., Stanyon, C. A., Finley, R. L., Jr., White, K. P., Braverman, M., Jarvie, T., Gold, S., Leach, M., Knight, J., Shimkets, R. A., McKenna, M. P., Chant, J., and Rothberg, J. M. (2003) *Science* **302,** 1727–1736
32. Bartel, P. L., and Fields, S. (1995) *Methods Enzymol.* **254,** 241–263
33. Hermida-Matsumoto, L., and Resh, M. D. (2000) *J. Virol.* **74,** 8670–8679
34. von Schwedler, U. K., Stemmler, T. L., Klishko, V. Y., Li, S., Albertine, K. H., Davis, D. R., and Sundquist, W. I. (1998) *EMBO J.* **17,** 1555–1568
35. Elbashir, S. M., Harborth, J., Lendeckel, W., Yalcin, A., Weber, K., and Tuschl, T. (2001) *Nature* **411,** 494–498
36. Welker, R., Hohenberg, H., Tessmer, U., Huckhagel, C., and Krausslich, H. G. (2000) *J. Virol.* **74,** 1168–1177
37. Dettenhofer, M., and Yu, X. F. (1999) *J. Virol.* **73,** 1460–1467
38. Groβ, I., Hohenberg, H., and Krausslich, H. G. (1997) *Eur. J. Biochem.* **249,** 592–600
39. Xu, Z., Liang, L., Wang, H., Li, T., and Zhao, M. (2003) *Biochem. Biophys. Res. Commun.* **311,** 1057–1066
40. Begley, D., Murphy, A. M., Hiu, C., and Tsubota, S. I. (1995) *Mol. Gen. Genet.* **248,** 69–78
41. Pornillos, O., Alam, S. L., Rich, R. L., Myszka, D. G., Davis, D. R., and Sundquist, W. I. (2002) *EMBO J.* **21,** 2397–2406
42. Deleted in proof
43. Bowers, K., Lottridge, J., Helliwell, S. B., Goldthwaite, L. M., Luzio, J. P., and Stevens, T. H. (2004) *Traffic* **5,** 194–210
44. Finken-Eigen, M., Rohricht, R. A., and Kohrer, K. (1997) *Curr. Genet.* **31,** 469–480
45. Babst, M., Sato, T. K., Banta, L. M., and Emr, S. D. (1997) *EMBO J.* **16,** 1820–1831
46. Babst, M., Wendland, B., Estepa, E. J., and Emr, S. D. (1998) *EMBO J.* **17,** 2982–2993
47. Yoshimori, T., Yamagata, F., Yamamoto, A., Mizushima, N., Kabeya, Y., Nara, A., Miwako, I., Ohashi, M., Ohsumi, M., and Ohsumi, Y. (2000) *Mol. Biol. Cell* **11,** 747–763
48. Scheuring, S., Rohricht, R. A., Schoning-Burkhardt, B., Beyer, A., Muller, S., Abts, H. F., and Kohrer, K. (2001) *J. Mol. Biol.* **312,** 469–480
49. Fujita, H., Yamanaka, M., Imamura, K., Tanaka, Y., Nara, A., Yoshimori, T., Yokota, S., and Himeno, M. (2003) *J. Cell Sci.* **116,** 401–414
50. Hislop, J. N., Marley, A., and von Zastrow, M. (2004) *J. Biol. Chem.* **279,** 22522–22531
51. Patnaik, A., Chau, V., and Wills, J. W. (2000) *Proc. Natl. Acad. Sci. U. S. A.* **97,** 13069–13074
52. Tanzi, G. O., Piefer, A. J., and Bates, P. (2003) *J. Virol.* **77,** 8440–8447
53. Martin-Serrano, J., Perez-Caballero, D., and Bieniasz, P. D. (2004) *J. Virol.* **78,** 5554–5563

54. Pornillos, O., Alam, S. L., Davis, D. R., and Sundquist, W. I. (2002) *Nat. Struct. Biol.* **9,** 812–817
55. Muller, B., Patschinsky, T., and Krausslich, H. G. (2002) *J. Virol.* **76,** 1015–1024
56. Ott, D. E., Coren, L. V., Johnson, D. G., Kane, B. P., Sowder, R. C., II, Kim, Y. D., Fisher, R. J., Zhou, X. Z., Lu, K. P., and Henderson, L. E. (2000) *Virology* **266,** 42–51
57. Briggs, J. A., Simon, M. N., Gross, I., Kräusslich, H. G., Fuller, S. D., Vogt, V. M., and Johnson, M. C. (2004) *Nat. Struct. Mol. Biol.* **11,** 672–675
58. Thery, C., Regnault, A., Garin, J., Wolfers, J., Zitvogel, L., Ricciardi-Castagnoli, P., Raposo, G., and Amigorena, S. (1999) *J. Cell Biol.* **147,** 599–610
59. Denzer, K., Kleijmeer, M. J., Heijnen, H. F., Stoorvogel, W., and Geuze, H. J. (2000) *J. Cell Sci.* **113,** 3365–3374
60. Thery, C., Boussac, M., Veron, P., Ricciardi-Castagnoli, P., Raposo, G., Garin, J., and Amigorena, S. (2001) *J. Immunol.* **166,** 7309–7318
61. Carter, C. A. (2002) *Trends Microbiol.* **10,** 203–205
62. Gottwein, E., Bodem, J., Muller, B., Schmechel, A., Zentgraf, H., and Krausslich, H. G. (2003) *J. Virol.* **77,** 9474–9485
63. VanDemark, A. P., Hofmann, R. M., Tsui, C., Pickart, C. M., and Wolberger, C. (2001) *Cell* **105,** 711–720
64. McKenna, S., Hu, J., Moraes, T., Xiao, W., Ellison, M. J., and Spyracopoulos, L. (2003) *Biochemistry* **42,** 7922–7930
65. Li, L., and Cohen, S. N. (1996) *Cell* **85,** 319–329
66. Wagner, K. U., Krempler, A., Qi, Y., Park, K., Henry, M. D., Triplett, A. A., Riedlinger, G., Rucker, I. E., and Hennighausen, L. (2003) *Mol. Cell. Biol.* **23,** 150–162
67. Wolf, E., Kim, P. S., and Berger, B. (1997) *Protein Sci.* **6,** 1179–1189
68. Lupas, A., Van Dyke, M., and Stock, J. (1991) *Science* **252,** 1162–1164
69. Gasteiger, E., Gattiker, A., Hoogland, C., Ivanyi, I., Appel, R. D., and Bairoch, A. (2003) *Nucleic Acids Res.* **31,** 3784–3788
70. Hammond, S. M., Caudy, A. A., and Hannon, G. J. (2001) *Nat. Rev. Genet.* **2,** 110–119
71. Elbashir, S. M., Harborth, J., Weber, K., and Tuschl, T. (2002) *Methods* **26,** 199–213
72. Shi, Y. (2003) *Trends Genet.* **19,** 9–12
73. Schwarz, D. S., Hutvagner, G., Haley, B., and Zamore, P. D. (2002) *Mol. Cell* **10,** 537–548
74. Chiu, Y. L., and Rana, T. M. (2002) *Mol. Cell* **10,** 549–561
75. Martinez, J., Patkaniowska, A., Urlaub, H., Luhrmann, R., and Tuschl, T. (2002) *Cell* **110,** 563–574

CHAPTER 4

ESCRT-III RECOGNITION BY VPS4 ATPASES

Melissa D. Stuchell-Brereton, Jack J. Skalicky, Collin Kieffer, Mary Anne Karren, Sanaz Ghaffarian, and Wesley Sundquist

Reprinted from Nature, Vol. 449, pages 740-744, Copyright 2007.

Note: Cloning of CHMP and VPS4 constructs, purification of CHMP and VPS4 proteins, identification of C-terminal CHMP region required for VPS4 binding, biosensor experiments, homologue searches and alignments, NMR data collection, analysis of NMR data and determination of the solution structure of unbound VPS4B and of VPS4B in complex with CHMP2B (195-213) were performed by Melissa D. Stuchell-Brereton and contributed to Figures 1A, 1B, 2A, 4C, and Supplemental Table 1 and 2, and Supplemental Figures 3a, 3b, 3c, 3d, 4a, 4b, 4c, 4d, 4e, 4f, and 4g. Purification of VPS4A and CHMP1A proteins, NMR data collection, analysis of NMR data and determination of the solution structure of VPS4A in complex with CHMP1A were performed by Jack J. Skalicky and contributed to Figure 2B, 2C, 2D, 2E, 2F, Supplemental Table 1, and Supplemental Figures 1a, 1b, 1c, and 2. GFP-VPS4 cloning, localization studies, HIV-1 vector release and infectivity experiments, and biosensor experiments were performed by Collin Kieffer and contributed to Figures 4A, 4B, and Supplemental Figure 5. GFP-CPS cloning, CPS sorting assays, and Vps4p localization

studies in yeast were performed by Mary Anne Karren and contributed to Figures 3A, 3B, and Supplemental Figure 6. Cloning of constructs and production of protein were performed by Sanaz Ghaffarian and contributed to Figure 1. All Supplemental data is shown in Appendix B.

nature Vol 449|11 October 2007|doi:10.1038/nature06172

LETTERS

ESCRT-III recognition by VPS4 ATPases

Melissa D. Stuchell-Brereton[1]*, Jack J. Skalicky[1]*, Collin Kieffer[1], Mary Anne Karren[1], Sanaz Ghaffarian[1] & Wesley I. Sundquist[1]

The ESCRT (endosomal sorting complex required for transport) pathway is required for terminal membrane fission events in several important biological processes, including endosomal intraluminal vesicle formation[1,2], HIV budding[3] and cytokinesis[4]. VPS4 ATPases perform a key function in this pathway by recognizing membrane-associated ESCRT-III assemblies and catalysing their disassembly[5–7], possibly in conjunction with membrane fission. Here we show that the microtubule interacting and transport (MIT) domains of human VPS4A and VPS4B bind conserved sequence motifs located at the carboxy termini of the CHMP1–3 class of ESCRT-III proteins. Structures of VPS4A MIT–CHMP1A and VPS4B MIT–CHMP2B complexes reveal that the C-terminal CHMP motif forms an amphipathic helix that binds in a groove between the last two helices of the tetratricopeptide-like repeat (TPR) of the VPS4 MIT domain, but in the opposite orientation to that of a canonical TPR interaction. Distinct pockets in the MIT domain bind three conserved leucine residues of the CHMP motif, and mutations that inhibit these interactions block VPS4 recruitment, impair endosomal protein sorting and relieve dominant-negative VPS4 inhibition of HIV budding. Thus, our studies reveal how the VPS4 ATPases recognize their CHMP substrates to facilitate the membrane fission events required for the release of viruses, endosomal vesicles and daughter cells.

MIT domains are found in a number of proteins involved in cellular trafficking, where they frequently function as protein interaction modules[8,9]. The ESCRT-III proteins, in particular, interact with a series of different MIT-domain-containing proteins[10] including VPS4A and VPS4B[6,11], spastin[12], AMSH (associated molecule with the SH3 domain of STAM)[10,13–15], and others[10]. Biosensor binding experiments demonstrated that the human VPS4B MIT domain bound both full-length CHMP1B and a shorter, more soluble construct ($CHMP1B_{65–196}$) with dissociation constants of about 30 μM (Fig. 1a, dark blue and red curves)[11]. A series of amino-terminal deletion constructs were used to map the minimal VPS4B MIT-binding site on CHMP1B, and these experiments revealed that a construct spanning just the C-terminal 17 residues of CHMP1B bound the VPS4B MIT domain with nearly full affinity (Fig. 1a, green curve; K_d 34 ± 1 μM (mean ± s.d.). In contrast, a CHMP1B construct lacking this region ($CHMP1B_{65–180}$) did not bind (Fig. 1a, black curve), in good agreement with reports that deletion of the C terminus of CHMP3 blocks VPS4 and AMSH binding[14,16]. Similar binding data were obtained for the VPS4A MIT domain (not shown), indicating that the C-terminal end of CHMP1B is necessary and sufficient for VPS4 MIT binding.

The ten canonical human ESCRT-III proteins fall into two general classes (CHMP1–3 and CHMP4–6) based on sequence homology and functional similarities. These two classes can be further subdivided into the six different CHMP families, each of which corresponds to one of the six ESCRT-III-like proteins in yeast[7,17,18]. Sequence alignments revealed that three highly conserved leucine residues are arrayed in a heptad repeat at the C termini of CHMP1–3 proteins but not CHMP4–6 proteins (Fig. 2a, CHMP1A positions 187, 191 and 194). Mutation of either of the two most conserved leucine residues within CHMP1B decreased VPS4A and VPS4B MIT binding more than tenfold, confirming the importance of these residues for interactions between VPS4 MIT and CHMP1B (Fig. 1a, orange and teal curves and data not shown).

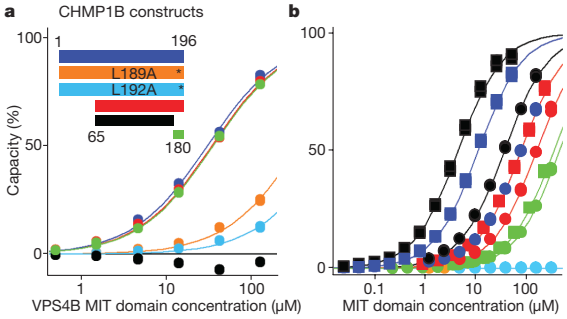

Figure 1 | VPS4 MIT–CHMP binding interactions. a, Biosensor binding isotherms showing VPS4B MIT binding to the wild-type and mutant CHMP1B proteins depicted schematically in the inset. The data demonstrate that the final 17 residues of CHMP1B are necessary and sufficient for full-affinity VPS4B MIT binding and that binding is inhibited by mutations in the two most conserved residues within this region (L189A and L192A). Duplicate data points are shown for each condition, and estimated dissociation constants derived from fits to single site binding models (curves) were as follows: CHMP1B, 29 ± 1 μM; $CHMP1B_{65–196}$, 33 ± 1 μM; $CHMP1B_{180–196}$, 34 ± 1 μM; $CHMP1B_{L189A}$, 353 ± 8 μM; $CHMP1B_{L192A}$, 810 ± 40 μM (means ± s.d.). Note that in other cases, VPS4 MIT domains bound even more tightly to isolated binding sites than to the corresponding full-length CHMP proteins, which is consistent with an autoinhibitory mechanism (refs 16, 29, 30; data not shown). **b**, Biosensor binding isotherms showing C-terminal peptides from CHMP1A and CHMP2B binding GST–VPS4A MIT and GST–VPS4B MIT under different solution conditions. The data show that both VPS4 MIT domains bind specifically to the CHMP1A and CHMP2B C termini, and that the affinities vary with different MIT domains, CHMP proteins and solution conditions. Representative data are shown for low salt and pH conditions ('L', 20 mM phosphate pH 5.5 (NMR conditions); squares) and medium salt and pH conditions ('M', 20 mM Tris-HCl pH 8.0, 100 mM NaCl; circles). Estimated dissociation constants derived from fits to single-site binding models were as follows: VPS4A MIT–$CHMP1A_{180–196}$ (black), 4.61 ± 0.02 μM (L) and 33.4 ± 0.2 μM (M); VPS4A MIT–$CHMP2B_{195–213}$ (red), 71.8 ± 0.3 μM (L) and 178 ± 1 μM (M); VPS4B MIT–$CHMP1A_{180–196}$ (blue), 13.4 ± 0.1 μM (L) and 74.0 ± 0.3 μM (M); VPS4B MIT–$CHMP2B_{195–213}$ (green), 273 ± 0.2 μM (L) and 402 ± 2 μM (M). Background binding of both CHMP peptides to control GST surfaces was negligible under both conditions, as shown for the medium-salt conditions ($CHMP1A_{180–196}$, orange; $CHMP2B_{195–213}$, cyan).

[1]Department of Biochemistry, Room 4100, 15 N. Medical Drive East, University of Utah, Salt Lake City, Utah 84112-5650, USA.
*These authors contributed equally to this work.

To assess the generality of VPS4 MIT binding to the C termini of the CHMP1–3 proteins, peptides corresponding to these regions of CHMP1A, CHMP1B, CHMP2A and CHMP2B were tested and shown to bind the MIT domains of VPS4A and VPS4B in every case (Fig. 1b, Supplementary Fig. 1, and data not shown). Thus, this sequence motif constitutes a generalized VPS4 MIT-binding site. In contrast, binding of VPS4 MIT to proteins of the CHMP4–6 class was much more variable and the binding site did not map to the C terminus of CHMP6 (the one case studied in detail). VPS4 MIT domains can therefore also bind a subset of the CHMP4–6 proteins, but the recognition mode is different and will be described elsewhere.

Our initial surveys revealed that dissociation constants for MIT binding to CHMP1A, CHMP1B, CHMP2A and CHMP2B peptides varied throughout the micromolar range, with tighter binding generally associated with VPS4A, with reduced temperatures, with reduced ionic strengths and with slightly acidic conditions. Several of these trends are evident in the isotherms for VPS4 MIT domains binding to $CHMP1A_{180–196}$ and $CHMP2B_{195–213}$ (Fig. 1b). Representative strong (VPS4A MIT–$CHMP1A_{180–196}$; K_d 4.6 μM) and weak (VPS4B MIT–$CHMP2B_{195–213}$; K_d 273 μM) complexes were selected for structural studies by NMR. Studies of VPS4A MIT–$CHMP1A_{180–196}$ and free VPS4B MIT were straightforward and yielded high-quality structures (Fig. 2, Supplementary Figs 1–3 and Supplementary Table 1), whereas assignment of intermolecular nuclear Overhauser effects in the weaker VPS4B MIT–$CHMP2B_{195–213}$ complex required reference to the VPS4A MIT–$CHMP1A_{180–196}$ structure (Supplementary Fig. 4, Supplementary Table 1 and Supplementary Methods). Thus, although the two VPS4 MIT–CHMP structures were similar, only the VPS4A MIT–$CHMP1A_{180–196}$ complex is described here in detail.

N-terminal domains of AAA ATPases generally dictate substrate specificity and therefore vary considerably in structure[19]. The VPS4A MIT domain is a three-helix bundle[11,20], and $CHMP1A_{180–196}$ forms a fourth helix that binds in the groove between helices 2 and 3 (Fig. 2b, c). The three conserved $CHMP1A_{180–196}$ leucine residues line one side of the amphipathic helix, and each binds in a hydrophobic pocket along the groove (Fig. 2c–f). These interactions seem to constitute the primary recognition determinants, but complementary salt bridges are also made by three of the adjacent conserved CHMP1A residues (Glu 184, Arg 190 and Arg 195; see Fig. 2). The structure nicely explains existing mutagenesis data showing the importance of several MIT residues for CHMP binding[11]. In particular, the VPS4A MIT Leu 64 residue has a critical function in helping to define all three MIT-binding pockets (highlighted in blue in Fig. 2c–f), and an L64A mutation decreases CHMP1B binding more than 30-fold[11]. The structures indicated that an Asp residue at this position would weaken binding even further by interacting unfavourably with all three conserved CHMP1–3 leucine residues, and, indeed, VPS4A MIT_{L64D} did not detectably bind glutathione *S*-transferase (GST)-tagged $CHMP1B_{180–196}$ at protein concentrations up to 250 μM (Supplementary Fig. 5). A VPS4A MIT E68A mutation also decreased the CHMP1B binding affinity 2–3-fold[11], which is consistent with the conserved salt bridge observed between VPS4A Glu 68 and CHMP1A Arg 190.

The structures further revealed that two previous proposals for MIT–CHMP interactions were incorrect. Specifically, CHMP1–3 proteins do not bind between MIT helices 1 and 2 to complete a canonical four-helix bundle[20], nor does the binding of the CHMP helix between MIT helices 2 and 3 complete a second paired tetratricopeptide helical repeat[11]. Instead, the CHMP helix binds parallel to MIT helix 3, whereas a TPR-like interaction would have the opposite orientation. Hence, although the TPR-like disposition of the three MIT helices helps to define the geometry of the CHMP binding site, the interaction mode has not previously been observed.

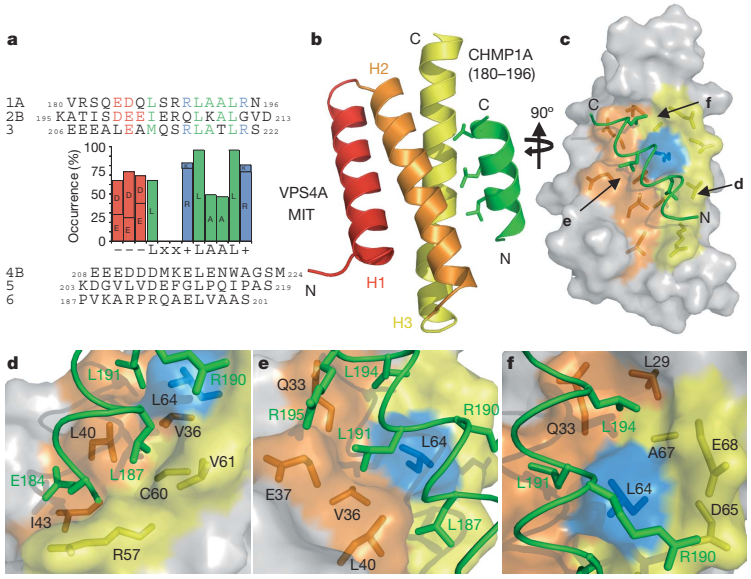

Figure 2 | Structural basis for VPS4 MIT recognition of CHMP1–3. **a**, Alignments of ESCRT-III protein C termini. C-terminal sequences of human proteins from the six CHMP classes are shown explicitly, together with a graph showing the degree of sequence conservation within aligned CHMP1–3 C termini (50 sequences; see Supplementary Table 2) and the consensus sequence (below the graph). Note that ESCRT-III proteins of the CHMP4–6 class do not conform to the consensus. **b**, Solution structure of the VPS4A MIT–$CHMP1A_{180–196}$ complex, with the three conserved $CHMP1A_{180–196}$ leucines shown explicitly. This helical colour scheme is also used in **c**–**f**. **c**, Structure of the VPS4A MIT–$CHMP1A_{180–196}$ complex. The MIT domain is shown in a space-filling model with Leu 64 highlighted in blue; important residues on both sides of the interface are shown explicitly. Arrows denote the approximate orientations of the three leucine-binding pockets shown in **d**–**f**. **d**–**f**, Close-up views of the three leucine-binding pockets of the VPS4A MIT domain showing the hydrophobic pocket views in detail, as well as complementary charge interactions between Glu 184 and Arg 57 (**d**), between Arg 195 and Glu 37 (**e**), and between Arg 190 and Glu 68 (Asp 65) (**f**); CHMP1A residues are listed first.

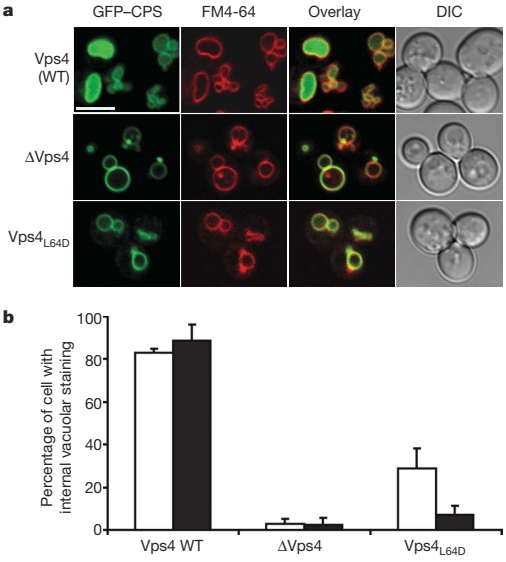

Figure 3 | The Vps4 MIT Leu64Asp mutation inhibits membrane protein sorting into the vacuolar lumen. **a**, Confocal fluorescence slices of live yeast cells showing localization of the model membrane protein cargo, GFP–CPS, in the presence of wild-type (WT) Vps4 (top row), no Vps4 (middle row) or $Vps4_{L64D}$ (bottom row), at 30 °C. FM4-64 staining (red) was used to define the limiting vacuolar membrane (open circles) and to reveal class E compartments (intense puncta in the middle and bottom rows). Overlaid fluorescence and differential interference contrast (DIC) images are shown in the right two columns for reference. Scale bar, 5 μm. **b**, Graphic quantification of the experiment shown in **a**, demonstrating that the $Vps4_{L64D}$ mutant inhibits GFP–CPS trafficking into the lumen of the vacuole. GFP–CPS localization was examined at 30 °C (open columns) and 37 °C (filled columns). Data are from three independent experiments (100 cells per experiment); error bars indicate s.d.

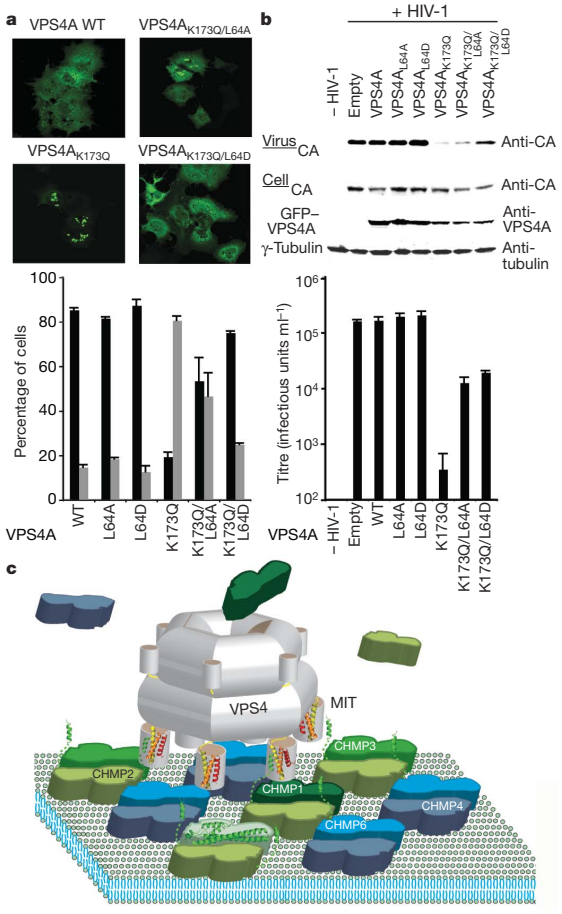

Figure 4 | Secondary MIT Leu 64 mutations decrease endosomal recruitment and inhibition of HIV-1 budding by VPS4A proteins that lack ATP-binding activity. **a**, Upper panels: confocal fluorescence slices showing representative distributions of wild-type (WT) GFP–VPS4A, GFP–$VPS4A_{K173Q}$, GFP–$VPS4A_{K173Q/L64A}$ and GFP–$VPS4A_{K173Q/L64D}$, in transfected COS7 cells. Lower panel: quantification showing that the K173Q mutation causes VPS4A to become trapped on aberrant endosomal membranes (class E compartments) and that secondary mutations at Leu 64 restore the cytoplasmic localization of VPS4A partly (L64A) or almost fully (L64D). Black columns, diffuse staining; grey columns, punctate staining. Data are from two independent experiments (at least 100 cells per experiment); error bars indicate s.d. **b**, Secondary L64A and L64D mutations decrease dominant inhibition of HIV-1 vector release and infectivity by GFP–$VPS4A_{K173Q}$. Lanes 3–8 show HIV-1 vector titres (lower panel) and virion release (upper panels) on co-expression with GFP–VPS4A (lanes 3, negative control), GFP–$VPS4A_{L64A}$ (lanes 4, negative control), GFP–$VPS4A_{L64D}$ (lanes 5), GFP–$VPS4_{K173Q}$ (lanes 6, positive control) or the doubly mutant GFP–$VPS4_{K173Q/L64A}$ (lanes 7) or GFP–$VPS4_{K173Q/L64D}$ (lanes 8) proteins. Virion release (top panel, virus) was assayed by western blot detection of virion-associated CA proteins. The lower western blots show, respectively, cell-associated Gag, exogenous GFP–VPS4A proteins and a γ-tubulin loading control. Controls lacking HIV-1 vector and exogenous GFP–VPS4A are shown in lanes 1 and 2, respectively. Vector titres (infectious units ml^{-1}) are shown in the bottom panel (triplicate measurements; error bars indicate s.d.). **c**, Schematic model showing VPS4 recruitment to the membrane-associated ESCRT-III lattice. An idealized membrane-associated ESCRT-III lattice, based on the CHMP3 crystal structure and lattice contacts[2,29], is shown with the C-terminal tails on the CHMP1–3 subunits exposed to interact with the MIT domains of a dodecameric VPS4 protein (grey). The VPS4 ATPase activity releases the assembled ESCRT-III lattice from the membrane and may also be coupled to vesicle formation (not shown).

Yeast Vps4 is required for the formation of intraluminal vesicles that transport membrane proteins into the late endosome and ultimately into the lumen of the vacuole[5,6]. Loss of Vps4 activity therefore induces the formation of aberrant endosomes (termed class E compartments) and inhibits membrane protein cargoes such as green fluorescent protein-labelled carboxypeptidase S (GFP–CPS) from accumulating within the vacuole (Fig. 3; compare rows 1 and 2). A single L64D point mutation within the Vps4 MIT domain also impaired the vacuolar accumulation of the GFP–CPS cargo significantly at 30 °C and almost entirely at 37 °C, showing that the structurally characterized VPS4 MIT–ESCRT-III interface is required for efficient endosomal protein sorting.

Mutations that block ATP binding by Vps4 (for example $Vps4_{K179Q}$) also induce class E compartment formation; in this case all of the ESCRT machinery, including Vps4 itself, remains trapped on the class E compartments, leading to punctate Vps4 staining in virtually every cell (Supplementary Fig. 6)[5,6]. However, the secondary L64D MIT-domain mutation substantially redistributed the $Vps4_{L64D/K179Q}$ protein from class E compartments back into the cytoplasm (Supplementary Fig. 6). Thus, this mutation inhibits protein sorting at least in part by preventing the recruitment of Vps4 to endosomal membranes.

The importance of the MIT–CHMP interaction for VPS4 recruitment to mammalian endosomes was also tested by comparing the cellular distributions of different exogenously expressed GFP–VPS4A fusion proteins (Fig. 4a). As in yeast, VPS4 ATP-binding mutants (for example $VPS4A_{K173Q}$) induce the formation of mammalian class E compartments that trap VPS4 and other ESCRT

machinery on their extended surfaces (Fig. 4a; compare VPS4A with $VPS4A_{K173Q}$)[6,21,22]. Quantitative analyses revealed that wild-type GFP–VPS4A was distributed diffusely throughout cytoplasm in 85% of cells, whereas GFP–$VPS4A_{K173Q}$ was trapped on punctate class E compartments in 79% of cells (Fig. 4a, lower panel). However, the secondary L64A mutation significantly decreased punctate/class E localization of $VPS4A_{K173Q/L64A}$ (to 47%), and the more detrimental L64D mutation decreased punctate/class E localization even further (25%), to nearly the same level as that of the wild-type protein (15%). The redistribution of doubly mutant VPS4A proteins is particularly significant for two reasons: first because these experiments were performed in the presence of endogenous wild-type VPS4A and VPS4B, which probably co-polymerize with the $VPS4_{K173Q/L64A,D}$ mutants and augment endosomal recruitment, and second because LIP5/Vta1, a VPS4 cofactor, seems to interact with both VPS4 and ESCRT-III proteins and may therefore also contribute to VPS4 recruitment[23–25].

We also tested whether the secondary L64A and L64D mutations decreased the dominant inhibition of HIV-1 release and infectivity by the $VPS4A_{K173Q}$ mutant. As reported previously[26], overexpression of the $VPS4A_{K173Q}$ mutant strongly inhibited HIV-1 release, decreasing infectious titres more than 500-fold (Fig. 4b). However, incorporation of secondary L64A or L64D mutations restored virus release and infectivity 35-fold and 55-fold, respectively, albeit to levels that were still about tenfold below those seen for wild-type VPS4A. Although the incomplete rescue by the $VPS4A_{K173Q/L64A,D}$ double mutants probably reflects a complex combination of competing effects, this experiment indicates that secondary Leu 64 mutations decrease the severity of class E compartment formation and thereby release endogenous ESCRT machinery to function in virus budding.

VPS4 enzymes are composed of three different functional elements: the N-terminal MIT domain, which binds the ESCRT-III lattice, a central AAA ATPase cassette, which mediates oligomerization and hydrolyses ATP, and a β-domain, which is inserted into the small domain of the ATPase cassette and is required for LIP5/Vta1 cofactor binding[27]. VPS4 enzymes assemble into dodecamers composed of two stacked hexameric rings, with MIT domains positioned above a large central chamber created within one of the two asymmetric rings (Fig. 4c; Z. Yu, G. Gonciarz, W. I. Sundquist, C. P. Hill and G. J. Jensen, personal communication). The ESCRT-III lattice is not yet fully characterized, but biochemical and crystallographic analyses[16,28–30] have shown that ESCRT-III protein oligomerization and membrane binding are autoinhibited by terminal elements that include the C-terminal helices described here. Removal of these elements promotes CHMP3 dimerization in solution and permits CHMP3 to be crystallized in protein 'strips' that contain two distinct dimer interfaces and create a continuous basic membrane-binding surface[28]. ESCRT-III membrane association may therefore serve to expose (and concentrate) the C-terminal CHMP1–3 helices. This oligomeric array of exposed binding sites would then promote the recruitment and assembly of dodecameric VPS4 enzymes by means of their MIT domains. The MIT domains, in turn, seem to reside at the ends of flexible tethers[27,28] and could therefore 'feed' ESCRT-III subunits into the open central chamber of the assembled enzyme.

METHODS SUMMARY

Biosensor binding experiments. Biosensor binding experiments were performed as described[11,26] with purified VPS4B MIT protein binding to immobilized GST–CHMP1B proteins (Fig. 1a) or C-terminal CHMP peptides binding to immobilized GST–VPS4 MIT proteins (Fig. 1b). All binding isotherms were fitted to simple 1:1 binding models.

Structural studies by NMR. Solution structures of VPS4A/VPS4B MIT–CHMP complexes were determined with NMR spectroscopic analyses of two sets of mixed isotope-labelled samples (all in fast exchange): $^{13}C,^{15}N$-VPS4A/VPS4B MIT plus excess $^{12}C,^{14}N$-$CHMP1A_{180–196}$/$CHMP2B_{195–213}$ and excess $^{12}C,^{14}N$-VPS4A/VPS4B MIT plus $^{13}C,^{15}N$-$CHMP1A_{180–196}$/$CHMP2B_{195–213}$. Bound structures were determined for the $^{13}C,^{15}N$-labelled component in each sample, and then docked to create binary complexes by using data from half-filtered nuclear Overhauser enhancement spectroscopy.

GFP–CPS sorting in yeast cells. *vps4Δ* yeast cells (SEY6210 genetic background) harbouring pRS415*MET25+GFP–CPS* (GFP–CPS expression) and either pRS416+*VPS4* or pRS416+$vps4_{L64D}$ (Vps4 expression) or an empty control plasmid were imaged by confocal microscopy and scored for GFP fluorescence that was primarily at the limiting vacuolar membrane or primarily within the vacuolar lumen. Yeast class E compartments and vacuolar membranes were revealed by staining with FM4-64.

GFP–VPS4 localization in mammalian cells. COS7 cells grown on coverslips were transfected with wild-type and mutant enhanced green fluorescent protein (EGFP)–VPS4A expression vectors[26]. Cells were fixed 18 h after transfection, imaged by confocal fluorescence microscopy, and scored as having either cytoplasmic or punctate GFP–VPS4 distributions.

HIV-1 vector release and infectivity. 293T cells were transfected with EGFP–VPS4 expression constructs together with an HIV-1 vector system (pCMVΔR8.2 plus pWPTS-nlsLacZ plus phCMV-VSVG). Cells and supernatants containing virions were harvested separately 48 h after transfection. Cellular protein expression levels and virion release were analysed by western blotting, and vector titres were determined by transducing HeLa-M cells.

Full protocols. Detailed methods describing sequence alignments, protein expression and purification, binding studies, NMR structure determinations, cell biology and virology experiments are provided in Supplementary Methods.

Received 2 June; accepted 15 August 2007.

1. Hurley, J. H. & Emr, S. D. The ESCRT complexes: structure and mechanism of a membrane-trafficking network. *Annu. Rev. Biophys. Biomol. Struct.* **35,** 277–298 (2006).
2. Williams, R. L. & Urbe, S. The emerging shape of the ESCRT machinery. *Nature Rev. Mol. Cell Biol.* **8,** 355–368 (2007).
3. Morita, E. & Sundquist, W. I. Retrovirus budding. *Annu. Rev. Cell Dev. Biol.* **20,** 395–425 (2004).
4. Carlton, J. G. & Martin-Serrano, J. Parallels between cytokinesis and retroviral budding—a role for the ESCRT machinery. *Science* **316,** 1908–1912 (2007).
5. Babst, M., Sato, T. K., Banta, L. M. & Emr, S. D. Endosomal transport function in yeast requires a novel AAA-type ATPase, Vps4p. *EMBO J.* **16,** 1820–1831 (1997).
6. Babst, M., Wendland, B., Estepa, E. J. & Emr, S. D. The Vps4p AAA ATPase regulates membrane association of a Vps protein complex required for normal endosome function. *EMBO J.* **17,** 2982–2993 (1998).
7. Babst, M., Katzmann, D., Estepa-Sabal, E., Meerloo, T. & Emr, S. Escrt-III. An endosome-associated heterooligomeric protein complex required for mvb sorting. *Dev. Cell* **3,** 271–282 (2002).
8. Phillips, S. A., Barr, V. A., Haft, D. H., Taylor, S. I. & Haft, C. R. Identification and characterization of SNX15, a novel sorting nexin involved in protein trafficking. *J. Biol. Chem.* **276,** 5074–5084 (2001).
9. Ciccarelli, F. D. *et al.* The identification of a conserved domain in both spartin and spastin, mutated in hereditary spastic paraplegia. *Genomics* **81,** 437–441 (2003).
10. Tsang, H. T. *et al.* A systematic analysis of human CHMP protein interactions: Additional MIT domain-containing proteins bind to multiple components of the human ESCRT III complex. *Genomics* **88,** 333–346 (2006).
11. Scott, A. *et al.* Structure and ESCRT-III protein interactions of the MIT domain of human VPS4A. *Proc. Natl Acad. Sci. USA* **102,** 13813–13818 (2005).
12. Reid, E. *et al.* The hereditary spastic paraplegia protein spastin interacts with the ESCRT-III complex-associated endosomal protein CHMP1B. *Hum. Mol. Genet.* **14,** 19–38 (2005).
13. McCullough, J. *et al.* Activation of the endosome-associated ubiquitin isopeptidase AMSH by STAM, a component of the multivesicular body-sorting machinery. *Curr. Biol.* **16,** 160–165 (2006).
14. Agromayor, M. & Martin-Serrano, J. Interaction of AMSH with ESCRT-III and deubiquitination of endosomal cargo. *J. Biol. Chem.* **281,** 23083–23091 (2006).
15. Ma, Y. M. *et al.* Targeting of AMSH to endosomes is required for epidermal growth factor receptor degradation. *J. Biol. Chem.* **282,** 9805–9812 (2007).
16. Zamborlini, A. *et al.* Release of autoinhibition converts ESCRT-III components into potent inhibitors of HIV-1 budding. *Proc. Natl Acad. Sci. USA* **103,** 19140–19145 (2006).
17. Howard, T. L., Stauffer, D. R., Degnin, C. R. & Hollenberg, S. M. CHMP1 functions as a member of a newly defined family of vesicle trafficking proteins. *J. Cell Sci.* **114,** 2395–2404 (2001).
18. von Schwedler, U. K. *et al.* The protein network of HIV budding. *Cell* **114,** 701–713 (2003).
19. Hanson, P. I. & Whiteheart, S. W. AAA+ proteins: have engine, will work. *Nature Rev. Mol. Cell Biol.* **6,** 519–529 (2005).
20. Takasu, H. *et al.* Structural characterization of the MIT domain from human Vps4b. *Biochem. Biophys. Res. Commun.* **334,** 460–465 (2005).
21. Bishop, N. & Woodman, P. TSG101/mammalian VPS23 and mammalian VPS28 interact directly and are recruited to VPS4-induced endosomes. *J. Biol. Chem.* **276,** 11735–11742 (2001).

22. Fujita, H. *et al.* A dominant negative form of the AAA ATPase SKD1/VPS4 impairs membrane trafficking out of endosomal/lysosomal compartments: class E vps phenotype in mammalian cells. *J. Cell Sci.* **116,** 401–414 (2003).
23. Bowers, K. *et al.* Protein–protein interactions of ESCRT complexes in the yeast *Saccharomyces cerevisiae*. *Traffic* **5,** 194–210 (2004).
24. Ward, D. M. *et al.* The role of LIP5 and CHMP5 in multivesicular body formation and HIV-1 budding in mammalian cells. *J. Biol. Chem.* **280,** 10548–10555 (2005).
25. Shiflett, S. L. *et al.* Characterization of Vta1p, a class E Vps protein in *Saccharomyces cerevisiae*. *J. Biol. Chem.* **279,** 10982–10990 (2004).
26. Garrus, J. E. *et al.* Tsg101 and the vacuolar protein sorting pathway are essential for HIV-1 budding. *Cell* **107,** 55–65 (2001).
27. Scott, A. *et al.* Structural and mechanistic studies of VPS4 proteins. *EMBO J.* **24,** 3658–3669 (2005).
28. Muziol, T. *et al.* Structural basis for budding by the ESCRT-III factor CHMP3. *Dev. Cell* **10,** 821–830 (2006).
29. Lin, Y., Kimpler, L. A., Naismith, T. V., Lauer, J. M. & Hanson, P. I. Interaction of the mammalian endosomal sorting complex required for transport (ESCRT) III protein hSnf7-1 with itself, membranes, and the AAA+ ATPase SKD1. *J. Biol. Chem.* **280,** 12799–12809 (2005).
30. Shim, S., Kimpler, L. A. & Hanson, P. I. Structure/function analyses of four core ESCRT-III reveals common regulatory role for extreme C-terminal domain. *Traffic* **8,** 1068–1079 (2007).

Supplementary Information is linked to the online version of the paper at www.nature.com/nature.

Acknowledgements We thank R. Rich, D. Myszka and S. Endicott for support; D. Winge for amino acid analysis; J. Shaw for reagents and expertise; and S. Alam for NMR expertise. W.I.S. received funding from the NIH.

Author Information Atomic coordinates for VPS4A MIT–CHMP1A$_{180–196}$, free VPS4B MIT and VPS4B MIT–CHMP2B$_{195–213}$ are deposited in the Protein Data Bank under accession numbers 2jq9, 2jqh and 2jqk, respectively. Reprints and permissions information is available at www.nature.com/reprints. Correspondence and requests for materials should be addressed to W.I.S. (wes@biochem.utah.edu).

CHAPTER 5

CONCLUSIONS AND FUTURE DIRECTIONS

Summary and Conclusions

The research described within this dissertation made a significant contribution to the general understanding of the protein network required for both vesicle formation at the multivesicular body (MVB) and the release of HIV-1 from host cells during virus budding. Prior to the research described in Chapters 1-4, the cellular factors TSG101 (tumor susceptibility gene 101) and VPS28 (vacuolar protein sorting 28) were known to be required for efficient HIV-1 budding (Garrus et al., 2001; Martin-Serrano et al., 2001; Martin-Serrano et al., 2003). This discovery led to further investigation of their native functions in protein sorting at the late endosome or MVB, where our studies were guided by the genetically defined yeast ESCRT (endosomal sorting complex required for transport) pathway (Babst et al., 2000; Bishop & Woodman, 2001; Hurley & Emr, 2006; Saksena et al., 2007). The similar topologies of vesicle formation at the MVB and HIV-1 budding suggested that characterizing the human ESCRT pathway would help to understand virus budding.

To define the human ESCRT pathway, we used bioinformatic approaches to identify 22 putative human homologs of yeast ESCRT proteins. Chapter 2 described not only the identification of these human ESCRT proteins but also their protein-protein interaction network, which proved to be similar to that of the yeast system. The

identification of human ESCRT complexes and their interactions has advanced our understanding of ESCRT pathway functions not only in retroviral budding, but also the ESCRT-mediated processes of cellular protein sorting, MVB vesicle formation and cytokinesis (Azmi et al., 2008; Carlton et al., 2008; Fujita et al., 2004; Im et al., 2009; Katoh et al., 2005; Kieffer et al., 2008; Langelier et al., 2006; Lin et al., 2005; McCullough et al., 2008; Muziol et al., 2006; Pires et al., 2009; Scott et al., 2005b; Shim et al., 2007; Shim et al., 2008; Stuchell-Brereton et al., 2007; Tsang et al., 2006; Usami et al., 2007; Xiao et al., 2008; Yorikawa et al., 2005; Zamborlini et al., 2006; Zhou et al., 2009).

The well characterized yeast ESCRT system facilitated the identification of a large number of human counterparts. However, not all components of the human ESCRT pathway could be identified based on sequence homology alone. ESCRT-I, as described in Chapter 3, is the first committed complex of the ESCRT pathway (Garrus et al., 2001; Martin-Serrano et al., 2001; Martin-Serrano et al., 2003). Prior to publication of the work described in Chapter 3, three yeast ESCRT-I components had been identified: Vps23p, Vps28p, and Vps37p. Sequence similarities made it straightforward to identify the human homologs of Vps23p and Vps28p, as TSG101 and VPS28, respectively. However, the human homolog of Vps37p was not obvious, apparently owing to significant primary sequence divergence. We therefore pursued more sophisticated bioinformatics approaches to identify human VPS37 candidates. Chapter 3 describes the identification of four putative human VPS37 proteins and the characterization of the interaction between one of these proteins, termed VPS37B, and another ESCRT-I subunit, TSG101. Identification of the human VPS37 proteins led to a more complete

description of the human ESCRT-I complex (Bache et al., 2004; Eastman et al., 2005; Stuchell et al., 2004). Several labs have since published important papers identifying MVB12 as the final ESCRT-I subunit and demonstrating its functional importance in yeast and human ESCRT-I (Chu et al., 2006; Curtiss et al., 2006; Morita et al., 2007; Oestreich et al., 2006; Oestreich et al., 2007). Moreover, the discovery of VPS37 and MVB12 laid the groundwork necessary for structural studies of the ESCRT-I quaternary complex (Kostelansky et al., 2007; Kostelansky et al., 2006).

Having obtained a more complete picture of the human ESCRT pathway, the remainder of my thesis research focused on understanding mechanistic details of the final fission step of vesicle formation or virus budding. VPS4 is the only known enzyme in the ESCRT pathway and its ability to hydrolyze ATP is thought to be required for recycling the assembled ESCRT machinery (Babst et al., 1998; Bishop & Woodman, 2000; Fujita et al., 2003; Garrus et al., 2001; Martin-Serrano et al., 2003; Wollert et al., 2009; Yoshimori et al., 2000). VPS4 interacts with at least a subset of the large ESCRT-III family of proteins (Bowers et al., 2004; Scott et al., 2005b; von Schwedler et al., 2003), which are believed to form lattices on endosomal membranes (Babst et al., 2002; Muziol et al., 2006; Scott et al., 2005b). These interactions, together with the enzymatic activity of VPS4, are both required for endosomal protein sorting and recycling of ESCRT pathway components (Babst et al., 1998; Kieffer et al., 2008; Lata et al., 2008b; Lin et al., 2005; Nickerson et al., 2006; Shim et al., 2008; Stuchell-Brereton et al., 2007). The final research goal of my thesis was to understand the interaction between ESCRT-III and the VPS4 complex.

Biochemical and structural studies have helped us to understand how the VPS4 AAA (ATPases associated with diverse cellular activities) ATPases, can bind ESCRT-III proteins and help facilitate recycling of the assembled ESCRT machinery. In 2005, VPS4 was reported to be composed of three different regions: an N-terminal microtubule interacting and trafficking (MIT) domain, a C-terminal AAA ATPase cassette, and a three-stranded, anti-parallel β -domain that is inserted into the small domain of the ATPase cassette (Scott et al., 2005a; Scott et al., 2005b; Takasu et al., 2005). The crystal structure of monomeric VPS4A revealed that the protein resembled another AAA ATPase, p97, and allowed us to model the hexameric rings formed by VPS4 by analogy to the structurally characterized p97 ring (Scott et al., 2005a; Zhang et al., 2000). This model also suggested that VPS4 might act like other known protein unfolding ATPases by feeding substrates, the ESCRT-III components, through the central pore of the VPS4 ring (Sauer et al., 2004). Other AAA ATPases recognize their substrates using N-terminal domains, suggesting that the N-terminal MIT domain might bind ESCRT-III proteins (Sauer et al., 2004; Scott et al., 2005a). This model was tested, as described in Appendix A, by showing that the isolated MIT regions of the VPS4 proteins could bind directly with ESCRT-III proteins (Scott et al., 2005b). These studies also revealed that the MIT domains were unusual three helix bundles. Finally, mapping studies revealed that the VPS4A MIT domain bound the C-terminal half of CHMP1B (charged multivesicular body protein 1B) (Scott et al., 2005b).

To ascertain exactly how VPS4/MIT domains recognize their ESCRT-III substrates, I mapped the MIT binding sites on ESCRT-III proteins more precisely and determined two ESCRT-III/VPS4 co-structures using NMR spectroscopy (Stuchell-

Brereton et al., 2007). Chapter 4 and Appendix B of this dissertation mapped MIT binding sites to amphipathic helices, termed MIT-interacting motifs 1 (MIM1), at the C-termini of a subset of the ESCRT-III proteins (Obita et al., 2007; Stuchell-Brereton et al., 2007; Zamborlini et al., 2006). The C-termini of both CHMP1A and CHMP2B each formed helices that bound between helices 2 and 3 of the MIT domain, in an orientation parallel to MIT helix 3 (Obita et al., 2007; Stuchell-Brereton et al., 2007). Similar MIM elements were also identified in a subset of the CHMP proteins (CHMP1A, CHMP1B, CHMP2A, CHMP2B, and CHMP3) based on biochemical analyses (Obita et al., 2007; Shim et al., 2007; Stuchell-Brereton et al., 2007). Following the publication of the VPS4/CHMP1-3 co-structures, the MIM1 elements in ESCRT-III proteins were also been shown to bind other MIT-domain containing proteins, including AMSH, UBPY and Vta1/LIP5 (Agromayor & Martin-Serrano, 2006; Azmi et al., 2008; Lata et al., 2008a; Lottridge et al., 2006; McCullough et al., 2006; Row et al., 2007; Xiao et al., 2008; Zamborlini et al., 2006). Thus MIM1-MIT interactions are a ubiquitous feature of the ESCRT pathway. In addition, a second distinct MIM element, termed MIM2, was identified in a second subset of CHMP proteins, and a structure of the CHMP6 MIM2 – VPS4 MIT complex was determined (Kieffer et al., 2008). The MIM2 element is an extended strand that binds between MIT helices 1 and 3, again in an orientation parallel to helix 3. MIM2 binding was also shown to be necessary for VPS4 recruitment as well as efficient protein sorting and HIV-1 budding, indicating that the MIT-MIM2 interactions are also important components of the ESCRT pathway (Kieffer et al., 2008; Obita et al., 2007; Shim et al., 2007; Stuchell-Brereton et al., 2007).

Current Models for ESCRT-III and VPS4 Function

Significant progress has been made in the past ten years in understanding the molecular mechanism by which the ESCRT pathway facilitates vesicle formation at the late endosome, HIV-1 budding and the abscission step of cytokinesis. The current model for MVB formation suggests that cargo is recognized by ESCRT-0 and ESCRT-I is subsequently recruited to protein sorting sites on late endosomes through direct interactions with the HRS/Vps27p subunit of ESCRT-0 (Bache et al., 2003; Bilodeau et al., 2003; Katzmann et al., 2003; Pornillos et al., 2003). ESCRT-I sequentially recruits ESCRT-II (Gill et al., 2007; Pineda-Molina et al., 2006; Teo et al., 2006), which interacts with the CHMP6/VPS20 subunit of ESCRT-III to initiate polymerization of the ESCRT-III subunit CHMP4/Snf7p into a ring that forms within the neck of the newly forming vesicle (Hanson et al., 2008; Im et al., 2009; Saksena et al., 2009; Teis et al., 2008; Wollert et al., 2009). It is believed that ESCRT-I/ESCRT-II and ESCRT-III polymers can stabilize membrane curvature at the bud neck (Fabrikant et al., 2009; Hanson et al., 2008; Im et al., 2009; Saksena et al., 2009; Wollert et al., 2009). CHMP4/SNF7 polymerization, in turn, recruits the remaining ESCRT-III components, CHMP3/VPS24 and CHMP2/VPS2 (Nickerson et al., 2006; Saksena et al., 2009; Teis et al., 2008). These ESCRT subunits may then from an enclosing "dome" that juxtaposes the membranes for fission (Fabrikant et al., 2009; Lata et al., 2009). Finally, the VPS4 AAA ATPases are recruited and utilize ATP hydrolysis to recycle ESCRT components, allowing for multiple rounds of vesicle formation (Fabrikant et al., 2009; Ghazi-Tabatabai et al., 2008; Im et al., 2009; Lata et al., 2008b; Wollert et al., 2009).

Although the characterization of the ESCRT pathway has come a long way in the past 10 years, there are still many unanswered mechanistic questions. Reconstitution of vesicle formation using pure recombinant yeast ESCRT proteins offers a powerful tool for mechanistic studies. For example, recent *in vitro* reconstitution assays indicate that the ESCRT-III components can facilitate the membrane scission event without the aid of VPS4 ATP hydrolysis (Wollert et al., 2009). This model suggests that VPS4 is not required for vesicle fission; but is required to remove ESCRT-III from the membrane and recycle the subunits for further rounds of vesicle formation (Wollert et al., 2009). The precise roles of the different ESCRT-III subunits are also emerging. The ESCRT-III subunits are recruited in a sequential manner, both *in vitro* and *in vivo*. CHMP6/Vps20 recruits CHMP4/Snf7, which polymerizes and recruits CHMP3/Vps24, leading to CHMP2/Vps2 binding (Saksena et al., 2009; Teis et al., 2008). CHMP2/Vps2 and CHMP3/Vps24 can form closed tubes, even dome shaped caps on tubes, *in vitro* (Fabrikant et al., 2009; Ghazi-Tabatabai et al., 2008; Lata et al., 2008b). A recent computational analysis argues that these domes have sufficient binding energy to deform the tubular membrane to the point where the tube closes and ultimately fuses, releasing the newly formed vesicle (Fabrikant et al., 2009). Future studies will focus on testing the "dome" model for membrane fission, and the detailed mechanisms by which VPS4 disassembles the membrane-bound ESCRT machinery.

References

Agromayor M, Martin-Serrano J (2006) Interaction of AMSH with ESCRT-III and deubiquitination of endosomal cargo. *The Journal of biological chemistry* **281:** 23083-23091

Azmi IF, Davies BA, Xiao J, Babst M, Xu Z, Katzmann DJ (2008) ESCRT-III family members stimulate Vps4 ATPase activity directly or via Vta1. *Developmental cell* **14:** 50-61

Babst M, Katzmann D, Estepa-Sabal E, Meerloo T, Emr S (2002) Escrt-III. An endosome-associated heterooligomeric protein complex required for mvb sorting. *Developmental cell* **3:** 271-282

Babst M, Odorizzi G, Estepa EJ, Emr SD (2000) Mammalian tumor susceptibility gene 101 (TSG101) and the yeast homologue, Vps23p, both function in late endosomal trafficking. *Traffic (Copenhagen, Denmark)* **1:** 248-258

Babst M, Wendland B, Estepa EJ, Emr SD (1998) The Vps4p AAA ATPase regulates membrane association of a Vps protein complex required for normal endosome function. *The EMBO journal* **17:** 2982-2993

Bache KG, Brech A, Mehlum A, Stenmark H (2003) Hrs regulates multivesicular body formation via ESCRT recruitment to endosomes. *The Journal of cell biology* **162:** 435-442

Bache KG, Slagsvold T, Cabezas A, Rosendal KR, Raiborg C, Stenmark H (2004) The Growth-Regulatory Protein HCRP1/hVps37A is a Subunit of Mammalian ESCRT-I and Mediates Receptor Downregulation. *Molecular biology of the cell* **15:** 4337-4346

Bilodeau PS, Winistorfer SC, Kearney WR, Robertson AD, Piper RC (2003) Vps27-Hse1 and ESCRT-I complexes cooperate to increase efficiency of sorting ubiquitinated proteins at the endosome. *The Journal of cell biology* **163:** 237-243

Bishop N, Woodman P (2000) ATPase-defective mammalian VPS4 localizes to aberrant endosomes and impairs cholesterol trafficking. *Molecular biology of the cell* **11:** 227-239

Bishop N, Woodman P (2001) TSG101/mammalian VPS23 and mammalian VPS28 interact directly and are recruited to VPS4-induced endosomes. *The Journal of biological chemistry* **276:** 11735-11742

Bowers K, Lottridge J, Helliwell SB, Goldthwaite LM, Luzio JP, Stevens TH (2004) Protein-protein interactions of ESCRT complexes in the yeast Saccharomyces cerevisiae. *Traffic (Copenhagen, Denmark)* **5:** 194-210

Carlton JG, Agromayor M, Martin-Serrano J (2008) Differential requirements for Alix and ESCRT-III in cytokinesis and HIV-1 release. *Proceedings of the National Academy of Sciences of the United States of America* **105:** 10541-10546

Chu T, Sun J, Saksena S, Emr SD (2006) New component of ESCRT-I regulates endosomal sorting complex assembly. *The Journal of cell biology* **175:** 815-823

Curtiss M, Jones C, Babst M (2007) Efficient Cargo Sorting by ESCRT-I and the Subsequent Release of ESCRT-I from MVBs Requires the Subunit Mvb12. *Molecular biology of the cell* **18:** 636-645

Eastman SW, Martin-Serrano J, Chung W, Zang T, Bieniasz PD (2005) Identification of human VPS37C, a component of endosomal sorting complex required for transport-I important for viral budding. *The Journal of biological chemistry* **280:** 628-636

Fabrikant G, Lata S, Riches JD, Briggs JA, Weissenhorn W, Kozlov MM (2009) Computational model of membrane fission catalyzed by ESCRT-III. *PLoS computational biology* **5:** e1000575

Fujita H, Umezuki Y, Imamura K, Ishikawa D, Uchimura S, Nara A, Yoshimori T, Hayashizaki Y, Kawai J, Ishidoh K, Tanaka Y, Himeno M (2004) Mammalian class E Vps proteins, SBP1 and mVps2/CHMP2A, interact with and regulate the function of an AAA-ATPase SKD1/Vps4B. *Journal of cell science* **117:** 2997-3009

Fujita H, Yamanaka M, Imamura K, Tanaka Y, Nara A, Yoshimori T, Yokota S, Himeno M (2003) A dominant negative form of the AAA ATPase SKD1/VPS4 impairs membrane trafficking out of endosomal/lysosomal compartments: class E vps phenotype in mammalian cells. *Journal of cell science* **116:** 401-414

Garrus JE, von Schwedler UK, Pornillos OW, Morham SG, Zavitz KH, Wang HE, Wettstein DA, Stray KM, Cote M, Rich RL, Myszka DG, Sundquist WI (2001) Tsg101 and the vacuolar protein sorting pathway are essential for HIV-1 budding. *Cell* **107:** 55-65

Ghazi-Tabatabai S, Saksena S, Short JM, Pobbati AV, Veprintsev DB, Crowther RA, Emr SD, Egelman EH, Williams RL (2008) Structure and disassembly of filaments formed by the ESCRT-III subunit Vps24. *Structure* **16:** 1345-1356

Gill DJ, Teo H, Sun J, Perisic O, Veprintsev DB, Emr SD, Williams RL (2007) Structural insight into the ESCRT-I/-II link and its role in MVB trafficking. *The EMBO journal* **26:** 600-612

Hanson PI, Roth R, Lin Y, Heuser JE (2008) Plasma membrane deformation by circular arrays of ESCRT-III protein filaments. *The Journal of cell biology* **180:** 389-402

Hurley JH, Emr SD (2006) The ESCRT complexes: structure and mechanism of a membrane-trafficking network. *Annual review of biophysics and biomolecular structure* **35:** 277-298

Im YJ, Wollert T, Boura E, Hurley JH (2009) Structure and function of the ESCRT-II-III interface in multivesicular body biogenesis. *Developmental cell* **17:** 234-243

Katoh K, Suzuki H, Terasawa Y, Mizuno T, Yasuda J, Shibata H, Maki M (2005) The penta-EF-hand protein ALG-2 directly interacts with the ESCRT-I component TSG101 and Ca 2+-dependently colocalizes to aberrant endosomes with dominant-negative AAA ATPase SKD1/Vps4B. *The Biochemical journal* **391:** 677-685

Katzmann DJ, Stefan CJ, Babst M, Emr SD (2003) Vps27 recruits ESCRT machinery to endosomes during MVB sorting. *The Journal of cell biology* **162:** 413-423

Kieffer C, Skalicky JJ, Morita E, De Domenico I, Ward DM, Kaplan J, Sundquist WI (2008) Two distinct modes of ESCRT-III recognition are required for VPS4 functions in lysosomal protein targeting and HIV-1 budding. *Developmental cell* **15:** 62-73

Kostelansky MS, Schluter C, Tam YY, Lee S, Ghirlando R, Beach B, Conibear E, Hurley JH (2007) Molecular architecture and functional model of the complete yeast ESCRT-I heterotetramer. *Cell* **129:** 485-498

Kostelansky MS, Sun J, Lee S, Kim J, Ghirlando R, Hierro A, Emr SD, Hurley JH (2006) Structural and functional organization of the ESCRT-I trafficking complex. *Cell* **125:** 113-126

Langelier C, von Schwedler UK, Fisher RD, De Domenico I, White PL, Hill CP, Kaplan J, Ward D, Sundquist WI (2006) Human ESCRT-II complex and its role in human immunodeficiency virus type 1 release. *Journal of virology* **80:** 9465-9480

Lata S, Roessle M, Solomons J, Jamin M, Gottlinger HG, Svergun DI, Weissenhorn W (2008a) Structural basis for autoinhibition of ESCRT-III CHMP3. *Journal of molecular biology* **378:** 818-827

Lata S, Schoehn G, Jain A, Pires R, Piehler J, Gottlinger HG, Weissenhorn W (2008b) Helical structures of ESCRT-III are disassembled by VPS4. *Science* **321:** 1354-1357

Lata S, Schoehn G, Solomons J, Pires R, Gottlinger HG, Weissenhorn W (2009) Structure and function of ESCRT-III. *Biochemical Society transactions* **37:** 156-160

Lin Y, Kimpler LA, Naismith TV, Lauer JM, Hanson PI (2005) Interaction of the mammalian endosomal sorting complex required for transport (ESCRT) III protein hSnf7-1 with itself, membranes, and the AAA+ ATPase SKD1. *The Journal of biological chemistry* **280:** 12799-12809

Lottridge JM, Flannery AR, Vincelli JL, Stevens TH (2006) Vta1p and Vps46p regulate the membrane association and ATPase activity of Vps4p at the yeast multivesicular body. *Proceedings of the National Academy of Sciences of the United States of America* **103:** 6202-6207

Martin-Serrano J, Zang T, Bieniasz PD (2001) HIV-1 and Ebola virus encode small peptide motifs that recruit Tsg101 to sites of particle assembly to facilitate egress. *Nature medicine* **7:** 1313-1319

Martin-Serrano J, Zang T, Bieniasz PD (2003) Role of ESCRT-I in Retroviral Budding. *Journal of virology* **77:** 4794-4804

McCullough J, Fisher RD, Whitby FG, Sundquist WI, Hill CP (2008) ALIX-CHMP4 interactions in the human ESCRT pathway. *Proceedings of the National Academy of Sciences of the United States of America* **105:** 7687-7691

McCullough J, Row PE, Lorenzo O, Doherty M, Beynon R, Clague MJ, Urbe S (2006) Activation of the endosome-associated ubiquitin isopeptidase AMSH by STAM, a component of the multivesicular body-sorting machinery. *Curr Biol* **16:** 160-165

Morita E, Sandrin V, Alam SL, Eckert DM, Gygi SP, Sundquist WI (2007) Identification of human MVB12 proteins as ESCRT-I subunits that function in HIV budding. *Cell host & microbe* **2:** 41-53

Muziol T, Pineda-Molina E, Ravelli RB, Zamborlini A, Usami Y, Gottlinger H, Weissenhorn W (2006) Structural basis for budding by the ESCRT-III factor CHMP3. *Developmental cell* **10:** 821-830

Nickerson DP, West M, Odorizzi G (2006) Did2 coordinates Vps4-mediated dissociation of ESCRT-III from endosomes. *The Journal of cell biology* **175:** 715-720

Obita T, Saksena S, Ghazi-Tabatabai S, Gill DJ, Perisic O, Emr SD, Williams RL (2007) Structural basis for selective recognition of ESCRT-III by the AAA ATPase Vps4. *Nature* **449:** 735-739

Oestreich AJ, Davies BA, Payne JA, Katzmann DJ (2006) Mvb12 Is a Novel Member of ESCRT-I Involved in Cargo Selection by the MVB Pathway. *Molecular biology of the cell* **18:** 646-657

Oestreich AJ, Davies BA, Payne JA, Katzmann DJ (2007) Mvb12 is a novel member of ESCRT-I involved in cargo selection by the multivesicular body pathway. *Molecular biology of the cell* **18:** 646-657

Pineda-Molina E, Belrhali H, Piefer AJ, Akula I, Bates P, Weissenhorn W (2006) The crystal structure of the C-terminal domain of Vps28 reveals a conserved surface required for Vps20 recruitment. *Traffic (Copenhagen, Denmark)* **7:** 1007-1016

Pires R, Hartlieb B, Signor L, Schoehn G, Lata S, Roessle M, Moriscot C, Popov S, Hinz A, Jamin M, Boyer V, Sadoul R, Forest E, Svergun DI, Gottlinger HG, Weissenhorn W (2009) A crescent-shaped ALIX dimer targets ESCRT-III CHMP4 filaments. *Structure* **17:** 843-856

Pornillos O, Higginson DS, Stray KM, Fisher RD, Garrus JE, Payne M, He GP, Wang HE, Morham SG, Sundquist WI (2003) HIV Gag mimics the Tsg101-recruiting activity of the human Hrs protein. *The Journal of cell biology* **162:** 425-434

Row PE, Liu H, Hayes S, Welchman R, Charalabous P, Hofmann K, Clague MJ, Sanderson CM, Urbe S (2007) The MIT domain of UBPY constitutes a CHMP binding and endosomal localization signal required for efficient epidermal growth factor receptor degradation. *The Journal of biological chemistry* **282:** 30929-30937

Saksena S, Sun J, Chu T, Emr SD (2007) ESCRTing proteins in the endocytic pathway. *Trends in biochemical sciences* **32:** 561-573

Saksena S, Wahlman J, Teis D, Johnson AE, Emr SD (2009) Functional reconstitution of ESCRT-III assembly and disassembly. *Cell* **136:** 97-109

Sauer RT, Bolon DN, Burton BM, Burton RE, Flynn JM, Grant RA, Hersch GL, Joshi SA, Kenniston JA, Levchenko I, Neher SB, Oakes ES, Siddiqui SM, Wah DA, Baker TA (2004) Sculpting the proteome with AAA(+) proteases and disassembly machines. *Cell* **119:** 9-18

Scott A, Chung HY, Gonciarz-Swiatek M, Hill GC, Whitby FG, Gaspar J, Holton JM, Viswanathan R, Ghaffarian S, Hill CP, Sundquist WI (2005a) Structural and mechanistic studies of VPS4 proteins. *The EMBO journal* **24:** 3658-3669

Scott A, Gaspar J, Stuchell-Brereton MD, Alam SL, Skalicky JJ, Sundquist WI (2005b) Structure and ESCRT-III protein interactions of the MIT domain of human VPS4A. *Proceedings of the National Academy of Sciences of the United States of America* **102:** 13813-13818

Shim S, Kimpler LA, Hanson PI (2007) Structure/function analysis of four core ESCRT-III proteins reveals common regulatory role for extreme C-terminal domain. *Traffic (Copenhagen, Denmark)* **8:** 1068-1079

Shim S, Merrill SA, Hanson PI (2008) Novel interactions of ESCRT-III with LIP5 and VPS4 and their implications for ESCRT-III disassembly. *Molecular biology of the cell* **19:** 2661-2672

Stuchell-Brereton MD, Skalicky JJ, Kieffer C, Karren MA, Ghaffarian S, Sundquist WI (2007) ESCRT-III recognition by VPS4 ATPases. *Nature* **449:** 740-744

Stuchell MD, Garrus JE, Muller B, Stray KM, Ghaffarian S, McKinnon R, Krausslich HG, Morham SG, Sundquist WI (2004) The Human Endosomal Sorting Complex Required for Transport (ESCRT-I) and Its Role in HIV-1 Budding. *The Journal of biological chemistry* **279:** 36059-36071

Takasu H, Jee JG, Ohno A, Goda N, Fujiwara K, Tochio H, Shirakawa M, Hiroaki H (2005) Structural characterization of the MIT domain from human Vps4b. *Biochemical and biophysical research communications* **334:** 460-465

Teis D, Saksena S, Emr SD (2008) Ordered assembly of the ESCRT-III complex on endosomes is required to sequester cargo during MVB formation. *Developmental cell* **15:** 578-589

Teo H, Gill DJ, Sun J, Perisic O, Veprintsev DB, Vallis Y, Emr SD, Williams RL (2006) ESCRT-I core and ESCRT-II GLUE domain structures reveal role for GLUE in linking to ESCRT-I and membranes. *Cell* **125:** 99-111

Tsang HT, Connell JW, Brown SE, Thompson A, Reid E, Sanderson CM (2006) A systematic analysis of human CHMP protein interactions: Additional MIT domain-containing proteins bind to multiple components of the human ESCRT III complex. *Genomics* **88:** 333-346

Usami Y, Popov S, Gottlinger HG (2007) Potent rescue of human immunodeficiency virus type 1 late domain mutants by ALIX/AIP1 depends on its CHMP4 binding site. *Journal of virology* **81:** 6614-6622

von Schwedler UK, Stuchell M, Muller B, Ward DM, Chung HY, Morita E, Wang HE, Davis T, He GP, Cimbora DM, Scott A, Krausslich HG, Kaplan J, Morham SG, Sundquist WI (2003) The protein network of HIV budding. *Cell* **114:** 701-713

Wollert T, Wunder C, Lippincott-Schwartz J, Hurley JH (2009) Membrane scission by the ESCRT-III complex. *Nature* **458:** 172-177

Xiao J, Xia H, Zhou J, Azmi IF, Davies BA, Katzmann DJ, Xu Z (2008) Structural basis of Vta1 function in the multivesicular body sorting pathway. *Developmental cell* **14:** 37-49

Yorikawa C, Shibata H, Waguri S, Hatta K, Horii M, Katoh K, Kobayashi T, Uchiyama Y, Maki M (2005) Human CHMP6, a myristoylated ESCRT-III protein, interacts directly with an ESCRT-II component EAP20 and regulates endosomal cargo sorting. *The Biochemical journal* **387:** 17-26

Yoshimori T, Yamagata F, Yamamoto A, Mizushima N, Kabeya Y, Nara A, Miwako I, Ohashi M, Ohsumi M, Ohsumi Y (2000) The mouse SKD1, a homologue of yeast Vps4p, is required for normal endosomal trafficking and morphology in mammalian cells. *Molecular biology of the cell* **11:** 747-763

Zamborlini A, Usami Y, Radoshitzky SR, Popova E, Palu G, Gottlinger H (2006) Release of autoinhibition converts ESCRT-III components into potent inhibitors of HIV-1 budding. *Proceedings of the National Academy of Sciences of the United States of America* **103:** 19140-19145

Zhang X, Shaw A, Bates PA, Newman RH, Gowen B, Orlova E, Gorman MA, Kondo H, Dokurno P, Lally J, Leonard G, Meyer H, van Heel M, Freemont PS (2000) Structure of the AAA ATPase p97. *Molecular cell* **6:** 1473-1484

Zhou X, Pan S, Sun L, Corvera J, Lee YC, Lin SH, Kuang J (2009) The CHMP4b- and Src-docking sites in the Bro1 domain are autoinhibited in the native state of Alix. *The Biochemical journal* **418:** 277-284

APPENDIX A

STRUCTURE AND ESCRT-III PROTEIN INTERACTIONS OF THE MIT DOMAIN OF HUMAN VPS4A

Anna Scott, Jason Gaspar, Melissa D. Stuchell-Brereton, Steve L. Alam,

Jack J. Skalicky and Wesley I. Sundquist

Reprinted from the Proceedings of the National Academy of Science, USA,

Vol. 102, pages 13813-13818, Copyright 2005.

Note: Work described in this appendix was largely performed by Anna Scott and Jason Gaspar. CHMP1B constructs were designed and constructed by Melissa D. Stuchell-Brereton. Identification of the MIT domain as the region of VPS4A required for VPS4A/ESCRT-III CHMP1B protein interaction was determined by Anna Scott and Melissa D. Stuchell-Brereton via GST-pulldown experiments prior to this publication.

Structure and ESCRT-III protein interactions of the MIT domain of human VPS4A

Anna Scott, Jason Gaspar, Melissa D. Stuchell-Brereton, Steven L. Alam, Jack J. Skalicky, and Wesley I. Sundquist*

Department of Biochemistry, 20 N, 1900 E, University of Utah School of Medicine, Salt Lake City, UT 84132-3201

Edited by John M. Coffin, Tufts University School of Medicine, Boston, MA, and approved August 8, 2005 (received for review March 16, 2005)

The VPS4 AAA ATPases function both in endosomal vesicle formation and in the budding of many enveloped RNA viruses, including HIV-1. VPS4 proteins act by binding and catalyzing release of the membrane-associated ESCRT-III protein lattice, thereby allowing multiple rounds of protein sorting and vesicle formation. Here, we report the solution structure of the N-terminal VPS4A microtubule interacting and transport (MIT) domain and demonstrate that the VPS4A MIT domain binds the C-terminal half of the ESCRT-III protein, CHMP1B (K_d = 20 ± 13 μM). The MIT domain forms an asymmetric three-helix bundle that resembles the first three helices in a tetratricopeptide repeat (TPR) motif. Unusual interhelical interactions are mediated by a series of conserved aromatic residues that form coiled-coil interactions between the second two helices and also pack against the conserved alanines that interdigitate between the first two helices. Mutational analyses revealed that a conserved leucine residue (Leu-64) on the third helix that would normally bind the fourth helix in an extended TPR is used to bind CHMP1B, raising the possibility that ESCRT-III proteins may bind by completing the TPR motif.

HIV | budding | vacuolar protein sorting | multivesicular body | NMR

Proteins targeted for lysosomal degradation are sorted into vesicles that bud into late endosomal compartments called multivesicular bodies (MVB). Once formed, multivesicular bodies can undergo several different fates, either serving as long-term storage compartments, fusing with lysosomes to deliver the internal vesicles and their contents for degradation, or fusing with the plasma membrane to release the vesicles as extracellular "exosomes." The MVB functions in a number of important biological processes, including receptor down-regulation, antigen presentation, intercellular communication, and development (for reviews, see refs. 1–4). Moreover, a number of enveloped RNA viruses, including HIV-1, usurp cellular proteins involved in MVB biogenesis to facilitate virus budding, a process that shares many similarities with MVB vesicle formation (5, 6).

MVB vesicle formation and protein sorting require a complex set of protein machinery (the class E proteins) originally identified in yeast genetic screens (2, 7). Subsequent studies have identified at least one human homolog for every yeast class E protein (5), indicating that the MVB pathway is conserved across eukaryotes. Most class E proteins function as components of one of three endosomal sorting complexes required for transport (ESCRT-I, -II, and -III), which are sequentially recruited to sites of MVB protein sorting and vesicle formation (8). The ESCRT-III proteins are the last to assemble, and are thought to form a membrane-associated lattice that functions in the final stages of protein sorting and vesicle formation (2, 8). Humans have a total of 10 ESCRT-III-like proteins (the "CHMP" proteins) that can be subdivided into six families corresponding to the six ESCRT-III proteins in yeast (5, 9). Four of the ESCRT-III protein families (corresponding to CHMP-2, -3, -4, and -6) are considered core ESCRT-III components, whereas the other two families (CHMP-1 and CHMP-5) may play regulatory or peripheral roles (8). The ESCRT-III proteins, in turn, recruit the VPS4 AAA ATPases to sites of MVB vesicle formation (10). This recruitment appears to occur through direct protein–protein interactions, because both human and yeast ESCRT-III proteins bind directly to VPS4 proteins (11–13). Subsequent release of ESCRT complexes from the membrane requires the ATPase activity of the VPS4 proteins (9, 10, 14–17). Thus, the VPS4 ATPases allow the ESCRT machinery to recycle through multiple rounds of vesicle formation and may also provide the energy necessary for protein sorting and/or vesicle formation.

Humans and other mammals have two highly related VPS4 proteins (designated VPS4A and VPS4B/SKD1) that are 80% identical to one another and ≈60% identical to the yeast VPS4 protein (17). Like other AAA ATPases, the VPS4 proteins have modular structures, with an N-terminal substrate recognition domain preceding the canonical AAA ATPase cassette (Fig. 1) (18, 19). Although the catalytic domains are highly conserved, distinct substrate specificities are created through the use of different N-terminal domains. The N-terminal domains of the VPS4 proteins belong to a family called MIT (microtubule interacting and trafficking) domains (20, 21). MIT domains are found in other AAA ATPases, such as spastin, and are also present in proteins that lack ATPase domains, such as SNX15 and PalB/calpain-7. Several recent yeast two-hybrid studies have indicated that at least some MIT domains may act as protein recognition modules that bind ESCRT-III/CHMP proteins (13, 22). However, detailed biochemical or structural analyses have not yet been performed for any MIT domain. Here, we describe the structure and protein–protein interactions of the VPS4A MIT domain.

Experimental Procedures

Supporting Information. Further details can be found in Tables 1 and 2 and Figs. 5–7, which are published as supporting information on the PNAS web site.

MIT Domain Alignments. The MIT domain sequence alignment (Fig. 1) matches that presented previously (21, 23), except that the third helices in spastin, spartin, and tobacco mosaic virus (TMV) helicase were manually adjusted by first aligning spastin with VPS4A and VPS4B by using CLUSTALW (24), and then aligning spartin and TMV helicase with spastin. This procedure optimized the alignment of highly conserved residues without altering the 50% consensus sequence.

Cloning. DNA encoding VPS4A residues 1–84, 1–122, or 1–437 (full length) or VPS4B 1–129 or 1–444 (full length) was amplified from EST templates (ATCC 81449 and 6216963) (25). The 5′ PCR primer also reintroduced the first five amino acids that were missing from the VPS4A EST sequence. DNA fragments were cloned into NdeI/BamH1 sites of pET16b (Novagen), modified

This paper was submitted directly (Track II) to the PNAS office.

Abbreviations: MVB, multivesicular body; TPR, tetratricopeptide repeats.

Data deposition: The model coordinates and assignments have been deposited in the Protein Data Bank, www.pdb.org (PDB ID code 1YXR).

*To whom correspondence should be addressed. E-mail: wes@biochem.utah.edu.

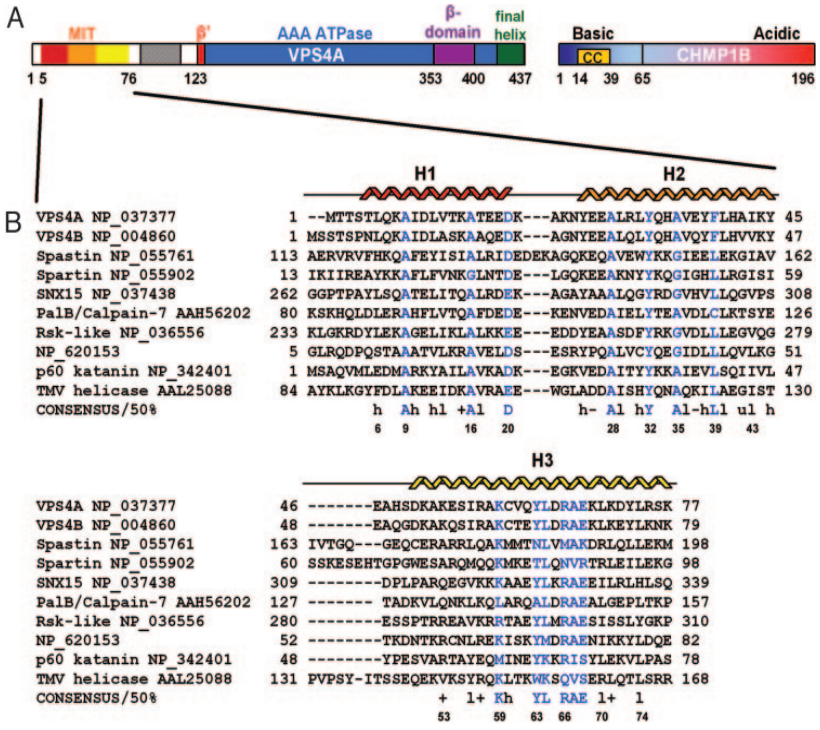

Fig. 1. Sequences and features of VPS4A, CHMP1B, and MIT domains. (*A*) Schematic illustrations of human VPS4A (19) and CHMP1B. The predicted coiled-coil (CC) of CHMP1B was identified at a probability of 0.17 by using MULTICOIL (41). (*B*) Sequence alignment of known MIT domains from eight human proteins (*Upper*) and two proteins lacking human homologs. The ''consensus'' sequence (*Lower*) was derived from all 116 MIT domains in the SMART database (23). Highly conserved residues (>50% identity) are shown in blue, and residue types conserved in >50% of the sequences are shown in lowercase (h, hydrophobic; +, positively charged; -, negatively charged; u, Ala or Gly; l, Ile, Val, or Leu). Numbering corresponds to VPS4A.

to encode a TEV protease site after the N-terminal His-10 tag. Site directed mutants were created by using the QuikChange method (Stratagene). DNA fragments encoding CHMP1B residues 65–196 and 1–196 (full length) were amplified from a HeLa cDNA library (Stratagene) (26), and cloned into the NdeI/BamHI sites of a modified pGEX2T vector that encoded a TEV protease cleavage site. All constructs were verified by DNA sequencing.

Protein Expression and Purification. Protein expression and purification protocols were similar for the different VPS4 proteins, and are described for $VPS4A_{1–122}$. His-10-$VPS4A_{1–122}$ was expressed in 2-liter cultures of BL21(DE3) *Escherichia coli* cells grown in LB or in M9 media supplemented with either 2 g/liter $^{15}NH_4Cl$ or 2 g/liter $^{15}NH_4Cl$ and 2 g/liter $^{13}C_6$-glucose. Expression was induced (4 h at 27°C) with 0.5 mM IPTG (A_{600} = 0.65). Subsequent steps were performed at 4°C. Cells were harvested and resuspended in lysis buffer (50 mM Tris, pH 8.0/50 mM imidazole/500 mM NaCl) supplemented with protease inhibitors (Roche Diagnostics) and lysed with 1 mg/ml lysozyme followed by sonication. The lysate was clarified by centrifugation (45 min, 35,000 × *g*), and the soluble protein purified by nickel Sepharose chromatography (Amersham Pharmacia). His-10-$VPS4A_{1–122}$ eluted at ≈400 mM imidazole from a linear gradient of 50–750 mM imidazole in lysis buffer. Protein fractions were pooled and dialyzed sequentially against two changes of cleavage buffer (20 mM Tris·HCl, pH 8.0/100 mM NaCl/5 mM EDTA), with 1 mM DTT replacing EDTA in the second change. The His-10 tag was removed by incubation with TEV protease (1 mg per 100 mg of protein, 12 h, 27°C) followed by anion exchange chromatography (Q Sepharose, Amersham Pharmacia). Flow-through fractions containing $VPS4A_{1–122}$ were concentrated to ≈4 ml, and the protein was purified to homogeneity by gel filtration chromatography (S75, Amersham Pharmacia). This procedure typically yielded ≈30 mg of $VPS4A_{1–122}$. TEV cleavage left two nonnative residues at the N terminus (Gly–His), which are not included in our numbering scheme. The protein was verified by N-terminal sequencing (G-H-M-T-T-S-T) and electrospray mass spectrometry ($MW_{exp.}$ = 14,168 Da, $MW_{calc.}$ = 14,167 Da).

GST Pull-Down Experiments. *E. coli* (30-ml cultures) expressing either GST or GST-$CHMP1B_{65–196}$ were pelleted, resuspended in 5 ml of lysis buffer (50 mM Tris·HCl, pH 7.4/50 mM NaCl/5 mM 2-mercaptoethanol), and lysed with 75 μl of 10 mg/ml lysozyme (20 min, 4°C) followed by addition of 100 μl of 5% deoxycholate (20 min) and sonication. Soluble proteins were collected after centrifugation for 45 min at 13,200 × *g*. Binding reactions (1 h at 4°C) contained 35 μM GST or GST-$CHMP1B_{65–196}$, 60 μM VPS4A or 300 μM $VPS4A_{1–84}$, and 100 μl glutathione agarose slurry (Amersham Pharmacia) in 190 ml total volume buffer (20 mM Tris·HCl, pH 8.0/100 mM NaCl/2 mM $MgCl_2$/2 mM $CaCl_2$/5 mM 2-mercaptoethanol/0.02% Nonidet P-40/5% glycerol). Unbound proteins were removed in three 1.2-ml buffer washes. Bound proteins were eluted from the matrix by boiling in 100 μl of 2× SDS/PAGE buffer and detected by SDS/PAGE.

Biosensor Binding Experiments. Biosensor binding experiments used a BIACORE 2000 with research-grade CM4 sensor chips. Approximately 5 kRU of anti-GST Ab was immobilized by amine-coupling, and GST-CHMP proteins or GST alone (ref-

erence) were captured in running buffer (≈0.5 kRU, 20 mM Tris, pH 8.0/100 mM NaCl/1 mM DTT/0.2 mg/ml BSA/0.005% P20). GST-CHMP proteins were either purified by glutathione affinity chromatography or captured directly from soluble *E. coli* lysates (no difference in binding was noted). Purified VPS4A MIT proteins were injected in running buffer (0–450 μM, 50 μl/min, 20°C). Data were collected at 2 Hz during 30-s association and dissociation phases and equilibrium binding isotherms fit to simple 1:1 binding models (27). VPS4A MIT proteins in running buffer were injected in duplicate or triplicate. Sensorgrams for wild-type $VPS4A_{1–84}$ and L64A mutant $VPS4A_{1–84}$ binding immobilized GST-$CHMP1B_{65–196}$ are given in Fig. 7*B*.

NMR Spectroscopy. NMR samples were 3 mM protein in 20 mM sodium phosphate (pH 5.5), 50 mM NaCl, 90% H_2O/10% D_2O. Spectra were recorded at 25°C on a Varian Inova 600 NMR spectrometer equipped with a triple-resonance $^1H/^{13}C/^{15}N$ probe and *z* axis pulsed-field gradients. Data were processed with FELIX (Accelrys, San Diego), and resonances were assigned by using standard approaches within the SPARKY program (T. D. Goddard and D. G. Kneller, University of California, San Francisco) (see Tables 1 and 2). Complete resonance assignments were obtained, with eight exceptions: H48 H^N, F39 H^ζ, K83 H^γ H^δ H^ε, and M1, M114, and M119 H^ε. Stereospecific assignments were obtained from GLOMSA (28) for six pairs of methylene protons: E18H^β, E18H^γ, N24H^β, E27H^β, Y38H^β, and E39H^β. Backbone torsion angles were estimated from ^{13}C chemical shifts by using TALOS (42). All prolines were in the *trans* conformation, as confirmed by intense Xxx(H^α)-Pro(Hδ) sequential NOESY cross peaks and $^{13}C^\beta$ and $^{13}C^\gamma$ chemical shifts typical of *trans*-Pro (29).

Structure Calculations. NOE coordinates and intensities were obtained by using the tools in SPARKY. NOE assignments were obtained and initial structures calculated by using automated NOE assignment together with torsion angle dynamics as implemented in CYANA (28). A total of 100 randomized conformers were "folded" into 3D structures by introducing NOE constraints in a step-wise manner by using the criteria of chemical shift agreement, network anchoring, and consistency with an initial fold. Each conformer was subjected to 10,000 steps of torsion angle dynamics per cycle (seven cycles). The 20 structures with the lowest final CYANA target function values were then subjected to restrained energy minimization in CNS (30) using the final CYANA NOE and torsion angle constraints, as well as helical hydrogen bond restraints based upon chemical shift indices and local NOE patterns (Fig. 5). Structures were validated by using PROCHECK-NMR and AQUA (31) and visualized by using PYMOL (DeLano Scientific).

Results and Discussion

VPS4A MIT Domain Structure Determination. N-terminal fragments of VPS4A and VPS4B were screened for their feasibility for NMR structural studies. The two fragments tested, $VPS4A_{1–122}$ and $VPS4B_{1–129}$, were designed to span the entire region of VPS4B that was disordered in our recent crystal structure of the full-length protein (residues 1–122) (19). Both $VPS4A_{1–122}$ and $VPS4B_{1–129}$ exhibited reasonable amide proton and nitrogen chemical shift dispersion, but $VPS4B_{1–129}$ NH resonance linewidths and intensities varied, whereas the $VPS4A_{1–122}$ spectrum was of uniformly high quality. Therefore, this protein was selected for high-resolution structural studies.

Essentially complete proton resonance assignments were obtained for $VPS4A_{1–122}$ by using a standard suite of NMR experiments (Table 1). Analyses of short- and medium-range NOE patterns, $^3J_{HNHA}$ couplings, and ^{13}C chemical shift indices indicated the presence of three well defined helices (residues 5–20, 25–45, and 50–76), a fourth region with helical propensity

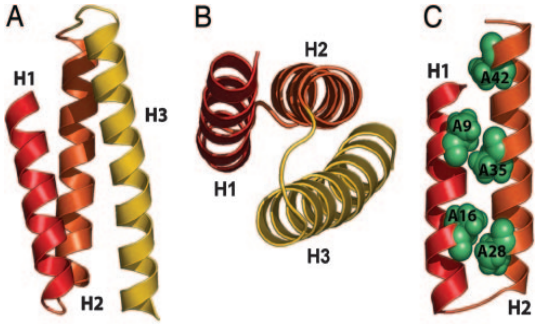

Fig. 2. $VPS4A_{5–76}$ MIT domain structure. (*A*) Ribbon diagram of the VPS4A MIT domain (residues 5–76). (*B*) View down the three helix bundle of the MIT domain, emphasizing the asymmetry in the disposition of the three helices. (*C*) "Alanine zipper" connecting $VPS4A_{5–76}$ MIT helices 1 and 2. The five conserved alanine side chains within this motif are shown explicitly.

(105–114), and random coil secondary structure elsewhere (Fig. 5). $VPS4A_{1–122}$ residues 77–122, including the final nascent helix, lacked any detectable long-range NOEs, and were therefore excluded from structure calculations. VPS4 residues 5–76 formed a tightly packed, well ordered structure as judged by the excellent agreement between different structures (0.26-Å backbone heavy atom rms deviation for 20 calculated structures), good geometries, low residual energies, and a lack of NOE violations (see Table 2 and Fig. 6).

Structure of the VPS4A MIT Domain. The MIT domain of VPS4A (residues 5–76) forms an antiparallel three helix bundle (Fig. 2*A*). The three helices wrap with a left superhelical twist, and are disposed asymmetrically onto three corners of a square (Fig. 2*B*). The third helix is longer than the first two, and has an ≈10° bend centered about residue Tyr-63. Helices 2 and 3 form a two-stranded, antiparallel coiled coil, and interact with canonical "knobs in holes" side chain interactions (32, 33) (Fig. 3). This interaction explains the predicted coiled-coil propensity of the third helix (10), and also explains the conservation of hydrophobic residues across MIT domains at helix 2 positions 25, 29, 32, 36, 39, and 43 and helix 3 positions 56, 60, 63, 67, 70, and 74 (see Fig. 1), because these residues correspond to the alternating **a** (+1) and **d** (+4) positions in the heptad repeats of the coiled coil. However, the coiled coil formed between helices 2 and 3 is unusual in that it is mediated by conserved aromatic (as opposed to aliphatic) side chains at positions 25, 32, 39, and 63.

In contrast, helices 1 and 2 do not form a canonical coiled coil, but rather interact through a motif that could be described as an "alanine zipper." As shown in Figs. 2*C* and 3, the closest contacts between the two helices are mediated by five alanine residues, two from helix 1 (Ala-9 and Ala-16), and three from helix 2 (Ala-28, Ala-35, and Ala-42). Each set of alanines is separated by seven residues, and the side chains therefore project from the same side of the helix with a spacing of two helical turns. However, unlike the side chains in a coiled coil, the alanines project directly toward the partner helix, and form an interdigitating strip between the two helices (Fig. 2*C*). As shown in Fig. 3, all of these alanines sit between hydrophobic residues that project from the +4 and +5 positions on the partner helix (numbering relative to the preceding alanine). The distance between helices 1 and 2 in the MIT domain of VPS4A is not unusual (≈10 Å), but this packing distance can only readily accommodate small side chains such as Ala and Gly at the five zipper positions (9, 16, 28, 35, and 42). Importantly, these alanines or glycines are highly conserved, particularly within the center of the zipper, with ≥93% conservation of Ala or Gly at

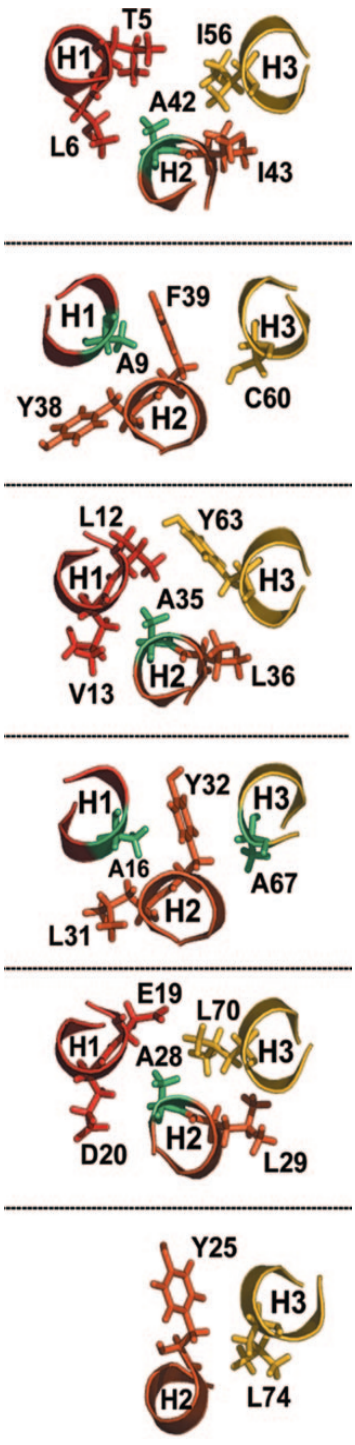

Fig. 3. Side chain interactions at the different layers of the VPS4A MIT three-helix bundle. Sequential amino acid layers in the three helix bundle of the VPS4A MIT domain. Note that side chain interactions between helices 2 (H2) and 3 (H3) follow canonical alternating ''knobs into holes'' interactions between residues at helix positions +1 (A) and +4 (D), whereas side chain packing between helices 1 (H1) and 2 (H2) is different because alternating alanine residues (highlighted in green) project almost directly at the pairing helix and are sandwiched between hydrophobic side chains from the +4 and +5 positions (relative to the preceding alanine) in the pairing helix.

positions 9, 16, 28, and 35 in the 116 known MIT domain sequences (23). Therefore, analogous interhelical packing interactions likely exist in all MIT domains.

Importantly, the alanine zipper formed between the first two helices is linked structurally to the aromatic coiled coil formed between the second two helices, so that the entire three-helix bundle of the MIT domain can be considered a single structural motif. Specifically, the two alanines from helix 1 (Ala-9 and Ala-16) pack between conserved central aromatic residues from helix 2 (Tyr-32 and Phe-39). Similarly, the three alanines on helix 2 (Ala-28, Ala-35, and Ala-42) pack against aromatic/large hydrophobic side chains from the heptad repeat of helix 3 (Leu-70, Tyr-63, and Ile-56). Thus, the central strip of aromatic residues between helices 2 and 3 simultaneously buttresses the alanine zipper and participates in coiled-coil formation, and apparently serves to hold the three helices at a proper angle (see Figs. 2*B* and 3).

The closest known structural matches to the VPS4A MIT domain occur for two distinct classes of helical bundles (34). The first class corresponds to the first three helices within canonical four helix bundles. In the best matches, the three MIT domain helices align with the first three helices of the four helix bundles with backbone atom rms deviations of ≈2 Å (e.g., α-1 catenin; Protein Data Bank ID 1h6g, Dali *z* score = 8.1, backbone atom rms deviation = 2.0 over 74 residues). However, as emphasized above, the interhelical side chain packing interactions of the $VPS4A_{5–76}$ MIT domain are quite distinct from those of canonical four helix bundles, and it therefore seems unlikely that MIT domains bind their partners by completing the four helix bundle. The second class of similar structures correspond to helices within tetratricopeptide repeats (TPR). For example, the three MIT domain helices align well with the first three helices in the TPR of FKBP51 (Protein Data Bank ID 1kt0, Dali *z* score = 8.7, backbone atom rms deviation = 2.1 over 70 residues in helices 1–3, see Fig. 4 *D* and *E*). TPR motifs are repeats of paired helices composed of two different types of interhelical interactions: an A/B interaction within each helical pair and a B/A′ interaction that links one helix pair to the next (35). TPR and MIT domain helices are similar in that: (*i*) the helices have similar spatial dispositions, (*ii*) an Ala/Gly zipper pairs the first two helices (the A/B interaction), and (*iii*) conserved aromatic residues perform similar roles in helping to bridge the first helix pair and the following repeat (the B/A′ interaction). In a TPR, the fourth (B′) helix, which is absent in the MIT domain, binds the third helix and we envision that an analogous interaction could mediate the intermolecular interaction with CHMP1B (see below).

The VPS4A MIT Domain Binds the C-Terminal Region of CHMP1B. To begin to define how the VPS4 ATPases interact with the assembled ESCRT-III lattice, we mapped the sites of interaction between the VPS4A and CHMP1B proteins. The 10 different human CHMP proteins exhibit only modest pairwise sequence identities (12–65%), but nevertheless share a number of common features, including similar sizes (210 ± 20 residues), predicted coiled-coil motifs, and highly asymmetric charge distributions (9). CHMP1B is typical of other CHMP proteins in that the first 64 residues are highly basic [predicted isoelectric point (PI) of 10.1] and contain a predicted coiled coil (see Fig. 1), whereas the C-terminal 132 residues are highly acidic (predicted PI of 4.5) and lack predicted coiled-coil motifs. We have previously used GST pull-down assays to demonstrate that both VPS4A and VPS4B bind to a series of full-length ESCRT-III proteins, including CHMP1B (12). As shown in Fig. 4*A*, the full-length recombinant VPS4A protein also bound a C-terminal fragment of GST-CHMP1B (residues 65–196), but not GST alone (compare lanes 4 and 5). Thus, VPS4A does not interact with the CHMP1B coiled-coil/basic region as had been pre-

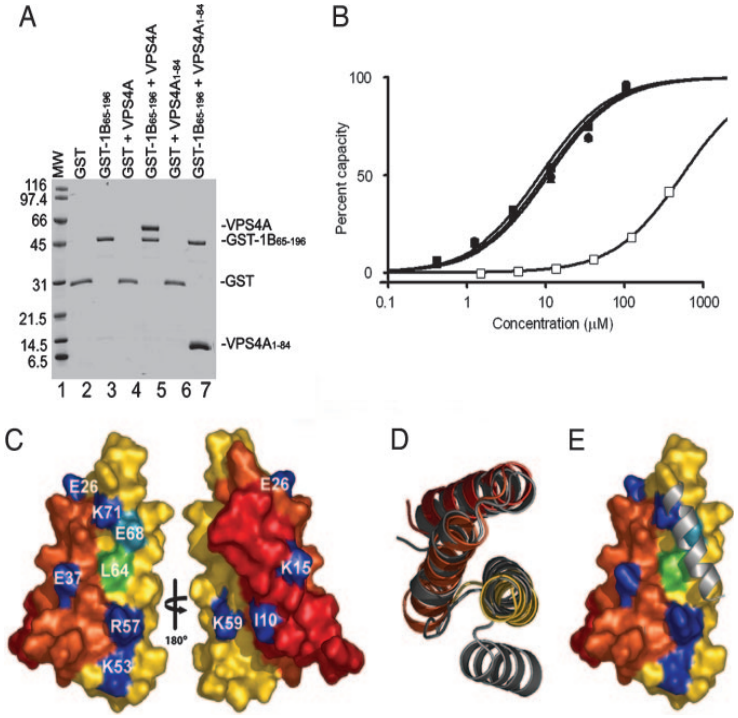

Fig. 4. Interactions between VPS4A and CHMP1B proteins. (*A*) GST pull-downs demonstrating that both full-length VPS4A and its isolated MIT domain ($VPS4A_{1–84}$) bind GST-$CHMP1B_{65–196}$ (denoted GST-$1B_{65–196}$, lanes 5 and 7) but not GST alone (lanes 4 and 6). Molecular weight standards (MW, lane 1), pure GST (lane 2), and pure GST-$CHMP1B_{65–196}$ (lane 3) are shown for reference. (*B*) Biosensor binding isotherms showing wild-type (WT) and L64A mutant $VPS4A_{1–84}$ proteins binding GST-CHMP1B and GST-$CHMP1B_{65–196}$. Filled circles, WT $VPS4A_{1–84}$ binding full-length GST-CHMP1B captured from *E. coli* extracts; filled triangles, WT $VPS4A_{1–84}$ binding GST-$CHMP1B_{65–196}$ captured from *E. coli* extracts; filled squares, WT $VPS4A_{1–84}$ binding affinity purified GST-$CHMP1B_{65–196}$; open squares, $VPS4A_{1–84}$ L64A binding affinity purified GST-$CHMP1B_{65–196}$. Binding to the GST control surface was negligible (not shown). Dissociation constants (μM) for WT $VPS4A_{1–84}$ binding were: CHMP1B = 20 ± 13 and $CHMP1B_{65–196}$ = 13 ± 6 μM; and were >500 μM for $VPS4A_{1–84}$ L64A binding to both constructs (minimum three independent measurements). (*C*) VPS4A MIT surface renderings showing the locations and identities of conserved residues. Conserved residues are color-coded based on the reduction in $CHMP_{65–196}$ binding affinity for alanine substitution mutations: dark blue, <3-fold change; light blue, 3- to 30-fold reduction; green, >30-fold reduction. Dissociation constants were: WT, 13 ± 6 μM; I10A, 17 ± 1 μM; K15A, 14 ± 1 μM; E26A, 8 ± 1 μM; E37A, 16 ± 2 μM; K53A, 20 ± 2 μM; R57A, 34 ± 4 μM; K59A, 9 ± 1 μM; L64A, >500 μM; E68A, 55 ± 4 μM; K71A, 18 ± 2 μM (minimum of two independent measurements). (*D*) Overlays of the first four helices of the TPR domain of FKBP51 (gray) with the MIT domain of VPS4A. The overlay shows the similarity of the structures and the position of the second paired helix (fourth overall) in the FKBP51 TPR domain, which is missing in the VPS4A MIT domain. (*E*) Side view of the overlay in *D*, but with the VPS4A MIT domain shown in a space filling model and color coded as in *C*. The figure emphasizes that residues required for CHMP1B binding (green, light blue) map to the same surface as the binding site for the second paired helix of the FKBP51 TPR domain.

dicted (10), but instead binds the protein's acidic C-terminal region. These data are consistent with other recent experiments showing that C-terminal regions of other CHMP proteins bind VPS4 in extracts (13, 36).

As discussed above, the ESCRT-III proteins are apparently substrates for the VPS4 ATPases (9, 10, 14–17) and AAA ATPase substrate recognition is typically meditated by the N-terminal domain (reviewed in ref. 18). Therefore, we tested whether the N-terminal MIT domain of VPS4A alone ($VPS4A_{1–84}$) could bind CHMP1B proteins. As shown in Fig. 4*A*, $VPS4A_{1–84}$ bound GST-$CHMP1B_{65–196}$, but not GST alone (compare lanes 6 and 7). Thus, the VPS4A MIT domain alone contains CHMP1B binding activity. This observation was confirmed and quantitated in biosensor binding experiments, in which soluble monomeric $VPS4A_{1–84}$ bound specifically to immobilized GST-CHMP1B proteins. VPS4A MIT domain binding and dissociation were rapid at 20°C, and dissociation constants were therefore obtained by analyzing equilibrium binding phases (see Fig. 7*B* for representative sensorgrams). As shown in Fig. 4*B*, the MIT domain bound with equal affinity to both full-length GST-CHMP1B (K_d = 20 ± 13 μM) and GST-$CHMP1B_{65–196}$ (K_d = 13 ± 6 μM). Thus, a C-terminal CHMP1B fragment that contains the acidic region but lacks the predicted coiled-coil contributes all of the energetically significant VPS4A MIT binding contacts.

Biosensor binding assays were also used to map the interaction surface on the VPS4A MIT domain. We reasoned that the binding site might feature a cluster of conserved, surface-exposed residues, particularly hydrophobic residues. As discussed above, interhelical packing interactions rationalize the conservation of all hydrophobic residues found with >50% frequency in the MIT domain, with the sole exception of Leu-64, which is exposed on the surface of helix 3 (see Figs. 1 and 4*C*). Most of the remaining hydrophobic residues that lack strict sequence conservation also appear to perform structural roles, as do a conserved pair of charged residues, Asp-20 and Arg-66, which approach one another across the interface between helices 1 and 2, where they may interact to form a salt bridge. This leaves nine solvent-exposed residues that are conserved at >50% identity and that appear unlikely to perform important structural roles within the three helix bundle (Lys/Arg-15, Glu/Asp-26, Glu/Asp-37, Arg/Lys-53, Arg/Lys-57, Lys-59, Leu-64, Glu-68, and Lys/Arg-71). We created an ensemble of proteins that contained single alanine substitution mutations at each conserved position, as well as in the exposed Ile-10 residue. Al-

though Ile-10 is <50% conserved across all MIT domains, this position is typically hydrophobic and lies on the face opposite Leu-64.

As summarized in Fig. 4 *B–E*, the affinity of CHMP1B (and $CHMP1B_{65–96}$) binding was reduced very substantially (>30-fold) by the $VPS4A_{1–84}$ L64A mutation. An alanine substitution mutation in the adjacent Glu-68 residue also reduced CHMP1B binding affinity, albeit modestly (3.5-fold). None of the other mutants altered the CHMP1B binding affinity significantly (<3-fold). Importantly, an [^{1}H,^{15}N] HSQC spectrum of the $VPS4A_{1–84}$ L64A protein confirmed that this mutation did not alter the overall fold of the MIT domain (see Fig. 7*A*). Therefore, we conclude that CHMP1B contacts the Leu-64/Glu-68 patch directly. As shown in Fig. 4*E*, this patch corresponds to the surface of helix 3 that would normally interact with the fourth helix in a TPR motif. Thus, the short TPR in the MIT domain has adapted to bind a target protein in trans, rather than a fourth helix in cis, raising the intriguing possibility that helices from the ESCRT-III proteins may bind by completing or extending the TPR.

Potential Biological Implications. MIT domains are found in proteins that function in important biological processes such as endosomal protein sorting (VPS4, SNX15, spastin) (10, 20, 22), virus budding (VPS4) (25), microtubule organization (spastin) (21, 22, 37, 38), and maintenance of motor neuron function (spastin and spartin) (22, 39). The general conservation of key structural residues indicates that all MIT domains will form three-helix bundles that are similar to the VPS4A MIT domain structure presented here.

Our data also demonstrate that the MIT domain of VPS4A binds directly to the C-terminal acidic region of the ESCRT-III protein, CHMP1B, and to analogous regions on other human CHMP proteins (data not shown). These interactions seem functionally important because recruitment of VPS4 proteins to endosomal membranes requires both the C-terminal half of CHMP proteins (40) and the MIT domains of VPS4 proteins (10). Interestingly, another MIT domain-containing protein, spastin, is also a CHMP1B-binding protein and the MIT domain is again required for this interaction (22). As shown in Fig. 1, the key Leu-64 residue in helix 3 critical for the VPS4A/CHMP1B interaction is also conserved in the spastin MIT domain. This domain again precedes a AAA ATPase cassette, raising the possibility that spastin may perform at least some functions that are analogous to those of the two better characterized human VPS4 proteins. Indeed, although the binding partners for most MIT domain proteins have not yet been determined experimentally, the apparent conservation of the exposed leucine on helix 3 suggests that other human MIT domain proteins such as SNX15, which again seems to function in endosomal protein sorting (20), may also interact functionally with ESCRT-III proteins.

We thank Tom Alber for helpful discussions on helical packing interactions, Darrell Davis for his efforts on behalf of the University of Utah Biomolecular NMR Center, and David Myszka and Phini Katsamba for performing the biosensor binding experiments. This work was funded by National Institutes of Health Grant AI51174 (to W.I.S.).

1. Murk, J. L., Stoorvogel, W., Kleijmeer, M. J. & Geuze, H. J. (2002) *Semin. Cell Dev. Biol.* **13,** 303–311.
2. Katzmann, D. J., Odorizzi, G. & Emr, S. D. (2002) *Nat. Rev. Mol. Cell Biol.* **3,** 893–905.
3. Gruenberg, J. & Stenmark, H. (2004) *Nat. Rev. Mol. Cell Biol.* **5,** 317–323.
4. de Gassart, A., Geminard, C., Hoekstra, D. & Vidal, M. (2004) *Traffic* **5,** 896–903.
5. Morita, E. & Sundquist, W. I. (2004) *Annu. Rev. Cell Dev. Biol.* **20,** 395–425.
6. Demirov, D. G. & Freed, E. O. (2004) *Virus Res.* **106,** 87–102.
7. Raymond, C. K., Howald-Stevenson, I., Vater, C. A. & Stevens, T. H. (1992) *Mol. Biol. Cell* **3,** 1389–1402.
8. Babst, M., Katzmann, D., Estepa-Sabal, E., Meerloo, T. & Emr, S. (2002) *Dev. Cell* **3,** 271–282.
9. Howard, T. L., Stauffer, D. R., Degnin, C. R. & Hollenberg, S. M. (2001) *J. Cell Sci.* **114,** 2395–2404.
10. Babst, M., Wendland, B., Estepa, E. J. & Emr, S. D. (1998) *EMBO J.* **17,** 2982–2993.
11. Martin-Serrano, J., Yaravoy, A., Perez-Caballero, D. & Bieniasz, P. D. (2003) *Proc. Natl. Acad. Sci. USA* **100,** 12414–12419.
12. von Schwedler, U. K., Stuchell, M., Muller, B., Ward, D. M., Chung, H. Y., Morita, E., Wang, H. E., Davis, T., He, G. P., Cimbora, D. M., *et al.* (2003) *Cell* **114,** 701–713.
13. Yeo, S. C., Xu, L., Ren, J., Boulton, V. J., Wagle, M. D., Liu, C., Ren, G., Wong, P., Zahn, R., Sasajala, P., *et al.* (2003) *J. Cell Sci.* **116,** 3957–3970.
14. Finken-Eigen, M., Rohricht, R. A. & Kohrer, K. (1997) *Curr. Genet.* **31,** 469–480.
15. Yoshimori, T., Yamagata, F., Yamamoto, A., Mizushima, N., Kabeya, Y., Nara, A., Miwako, I., Ohashi, M., Ohsumi, M. & Ohsumi, Y. (2000) *Mol. Biol. Cell* **11,** 747–763.
16. Bishop, N. & Woodman, P. (2000) *Mol. Biol. Cell* **11,** 227–239.
17. Scheuring, S., Rohricht, R. A., Schoning-Burkhardt, B., Beyer, A., Muller, S., Abts, H. F. & Kohrer, K. (2001) *J. Mol. Biol.* **312,** 469–480.
18. Dougan, D. A., Mogk, A., Zeth, K., Turgay, K. & Bukau, B. (2002) *FEBS Lett.* **529,** 6–10.
19. Scott, A., Chung, H.-Y., Gonciarz-Swiatek, M., Hill, G. C., Whitby, F. G., Gaspar, J., Holton, J. M., Viswanathan, R., Ghaffarian, S., Hill, C. P. & Sundquist, W. I. (2005) *EMBO J.*, in press.
20. Phillips, S. A., Barr, V. A., Haft, D. H., Taylor, S. I. & Haft, C. R. (2001) *J. Biol. Chem.* **276,** 5074–5084.
21. Ciccarelli, F. D., Proukakis, C., Patel, H., Cross, H., Azam, S., Patton, M. A., Bork, P. & Crosby, A. H. (2003) *Genomics* **81,** 437–441.
22. Reid, E., Connell, J., Edwards, T. L., Duley, S., Brown, S. E. & Sanderson, C. M. (2005) *Hum. Mol. Genet.* **14,** 19–38.
23. Letunic, I., Copley, R. R., Schmidt, S., Ciccarelli, F. D., Doerks, T., Schultz, J., Ponting, C. P. & Bork, P. (2004) *Nucleic Acids Res.* **32,** D142–D144.
24. Pearson, W. R. & Lipman, D. J. (1988) *Proc. Natl. Acad. Sci. USA* **85,** 2444–2448.
25. Garrus, J. E., von Schwedler, U. K., Pornillos, O. W., Morham, S. G., Zavitz, K. H., Wang, H. E., Wettstein, D. A., Stray, K. M., Cote, M., Rich, R. L., *et al.* (2001) *Cell* **107,** 55–65.
26. von Schwedler, U. K., Stray, K. M., Garrus, J. E. & Sundquist, W. I. (2003) *J. Virol.* **77,** 5439–5450.
27. Myszka, D. G. (1999) *J. Mol. Recognit.* **12,** 279–284.
28. Guntert, P. (2004) *Methods Mol. Biol.* **278,** 353–378.
29. Schubert, M., Labudde, D., Oschkinat, H. & Schmieder, P. (2002) *J. Biomol. NMR* **24,** 149–154.
30. Brunger, A. T., Adams, P. D., Clore, G. M., DeLano, W. L., Gros, P., Grosse-Kunstleve, R. W., Jiang, J. S., Kuszewski, J., Nilges, M., Pannu, N. S., *et al.* (1998) *Acta Crystallogr. D* **54,** 905–921.
31. Laskowski, R. A., Rullmannn, J. A., MacArthur, M. W., Kaptein, R. & Thornton, J. M. (1996) *J. Biomol. NMR* **8,** 477–486.
32. Crick, F. H. C. (1953) *Acta Crystallogr.* **6,** 689–697.
33. Walshaw, J. & Woolfson, D. N. (2001) *J. Mol. Biol.* **307,** 1427–1450.
34. Holm, L. & Sander, C. (1995) *Trends Biochem. Sci.* **20,** 478–480.
35. D'Andrea, L. D. & Regan, L. (2003) *Trends Biochem. Sci.* **28,** 655–662.
36. Fujita, H., Umezuki, Y., Imamura, K., Ishikawa, D., Uchimura, S., Nara, A., Yoshimori, T., Hayashizaki, Y., Kawai, J., Ishidoh, K., *et al.* (2004) *J. Cell Sci.* **117,** 2997–3009.
37. Errico, A., Ballabio, A. & Rugarli, E. I. (2002) *Hum. Mol. Genet.* **11,** 153–163.
38. Trotta, N., Orso, G., Rossetto, M. G., Daga, A. & Broadie, K. (2004) *Curr. Biol.* **14,** 1135–1147.
39. Patel, H., Cross, H., Proukakis, C., Hershberger, R., Bork, P., Ciccarelli, F. D., Patton, M. A., McKusick, V. A. & Crosby, A. H. (2002) *Nat. Genet.* **31,** 347–348.
40. Lin, Y., Kimpler, L. A., Naismith, T. V., Lauer, J. M. & Hanson, P. I. (2005) *J. Biol. Chem.* **280,** 12799–12809.
41. Wolf, E., Kim, P. S. & Berger, B. (1997) *Protein Sci.* **6,** 1179–1189.
42. Cornilescu, G., Delaglio, F. & Bax, A. (1999) *J. Biomol. NMR* **13,** 289–302.

APPENDIX B

ESCRT-III RECOGNITION BY VPS4 ATPASES SUPPLEMENTAL MATERIAL

Melissa D. Stuchell-Brereton, Jack J. Skalicky, Collin Kieffer, Mary Anne Karren, Sanaz Ghaffarian, and Wesley Sundquist

Reprinted from Nature, Vol. 449, Supplemental Material pages 1-19, Copyright 2007.

Note: Cloning of CHMP and VPS4 constructs, purification of CHMP and VPS4 proteins, identification of C-terminal CHMP region required for VPS4 binding, biosensor experiments, homologue searches and alignments, NMR data collection, analysis of NMR data and determination of the solution structure of unbound VPS4B and of VPS4B in complex with CHMP2B (195-213) were performed by Melissa D. Stuchell-Brereton and contributed to Supplemental Table 1 and 2, and Supplemental Figures 3a, 3b, 3c, 3d, 4a, 4b, 4c, 4d, 4e, 4f, and 4g. Purification of VPS4A and CHMP1A proteins, NMR data collection, analysis of NMR data and determination of the solution structure of VPS4A in complex with CHMP1A were performed by Jack J. Skalicky and contributed to Supplemental Table 1 and Supplemental Figures 1a, 1b, 1c, and 2. GFP-VPS4 cloning, localization studies, HIV-1 vector release and infectivity experiments, and biosensor experiments were performed by Collin Kieffer and contributed to Supplemental Figure 5. GFP-CPS cloning, CPS sorting assays, and Vps4p localization studies in yeast were performed by Mary Anne Karren and contributed to Supplemental Figure 6.

doi: 10.1038/ nature06 172

SUPPLEMENTARY INFORMATION

Supplemental Table 1. Structural Statistics for VPS4A MIT-CHMP1A$_{180-196}$, VPS4B MIT, and VPS4B MIT-CHMP2B$_{195-213}$

	VPS4A MIT-CHMP1A$_{180-196}$	VPS4B MIT	VPS4B MIT-CHMP2B$_{195-213}$
NMR distance and dihedral constraints			
Distance constraints			
Total NOE	1311	1769	1625
Intra-residue	309	426	338
Inter-residue	1002	1343	1287
Sequential (|i – j| = 1)	333	418	403
Medium-range (2 ≥ |i – j| ≤ 5)	391	538	487
Long-range (|i – j| > 5)	215	387	336
Intermolecular (MIT – CHMP)	63		61
Hydrogen bonds	59	55	61
Total dihedral angle restraints	152	120	140
ϕ	76	60	70
ψ	76	60	70
Structure statistics			
Violations (mean, s.d.)			
Distance constraints (Å)	0.002, 0.002	0.003, 0.005	0.003, 0.004
Dihedral angle constraints (º)	0.030, 0.025	0.035, 0.025	0.034, 0.027
Max. distance constraint violation (Å)	0.017	0.065	0.026
Max. dihedral angle violation (º)	0.1	0.103	0.125
Deviations from idealized geometry (r.m.s.deviation)			
Bond lengths (Å)	0.0003	0.0003	0.0004
Bond angles (º)	0.29	0.25	0.25
Impropers (º)	0.08	0.79	0.81
Average pairwise r.m.s. deviation[1] (Å)			
All heavy atoms	1.25 ± 0.14	1.07 ± 0.08	1.16 ± 0.10
Backbone atoms (Cα, C, N, O)	0.63 ± 0.26	0.37 ± 0.07	0.64 ± 0.10

[1]Average pairwise r.m.s. deviation was calculated using the 20 lowest energy CNS structures. Structures were superimposed using residues 5-75 and 185-196 for VPS4A MIT-CHMP1A$_{180-196}$, 10-81 for VPS4B MIT, and 10-81 and 200-213 for VPS4B MIT-CHMP2B$_{195-213}$.

Ramachandran statistics (most favored%, additionally allowed%, generously allowed%) are: VPS4A MIT-CHMP1A$_{180-196}$ (93.7, 6.3, 0); VPS4B MIT (95.1, 4.9, 0); and VPS4B MIT-CHMP2B$_{195-213}$ (94.7, 5.1, 0.2).

Structure coordinates have been deposited in the PDB with the following codes: VPS4A MIT-CHMP1A$_{180-196}$, rcsb100153 and PDB ID code 2jq9; VPS4B MIT, rcsb100161 and PDB ID code 2jqh; and VPS4B MIT- CHMP2B$_{195-213}$, rcsb100164 and PDB ID code 2jqk.

doi: 10.1038/ nature06 172

Supplemental Table 2.

CHMP Protein Family	Organism	NCBI Accession Number	C-terminal Sequence
1A	Homo Sapiens	Q9HD42	SQEDQLSRRLAALRN
1B	Homo Sapiens	AAG01449	AEQDELSQRLARLRDQV
2A	Homo Sapiens	NP_940818	DADADLEERLKNLRRD
2B	Homo Sapiens	NP_054762	ISDEEIERQLKALGVD
3	Homo Sapiens	NP_057163	EALEAMQSRLATLRS
1	Macaca mulatta	XP_001103984	SQEDQLSRRLAALRN
2	Macaca mulatta	XP_001104442	ISDEEIERQLKALGVD
3	Macaca mulatta	XP_001086438	AAEMEIDRILFEITADVFHNT
1A	Mus musculus	NP_663581	SQEDQLSRRLAALRN
1B	Mus musculus	NP_077152	AEQDELSQRLARLRDQV
2A	Mus musculus	NP_081161	DADADLEERLKNLRRD
2B	Mus musculus	NP_081155	ISDEEIERQLKALGVD
3	Mus musculus	NP_080059	EDLEAMQSRLATLRS
1A	Rattus norvegicus	NP_001076782	SQEDQLSRRLAALRN
1B	Rattus norvegicus	XP_001067633	AEQDELSQRLARLRDQV
2A	Rattus norvegicus	XP_344861	DADADLEERLKNLRRD
2B	Rattus norvegicus	XP_001063932	ISDEEIERQLKALGVD
3	Rattus norvegicus	NP_758834	EDLEAMQSRLATLRS
1	Caenorhabditis elegans	NP_490974	SEDKDLTERLAALRNM
2A	Caenorhabditis elegans	NP_496717	DVDDDLQARLDQLRRE
2B	Caenorhabditis elegans	NP_493357	ADFDDLEAQLARLRS
3	Caenorhabditis elegans	NP_494919	EDFEGMAQRLAELRD
1A	Xenopus laevis	AAH68657	TQEDQLSRRLASLRN
1B	Xenopus laevis	Q7SZB5	TEQDELSQRLARLRDQV
2A	Xenopus laevis	Q6IP52	DADADLEERLNNLRRD
2B	Xenopus laevis	Q7SYR0	ISDEEIERQLKALGVD
2B	Xenopus laevis	Q66IV6	ISDEEIERQLKALGVD
3	Xenopus laevis	Q6NRM7	EDLEAMHSRLAALRS
1	Drosophila melanogaster	NP_649051	QEQDELTQRLARLRQAE
2A	Drosophila melanogaster	NP_651455	DADADLQARLDKLRKD
2B	Drosophila melanogaster	NP_647947	RTEKDIADQLAKLRSS
3	Drosophila melanogaster	NP_649451	EELQEMQSRLASLRS
1	Anopheles gambiae	XP_316550	TEQDELTARLARLRQAE
2	Anopheles gambiae	XP_321862	DADADLQARLDNLRRE
3	Anopheles gambiae	EAA05411	DDMKEMQNRLQALRS
1	Arabidopsis thaliana	AAF99815	VEEDDLTRRLAELKAR
2A	Arabidopsis thaliana	NP_565336	GIDSDLQARLDNLRKM
2B	Arabidopsis thaliana	ADD10675	SGIDELEKRLAALR
2B	Arabidopsis thaliana	NP_563696	SGIDELEKRLAALR
3	Arabidopsis thaliana	NP_197686	EELEEIRARLAKVRS
1A	Leishmania infantum JPCM5	XP_001468271	VDEDDIAERLKALQAL
1B	Leishmania infantum JPCM5	XP_001469249	VEEDDLEAKFAQLRGR
2	Leishmania infantum JPCM5	XP_001466503	ETDEELDARLAALKASM
3	Leishmania infantum JPCM5	XP_001469672	--EDELMEKFNALRNS
1	Saccharomyces cerevisiae	NP_012961	EKEDKLAQRLRALRG
2	Saccharomyces cerevisiae	NP_012924	NPDDDLQARLNTLKKQT
3	Saccharomyces cerevisiae	CAA81876	RMVNEMRERLRALQN
1	Schizosaccharomyces pombe	NP_596562	VEDDNLQERLRALRS
2	Schizosaccharomyces pombe	CAB90130	KTEDNLQARLDELAKR
3	Schizosaccharomyces pombe	NP_594587	EQLLDIRDKLDALKS

doi: 10.1038/ nature06 172

Supplemental Figure Captions

Supplemental Figure 1 | NMR Spectra of the VPS4A MIT-CHMP1A$_{180-196}$ Complex.
a, Overlay of 2D [^{15}N, ^{1}H] HSQC spectra for ^{15}N-labeled VPS4A MIT titrated with unlabeled CHMP1A$_{180-196}$ peptide. Spectra are colored according to the number of molar equivalents CHMP1A$_{180-196}$ added: red, 0 equivalents; cyan, 0.35 equivalents; purple, 0.65 equivalents; and blue, 1.15 equivalents. Aliased arginine N$^{\varepsilon}$H$^{\varepsilon}$ resonances are shown in green, yellow, white, and cyan, respectively. Right panels show expanded regions of the left spectrum.
b, Comparative NH backbone chemical shifts from the 0 and 1.15 equivalent titration points in **a** mapped on the VPS4A MIT–CHMP1A$_{180-196}$ structure. Red denotes NH signals with composite $\Delta\delta > 5$, where $\Delta\delta=25((\Delta\delta_{HN})^2 + (\Delta\delta_N/5)^2)^{0.5}$.
c, Strip plots from 3D [^{1}H,^{13}C/^{15}N, ^{1}H] NOESY (blue) and 3D F1-^{13}C^{15}N-filtered [^{1}H,^{13}C/^{15}N,^{1}H] NOESY (red) for six different CH strips from residues within the VPS4A MIT–CHMP1A interface. Horizontal lines denote assigned inter-molecular NOEs and assignments are given to the right of the corresponding strips.

Supplemental Figure 2 | Structure of the VPS4A MIT-CHMP1A$_{180-196}$ Complex.
Superposition of the twenty lowest penalty structures of the VPS4A MIT-CHMP1A$_{180-196}$ complex. Structure statistics are given in Supplemental Table 1. Color coding here and throughout is the same as in Fig. 2b.

Supplemental Figure 3 | Structures and Comparisons of the VPS4B MIT Domains
a, Superposition of the twenty lowest penalty structures of the free VPS4B MIT Domain. Structure statistics are given in Supplemental Table 1.
b, Ribbon diagrams showing the superposition of the free VPS4B MIT domain (colored) and the free VPS4A MIT domain (grey), rmsd = 1.14 Å. Superpositions in parts b-d were on all heavy atoms within the three helices of the VPS4A and VPS4B MIT domains (VPS4A residues 6-22, 25-45, 50-75 and VPS4B residues 8-24, 27-47, 52-83).
c, Ribbon diagrams showing the superposition of the free VPS4A MIT domain (colored) and the same domain within the VPS4A MIT-CHMP1A$_{180-196}$ complex (grey), rmsd = 0.86 Å.
d, Ribbon diagrams showing the superposition of the free VPS4B MIT domain (colored) and the same domain within the VPS4B MIT-CHMP2B$_{195-213}$ complex (grey), rmsd = 0.73 Å.

Supplemental Figure 4 | Structure of the VPS4B MIT-CHMP2B$_{195-213}$ Complex.
a, Superposition of the twenty lowest penalty structures of the VPS4B MIT-CHMP1A$_{195-213}$ complex. Structure statistics are given in Supplemental Table 1.
b, Ribbon diagram of the VPS4B MIT-CHMP2B$_{195-213}$ complex, with the three conserved leucine residues shown explicitly.
c, Structure of the VPS4B MIT-CHMP2B$_{195-213}$ complex. The MIT domain is shown in a space filling model with the Leu66 residue highlighted in blue, and with important residues on both sides of the interface shown explicitly. Arrows denote the approximate orientations of the three leucine binding pocket views shown in parts d-f.
d-f, Close up views of the three leucine binding pockets of the VPS4B MIT domain showing the hydrophobic pockets in detail, as well as salt bridge and hydrogen bonding interactions between D200-R59 and Q206-E70 (CHMP2B residues listed first).

Supplemental Figure 5 | VPS4A MIT-CHMP1B Binding Interactions

doi: 10.1038/ nature06 172

Biosensor binding isotherms showing wild type and mutant VPS4A MIT binding to immobilized GST-CHMP1B$_{180-196}$ proteins. The data demonstrate that mutation of the VPS4A Leu64 residue severely inhibits CHMP1B binding and that the L64D mutation is even more detrimental than the L64A mutation. Duplicate data points are shown for each condition, and estimated dissociation constants derived from fits to single site binding models (curves) were wt VPS4A MIT = 19.0 ± 0.1μM and VPS4A MIT$_{L64A}$ ~3.36 ± 0.2 mM. VPS4A MIT$_{L64D}$ binding was undetectable at the highest concentration tested (250 μM). Estimated errors in dissociation constants were derived from statistical fits of duplicate binding data to 1:1 binding models and the dissociation constant for the VPS4A MIT-CHMP1B$_{180-196}$ interaction (K_D=19 μM, M buffer) was in good agreement with previous measurements for VPS4A binding to full length CHMP1B (K_D=20 ±13 μM, M buffer)[2].

Supplemental Figure 6 | The Yeast Vps4p MIT Leu64Asp Mutation Inhibits Recruitment of GFP-Vps4p to Class E Compartments.

a, Confocal fluorescence slices showing localization of GFP-Vps4p$_{K179Q}$ (top row), and GFP-Vps4p$_{L64D/K179Q}$ (bottom row) in yeast. FM4-64 staining (red) was used to define the limiting vacuolar membrane (open circles) and to visualize class E compartments (intense puncta). Overlaid and differential interference contrast (DIC) images are shown in the final two rows for reference and the scale bar is 5 μm.

b, Graphic quantification of the experiment shown in **a**, demonstrating that the Vps4p$_{K179Q}$ protein localizes to Class E compartments and that the secondary L64D mutation redistributes the Vps4p$_{L64D/K179Q}$ protein back into the cytoplasm.

doi: 10.1038/ nature06 172

Supplemental Discussion

As expected, the VPS4A and VPS4B MIT domains adopt similar structures, and all three helices overlayed with rmsd values that were only slightly larger than their coordinate errors (Supplemental Figure 3). Furthermore, neither domain changed structure significantly upon CHMP peptide binding, indicating that MIT domains are preformed binding modules. Both CHMP peptides exhibited some helical character prior to binding, but changes in chemical shift indices indicated that the peptides became substantially more helical when they bound the MIT domain. Both complexes exhibit a similar amount of total buried surface area (VPS4A MIT-CHMP1A$_{180-196}$ = 1040Å^2, VPS4B MIT- CHMP2B$_{195-213}$ = 1007Å^2).

Previous studies of isolated VPS4 MIT domains have provided structural explanations for the sequence conservation at a number of positions that stabilize the TPR-like disposition of the three helix bundle[1,2]. The MIT-CHMP complex structures now rationalize the weaker sequence conservation at several additional positions that help define the three binding pockets for the conserved CHMP leucines, including: L29 and Q33 (Leu194 binding pocket), Val36 (Leu191 binding pocket), and Leu40 (Leu187 binding pocket) (VPS4A MIT/CHMP1A numbering). Although the VPS4A MIT-CHMP1A$_{180-196}$ and VPS4B MIT-CHMP2B$_{195-213}$ complexes adopted very similar structures, the VPS4B MIT- CHMP2B$_{195-213}$ interaction was approximately 50-fold weaker (Fig. 1b). To a large extent, this appears to be because the CHMP1A tail conforms perfectly to the $_{187}$LxxRLAALR$_{195}$ core consensus sequence, whereas the CHMP2B tail differs from the consensus at four positions ($_{204}$IxxQLKALG$_{211}$). As a result: 1) the Arg195-Glu37 salt bridge in the VPS4A MIT-CHMP1A complex is lost in the VPS4B MIT-CHMP2B complex (Gly211-Gln39), 2) the Arg190-Glu68 salt bridge in the VPS4A MIT-CHMP1A complex is replaced by a simple hydrogen bonding interaction in the VPS4B MIT-CHMP2B complex (Gln206-Glu70), 3) the conserved Leu187 residue of CHMP1A is replaced

doi: 10.1038/ nature06 172

by an isoleucine in CHMP2B (Ile203), and 4) the consensus Ala-Ala motif ($_{192}$AA$_{193}$ in CHMP1A) may augment the binding affinity indirectly by contributing to helical propensity, (vs. the $_{208}$KA$_{209}$ sequence in CHMP2B), even though these residues do not directly contact the MIT domain. Similarly, the weaker binding typically seen for the VPS4B MIT domain appears to reflect substitutions at VPS4A Val61 (Leu187 binding pocket) vs. VPS4B Thr63, VPS4A Ile43 (Leu184 binding pocket) vs. VPS4B Val45, and VPS4A Glu37 (salt bridge with Arg195 salt bridge, CHMP1A numbering) vs. VPS4B Gln39. Thus, the complex structures explain the sequence conservation on both sides of the interface, and can also rationalize the gradient of binding affinities observed for different MIT-CHMP complexes.

doi: 10.1038/ nature06 172

Full Methods

ESCRT-III Protein Sequence Alignments

50 different CHMP1-3 protein sequences from 12 model organisms were identified using BLAST searches[3] (Supplemental Table 2). C-terminal sequence alignments were created in Clustal W (http://align.genome.jp) by aligning the final 14-21 residues of each sequence.

Yeast Strains

Standard yeast genetic methods were used for the construction, transformation, and growth of yeast[4,5]. The *VPS4* open reading frame (ORF) was replaced with the KanMX cassette generated from pFA6-KanMX4[6] using homologous recombination[7] in the SEY6210 genetic background[8] (MATa; *leu2-3,112 ura3-52 his3-Δ200 trp1-Δ901 lys2-801 suc2-Δ9*).

Expression Constructs and Plasmids

VPS4 MIT Domains. DNA encoding residues 1-84 of human VPS4A and 1-86 of VPS4B were amplified from EST templates (ATCC 81449 and 6216963)[9,10] and cloned into the (5')*Nde*I/(3')*BamH*I sites of a pET16b (Novagen) plasmid modified to encode a TEV protease site after the N-terminal His_{10} tag (WISP00-71). The resulting expression constructs were designated WISP05-43 (VPS4A) and WISP04-153 (VPS4B). Expression constructs for the VPS4A MIT_{L64A}[2] (WISP07-119) and VPS4A MIT_{L64D} (WISP07-120) were made by the QuikChange method (Stratagene). The wt VPS4 MIT constructs were also subcloned into the (5')*Nde*I/(3')*BamH*I sites of pGEX-2T (Amersham) plasmid modified to encode a TEV protease site after the N-terminal GST tag, to create expression constructs for GST-$VPS4A_{1-84}$ (WISP07-60) and GST-$VPS4B_{1-86}$ (WISP04-155).

CHMP1B. Expression constructs for GST-$CHMP1B_{1-196}$ (full length) and GST-$CHMP1B_{65-196}$ have been described[2]. Analogous expression constructs for GST-$CHMP1B_{180-196}$ (WISP06-22) and GST-$CHMP1B_{65-180}$ (WISP06-12), GST-$CHMP1B_{L189A}$ (WISP06-23), and GST-$CHMP1B_{L192A}$ (WISP06-24) were created by the QuikChange method using the CHMP1B and $CHMP1B_{65-196}$ expression constructs as templates.

$CHMP1A_{180-196}$ and $CHMP2B_{195-213}$. Expression constructs for $(His)_{10}$-TrpΔLE-$CHMP1A_{180-196}$ (WISP06-62) and TrpΔLE-$CHMP2B_{195-213}$ (WISP07-61) fusions were initially created by the QuikChange method using the TrpΔLE-Pro-ω-MVIIA-Gly template plasmid[11].

Yeast Vps4p Expression Constructs. Expression constructs for yeast Vps4p were created by amplifying a fragment containing the yeast *VPS4* ORF and ~250 bases up and downstream using wild-type yeast genomic DNA as a template. The amplified fragment was inserted at (5')*BamH1/*(3')*Sal1* sites of pRS416 (ATCC) to create WISP07-95, and this plasmid was mutated using the QuikChange method to create an expression construct for $Vps4p_{L64D}$ (WISP07-97).

GFP-Vps4p. The yeast *VPS4* ORF was amplified from wild-type yeast genomic DNA and cloned into (5')*BamH1/*(3')*Xho1* sites of pRS415*MET25-GFP*[12]. A single base pair was removed from the multiple cloning site using QuikChange mutagenesis to generate the in-frame GFP fusion construct (WISP07-90). *vps4* mutations were introduced using the QuikChange method to create expression constructs for $Vps4p_{K179Q}$ (WISP07-92) and $Vps4p_{K179Q,L64D}$ (WISP07-93).

GFP-CPS Constructs. The gene for carboxypeptidase S was amplified from wild-type yeast genomic DNA and cloned into (5')*BamH1/*(3')*Xho1* sites of WISP07-90 in place of the ORF for *VPS4* to create WISP07-94.

doi: 10.1038/ nature06 172

GFP-VPS4 Constructs. The mammalian expression constructs for EGFP-VPS4A and EGFP-VPS4A$_{K173Q}$ have been described[9], and mutations were introduced using the QuikChange method to create constructs for VPS4$_{L64A}$ (WISP07-98), VPS4$_{L64D}$ (WISP07-99), VPS4$_{K173Q/L64A}$ (WISP07-100), and VPS4$_{K173Q/L64D}$ (WISP07-101).

Protein Expression and Purification

Wild type and mutant VPS4A and VPS4B MIT domains were expressed in BL21(DE3) *E. coli* cells grown in 2-liter cultures of LB or M9 media (2 g/liter $^{15}NH_4Cl$ or 2 g/liter $^{15}NH_4Cl$ and 2 g/liter $^{13}C_6$-glucose). Protein expression was induced (4-12 h, 23°C) with 0.5 mM IPTG (A_{600} = 0.65). Cells were harvested and resuspended in 50 mM Tris pH 8.0, 50 mM imidazole, 500 mM NaCl, and protease inhibitors (Roche Diagnostics) and lysed with 1 mg/mL lysozyme followed by sonication. Lysates were clarified by centrifugation (45 min., 17,000 rpm), and the soluble MIT domains purified by nickel affinity chromatography (chelating sepharose, Amersham Pharmacia). His$_{10}$-VPS4 MIT domains eluted at ~500 mM imidazole from a linear gradient of 50-750 mM imidazole in the lysis buffer. Protein fractions were collected and dialyzed against two changes of 20 mM Tris pH 8.0, 100 mM NaCl, and 5 mM EDTA replacing EDTA in the second change with 1 mM DTT. The His$_{10}$ tag was removed by incubation with TEV protease (1 mg TEV per 100 mg VPS4 protein, 12 h, 23°C) followed by anion exchange chromatography (Q sepharose, Amersham Pharmacia). Flow-through fractions containing VPS4 MIT were concentrated to ~2 ml, and the proteins were purified to homogeneity by gel filtration chromatography (S75, Amersham Pharmacia). This procedure typically yielded ~30 mg of VPS4A MIT and ~20 mg of VPS4B MIT. TEV cleavage left two nonnative residues at the N-terminus of VPS4A MIT (Gly-His) and three nonnative residues at the N-terminus of VPS4B MIT (Gly-His-Met), which are not included in our numbering scheme. Proteins were verified by N-terminal sequencing and electrospray mass spectrometry.

Peptide Synthesis/Expression and Purification

Unlabeled CHMP1A$_{180-196}$ and CHMP2B$_{195-213}$ were prepared by solid phase synthesis and purified by reversed phase HPLC. CHMP1A$_{180-196}$ and CHMP2B$_{195-213}$ were also expressed in bacteria as TrpΔLE peptide fusions for isotopic ^{13}C- and ^{15}N-labeling. The recombinant peptides were purified from inclusion bodies, with an additional nickel affinity chromatography step (6M urea) for (His)$_{10}$-TrpΔLE-CHMP1A$_{180-196}$. The fusion peptides were then cleaved using cyanogen bromide in 70% formic acid[13,14], and the desired peptides were purified by reversed phase HPLC purification. Expected masses were confirmed by mass spectrometry, and final peptide concentrations were determined by amino acid analysis.

Biosensor Analyses

Biosensor binding experiments used BIACORE 2000 and 3000 instruments. Research-grade CM4 sensor chips were derivatized with anti-GST antibody by amine-coupling (5-6000 response units (RU) in Fig. 1a, 15 kRU in Fig. 1b). GST-CHMP1B proteins (Fig. 1a) or GST-VPS4 MIT proteins (Fig. 1b) or GST alone (reference) were captured directly from soluble *E. coli* lysates for 10 minutes at a flow rate of 10µl/min in running buffer (~0.77 kRU GST-CHMP1B proteins in Fig. 1a, ~2-3 kRU GST-MIT proteins in Fig. 1b, and ~3 kRU GST-CHMP1B180-196 protein in Supplemental Figure 5). Running buffers were: 20 mM Tris pH 8.0, 100 mM NaCl, 1 mM DTT, 0.2 mg/mL BSA, 0.005% P20 surfactant (Fig. 1a and "M" buffer in Fig. 1b and Supplemental Figure 5) or 20 mM sodium phosphate pH 5.5, 0.05%

doi: 10.1038/ nature06 172

P20, 0.4 mg/mL BSA ("L" buffer in Fig. 1b). Pure VPS4B MIT (Fig. 1a), CHMP peptides (Fig. 1b), or VPS4A MIT proteins (Supplemental Figure 5) at the designated concentrations were injected in duplicate (running buffer, 50 µL/min, 20ºC) and binding data were collected at 2 Hz during the 30 s association and dissociation phases. All interactions reached equilibrium rapidly and dissociated within seconds during the dissociation phase. To obtain equilibrium constants, the responses at 15 s were fit to a 1:1 binding interaction isotherm[15]. Note that although the estimated dissociation constant for the VPS4A MIT_{L64A}-$CHMP1B_{180-194}$ interaction is not reliable owing to weak binding (K_D~3.3 mM, see Supplemental Figure 5), this interaction is clearly stronger than the VPS4A MIT_{L64D}-$CHMP1B_{180-194}$ interaction, where binding was undetectable even at 250 µM VPS4A MIT_{L64D}.

NMR Sample Preparation and Screening

NMR titration experiments were initially used to screen different VPS4 MIT-CHMP peptide complexes, salt conditions, and temperatures to identify optimal complexes and solution conditions. Samples used for structure determinations were in NMR buffer (20 mM sodium phosphate pH 5.5, 90% H_2O, and 10% D_2O) except where noted. The following NMR samples were prepared and used for complex structure determinations: 1) 1.4 mM uniformly labeled ^{15}N-/^{13}C-labeled VPS4A MIT + 1.6 mM unlabeled $CHMP1A_{180-196}$ (NMR structure of bound VPS4A MIT and ID of intermolecular NOEs, K_D=4.6 µM, 98% occupancy) 2) 1.6 mM unlabeled VPS4A MIT in complex with 1.4 mM uniformly ^{15}N-/^{13}C-labeled $CHMP1A_{180-196}$ (NMR structure of bound $CHMP1A_{180-196}$ and ID of intermolecular NOEs, 98% occupancy), 3) 2.9 mM uniformly ^{15}N-/^{13}C-labeled VPS4B MIT in NMR buffer + 50 mM NaCl (NMR structure determination of free VPS4B MIT), 4) 0.48 mM uniformly ^{15}N-/^{13}C-labeled VPS4B MIT + 4.8 mM unlabeled $CHMP2B_{195-213}$ (NMR structure of bound VPS4B MIT and ID of intermolecular NOEs, K_D=273 µM, 94% occupancy) 5) 2.84 mM unlabeled VPS4B MIT in complex with 0.26 mM uniformly ^{15}N-/^{13}C-labeled $CHMP2B_{195-213}$ (NMR structure of bound $CHMP2B_{195-213}$ and and ID of intermolecular NOEs ,94% occupancy). All complexes were in fast exchange.

Data Collection and Resonance Assignment

Assignments were made using a standard suite of triple resonance NMR experiments[16] recorded at 25 ºC on Varian Inova 600 or 800 MHz NMR spectrometers equipped with triple-resonance ^1H/^{13}C/^{15}N probes (cryogenic probe, 600 MHz; room temperature probe, 800 MHz) and z-axis pulsed-field gradients. Data were processed with FELIX (Accelrys, San Diego), and resonances assigned using standard approaches within the SPARKY program (T.D. Goddard and D.G. Kneller, University of California, San Francisco).

Nearly complete resonance assignments were obtained for VPS4A MIT-$CHMP1A_{180-196}$ (96.4%, 13 stereospecific assignments), free VPS4B MIT (94.7%, 31 stereospecific assignments), and bound VPS4B MIT-$CHMP2B_{195-213}$ (98%, 14 stereospecific assignments). Backbone phi and psi torsion angles were estimated from $^{13}C\alpha$ chemical shifts using TALOS[17]. All prolines were in the trans conformation, as confirmed within CYANA by $^{13}C\beta$ and $^{13}C\gamma$ chemical shifts typical of trans-Pro[18] as part of the CYANA program[19]. The chemical shifts of $CHMP1A_{180-196}$ resonances in samples 1 and 2 (see above) were not identical due to slightly different VPS4A MIT-$CHMP1A_{180-196}$ molar ratios (and fast exchange conditions). Sample 1 CHMP1A resonance assignments were required for proper interpretation of intermolecular NOEs. These assignments were determined by adjusting the assignments in sample 2 using a combination of 2D F1/F2-$^{13}C^{15}N$ filtered [^1H, ^1H] NOESY[20,21] (60 ms mix time), 2D F1/F2-$^{13}C^{15}N$ filtered [^1H, ^1H] TOCSY (35, 55, 70 ms mix times), and analysis of 2D

doi: 10.1038/ nature06 172

[^{15}N, ^{1}H] HSQC (Supplemental Figure 1) and 2D [^{13}C, ^{1}H] HSQC titration curves. Double edited NOESY experiments were unnecessary owing to the small size of the system.

These procedures resulted in nearly complete resonance assignments for the bound CHMP1A$_{180-196}$ peptide in both samples 1 and 2. Chemical shift differences for bound VPS4A MIT in these samples were tracked using the titration data exclusively (Supplemental Figure 1).

Structure Calculations

Intra and intermolecular NOEs were obtained using 3D [^{1}H,^{13}C/^{15}N,^{1}H] NOESY and 3D F1-^{13}C^{15}N-filtered [^{1}H,^{13}C/^{15}N,^{1}H] NOESY experiments (60 msec mixing times). Intermolecular NOEs were obtained from the F1-^{13}C^{15}N-filtered [^{1}H,^{13}C/^{15}N,^{1}H] NOESY while intramolecular NOEs were obtained from differences between the 3D [^{1}H,^{13}C/^{15}N,^{1}H] NOESY and 3D F1-^{13}C^{15}N-filtered [^{1}H,^{13}C/^{15}N,^{1}H] NOESY. NOE coordinates (^{1}H, ^{15}N/^{13}C, ^{1}H) and intensities were obtained by using the tools in SPARKY (from T.D. Goddard and D.G. Kneller), and exported into CYANA[19] for structure calculations. NOEs were assigned and structures calculated using the automated NOE assignment module implemented in CYANA (Version 2.1)[19]. Intermolecular NOEs for both complexes were manually assigned and incorporated into the complex structure calculations using the "Keep" subroutine in CYANA. A number of additional peaks were present in the 3D [^{1}H,^{13}C/^{15}N,^{1}H] F1-^{13}C^{15}N-filtered NOESY spectra of VPS4B MIT-CHMP2B$_{195-213}$ owing to the very high excess of CHMP2B$_{195-213}$ peptide required to saturate this weaker-binding complex. The assigned VPS4A MIT-CHMP1A$_{180-196}$ structure was therefore used as a general "distance filter" to select the subset of NOE's kept.

Final CYANA calculations started with 1000 randomized conformers that were "folded" into 3D structures by introducing NOE constraints in a step-wise manner by using the criteria of chemical shift agreement, network anchoring, and consistency with an initial fold. Each conformer was subjected to 10,000 steps of torsion angle dynamics per cycle (seven cycles total). Final CYANA calculations included helical hydrogen bond restraints, derived from the preliminary structures. The 20 lowest energy CYANA structures were refined in CNS using a low temperature simulated annealing protocol. Structure statistics for VPS4A MIT-CHMP1A$_{180-196}$, free VPS4B, and VPS4B MIT-CHMP2B$_{195-213}$ are summarized in Supplemental Table 1. Structures were visualized, superimposed, and figures made using PYMOL (DeLano Scientific).

GFP-CPS Cargo Sorting Assays

vps4Δ yeast cells harboring pRS415*MET25+GFP-CPS*[22] and either pRS416+*VPS4*, pRS416+*vps4$_{L64D}$*, or an empty control vector were grown to log phase in selective media at 30 °C or 37 °C and scored for the presence of vacuolar GFP fluorescence primarily: 1) at the limiting vacuolar membrane, or 2) within the vacuolar lumen.

Yeast Class E compartments and vacuolar membranes were simultaneously visualized using FM4-64 staining[23]. Log phase cultures were incubated with 10 mg/μl FM4-64 dye (Molecular Probes)) at 30 °C or 37 °C for 15 min, washed, and incubated at 30 °C or 37 °C in selective media for 0.5-2 h prior to observation.

Vps4p Localization (Yeast)

For GFP-Vps4p localization studies, *vps4Δ* cells harboring pRS415*MET25+GFP-VPS4* or mutant alleles were grown to log phase at 30 °C, stained with FM4-64, and scored for one of three different phenotypes: 1) diffuse cytoplasmic, 2) diffuse + punctate, or 3) exclusively

doi: 10.1038/ nature06 172

punctate GFP fluorescence. FM4-64 staining was performed as described above. Equivalent expression levels of the wt and mutant GFP-Vps4p proteins were confirmed by western blotting (not shown).

Fluorescence Imaging (Yeast)

Yeast cells were visualized and protein localization was scored using a Zeiss Axioplan 2 Imaging microscope. Images used for figures were collected on an Olympus FV300 confocal fluorescence microscope using Fluoview 2.0.3.9 software. Quantified data shown in Fig. 3 and Supplemental Figure 6 are both from three independent data sets of 100 cells, and error bars reflect standard deviations.

Fluorescence Imaging (Mammalian Cells)

COS7 cells were seeded on collagen-coated glass coverslips in a 12-well plate at $8x10^4$ cells/well. 2 μg pEGFP-VPS4A DNA or mutant construct was transfected using 2.5 μl of lipofectamine 2000 (Invitrogen) per well according to the manufacturers instructions. Cells were fixed ~18 h post-transfection in 3% paraformaldehyde in phosphate buffered saline (PBS), washed once with 50 mM NH_4Cl in PBS, washed twice in 1% BSA in PBS and placed onto a microscope slide containing Fluoromount-G (Southern Biotech). Images were collected on an Olympus FV300 confocal fluorescence microscope using Fluoview 2.0.3.9 software. Data shown in Fig. 4a are from two independent experiments (≥100 cells/experiment), and errors reflect standard deviations.

Infectivity Assays

293T cells were seeded in 6-well plates at $8x10^5$ cells per well and co-transfected with the pEGFP-VPS4 expression construct and an HIV-1 vector system (packaging and transfer plasmids kindly provided by D. Trono, and envelope plasmid by J. Burns). Briefly, 12 μl FuGene 6 Transfection Reagent (Roche Diagnostics) was combined with 1 μg pCMVΔR8.2, 1μg pWPTS-nlsLacZ, 0.36 μg phCMV-VSVG, and 0.5 μg pEGFP-VPS4A plasmid per well according to manufacturer's instructions. Supernatants containing virions were harvested 48 h post-transfection, and used to infect HeLa-M cells[24] or used in virion release assays. Titers reported in Fig. 4b are from triplicate measurements, and errors reflect standard deviations.

Virion Release Assays

Viral supernatants and cell-associated proteins were prepared[25] and analyzed by western blotting was as described[26]. Primary antibodies used were rabbit anti-HIV-1 MA (1:50,000, from D. Trono), rabbit anti-HIV-1 CA UT415 (1:1000, Covance), rabbit anti-VPS4A UT289 (1:000, Covance), and mouse anti-γ-Tubulin GTU-88 (1:5000, Abcam). Proteins were detected using fluorescent secondary antibodies: 1) goat anti-rabbit ALEXA680nm (1:20,000, Molecular Probes) or 2) donkey anti-mouse IR800nm (1:10,000, Rockland) and visualized on an Odyssey scanner (LiCor Inc.).

doi: 10.1038/ nature06 172

Supplemental References

1. Takasu, H. et al. Structural characterization of the MIT domain from human Vps4b. *Biochem Biophys Res Commun* **334**, 460-5 (2005).
2. Scott, A. et al. Structure and ESCRT-III protein interactions of the MIT domain of human VPS4A. *Proc Natl Acad Sci U S A* **102**, 13813-8 (2005).
3. Gish, W. & States, D.J. Identification of protein coding regions by database similarity search. *Nat Genet* **3**, 266-72 (1993).
4. Guthrie, C. & Fink, G.R. (eds.). *Guide to yeast genetics and molecular biology*, 1-933 (Academic Press, San Diego, CA, 1991).
5. Sherman, F., Fing, G.R. & Hicks, J.B. *Methods in Yeast Genetics*, (Cold Spring Harbor Press, Cold Spring Harbor, NY, 1986).
6. Wach, A., Brachat, A., Pohlmann, R. & Philippsen, P. New heterologous modules for classical or PCR-based gene disruptions in Saccharomyces cerevisiae. *Yeast* **10**, 1793-808 (1994).
7. Rothstein, R. Targeting, disruption, replacement, and allele rescue: integrative DNA transformation in yeast. *Methods Enzymol* **194**, 281-301 (1991).
8. Wendland, B. & Emr, S.D. Pan1p, yeast eps15, functions as a multivalent adaptor that coordinates protein-protein interactions essential for endocytosis. *J Cell Biol* **141**, 71-84 (1998).
9. Garrus, J.E. et al. Tsg101 and the vacuolar protein sorting pathway are essential for HIV-1 budding. *Cell* **107**, 55-65 (2001).
10. von Schwedler, U.K. et al. The protein network of HIV budding. *Cell* **114**, 701-13 (2003).
11. Price-Carter, M., Gray, W.R. & Goldenberg, D.P. Folding of omega-conotoxins. 2. Influence of precursor sequences and protein disulfide isomerase. *Biochemistry* **35**, 15547-57 (1996).
12. Karren, M.A., Coonrod, E.M., Anderson, T.K. & Shaw, J.M. The role of Fis1p-Mdv1p interactions in mitochondrial fission complex assembly. *J Cell Biol* **171**, 291-301 (2005).
13. Dadlez, M. & Kim, P.S. Rapid formation of the native 14-38 disulfide bond in the early stages of BPTI folding. *Biochemistry* **35**, 16153-64 (1996).
14. Pornillos, O., Alam, S.L., Davis, D.R. & Sundquist, W.I. Structure of the Tsg101 UEV domain in complex with the PTAP motif of the HIV-1 p6 protein. *Nat Struct Biol* **9**, 812-7 (2002).
15. Myszka, D.G. Improving biosensor analysis. *J Mol Recognit* **12**, 279-84. (1999).
16. Cavanagh, J., Fairbrother, W.J., Palmer, A.G., 3rd & Skelton, N.J. *Protein NMR Spectroscopy, Principles and Practice*, (Academic Press, San Diego, 1996).
17. Cornilescu, G., Delaglio, F. & Bax, A. Protein backbone angle restraints from searching a database for chemical shift and sequence homology. *J Biomol NMR* **13**, 289-302. (1999).
18. Schubert, M., Labudde, D., Oschkinat, H. & Schmieder, P. A software tool for the prediction of Xaa-Pro peptide bond conformations in proteins based on 13C chemical shift statistics. *J Biomol NMR* **24**, 149-54 (2002).
19. Guntert, P. Automated NMR structure calculation with CYANA. *Methods Mol Biol* **278**, 353-78 (2004).
20. Zwahlen, C. et al. Methods for measurement of Intermolecular NOEs by multinuclear NMR Spectroscopy: Application to a bacteriophage lamda N-peptide/boxB RNA complex. *J. Am. Chem. Soc.* **119**, 6711-6721 (1997).

doi: 10.1038/ nature06 172

21. Petros, A.M. & Fesik, S.W. Nuclear magnetic resonance methods for studying protein-ligand complexes. *Methods Enzymol* **239**, 717-39 (1994).
22. Odorizzi, G., Babst, M. & Emr, S.D. Fab1p PtdIns(3)P 5-kinase function essential for protein sorting in the multivesicular body. *Cell* **95**, 847-58 (1998).
23. Vida, T.A. & Emr, S.D. A new vital stain for visualizing vacuolar membrane dynamics and endocytosis in yeast. *J Cell Biol* **128**, 779-92 (1995).
24. Ward, D.M. et al. The role of LIP5 and CHMP5 in multivesicular body formation and HIV-1 budding in mammalian cells. *J Biol Chem* **280**, 10548-55 (2005).
25. von Schwedler, U.K. et al. Proteolytic refolding of the HIV-1 capsid protein amino-terminus facilitates viral core assembly. *Embo J* **17**, 1555-68 (1998).
26. Langelier, C. et al. Human ESCRT-II complex and its role in human immunodeficiency virus type 1 release. *J Virol* **80**, 9465-80 (2006).

Supplemental Figure 1.

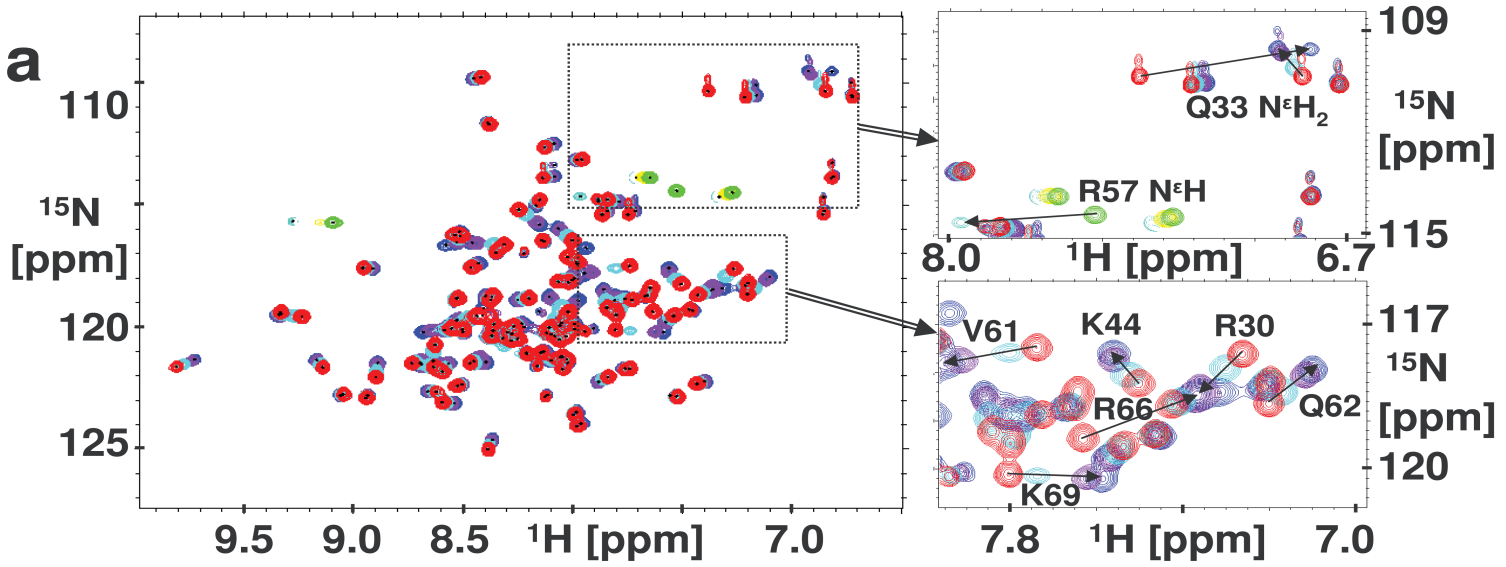

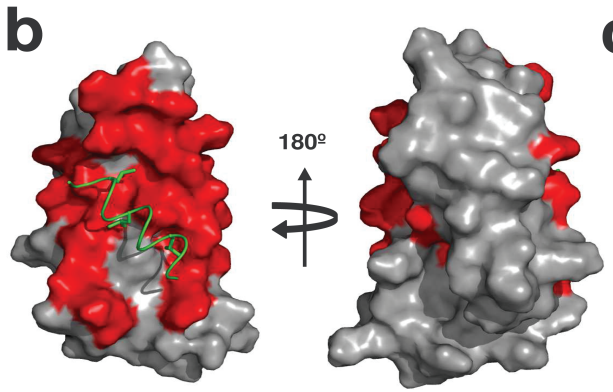

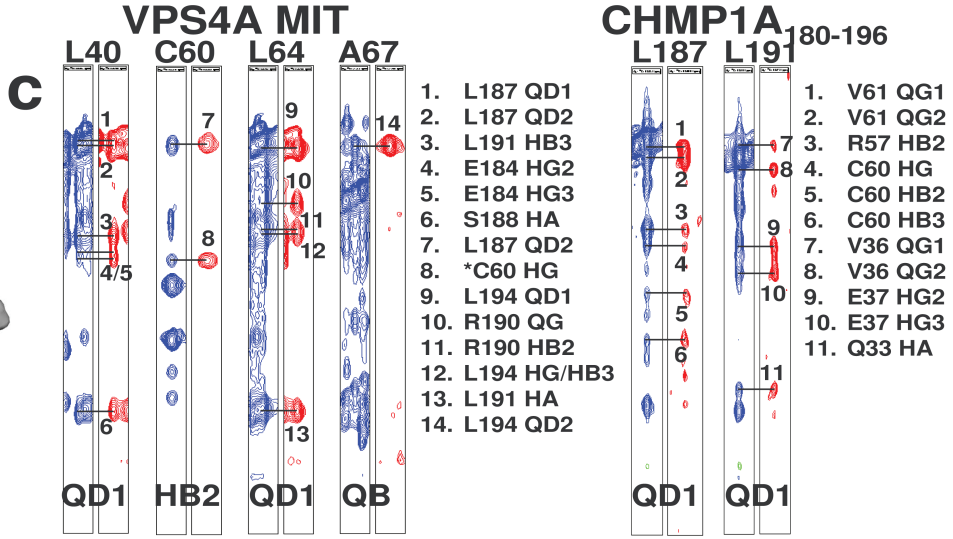

Supplemental Figure 2.

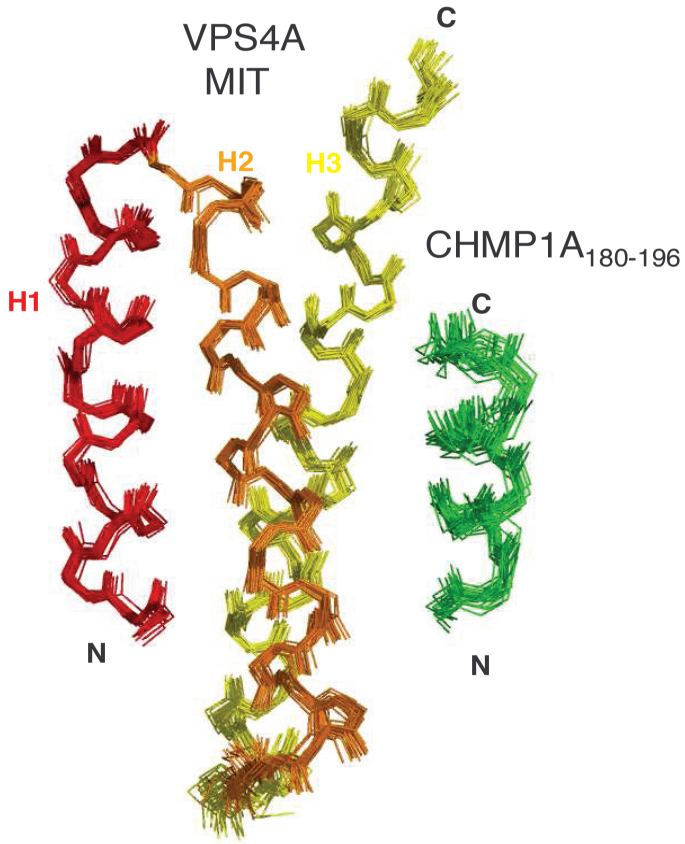

Supplemental Figure 3

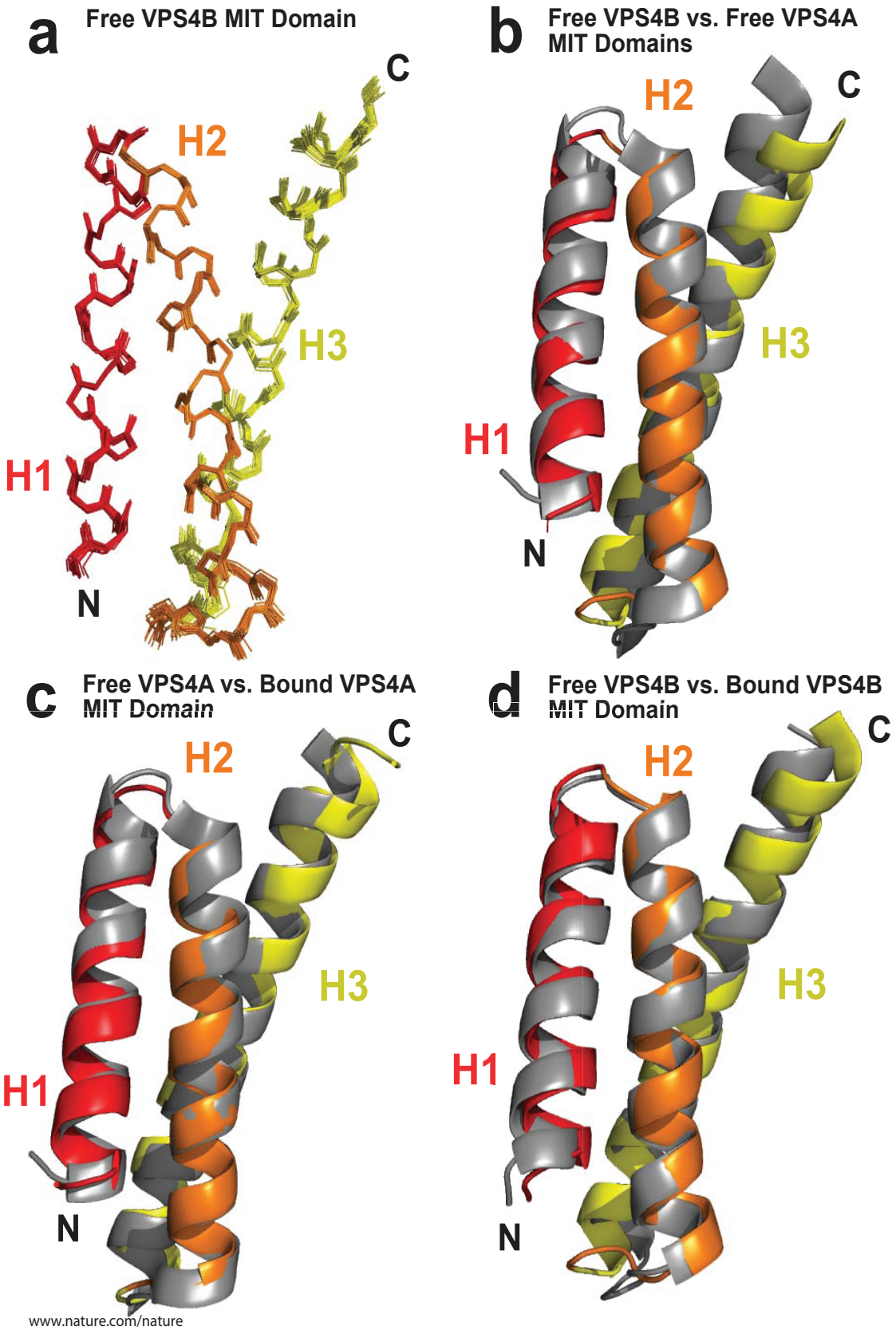

Supplemental Figure 4.

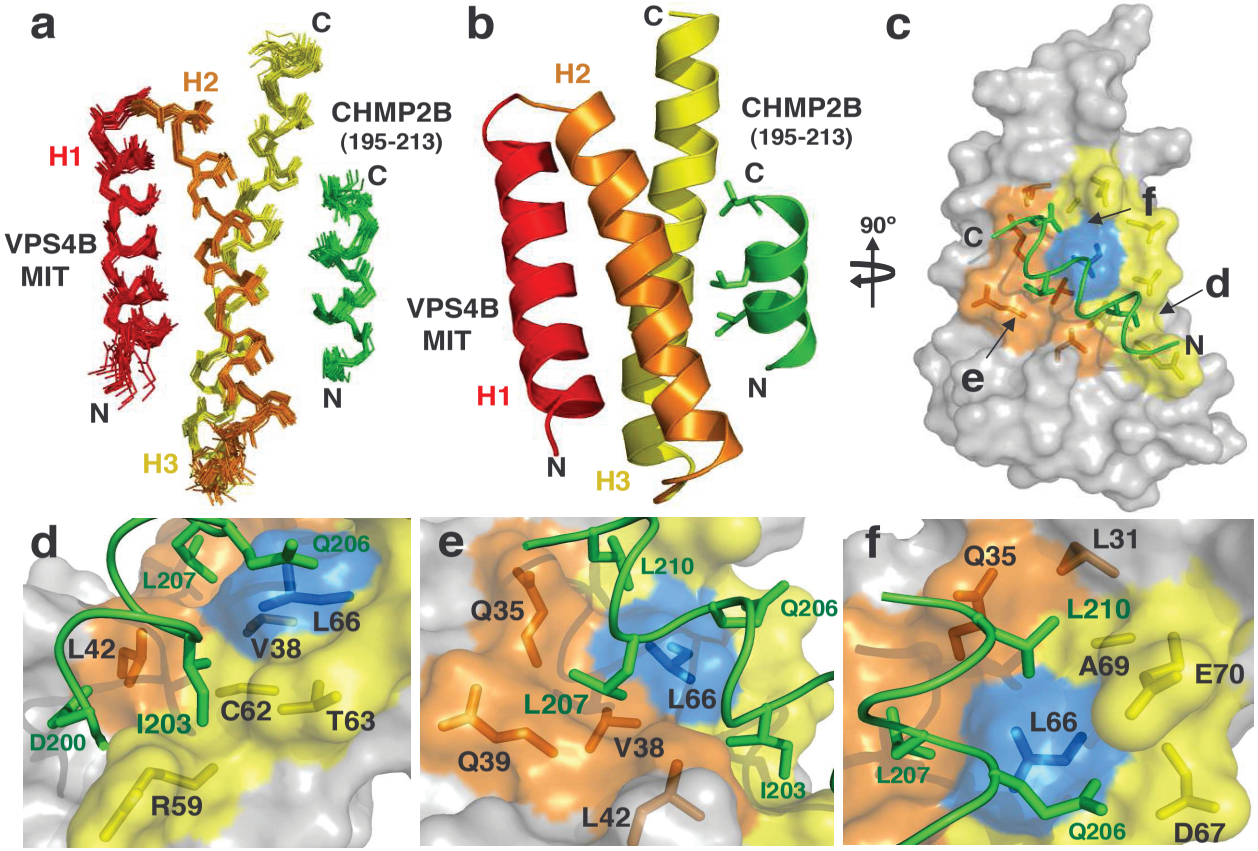

Supplemental Figure 5

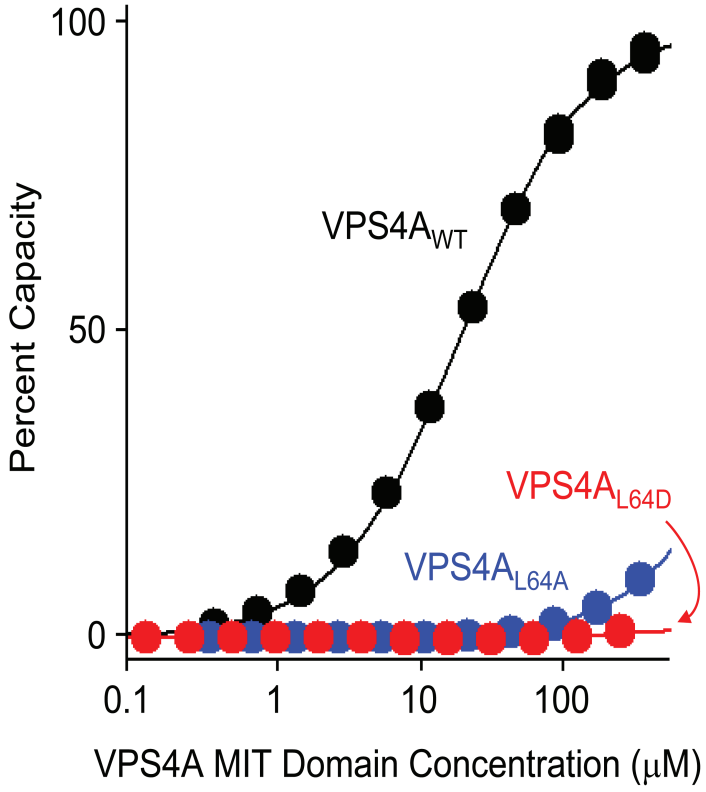

Supplemental Figure 6